DISCLAIMER:

This document does not meet the
current format guidelines of
the Graduate School at
The University of Texas at Austin.

It has been published for
informational use only.

The Dissertation Committee for Amey Shreekant Puranik Certifies that this is the approved version of the following dissertation:

Intelligent nanoscale hydrogels for the oral delivery of hydrophobic therapeutics

Committee:

Nicholas Peppas, Supervisor

Lydia Contreras

Isaac Sanchez

Jeanne Stachowiak

Hsin-Chih Yeh

Intelligent nanoscale hydrogels for the oral delivery of hydrophobic therapeutics

by

Amey Shreekant Puranik, B.Ch.E.

Dissertation

Presented to the Faculty of the Graduate School of

The University of Texas at Austin

in Partial Fulfillment

of the Requirements

for the Degree of

Doctor of Philosophy

The University of Texas at Austin

May 2015

Dedication

To my parents.

Acknowledgements

My tenure at the University of Texas at Austin has played a pivotal role in developing me professionally and personally. I have had the excellent fortune of working with some of the best researchers and future scientists – some young, some not-so-young - all of whom wholeheartedly embody the spirit of wanting to change the world.

Firstly, I would like to thank my advisor Dr. Nicholas Peppas for his enduring support, patience, and continued encouragement, and for being a constant source of motivation to me and countless other young researchers. His dedication to the advancement of the field and steadfast support for his students is testimony to his visionary and inspirational leadership. His research lab has spawned numerous world-renowned professors, scientists, and company leaders, and I consider myself privileged to belong to this great family of 'Peppamers'.

I would like to thank my parents for believing in me, and for enabling and empowering me to obtain the education and training that I desired. I have come a long way, literally and figuratively, and I am grateful to my parents for helping me achieve this feat. A big shout out to my friends back home in India for their constant support and encouragement, and for still staying in touch although we are many thousand miles apart.

This acknowledgment section would be grossly incomplete without thanking my fellow Peppamers – former and current lab mates. From starting out as the only friends I had in the western hemisphere to literally becoming my family away from home, I've had a great time getting to know each and every one of them. I would like to thank: Angela, Bill, Brandon, Brenda, Claire, Cody, David, David, Diane, bam Heidi, Jenny, Jonathan, John, Lindsey, Maggie, Marty, Mary, Mati, Michael, Rebekah, Sarena, and Stephanie for wonderful academic and

extracurricular discussions, as well as endless supply of support, encouragement, coffee, eggs, cookies, and chicken nuggettes. It has been a joy to be a part of all lab activities including but not limited to lab camping trips, lab lunches and lab parties.

I would like to acclaim the undergraduate research assistants who worked with me, for their support and help with experiments and scientific discussions regarding my research. I would like to thank – Ludovic Pao, Courtney Tanwar, and Vanessa White. Their efforts greatly influenced the impact of this research. It has been a pleasure to work with these young, enthusiastic researchers, and I'm certain of their success in all future endeavors. I would also like to thank the UT core facilities staff for their training and guidance with use of the various instruments mentioned in this thesis. Finally, I would like to acknowledge the funding sources for my work - the National Institutes of Health (NIH) and the Pratt Foundation.

Intelligent nanoscale hydrogels for the oral delivery of hydrophobic therapeutics

Amey Shreekant Puranik, PhD

The University of Texas at Austin, 2015

Supervisor: Nicholas A. Peppas

In this work, novel oral drug delivery formulations were developed for the administration of hydrophobic therapeutics, with the overarching goal of improving their solubility and permeability in the gastrointestinal tract. We have developed a set of four nanoscale hydrogels, formulated by incorporating different hydrophobic monomer components, and screen them for optimal physicochemical properties, drug loading and release, and ability to modulate intestinal permeability and P-glycoprotein related drug efflux. Here, we employ an evolved paradigm of *in vitro* tests to gauge the potential of these novel nanoscale carriers for the specific application of improving oral solubility and permeability of poorly water-soluble and less permeable therapeutics.

All the responsive nanoscale hydrogels are capable of undergoing a transition in size in response to change in pH. We capitalize on the interplay between the incorporated hydrophobic monomer choices and screened resulting physicochemical properties to determine an optimal nanoscale formulation. Depending upon the selection of the hydrophobic monomer, the sizes of the nanoparticles vary widely from 120 nm to about 500 nm at pH 7.4. We also evaluate cytocompatibility of the nanoparticle formulations in vitro in the presence of an intestinal epithelial cell mode to find that all formulations are reasonably cytocompatible. Subsequently,

we discuss some of the key findings and results of characterization studies that validate the success of achieving desired molecular architecture and physicochemical properties of the formulation. We then confirm the capacity of the nanocarrier to be able to load and release hydrophobic therapeutics in gastrointestinally relevant environments. Further, the ability of the nanocarriers to transport the hydrophobic therapeutic doxorubicin is determined by evaluating permeability of doxorubicin with intestinal epithelial cell monolayers. Furthermore, demonstrate functional abilities desired from a therapeutically relevant, oral delivery system is tested. Specifically, to overcome problems associated with P-glycoprotein related efflux and reduced drug permeability in the small intestine, we evaluated the ability of the nanoformulation to achieve therapeutic success in relevant and characteristic *in vitro* cancer cell lines. Finally, we make concluding remarks on the ability of the nanoparticles to function as improved formulations of hydrophobic therapeutics capable of performing and achieving the end-goal of delivering hydrophobic therapeutics orally for the treatment of cancer.

Contents

List of Tables 11

List of Figures 12

Chapter 1: Introduction 20

Chapter 2: Objectives of Proposed Research 23

Chapter 3: Cancer 26

3.1 Current State of Chemotherapy 28

3.2 Liver Cancer 30

Chapter 4: Oral Delivery of Hydrophobic Therapeutics 32

4.1 Classification of Hydrophobic Drugs 32

4.2 Hydrophobic Behavior Based on the Biopharmaceutics Classification System 32

4.3 Hydrophobic Behavior Based on the Biopharmaceutics Drug Disposition Classification System 34

4.4 Gastrointestinal Tract Physiology for Oral Delivery 35

4.5 Nanotechnology for Oral Delivery of Hydrophobic Drugs 37

4.6 References 44

Chapter 5: Delivery of Chemotherapeutics using Nanotechnology 55

5.1 Introduction 55

5.2. Current Standard of Care 56

5.2. Nanomaterials used in cancer therapy 57

5.4 Delivery to Primary Cancers 60

5.4 Delivery to Metastatic Cancers 68

5.5 Delivery for Anti-angiogenic Therapy 75

5.6 Delivery to Multidrug-Resistant Cancers 99

5.7 Conclusion 103

5.8 REFERENCES 104

Chapter 6: Synthesis and Characterization of pH-Responsive Nanoscale Hydrogels for Oral Delivery of Hydrophobic Therapeutics 120

6.1 Introduction 121

6.2 Physicochemical Characterization: Materials and Methods 124

6.3 Biological Characterization: Materials and Methods 131

6.4 Physicochemical Characterization: Results and discussion.....134
6.5 Biological Characterization: Results and discussion 143
6.6 Conclusions.....148
6.7 References.....194

Chapter 7: Modulation of Hydrophobic Solute Permeation through Anionic Crosslinked Hydrogels for Cancer Drug Delivery Applications 200
2.1 Introduction.....201
2.2 Materials and Methods.....201
2.3 Results and Discussion 207
2.4 Nano formulation dosage feasibility.....217
2.5 Conclusions.....218
2.6 References.....220

Chapter 8: Evaluation of the Effect of Nanoscale Hydrogels on the Permeability of Hydrophobic Therapeutics across *in vitro* Cell Models 245
8.1 Introduction.....246
8.2 Materials and Methods.....251
8.3 Results and Discussion 259
8.4 Conclusions.....269
8.5 References.....285

Chapter 9: Conclusions and Future Recommendations.....288

Appendices.....295
APPENDIX A: RECENT ADVANCES IN DRUG ELUTING STENTS .295
APPENDIX B: Background – Multidrug Resistant Proteins 311
APPENDIX C: BUILDING VASCULAR NETWORKS.....330

Bibliography 336

List of Tables

Table 6.1 – Q, e values of monomer components

Table 6.2 – Reactivity ratios for Methacrylic acid (designated as 1) and comonomers used in polymerization

Table 6.3 – Ratio of crystalline PEG to total PEG in the nanoparticle formulations.

Table 7.1: Powder X-ray diffraction peak values for doxorubicin-loaded formulations

Table 7.2: Doxorubicin loading efficiencies and partition coefficients with nanoscale hydrogel formulations at the end of the study. Calculated as % efficiency = C_o-C_t/C_o ; n= 3, Reported as mean +/- SD. K_d= c_m/c_e = $(c_0 - c_e)/c_e$;

Table 7.3: Permeability coefficients/slopes for the diffusion of doxorubicin through the membrane formulations.

Table 7.4: Membrane formulation and their permeability coefficients, partitioning coefficients, and diffusion coefficients

Table 8.1 Doxorubicin transport with nanoscale hydrogel formulations

Table 8.2 Doxorubicin transport with hydrogel formulations containing PEG and hydrogel formulations without PEG

List of Figures

Fig. 4.1: Efflux and uptake transporters present on the apical and basolateral sides of the small intestine. Adapted from [64].

Fig. 4.2: Schematic representation of pathways for intestinal transport: (a) transcellular active transport, (b) transcellular passive transport, and (c) paracellular transport through tight junctions. Adapted from [7].

Figure 6.1 – Schematic of the swelling behavior and drug release from a pH-responsive hydrogel for the oral delivery of doxorubicin, a hydrophobic therapeutic.

Figure 6.2 – Structures of monomers used in the emulsion polymerization procedure. MAA is the hydrophilic monomer, PEGMMA is used to form PEG grafts, and tetraethylene glycol dimethacrylate is the cross-linker. These monomers were maintained consistent for all four formulation syntheses.

Figure 6.3 – Structures of the four hydrophobic monomers used. Formulation containing, (a) tert-butyl methacrylate is denoted as P(MAA-g-PEG-co-tBMA), (b) n-butyl methacrylate is denoted as P(MAA-g-PEG-co-nBMA), (c) n-butyl acrylate is denoted as P(MAA-g-PEG-co-nBA), and (d) methyl methacrylate is denoted as P(MAA-g-PEG-co-MMA)

Figure 6.4 – Dynamic swelling data for P(MAA-g-PEG-co-tBMA). Data points shown are mean of measurements ± SD.

Figure 6.5 – Dynamic swelling data for P(MAA-g-PEG-co-nBMA). Data points shown are mean of measurements ± SD.

Figure 6.6 – Dynamic swelling data for P(MAA-g-PEG-co-nBMA). Data points shown are mean of measurements ± SD.

Figure 6.7 – Dynamic swelling data for P(MAA-g-PEG-co-MMA). Data points shown are mean of measurements ± SD.

Figure 6.8 – Dynamic Swelling behavior of all formulations as measured by dynamic light scattering. P(MAA-g-PEG-co-MMA) underwent the largest size increase upon increasing pH, while P(MAA-g-PEG-co-tBMA) underwent the smallest size increase. Data points shown are mean of measurements ± SD.

Figure 6.9 - Zeta potential measurements for all formulations. Nanoparticle surface charge typically increases from -17.5 to -20 mV at pH 7.5, to slightly less negative at lower pH. Data points shown are mean of measurements ± SD.

Figure 6.10 - Representative scanning electron micrograph images. Scale bars: (a) 300 nm, (b) 10 μm, (c) 100 nm, and (d) 500 nm

Figure 6.11 - Fourier Transform-Infrared (FTIR) spectra for P(MAA-g-PEG-co-tBMA). Y-axis: Relative Fraction Transmittance or (1-absorbance), X-axis: Wavenumbers (cm-1), wavenumber = 1/λ

Figure 6.12: Fourier Transform-Infrared (FTIR) spectra for P(MAA-g-PEG-co-nBMA). Y-axis: Relative Fraction Transmittance or (1-absorbance) X-axis: Wavenumbers (cm^{-1}), wavenumber = 1/λ

Figure 6.13: Fourier Transform-Infrared (FTIR) spectra for P(MAA-g-PEG-co-nBA). Y-axis: Relative Fraction Transmittance or (1-absorbance) X-axis: Wavenumbers (cm^{-1}), wavenumber = 1/λ

Figure 6.14: Fourier Transform-Infrared (FTIR) spectra for P(MAA-g-PEG-co-MMA). Y-axis: Relative Fraction Transmittance or (1-absorbance) X-axis: Wavenumbers (cm^{-1}), wavenumber = 1/λ

Figure 6.15 - FTIR spectra of all formulations. Light blue: P(MAA-g-PEG-co-tBMA); Red: P(MAA-g-PEG-co-MMA); Green: P(MAA-g-PEG-co-nBA); Blue:P(MAA-g-PEG-co-nBMA) ; Y axis: Fraction Transmittance

Figure 6.16 - 1H-NMR spectrum of P(MAA-g-PEG-co-tBMA)

Figure 6.16 - 1H-NMR spectrum of P(MAA-g-PEG-co- nBMA)

Figure 6.16 - 1H-NMR spectrum of P(MAA-g-PEG-co- nBA)

Figure 6.16 - 1H-NMR spectrum of P(MAA-g-PEG-co- MMA)

Figure 6.20 - Differential scanning calorimetry thermograms of P(MAA-co-tBMA-g-PEG) nanoparticle formulation (red), P(MAA-co-nBMA-g-PEG) nanoparticle formulation (green), P(MAA-co-nBA-g-PEG) nanoparticle formulation (red).

Figure 6.21 - DSC thermogram of P(MAA-co-tBMA-g-PEG) nanoparticle formulation as seen when subjected to a heat-cool-heat cycle.

Figure 6.22 - DSC thermogram of P(MAA-co-MMA-g-PEG) nanoparticle formulation as seen when subjected to a heat-cool-heat cycle.

Figure 6.23 - DSC thermogram of P(MAA-co-nBMA-g-PEG) nanoparticle formulation as seen when subjected to a heat-cool-heat cycle.

Figure 6.24 - DSC thermogram of P(MAA-co-nBA-g-PEG) nanoparticle formulation as seen when subjected to a heat-cool-heat cycle.

Figure 6.25 - TGA thermogram of the P(MAA-co-tBMA-g-PEG) polyanionic nanoparticles with nitrogen atmosphere. Weight Change % (green line) and derivative of Weight Change % with respect to time (blue line) are shown with increasing temperature.

Figure 6.26 - TGA thermogram of the P(MAA-co-MMA-g-PEG) polyanionic nanoparticles with nitrogen atmosphere. Weight Change % (green line) and derivative of Weight Change % with respect to time (blue line) are shown with increasing temperature.

Figure 6.27 - TGA thermogram of the P(MAA-co-nBMA-g-PEG) polyanionic nanoparticles with nitrogen atmosphere. Weight Change % (green line) and derivative of Weight Change % with respect to time (blue line) are shown with increasing temperature.

Figure 6.28 - TGA thermogram of the P(MAA-co-nBA-g-PEG) polyanionic nanoparticles with nitrogen atmosphere. Weight Change % (green line) and derivative of Weight Change % with respect to time (blue line) are shown with increasing temperature.

Figure 6.29 - *in vitro* cell proliferation % of evaluated by MTS assay for P(MAA-g-PEG-co-tBMA); n=4. Data are expressed as mean of measurements ± SD.

Figure 6.30 - *in vitro* cell proliferation % of evaluated by MTS assay for P(MAA-g-PEG-co-nBMA); n=4. Data are expressed as mean of measurements ± SD.

Figure 6.31 - *in vitro* cell proliferation % of evaluated by MTS assay for P(MAA-g-PEG-co-nBA); n=4. Data are expressed as mean of measurements ± SD.

Figure 6.32 - *in vitro* cell proliferation % of evaluated by MTS assay for P(MAA-g-PEG-co-MMA); n=4. Data are expressed as mean of measurements ± SD.

Figure 6.33 - *in vitro* cell viability % of evaluated by LDH assay for P(MAA-g-PEG-co-tBMA); n=4. Data are expressed as mean of measurements ± SD.

Figure 6.34 - *in vitro* cell viability % of evaluated by LDH assay for P(MAA-g-PEG-co-nBMA); n=4. Data are expressed as mean of measurements ± SD.

Figure 6.35 - *in vitro* cell viability % of evaluated by LDH assay for P(MAA-g-PEG-co-nBA); n=4. Data are expressed as mean of measurements ± SD.

Figure 6.36 - *in vitro* cell viability % evaluated by LDH assay for P(MAA-g-PEG-co-MMA); n=4. Data are expressed as mean of measurements ± SD.

Figure 6.37 **-** Mucoadhesion studies performed with a quartz crystal microbalance with (a) 0.001 mg/ml polymeric nanoparticles, (b) 0.5 mg/ml polymeric nanoparticles.

Figure 6.38 - Change in (a) mass and, (b) thickness of immobilized mucin owing adhesion of polymeric nanoparticles.

Figure 6.39 - Confocal microscopy images of fluorescently tagged polyanionic nanoparticles incubated with RAW 264.7 for 2 hr. Red: Alexa Fluor® 594 wheat-germ agglutinin (WGA); Blue: DAPI; Green: AlexaFluor® 488 tagged nanoparticles.

Figure 6.40 - Composite confocal microscopy images with merged color channels of fluorescently tagged polyanionic nanoparticles incubated with RAW 264.7 for 2 hr. Red: Alexa Fluor® 594 wheat-germ agglutinin (WGA); Blue: DAPI; Green: AlexaFluor® 488 tagged nanoparticles.

Figure 6.41 - Montage of Z-stack orthogonal view, with XZ –planes and YZ planes to visualize internalization of polyanionic nanoparticles.

Figure 6.42 - Montage of Z-stack orthogonal view, with XZ –planes and YZ planes to visualize internalization of polycationic nanoparticles.

Figure 7.1: Molecular structure of doxorubicin.

Figure 7.2: Formulation map showing nanoscale formulations for drug loading and relase studies, and powder X-ray diffraction. Micro or membrane formulations of the same component monomers had to be synthesized for compatibility with drug diffusion studies/cells and membrane partitioning.

Figure 7.3: Doxorubicin loading efficiencies with nanoscale hydrogel formulations. Calculated as % efficiency = C_o-C_t/C_o ; n= 3, data points shown are mean of measurements +/- SD. Loading efficiency among treatment groups is statistically significant with $p<0.05$.

Figure 7.4: Doxorubicin release efficiencies with nanoscale hydrogel formulations. Calculated as % efficiency = C_o-C_t/C_o ; n= 3, data points shown are mean of measurements +/- SD. Loading efficiency among treatment groups is statistically significant with $p<0.05$.

Figure 7.5: Powder X-ray diffraction pattern for free doxorubicin powder as obtained from manufacturer. Sharp peaks (indicated by red lines) imply a partially crystalline powder.

Figure 7.6: Powder X-ray diffraction pattern for doxorubicin loaded P(MAA-g-PEG-co-tBMA). Absence of any peaks implies an amorphous powder.

Figure 7.7: Powder X-ray diffraction pattern for doxorubicin loaded P(MAA-g-PEG-co-nBMA). Presence of peaks at 2θ=31.599, 45.322, 56.36 suggests powder is not fully amorphous and has a crystalline character to it.

Figure 7.8: Powder X-ray diffraction pattern for doxorubicin loaded P(MAA-g-PEG-co-nBA). Absence of any peaks implies an amorphous powder.

Figure 7.9: Powder X-ray diffraction pattern for doxorubicin loaded P(MAA-g-PEG-co-MMA). Absence of any peaks implies an amorphous powder

Figure 7.10: Elemental data scanning and Peak comparison. Powder X-ray diffraction pattern of Doxorubicin-loaded P(MAA-g-PEG-co-MMA) nanoscale hydrogels (blue) and compared with peaks of 5-beta-dihydrotestosterone standard, which has a structure similar to doxorubicin, implying presence of doxorubicin in amorphous powder.

Figure 7.11: Elemental data scanning and Peak comparison. Powder X-ray diffraction pattern of Doxorubicin-loaded P(MAA-g-PEG-co-MMA) nanoscale hydrogels (blue) and compared with peaks of L-lactide-poly(ethyleneglycol)

Figure 7.12: Elemental data scanning and Peak comparison. Powder X-ray diffraction pattern of Doxorubicin-loaded P(MAA-g-PEG-co-MMA) nanoscale hydrogels (blue) and compared with peaks of Succinic acid-2-urea

Figure 7.13: Elemental data scanning and Peak comparison. Powder X-ray diffraction pattern of Doxorubicin-loaded P(MAA-g-PEG-co-MMA) nanoscale hydrogels (blue) and compared with peaks of 3-(3-Methyltoluyl)-1,2,2-trimethylcyclopentanecarboxylic acid.

Figure 7.14: Elemental data scanning and Peak comparison. Powder X-ray diffraction pattern of Doxorubicin-loaded P(MAA-g-PEG-co-MMA) nanoscale hydrogels (blue) and compared with peaks of Indole-2-carboxylic acid 2,4-dinitrobenzoic acid.

Figure 7.15: Elemental data scanning and Peak comparison. Powder X-ray diffraction pattern of Doxorubicin-loaded P(MAA-g-PEG-co-MMA) nanoscale hydrogels (blue) and compared with peaks of 3-Aminobenzoic acid 5-nitroquinoline.

Figure 7.16: Schematic of solute diffusion cells or Valia-chen cells for drug diffusion studies.

Figure 7.17: Recipient cell concentration of doxorubicin in solute diffusion studies performed using diffusion cells and membrane formulations. Data points shown are expressed as mean +/- SD.

Figure 7.18: Calculation of slope for doxorubicin solute permeability studies conducted in Valia-Chen diffusion cells.

Figure 8.1: A schematic of the set-up for the transport studies conducted using Transwell® plates.

Figure 8.2: Doxorubicin transport with nanoscale hydrogel formulations. Studies were conducted with 1 mg/ml nanoscale hydrogel formulations incubated with Caco-2 cells and 0.15 mg/ml doxorubicin. n=4, Data points represent mean +/- SD.

Figure 8.3: Transport of doxorubicin in the presence of PEGylated formulation vs non-PEGylated formulations. Studies were conducted with 1 mg/ml hydrogel formulations incubated with Caco-2 cells and 0.15 mg/ml doxorubicin. n=4, Data points represent mean +/- SD.

Figure 8.4: Representative fluorescent micrographs of doxorubicin uptake by Caco-2 cells. Channel 1: cell nuclei in blue, Channel 2: doxorubicin, Channel 5: brightfield images.

Figure 8.5: Relative calcein retention in P-gp overexpressing multidrug resistant cells (H69/LX4) and parental cells (H69) upon incubation with calcein AM (a P-gp substrate) and P(MAA-co-tBMA-g-PEG) nanoscale hydrogel formulation. Increase in calcein retention can be observed beyond a concentration of 0.125 mg/ml. Relative calcein retention calculated by normalizing calcein fluorescence for sample to untreated parental cells. n=3, data points represent mean +/-SD.

Figure 8.6: Relative calcein retention in P-gp overexpressing multidrug resistant cells (H69/LX4) and parental cells (H69) upon incubation with calcein AM (a P-gp substrate) and P(MAA-co-nBMA-g-PEG) nanoscale hydrogel formulation. Relative calcein retention calculated by normalizing calcein fluorescence for sample to untreated parental cells. n=3, data points represent mean +/-SD.

Figure 8.7: Relative calcein retention in P-gp overexpressing multidrug resistant cells (H69/LX4) and parental cells (H69) upon incubation with calcein AM (a P-gp substrate) and P(MAA-co-nBA-g-PEG) nanoscale hydrogel formulation. Increased calcein retention was observed beyond a concentration of 0.5 mg/ml. Relative calcein retention calculated by normalizing calcein fluorescence for sample to untreated parental cells. n=3, data points represent mean +/-SD.

Figure 8.8: Relative calcein retention in P-gp overexpressing multidrug resistant cells (H69/LX4) and parental cells (H69) upon incubation with calcein AM (a P-gp substrate) and P(MAA-co-MMA-g-PEG) nanoscale hydrogel formulation. No significant increase in calcein retention was observed. Relative calcein retention calculated by normalizing calcein fluorescence for sample to untreated parental cells. n=3, data points represent mean +/-SD.

Figure 8.9: Cellular proliferation MTS assay with P(MAA-g-PEG-co-tBMA) and doxorubicin against doxorubicin-resistant H69/LX4 cells. n=4, data expressed as mean +/- SD.

Figure 8.10: Cellular proliferation MTS assay with P(MAA-g-PEG-co-nBMA) and doxorubicin against doxorubicin-resistant H69/LX4 cells. n=4, data expressed as mean +/- SD.

Figure 8.11: Cellular proliferation MTS assay with P(MAA-g-PEG-co-nBA) and doxorubicin against doxorubicin-resistant H69/LX4 cells. n=4, data expressed as mean +/- SD.

Figure 8.12: Cellular proliferation MTS assay with P(MAA-g-PEG-co-MMA) and doxorubicin against doxorubicin-resistant H69/LX4 cells. n=4, data expressed as mean +/- SD.

Chapter 1: Introduction

Despite momentous achievements in the field of tumor biology, cancer diagnosis and treatment, cancer continues to be the second leading cause of death in the US. Cancer continues to remain the lives of over half a million Americans each year, with one in every 4 deaths resulting from cancer. It is responsible for about 5 million hospitalizations among adults in a year.

Cancer begins as a localized, malignant tumor that can be successfully removed if detected at that stage. However, about 80% of the cancer cases are detected after cancer has spread to other organs of the body. Usually, the patient undergoes surgical resection of the primary tumor followed by chemotherapy or radiation therapy to eliminate any metastases or secondary tumor. Chemotherapy may be also used for shrinking the tumor to surgical proportions. While such therapies show increased success rates over the last decade, post-surgical cancer metastasis is responsible for 90% of all cancer-related deaths reflecting upon the need to develop more effective treatment modalities.

Primary and metastasized cancer hospitalizations alone account for a whopping $58 billion in costs, a number $15 billion higher than the combined costs for septicemia, osteoarthritis and atherosclerosis. Cancer-related surgeries specifically, account for an estimated 25% of the hospitalization costs, while intravenous, in-patient chemotherapy accounts for approximately 14%. At the present rate of cancer incidence, the financial burden associated with cancer is expected to increase by 39% in the next decade, primarily, due to establishment of specialized, targeted treatments requiring in-patient hospitalization.

The high direct and indirect costs associated with cancer treatment in addition to the discomfort incurred as a result of chemotherapy and subsequent loss of productivity; indicate the

need for further improvements in cancer treatment technologies. It is of critical importance that we address the shortcomings of the current treatment regimens for cancer or even find alternatives. Oral chemotherapeutic delivery can alleviate some of the side effects associated with intravenous chemotherapeutic administration and even supplant surgery as a treatment option, if the bioavailability of the cancer drug following intestinal absorption is good.

An inherent setback of small molecule cancer drugs is their hydrophobicity. Most cancer drugs are developed by modifying drug leads based on natural compounds. For example, doxorubicin, a commonly used cancer drug is obtained by modifying an antibiotic secreted by *Streptomyces peucetius*). Similarly, a lot of focus is devoted to develop anticancer drugs that selectively target cancerous cells, through high-throughput drug target screening and related technologies. Drug molecules that result from such a screening processes are rarely ever efficient in terms of deliverability, with about 60% of them being hydrophobic. Moreover, it is economically unfeasible to simply discard these recalcitrant, yet effective drugs and continue looking for hydrophilic drugs that can be easily delivered to the tumor target. Although there is an increasing trend to synthesize analogues of existing antineoplastic agents (eg. daunorubicin from doxorubicin) in a manner similar to that used to treat arteriosclerosis (eg. everolimus from sirolimus), the hydrophobicity issue remains to be resolved. There is no doubt that development of drug delivery systems capable of effectively delivering hydrophobic drug molecules for cancer and other diseases is the need of the hour. Such advancements in cancer therapy are imperative not only for increasing patient survival rates but also improving the quality of life of patients.

In this proposed thesis, *we focus on the development, characterization and optimization of nanoscale hydrogels for the oral delivery of hydrophobic agents*. Our overall goal is to

examine polymeric nanoparticles for their ability to load hydrophobic therapeutic agents, retain the drug during gastric transit, and release it in the small intestine. Such carriers can permit superior control over physicochemical properties that determine the fate of substance in the GI tract. Parameters such as the constituent hydrophobic monomer, cross linking density, and the hydrophobic monomer content will be controlled to exploit GI tract conditions for enhancing delivery of the hydrophobic drugs doxorubicin and tamoxifen, *in vitro*, across Caco-2 cell monolayers. Consequently, such oral drug delivery systems have the potential to overcome the innate drawbacks imposed by the molecular structure of hydrophobic chemotherapeutics.

Chapter 2: Objectives of Proposed Research

In this work, we propose the development of a novel oral drug delivery system for the administration of hydrophobic therapeutics. We first describe the motivation and rationale behind the design of such a system, and underline the need for the desired molecular architecture. We then move onto delineating the actual facile synthesis method used to produce such a system. Subsequently, we discuss some of the key findings and results of characterization studies led to examine and validating the success of achieving desired molecular architecture and physicochemical properties of the formulation. We then confirm the capacity of the nanocarrier to be able to load and release hydrophobic therapeutics in gastrointestinally relevant environments. Further, the ability of the nanocarriers to demonstrate functional abilities desired from a therapeutically relevant, oral delivery system is tested. Specifically, we establish the ability of the nanoformulation to achieve therapeutic success in relevant and characteristic cancer cell lines, with the overarching goal of corroborating hydrophobic drug delivery in an in vitro cell model. Finally, we make concluding remarks on the ability of the nanoparticles to function as improved formulations of hydrophobic therapeutics capable of performing and achieving end-goal of delivering hydrophobic therapeutics orally for the treatment of cancer; while, summarizing the results from our studies, and touching upon some of the inherent, ineluctable limitations of the system and enunciating modifications to design parameters and experimental studies for future reference. Here, we employ an evolved paradigm of in vitro tests to gauge the potential of these novel nanoscale carriers for the specific application of improving oral solubility and permeability of poorly soluble and less permeable therapeutics. We develop a set of four nanoscale hydrogels, formulated by incorporating different hydrophobic monomer

components, and screen them for optimal physicochemical properties, drug loading and release, and ability to modulate intestinal permeability.

In this proposed PhD thesis, we focus at achieving the following goals:

- To design, synthesize and characterize polyanionic nanoscale hydrogels that are capable of efficiently loading and release of hydrophobic therapeutics such as chemotherapeutics;
- To examine and compare the loading and release behaviors of different formulations and arrive at an optimal formulation
- To evaluate their *in vitro* cytocompatibility and transport properties across an intestinal epithelial model

We propose to design and develop methacrylic acid based nanoscale hydrogels, which will be optimized by varying hydrophobic monomer component, hydrophobic monomer percentage content and the cross linking density of the polymeric networks. We hypothesize that the use of hydrogels, which are optimized for better loading and release of hydrophobic therapeutics, can enhance the intestinal transport of such drugs and open up a window of opportunity for orally treating diseases that can be accessed through the blood stream. Finally, we intend to test the capacity of our oral drug delivery system to modulate intestinal permeability.

The specific aims of this research are:

- To synthesize and characterize methacrylic acid based polyanionic, nanoscale hydrogel networks for the oral delivery of hydrophobic therapeutic agents

- To design and develop a loading and release protocol for encapsulating hydrophobic drugs within the nanoscale hydrogels, and examine modulation of hydrophobic solute permeation through the gels
- To evaluate and compare the *in vitro* biocompatibility and transport properties of the developed nanoscale hydrogels

7

Chapter 3: Cancer

Cancer starts as a malignant tumor that has genetically lost its ability to undergo controlled growth and cellular division owing to mutations leading to overexpression of oncogenes and underexpression of tumor suppressor genes [11]. This malignant tumor dangerously and dramatically evolves into a pervasive disease with an intricate vasculature, by facile adoption of a set of principles commonly known as the hallmarks of cancer. Malicious tumor cells acquire self-sufficiency in growth signals and insensitivity to antigrowth signaling to conveniently overcome inherent growth regulatory constraints, which would otherwise limit normal cell growth and ensure homoeostasis. In fact cancer cells and adjacent normal cells rely on each other to acquire remarkable control of mitogenic growth signaling and the eventual growth factor independence [12,13].

Furthermore, cancer progresses by avoiding apoptosis, a characteristic that allows them to replicate uncontrollably and limitlessly. These burgeoning, aberrant cells explicably require unprecedented amounts of oxygen and nutrition to flourish. In a state of hypoxia, the tumorigenic tissue activates an otherwise dormant endothelium through proangiogenic factors and start building their own vascular network using proliferating and elongating endothelial cells [14]. Particularly, when a tumor reaches 2mm in diameter, oxygen is unable to diffuse throughout all cancer cells within the tumor [15]. Hypoxic cancer cells start a pro-angiogenic signaling process that ultimately translates into secretion of growth factors and extracellular matrix components (ECM) that induce the angiogenic process [16]. Angiogenesis sustains the continued growth of malignant tumors by providing oxygen and nutrients and disposing of waste products over the period of disease progression. These newly formed small blood vessels are critical for the survival and metastasis of the primary tumor to other organs of the body, spreading the

malignancy and advancing the stage of the disease. Compelling evidence in numerous mouse models of inhibition of the customary “angiogenic switch” that triggers the resilient foray of primary tumor cells to other body organs, has indicated halt of tumor growth and metastatic spread [17,18].

The process of angiogenesis is as complex as cancer itself, comprising of several steps and ancillary diffusible factors that facilitate the development of a supportive vascular network. As expected, cancer cells are equipped to escalate the production of proangiogenic factors and downregulating angiogenesis inhibitors, thus thwarting the natural balance of angiogenic factors. The initiation of angiogenesis involves extravasation of plasma proteins, degradation of extracellular matrix to allow migration of cells, followed by actual endothelial cell proliferation and migration, and capillary tube formation. Anti-angiogenic therapy is an approach, which circumvents the issue of metastasis by choking out overgrown tumors and enhances the therapeutic benefit achieved by anti-cancer drugs.

Eventually, tumor cells emigrate to other distant organs through such capillary sprouts and colonize those locations by adapting to the surrounding milieu over time [19]. Sometimes, these immigrating “micrometastases” (i.e., a small number of cancer cells that have spread beyond the original tumor) are able to camouflage themselves from diagnosis and detection by remaining dormant and not displaying the characteristic “hallmarks” evidenced by cancer cells [20]. These cells lack the potential to vigorously grow and replicate or activate angiogenesis when initially circulating systemically or settling in other organs. After several cycles of replication and evolution, ranging over a period of days to decades, they achieve enhanced survival capabilities and resume their cancerous behavior with unparalleled metastatic fury leading to unexpected tumor regression [21,22].

3.1 CURRENT STATE OF CHEMOTHERAPY

Intravenous administration of chemotherapeutics continues to be the beacon of hope for a majority of cancer malignancies, with the obvious caveat of systemic toxicity morbidly lining the therapeutic benefits earned. Success in chemotherapy requires dosage of hydrophobic therapeutics over sufficiently long exposure time periods and at concentrations that are above the therapeutic limit and lower than the toxic limit. In fact, a common strategy is to attack cancerous cells with a high payload of cytotoxic drug at one go, thereby not allowing cancer cells to build immunity for the drug or its structural analogues [23].

Systemic drug delivery has a merit in these regards, since it helps achieve high systemic concentrations of the drug after intravenous infusion permit cytotoxic drugs to reach distant organs at efficacious concentrations. Moreover, administration of a drug directly into the blood flow has the unique benefit of accessibility to a number of remote organs and tissues enabling eradication of micrometastases. With access to remote tissues and organs, a therapeutic luxury unavailable to other modes of treatment such as surgery or loco-regional drug delivery, intravenous administration has emerged to be the practical route of administering chemotherapeutics.

A pronounced increase in the concentration of the drug in the bloodstream also implies increased risk of normal cell and tissue drug exposure, thus, greatly limiting the cogency of the treatment. Thus, a major stumbling block in the employment of this ostensibly simple strategy is the off target effect of potentially cytotoxic chemotherapeutic drugs that persist in the bloodstream for prolonged time periods. In addition to serious side effects as result of exposure to normal cells and tissues, the actual procedure of intravenous administration of chemotherapeutics itself is accompanied by distinct challenges. The highly invasive procedure

uses major veins to distribute drugs effectively and can subject the patient to the perils of local complications resulting from the extravasation of drugs into proximate tissues [24].

Hydrophobic drugs are contrived into an intravenous formulation by utilizing surfactants (such as Cremophor EL) for enhancing their solubility in the saline fluid as well as blood stream [25]. Such surfactants have been known to stimulate hypersensitivity reactions at tissues close to the point of injection. Moreover, since many anticancer drugs dosages tenuously rely on the cell cycle and are schedule dependent, they require continuous administration; thereby eliminating the possibility of outpatient IV administrations. Although hospital admissions systemic administration is an invasive treatment modality, requiring hospital admissions, infusion supplies, surfactants and implantation of catheters in major blood vessels. These patent disadvantages reveal that intravenous administration is not only sophisticated but also cost prohibitive.

Other routes of administration such as oral or topical delivery are used only for a select number of cancers at specific stages of tumor growth [26]. Approaches such as topical (loco-regional) therapy rely on the premise of selective impingement of anticancer drugs to the diseased area eliminate the need for surgery or intravenous treatment while optimizing the benefits offered by both. However, this mode of application is excessively complex and requires highly skilled technical professionals [26].

Despite the obvious off-target effects of intravenous anticancer drug administration, one of the main reasons this potentially lethal strategy continues to dominate cancer treatment modalities is the lack of development in the sector of oral formulations for most hydrophobic cancer drugs [27]. Problems such as lack of availability of bioequivalent oral formulations for

most drugs, poor absorption of drugs across the epithelial layer and into the bloodstream, cytotoxic effects to the gastric inner lining and inconsistency in the tissue/plasma concentration of the drug transported across the GI tract beset the oral delivery of hydrophobic drugs [27]. Despite possessing the clear advantage of being the most convenient and comfortable mode of administration for cancer patients, the absence of innate mechanisms that can boost the ability of hydrophobic drugs to infiltrate the bloodstream after transit through the GI tract has been a fundamental impediment to the widespread applicability of this treatment modality.

3.2 LIVER CANCER

Liver cancer is defined as the uncontrolled, abnormal growth of hepatocytes in the liver. Owing to the ease of access that hepatocytes have to blood flow, liver cancer is typically diagnosed in its late metastatic stage, after the spread of cancerous cells to distant organs of the body through blood circulation. The causes of liver cancer are purported to be hepatitis B or C virus infection and even alcoholic cirrhosis. Liver cancer is the fifth most common cancer in the world and the third most common cancer-related cause of death with a five-year survival rate of less than 5% [28,29]. Advanced hepatocellular carcinoma (HCC), the metastatic form of the disease is known for the over-expression of p-glycoprotein and the resultant multidrug resistance [30-32]. Hence, liver cancer can serve as a multidrug resistant cancer model in addition to being a metastatic cancer model. Moreover, first pass metabolism in the liver is similar to intestinal first pass

metabolism owing to the presence of such efflux transporters [33]. As a result, drugs that can permeate through intestinal enterocytes may also be transported into hepatocytes. Liver cancer is an example disease model that can use an effective oral delivery system that can deliver the drug directly to the liver subsequent to intestinal absorption. Specifically, the nanoscale hydrogels will be used to enhance intestinal permeability of a chemotherapeutic drug, and the effect of the nanoscale hydrogel on modulation of P-gp will be studied.

In addition to chemotherapy, treatment for metastatic liver cancer involves dosage of Nexavar® (sorafenib), an orally active multikinase inhibitor that blocks the action of Vascular endothelial growth factor receptors (VEGFR) and hinders angiogenesis. However, sorafenib is used in conjunction with regular intravenous chemotherapy and is not an alternative to it. Recently, doxorubicin loaded poly(isohexyl cyanoacrylate) nanoparticles showed great promise against liver cancer. This nanoparticle formulation of doxorubicin, called as LivaTag® , is currently undergoing clinical trials and is administered intravenously.

Chapter 4: Oral Delivery of Hydrophobic Therapeutics

4.1 Classification of Hydrophobic Drugs

Classification standards proposed for orally delivered drugs declassified their common characteristics, enabling the pharmaceutical industry to develop strategies to deliver them more effectively. These classification systems afford a representation of the in vivo bioavailability of these drugs, based solely on the in vitro evaluation of properties such as solubility, permeability/metabolism and even dissolution rate. It is important to note that this classification system applies not just to pure drugs, but also to formulations/excipients containing the drug. Excipients/formulations that can reclassify the drug owing to their overall solubility/metabolic properties open up the opportunity to avoid in vivo bioequivalence studies. As a result, enhancement of solubility and permeability (or inhibition of efflux transporters) can be used as a guide to develop suitable oral drug delivery systems for chemotherapeutics. At present, the classification system and the related FDA policies are restricted to pure drugs or immediate release oral solid dosage forms (Excipient + active pharmaceutical ingredient). However, in the future, we foresee such a classification system and the FDA policies to serve as a basis in order to govern the outcomes of carriers delivering the drugs orally.

4.2 Hydrophobic Behavior Based on the Biopharmaceutics Classification System

The biopharmaceutics classification system (BCS) identifies aqueous solubility and intestinal permeability as the two fundamental parameters controlling drug absorption and

bioavailability following oral intake [1]. All drugs can be classified into four classes, namely: (i) Class I (high solubility, high permeability),

(ii) Class II (low solubility, high permeability),

(iii) Class III (high solubility, low permeability), and

(iv) Class IV (low solubility, low permeability).

Currently, the United States Food and Drug Administration (U.S. FDA) utilizes the BCS (which was developed by an academic, Prof. Gordon Amidon of the University of Michigan, and an FDA researcher, Dr. Vinod Shah during Amidon's sabbatical leave at FDA about twenty years ago) to waive *in vivo* bioequivalence studies and simplify regulatory pathways for BCS Class I drugs and/or solid dosage formulations incorporating the drug, if they display high solubility, and high intestinal permeability *in vitro* [2,3]. FDA's BCS guidance also recommends the use of Caco-2 cell monolayer transport studies to predict absorption of drugs in humans [4]. This oral drug delivery guidance system recognizes the intestinal jejunum to be the predominant site of drug absorption into the blood stream as it presents the largest surface area for permeation.

In addition to Class I drugs, Class II (low solubility, high permeability) drugs may stand a chance of getting waivers if their solid oral dosage is formulated to possess *in vivo* dissolution rates faster than the gastric emptying time or the GI transit time [2]. In general, Class II drugs have high permeability into intestinal enterocytes mainly due to high lipid solubility, which enhances partitioning of the drug into intestinal epithelial membranes and makes permeation through the lipophilic cell membranes rather easy.

4.3 HYDROPHOBIC BEHAVIOR BASED ON THE BIOPHARMACEUTICS DRUG DISPOSITION CLASSIFICATION SYSTEM

The Biopharmaceutics Drug Disposition Classification System (BDDCS) system developed by Wu and Benet further expands the concept of intestinal permeability to include metabolism in the intestine and liver [1]. Prof. Les Benet of the University of California at San Francisco was the original pioneer who analyzed drug transport in the GI tract but was omitted during the development of the BCS. He responded by providing a deep and thorough molecular and cellular evaluation of drug transport that corrected some of the shortcomings of the Amidon-Shah development. It is interesting that Benet and Amidon finally published an article together in 2008 [5]. In fact just this month, Benet and associates [6] published the most comprehensive analysis of drug transport in tissues and cells with a detailed understanding of the transport mechanisms and the various methods. Indeed, lipophilic compounds that permeate through the membrane of epithelial cells (in a transcellular manner) also exhibit affinity for metabolizing enzymes/efflux transporter related enzymes present in the intestine and liver [7,8].

BDDCS stipulates additional insight into mechanisms governing gastrointestinal permeability of drugs; mainly, efflux and absorptive transporters, metabolic routes of drug elimination, and the effect of concurrent food intake. This modified criteria for bioequivalence evaluation, thus, better envisages drug absorption, distribution, metabolism and excretion. Such classification gains unprecedented relevance in the case of cancer drugs, which display meager bioavailability subsequent to oral administration owing to efflux transporters.

BDDCS identifies and accounts for the fact that the more permeable lipophilic drugs are good substrates for cytochrome P450 enzymes (CYP) enzymes [9]. It notes that Class I high solubility/high permeability drugs avoid efflux transporters by saturating them, thereby ensuring

high bioavailability. *For hydrophobic cancer drugs, however, which belong to Class II and Class IV owing to their low solubility, the concentrations entering intestinal enterocytes is severely limited, making saturation of efflux transporters and enzymes impossible and leading to low bioavailability.* According to BDDCS, high-fat meals may enhance bioavailability of Class II and Class IV therapeutics. This increase in bioavailability is explained by inhibition of P-glycoprotein transporters after a high-fat meal and additional solubilization of the drugs in the intestinal lumen due to micelle formation [10].

4.4 GASTROINTESTINAL TRACT PHYSIOLOGY FOR ORAL DELIVERY

Drug delivery systems can enable protection of therapeutics from the highly variable, dynamic milieu encountered during transit through the GI tract [11]. The GI tract spans from the mouth to the large intestine, and is sub-divided into an "upper" region (comprising of the mouth, esophagus, and stomach) and a "lower" region (comprising of the small intestine- duodenum, jejunum, ileum, and, the large intestine- caecum, colon, rectum). Throughout its extent, the GI tract is covered with mucus-lined epithelial cells that tightly and selectively regulate the movement, retention and uptake of orally ingested therapeutics based on solubility, surface properties and intermolecular interactions [12-18].

In addition, the harsh environment of the GI tract has been programmed to safely and fastidiously absorb materials into the blood stream. For instance, the highly acidic setting of the stomach (~pH 2 in a state of fasting) and the bevy of enzymes (lipases, proteases, etc.) released to facilitate digestion can potentially degrade or deactivate the therapeutic function of most agents. Even doxorubicin, a relatively stable anthracycline, may be susceptible to degradation under gastric conditions, although the deleterious activity of doxorubicin against the gastric lining and encompassed enzymes is a bigger concern [19]. Also, retention of substances in the

stomach is subject to dietary and individual inconsistencies making transit times through the stomach highly variable [20]. Moreover, the gastric lining enclosing this acidic environment does not provide an opportunity for absorption into the bloodstream, precluding the stomach as a potential target for enhancing drug release into the bloodstream [21].

The highly digestive environment of the stomach is followed by the duodenum in the small intestine, wherein pancreatic enzymes and bile salts are released in a timely manner to further scavenge and effectively breakdown nutrients from foodstuffs. It is also important to note, that the pH of the GI tract lumen increases from a value of ~2 in the stomach to value of 5-6 in the duodenum and further to a value of 7 in the jejunum and ileum.

Conditions of drug stability are more favorable in the neutral pH of the small intestine than the acidic conditions of the stomach. However, the absorptive enterocytes of the small intestine are covered by a highly viscoelastic mucosal layer capable of clearing any drug released to the mucosal lumina through mucus clearance mechanisms [22]. Such clearance mechanisms are designed to proactively trap and efficiently expel any foreign bodies or particles that do not interact well with the mucosal layer [23]. Consequently, our drug carrier would be required to diffuse through the mucus layer or even adhere to it, in order to ensure retention of the drug at the release location.

Moreover, most hydrophobic anticancer drugs such as doxorubicin, paclitaxel, etc., are known to act as substrates for p-glycoprotein efflux pumps expressed on most intestinal epithelial cells [24]. Located on the apical side of the intestinal epithelium, these transporter proteins, selectively and actively transport certain molecules out of the intestinal epithelial cells [25,26]. Understandably, this natural detoxification mechanism primarily designed for purging

immunosuppressants, malevolently foils any advantage conferred by strategies to improve solubility and permeability of chemotherapeutics [27-29].

Despite the number of challenges faced by orally delivered therapeutics, the 8m long lower region of the GI tract does present 300-400 m^2 of surface area for drug absorption into the bloodstream owing to the presence of villi in the intestinal region [30]. Increasing the retention time of the drug in this region can facilitate drug absorption into systemic circulation. Improved retention of entities in the intestinal region can, in turn, be accomplished by encouraging interactions between the drug carrier and the mucus layer secreted by goblet cells. As a result, there has been increased focus on technologies that develop mucoadhesive carriers that can release therapeutics specifically in the intestinal region.

4.5 NANOTECHNOLOGY FOR ORAL DELIVERY OF HYDROPHOBIC DRUGS

4.5.1 Use of surfactants

Low molecular weight surfactants such as polyoxyethylated castor oil (Cremophor EL ~1200-1600 Da) are commonly used to facilitate the solubilization of hydrophobic drugs in the bloodstream during intravenous administration. On similar lines, Cremophor EL formulations of paclitaxel (a mitotic drug used to treat breast and lung cancers) called Paxoral™ have been tested in clinical studies to determine their efficacy at delivering the poorly water soluble payload orally [32]. However, severe toxicity of Cremophor EL at early stages of the transit through the GI tract (mouth and esophagus) has deterred widespread acceptance of surfactant-based formulations in oral cancer treatments. Moreover, surfactant-based micelles displayed premature release of paclitaxel in the upper GI tract posing a significant risk of cell and tissue damage to

the gastric lining [32,33].

4.5.2 Drug Nanocrystal Formation

Formulating nanocrystals of pure lipophilic drugs is a rapidly emerging pharmaceutical processing technology to greatly improve their surface area and, in turn, lead to increased dissolution velocity and saturation solubility in the intestinal lumen [34,35]. Also, these nanocrystals have demonstrated increased bioadhesion to the intestinal mucosal wall, thereby increasing retention time of the drug and maintaining high enough local drug concentrations to sustain a concentration gradient across the wall [36]. A combination of these factors translates into improved bioavailability of the drugs in the bloodstream.

Nanocrystals can be produced by precipitation and aggregation of drug solutions ("bottom up") or by reducing the particle size down to the nanoscale ("top down"). Nanocrystals can be precipitated out of solution by adding the drug solution to an organic solvent [37], although the use of organic solvents is considered discouraging. "Top down" approaches physically break down large particles into nanocrystals by milling and high-pressure homogenization, and are more amenable to scale-up for large scale processing.

Despite these advantages promoting widespread pharmaceutical use, it is important to note that this approach uses surfactants such as Tween 80, Tween 20, to stabilize the nanocrystals. The use of such hypersensitivity inducing surfactants in addition to the enhanced exposure of pure drug to the gastric lining can be a major cause of concern, especially for oral delivery of cytotoxic chemotherapeutics [32]. Furthermore, high bioavailability of such drugs implies higher systemic exposure to possibly toxic concentrations of anticancer drugs. Active targeting or passive targeting using the enhanced permeation and retention effect (EPR) to specific diseased organs can address this issue.

4.5.3 Beta Casein Nanoparticles

Synthetic or natural materials that can acquire an amphiphilic structure or can be combined with other components to possess an inner hydrophobic core have been a major focus of study. Beta-casein is one particular material that is interesting from the standpoint of oral delivery of hydrophobic drugs. A protein found in bovine milk, beta casein can be fashioned into forming a self-assembled micellar structure under environmental conditions contingent upon the pH, temperature, and ionic strength [38,39]. Previous studies have demonstrated the ability of beta-casein to preferentially associate to lipid-soluble entities such as vitamin D_3, vitamin A and sucrose esters by way of van der Waals interactions [40-42]. Effective delivery of a drug involves interplay of factors such as rate of release as well as the stability of the molecular association between the carrier and the entrapped drugs, so as to avoid premature release. It is of utmost importance to retain potentially cytotoxic drugs until they reach the desired site of release suggesting the need to design systems that can accommodate and release hydrophobic drugs in a stable and timely manner. Thermodynamics of the binding between beta-casein and lipophilic molecules and the stability of the micelles in aqueous has previously been verified [33], endorsing the use of beta-casein based micelles for such applications.

Shapira et al. [42] have investigated the utility of beta-casein micellar nanoparticles as enzymatically degradable drug delivery systems that can deliver hydrophobic drugs such as mitoxantrone for the treatment of gastric cancer. Beta-casein nanoparticles in the size range of 100-300 nm were formed by continuous addition of hydrophobic drug molecule to an aqueous solution of beta-casein in Phosphate Buffered Saline (PBS) at concentrations above and below the critical micellization concentration (CMC). Intermolecular hydrophobic interactions between the beta-casein molecules and amongst beta-casein-hydrophobic drug molecules are responsible

for entrapment of drug within the hydrophobic micellar core. Blocking contact amid the hydrophobic agent and the external hydrophilic environment in such a manner holds promise for solubilization of many cancer drugs. Versatility of beta-casein micelles in solubilizing a number of hydrophobic cancer drugs possessing diverse functional groups has also been demonstrated [43]. Once formed, beta casein nanoparticles retained the drug until they were subjected to degradative enzymatic conditions similar to the gastric environment indicating their utility for treatment of gastric malignancies. Under simulated gastric conditions, about 85-90% of the drug was released within 10-20 min of incubation [44], suggesting the prevalence of fast release kinetics. Tuning degradation rate by coating pure beta-casein nanoparticles with dietary fibers can facilitate targeting to other organs down the GI tract such as the colon. Despite great promise, the use of beta casein is restricted to gastric tumors mainly due to their degradability in the harsh enzymatic environment of the stomach.

4.5.4 Chitosan-based oral delivery systems

Chitosan is a naturally derived macromolecule that can be leveraged for improving drug solubility and loading while fulfilling the imperative requirement of biocompatibility. A rich body of work has focused on synthetically enhancing the properties of chitosan to tailor its ability to target specific cells or release drugs in a site-specific and controlled manner [45]. Two important parameters that can be controlled to modify the properties of chitosan particles are the molecular weight and the degree of deacetylation [46]. In addition, chitosan has a number of amine, hydroxyl and carboxylic groups that can be chemically modified to vary its physicochemical properties and influence drug deliverability.

Chitosan nanoparticles can be covalently crosslinked to cancer drugs, superparamagnetic oxides by using multifunctional agents such as glutaraldehyde, polyethylene glycol (PEG)

dicarboxylic acid, and acrylate-based molecules [47,48]. Free radical polymerization has been used to create chitosan hydrogel nanoparticles with distinct physical properties and achieve consistency in molecular weight distribution and particle size. De Moura et al. [49] achieved deliberate conformity in random polymerization by using equivalent amounts of poly(methyl methacrylate) that could match up to the amine functionality existing in chitosan.

Similarly, thiolated chitosan was used to increase solubility of hydrophobic polyalkylcyanoacrylates (PACA) by using a random free radical emulsion polymerization technique that led to the formation of hydrophobic core characterized by PACA and hydrophilic shell of chitosan [50]. The hydrophobic shell can possibly entrap hydrophobic drugs while the presence of thiolated chitosan can improve therapeutic level of the drugs owing to increased mucoadhesion.

A crucial touchstone for prolific oral delivery in the small intestine is the mucoadhesion of the drug carrier. Hydroxyl and amine groups in the glycoproteins predominant in intestinal mucus can establish strong hydrogen bonds with functional groups of chitosan leading to significantly higher retention times of the nanoparticles within the GI tract [23,51]. Improved mucoadhesive properties typically correlate with higher bioavailability of drugs in the bloodstream as the drug gets longer time periods to diffuse across the GI tract. Significantly improved mucoadhesion due to increased charge density in the case of chitosan, can however, also be a cause of concern since a longer contact time with epithelial cells can be potentially deleterious [52].

4.5.5 Dendrimers

Dendrimers are another important class of polymeric carriers that can solubilize hydrophobic anticancer drugs and enable transport of the covalently linked drug across the

intestinal epithelium. Chemically, dendrimers are nanoscale macromolecules possessing a unique functional architecture consisting of branches that can attach to drugs or targeting moieties for improved therapy. The layers of polymeric branches former after every generation form an external barrier that can retain the drugs captured within the inner core [52-56]. Polyamido amine (PAMAM) dendrimers have been reported to show superior transport properties across the mucosal GI tract into the bloodstream [57-59] and significantly improved biodistribution subsequent to intestinal absorption. These synthetic are able to permeate through intestinal barriers through passive transcellular and paracellular transport owing to sizes in the range of 1-5 nm [60-62].

Previous research work utilizing generation 4 (G4) PAMAM dendrimers for oral drug delivery exposed their instability in harsh acidic environments of pH 5 and were even shown to be toxic to intestinal epithelial cells restricting the concentrations of the dendrimer (and consequently, the drug too) that could be used [63]. Slow release kinetics, with only 40% of the drug releasing within 24 hours of incubation at a pH of 7.4, indicated a further barrier to their use [64]. More recently, Goldberg and coworkers [65] have conjugated the extremely lipophilic and cytotoxic campothecin to PAMAM dendrimers to increase solubility and reduce toxicity of DNA topoisomerase inhibitor, 7-ethyl-10-hydroxy campothecin. Modification in the number of conjugated molecules resulted in moderation of the surface charge on these dendrimers.

Previous studies have shown a tangible impact of surface charge of the dendrimers on the intestinal absorption of the polymer-drug conjugate in addition to the opening of tight junctions and the mechanism of transport [66]. It is hypothesized that a reduction in the surface charge of the dendrimer, typically by PEGylation, followed by an increase in the hydrophobicity of the polymer, leads to a decrease in the opening of tight junctions, and restricts transport to a

transcellular mechanism. Transport studies completed by Goldberg and associates [65] were able to demonstrate a notable increase in the uptake of the dendrimer-drug conjugate as opposed to the drug alone. This increase in uptake across the intestinal epithelium suggests synergy between transcellular, receptor mediated endocytosis and paracellular, diffusive mechanisms to facilitate transport of these generation 3.5 dendrimers across the intestine.

Thus, this class of polymers shows great promise for oral delivery although the need to covalently conjugate drugs to the polymer may chemically restrict certain drugs to be used in such formulations. The lack of any *in vivo* studies may limit discussions regarding any immune response that may be elicited by these polymers. Moreover, no insight was provided for only 50-60% release in the "simulated" target organ environment (liver) by enzymatic cleavage of the covalent bond between the drug and the polymer. Reliance on enzymatic cleavage and the slow release kinetics could potentially restrict practical application of these nanoscale delivery systems despite their remarkable ability to travel across intestinal barriers.

4.5.6 Self-nanoemulsifying drug delivery systems

One way of improving the prospects of oral delivery of hydrophobic drugs is the increase in the dissolution rate of the drug. Self-nanoemulsifying drug delivery system (SNEDDS) is an emulsification technology that increases the surface area available for a given volume of drug solution to diffuse out, thereby augmenting the dissolution rate of such pharmaceutics. Such systems are capsules fabricated using biopolymers such as gelatin and hydroxypropylmethyl cellulose (HPMC) and incorporate a dry mixture of oil and surfactant within. Upon absorption of gastric fluids, a stable oil-in-water emulsion results owing to stabilization by surfactants present in the encompassing capsule. These 150-200 nm nanoemulsion colloids have demonstrated

significantly high bioavailability of lipophilic drugs such as simsvastatin, atorvaststin, ezetimibe and exetimibe [67,68].

Hydrophobic molecules used in these devices are typically glycerides such as oleic acid, caprylic acid, glycerol monooleate, which are known to facilitate association with lipophilic drugs, enhance membrane permeation and even intestinal lymphatic transport [67,68]. Components such as these address metabolism-related issues impairing intestinal transport of lipophilic drugs by inhibiting gastric enzymes and hindering activity of the efflux transporter cytochrome p450. This increases overall permeability of the drug nanoemulsion across the intestine and justifies the subsequent high bioavailability of the drug.

These systems have, however, drawn criticism for their use of hypersensitivity inducing surfactants in their formulations. Surfactants such as Tween 80, Cremophor EL, and poloxamer 188 are known to induce severe hypersensitivity reactions when in contact with tissues [69-71]. Moreover, these nanoemulsions show significantly higher uptake in lymphoid tissues, suggesting their use may be restricted only to immune related diseases or the HIV/herpes-related cancers affecting the immune system such as Kaposi's sarcoma.

4.6 REFERENCES

[1] Amidon GL, Lennernas H, Shah VP, Crison JR. A theoretical basis for a biopharmaceutic durg classification – The correlation of in-vitro drug product dissolution and in-vivo bioavailability. Pharmaceutical Research 1995;12:413-20.

[2] U.S. Food and Drug Administration, Center for Drug Evaluation and Research. Guidance for Industry: Waiver of In Vivo Bioavailability and Bioequivalence Studies for Immediate-Release Solid Oral Dosage Forms Based on a Biopharmaceutics Classification System. 2000 August. Available from: http://www.

fda.gov/downloads/Drugs/GuidanceComplianceRegulatoryInformation/Guidances/ucm070246.pdf.

[3] Committee for Medicinal Products for Human Use, European Medicines Agency. Guideline on the Investigation of Bioequivalence. 2010 January 20. Available from: http://www.ema.europa.eu/docs/en_GB/document_library/Scientific_guideline/2010/01/WC500070039.pdf.

[4] Yan Y, Faustino PJ, Volpe DA, Lyon RC, Yu LX. Biopharmaceutics classification of selected beta-blockers: Solubility and permeability class membership. Mol Pharm. 2007;4:608–14.

[5] Benet LZ, Amidon GL, Barends DM, Lennernas H, Polli JE, Shah VP, et al. The use of BDDCS in classifying the permeability of marketed drugs. Pharmaceutical Research 2008;25:483-8.

[6] Estudante M, Morais JG, Soveral G, Benet LZ Intestinal drug transporters: An overview. Adv. Drug Deliv. Rev. 2012; DOI: 10.106/j.addr.2012.09.042.

[7] Takagi T, Ramachandran C, Bermejo M, Yamashita S, Yu LX, Amidon GL. A provisional biopharmaceutical classification of the top 200 oral drug products in the United States, Great Britain, Spain, and Japan. Molecular Pharmaceutics 2006;3:631-43.

[8] Chen M-L, Yu L. The Use of Drug Metabolism for Prediction of Intestinal Permeability. Molecular Pharmaceutics 2009;6:74-81.

[9] Smith DA. Design of drugs through a consideration of drug-metabolism and pharmacokinetics. European Journal of Drug Metabolism and Pharmacokinetics 1994;19:193-9.

[10] Custodio JM, Wu C-Y, Benet LZ. Predicting drug disposition, absorption/elimination/transporter interplay and the role of food on drug absorption. Advanced Drug Delivery Reviews 2008;60:717-33.

[11] Ruddy K, Mayer E, Partridge A. Patient adherence and persistence with oral anticancer treatment. CA - A Cancer Journal for Clinicians 2009;59:55–66.

[12] Zhang YC, Benet LZ. The gut as a barrier to drug absorption- Combined role of cytochrome P450 3A and P-glycoprotein. Clinical Pharmacokinetics 2001;40:159–68.

[13] Nusrat A, Turner JR, Madara JL. Molecular physiology and pathophysiology of tight junctions IV. Regulation of tight junctions by extracellular stimuli: nutrients, cytokines and immune cells. American Journal of Physiology - Gastrointestinal and Liver Physiology 2000;279:G851–7.

[14] McKay DM, Bienenstock J. The interaction between mast-cells and nerves in the gastrointestinal-tract. Immunology Today 1994;15:533–8.

[15] Montgomery RK, Mulberg AE, Grand RJ. Development of the human gastrointestinal tract: twenty years of progress. Gastroenterology 1999;116:702–31.

[16] Cheroutre H. Starting at the beginning: new perspectives on the biology of mucosal T cells. Annual Review of Immunology 2004;22:217–46.

[17] Thomsen L, Robinson TL, Lee JCF, et al. Interstitial cells of Cajal generate a rhythmic pacemaker current. Nature Medicine 1998;4:848–51.

[18] Maldonado-Contreras AL, McCormick BA. Intestinal epithelial cells and their role in innate mucosal immunity. Cell and Tissue Research 2011;343:5–12.

[19] Robison TW, Giri SN. Effects of chromic administration of doxorubicin on heart phospholipase-A2 activity and in vitro synthesis and degradation of prostaglandins in rats. Prostaglandins Leukotrienes and Medicine 1987;26:59-74.

[20] Prinderre P, Sauzet C, Fuxen C. Advances in gastro retentive drug-delivery systems. Expert Opinion on Drug Delivery 2011;8:1189-203.

[21] Brayden DJ, Mrsny RJ. Oral peptide delivery: prioritizing the leading technologies. Therapeutic delivery 2011;2:1567-73.

[22] Tang BC, Dawson M, Lai SK, Wang Y-Y, Suk JS, Yang M, et al. Biodegradable polymer nanoparticles that rapidly penetrate the human mucus barrier. Proceedings of the National Academy of Sciences of the United States of America 2009;106:19268-73.

[23] Lai SK, Wang Y-Y, Hanes J. Mucus-penetrating nanoparticles for drug and gene delivery to mucosal tissues. Advanced Drug Delivery Reviews 2009;61:158-71.

[24] Werle M. Natural and synthetic polymers as inhibitors of drug efflux pumps. Pharmaceutical Research 2008;25:500-11.

[25] Thiebaut F, Tsuruo T, Hamada H, Gottesman MM, Pastan I, Willingham MC. Cellular-localization of the multidrug resistance gene-product p-glycoprotein in normal human tissues. Proceedings of the National Academy of Sciences of the United States of America 1987;84:7735-8.

[26] Cordoncardo C, Obrien JP, Boccia J, Casals D, Bertino JR, Melamed MR. Expression of the multidrug resistance gene-product (p-glycoprotein) in human normal and tumor-tissues. Journal of Histochemistry & Cytochemistry 1990;38:1277-87.

[27] Varma MVS, Panchagnula R. Enhanced oral paclitaxel absorption with vitamin E-TPGS: Effect on solubility and permeability in vitro, in situ and in vivo. European Journal of Pharmaceutical Sciences 2005;25:445-53.

[28] Aungst BJ. Intestinal permeation enhancers. Journal of Pharmaceutical Sciences 2000;89:429-42.

[29] Woo JS, Lee CH, Shim CK, Hwang SJ. Enhanced oral bioavailability of paclitaxel by coadministration of the P-glycoprotein inhibitor KR30031. Pharmaceutical Research 2003;20:24-30.

[30] Keita AV, Soderholm JD, Ericson AC. Stress-induced barrier disruption of rat follicle-associated epithelium involves corticotropin-releasing hormone, acetylcholine, substance P, and mast cells. Neurogastroenterology and motility : the official journal of the European Gastrointestinal Motility Society 2010;22:770-8, e221-2.

[31] Takano M, Yumoto R, Murakami T. Expression and function of efflux drug transporters in the intestine. Pharmacology & Therapeutics 2006;109:137-61.

[32] Gelderblom H, Verweij J, Nooter K, Sparreboom A. Cremophor EL: the drawbacks and advantages of vehicle selection for drug formulation. European Journal of Cancer 2001;37:1590-8.

[33] R. Zana, Dynamics in micellar solutions of amphiphilic block copolymers, in: A.T. Hubbard (Ed.), Dynamics of Surfactant Self-Assemblies, CRC Press, Taylor & Francis Group, New York, 2005; 161–231.

[34] Hintz RJ, Johnson KC. The effect of particle-size distribution on dissolution rate and oral absorption. International Journal of Pharmaceutics 1989;51:9-17.

[35] Bohm BHL, Muller RH. Lab-scale production unit design for nanosuspensions of sparingly soluble cytotoxic drugs. Pharmaceutical Science & Technology Today 1999;2:336-9.

[36] Ponchel G, Montisci MJ, Dembri A, Durrer C, Duchene D. Mucoadhesion of colloidal particulate systems in the gastro-intestinal tract. European Journal of Pharmaceutics and Biopharmaceutics 1997;44:25-31.

[37] Gao L, Zhang D, Chen M. Drug nanocrystals for the formulation of poorly soluble drugs and its application as a potential drug delivery system. Journal of Nanoparticle Research 2008;10:845-62.

[38] Livney YD, Schwan AL, Dalgleish DG. A study of beta-casein tertiary structure by intramolecular crosslinking and mass spectrometry. Journal of Dairy Science 2004;87:3638-47.

[39] Swaisgood HE. Chemistry of the caseins. In: Fox PF, and McSweeney PLH, editors. Advanced dairy chemistry, volume 1, proteins, part A. New York: Kluwer Academic/Plenum Publishers 2003; 139–201.

[40] Forrest SA, Yada RY, Rousseau D. Interactions of vitamin D-3 with bovine beta-lactoglobulin A and beta-casein. Journal of Agricultural and Food Chemistry 2005;53:8003-9.

[41] Lietaer E, Poiffait A, Adrian J. Studies on the interaction between casein and vitamin A. Lebensmittel-Wissenschaft and Technologie 1991;24:39-45.

[42] Clark DC, Wilde PJ, Wilson DR, Wustneck R. The interaction of sucrose esters with beta-lactoglobulin and beta-casein from bovine milk. Food Hydrocolloids 1992;6:173-86

[43] Shapira A, Assaraf YG, Livney YD. Beta-casein nanovehicles for oral delivery of chemotherapeutic drugs'. Nanomedicine-Nanotechnology Biology and Medicine 2010;6:119-26.

[44] Shapira A, Assaraf YG, Epstein D, Livney YD. Beta-casein Nanoparticles as an Oral Delivery System for Chemotherapeutic Drugs: Impact of Drug Structure and Properties on Co-assembly. Pharmaceutical Research 2010;27:2175-86.

[45] Shapira A, Davidson I, Avni N, Assaraf YG, Livney YD. beta-Casein nanoparticle-based oral drug delivery system for potential treatment of gastric carcinoma: Stability, target-activated release and cytotoxicity. European Journal of Pharmaceutics and Biopharmaceutics 2012;80:298-305.

[46] Wang JJ, Zeng ZW, Xiao RZ, Xie T, Zhou GL, Zhan XR, et al. Recent advances of chitosan nanoparticles as drug carriers. International Journal of Nanomedicine 2011;6:765-74.

[47] Suknuntha K, Tantishaiyakul V, Worakul N, Taweepreda W. Characterization of muco- and bioadhesive properties of chitosan, PVP, and chitosan/PVP blends and release of amoxicillin from alginate beads coated with chitosan/PVP. Drug Development and Industrial Pharmacy 2011;37:408-18.

[48] Ohya Y, Shiratani M, Kobayashi H, Ouchi T. Release behavior of 5-fluorouracil from chitosan-gel nanospheres immobilizing 5-fluorouracil coated with polysaccharides and their cell-specific cytotoxicity. Journal of Macromolecular Science-Pure and Applied Chemistry 1994;A31:629-42.

[49] Qu J, Liu G, Wang Y, Hong R. Preparation of Fe3O4-chitosan nanoparticles used for hyperthermia. Advanced Powder Technology 2010;21:461-7.

[50] de Moura MR, Aouada FA, Mattoso LHC. Preparation of chitosan nanoparticles using methacrylic acid. Journal of Colloid and Interface Science 2008;321:477-83.

[51] Bravo-Osuna I, Vauthier C, Farabollini A, Palmieri GF, Ponchel G. Mucoadhesion mechanism of chitosan and thiolated chitosan-poly(isobutyl cyanoacrylate) core-shell nanoparticles. Biomaterials 2007;28:2233-43.

[52] Dudhani AR, Kosaraju SL. Bioadhesive chitosan nanoparticles: Preparation and characterization. Carbohydrate Polymers 2010;81:243-51.

[53] Kean T, Thanou M. Biodegradation, biodistribution and toxicity of chitosan. Advanced Drug Delivery Reviews 2010;62:3-11.

[54] Milhem OM, Myles C, McKeown NB, Attwood D, D'Emanuele A. Polyamidoamine Starburst (R) dendrimers as solubility enhancers. International Journal of Pharmaceutics 2000;197:239-41.

[55] Tomalia DA, Reyna LA, Svenson S. Dendrimers as multi-purpose nanodevices for oncology drug delivery and diagnostic imaging. Biochemical Society Transactions 2007;35:61-7.

[56] Duncan R, Izzo L. Dendrimer biocompatibility and toxicity. Advanced Drug Delivery Reviews 2005;57:2215-37.

[57] Lee CC, MacKay JA, Frechet JMJ, Szoka FC. Designing dendrimers for biological applications. Nature Biotechnology 2005;23:1517-26.

[58] Wiwattanapatapee R, Carreno-Gomez B, Malik N, Duncan R. Anionic PAMAM dendrimers rapidly cross adult rat intestine in vitro: A potential oral delivery system? Pharmaceutical Research 2000;17:991-8.

[59] D'Emanuele A, Jevprasesphant R, Penny J, Attwood D. The use of a dendrimer-propranolol prodrug to bypass efflux transporters and enhance oral bioavailability. Journal of Controlled Release 2004;95:447-53.

[60] Sweet DM, Kolhatkar RB, Ray A, Swaan P, Ghandehari H. Transepithelial transport of PEGylated anionic poly(amidoamine) dendrimers: Implications for oral drug delivery. Journal of Controlled Release 2009;138:78-85.

[61] El-Sayed M, Rhodes CA, Ginski M, Ghandehari H. Transport mechanism(s) of poly (amidoamine) dendrimers across Caco-2 cell monolayers. International Journal of Pharmaceutics 2003;265:151-7.

[62] Kitchens KM, Kolhatkar IB, Swaan PW, Ghandehari H. Endocytosis inhibitors prevent poly(amidoamine) dendrimer internalization and permeability across Ceco-2 cells. Molecular Pharmaceutics 2008;5:364-9.

[63] Jevprasesphant R, Penny J, Attwood D, D'Emanuele A. Transport of dendrimer nanocarriers through epithelial cells via the transcellular route. Journal of Controlled Release 2004;97:259-67.

[64] Kitchens KM, El-Sayed MEH, Ghandehari H. Transepithelial and endothelial transport of poly (amidoamine) dendrimers. Advanced Drug Delivery Reviews 2005;57:2163-76.

[65] Kolhatkar RB, Swaan P, Ghandehari H. Potential oral delivery of 7-Ethyl-10-hydroxy-camptothecin (SN-38) using poly(amidoamine) dendrimers. Pharmaceutical Research 2008;25:1723-9.

[66] Goldberg DS, Vijayalakshmi N, Swaan PW, Ghandehari H. G3.5 PAMAM dendrimers enhance transepithelial transport of SN38 while minimizing gastrointestinal toxicity. Journal of Controlled Release 2011;150:318-25.

[67] Sweet DM, Kolhatkar RB, Ray A, Swaan P, Ghandehari H. Transepithelial transport of PEGylated anionic poly(amidoamine) dendrimers: Implications for oral drug delivery. Journal of Controlled Release 2009;138:78-85.

[68] Dixit RP, Nagarsenker MS. Self-nanoemulsifying granules of ezetimibe: Design, optimization and evaluation. European Journal of Pharmaceutical Sciences 2008;35:183-92.

[69] Dabhi MR, Limbani MD, Sheth NR. Preparation and In Vivo Evaluation of Self-Nanoemulsifying Drug Delivery System (SNEDDS) Containing Ezetimibe. Current Nanoscience 2011;7:616-27.

[70] Date AA, Desai N, Dixit R, Nagarsenker M. Self-nanoemulsifying drug delivery systems: formulation insights, applications and advances. Nanomedicine 2010;5:1595-616.

[71] Wulff-Perez M, Galvez-Ruiz MJ, de Vicente J, Martin-Rodriguez A. Delaying lipid digestion through steric surfactant Pluronic F68: A novel in vitro approach. Food Research International 2010;43:1629-33.

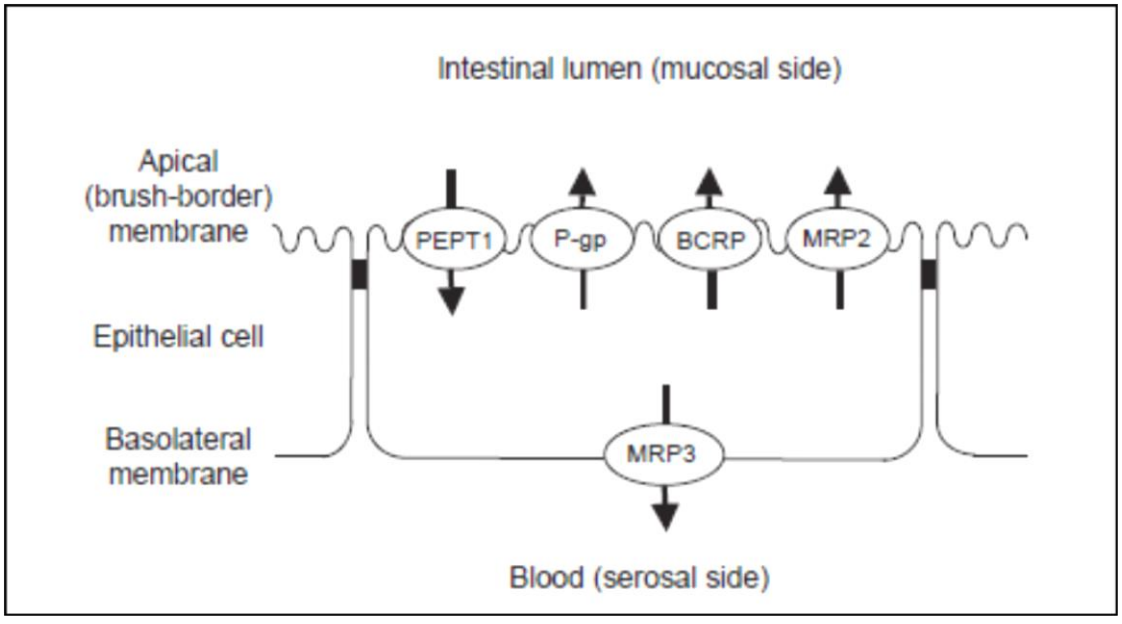

Figure 1: Efflux and uptake transporters present on the apical and basolateral sides of the small intestine. Adapted from [31].

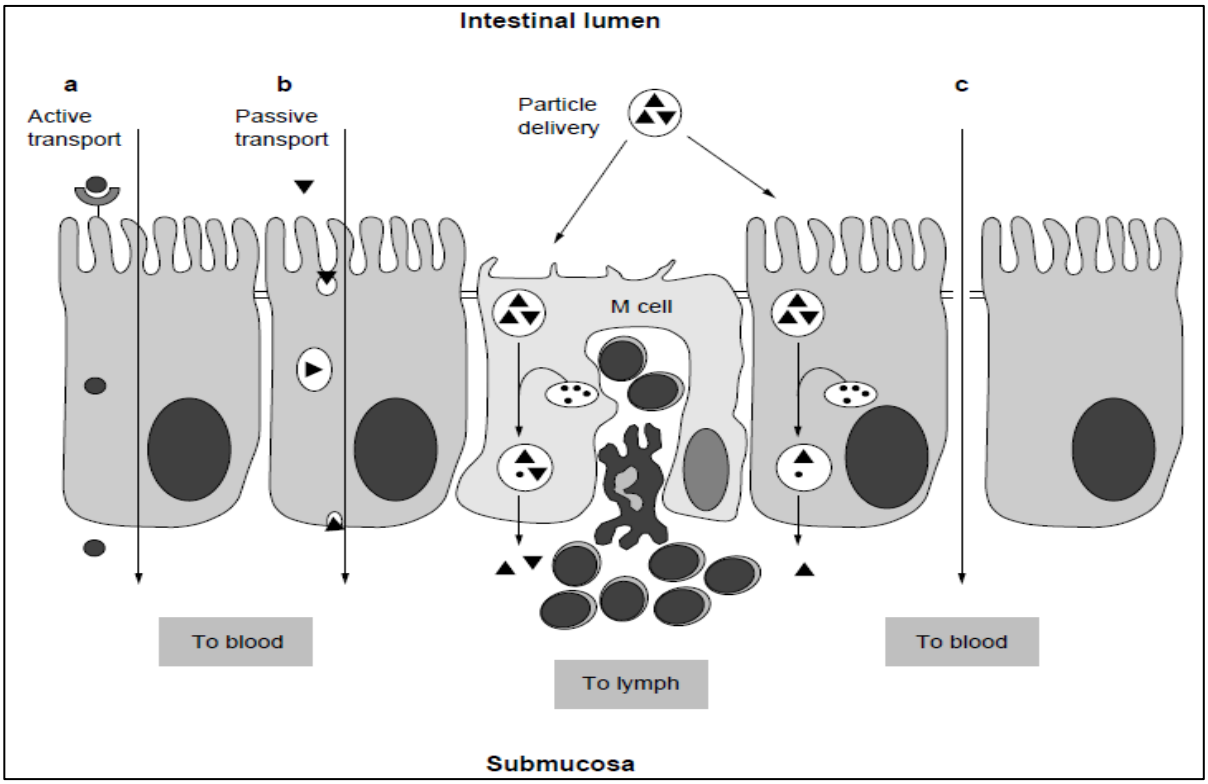

Figure 2: Schematic representation of pathways for intestinal transport: (a) transcellular active transport, (b) transcellular passive transport, and (c) paracellular transport through tight junctions. Adapted from [7].

Chapter 5: Delivery of Chemotherapeutics using Nanotechnology

5.1 INTRODUCTION

It is well understood that the size, charge and surface properties of nanomaterials will determine their physiological fate. In order to effectively design nanomaterials for cancer therapy, these parameters must be tailored to traverse the restrictions imposed by human and cancer physiology. While chemical synthesis and facile design procedures are widely reviewed, the precise effect of modulating these three key parameters to direct their biological fate in the context of cancer treatment is refreshed regularly. These properties can chemically engineered nanomaterials to increase likelihood of therapeutic success.

Rational design and engineering of nanomaterials requires elucidation of verifiable design criteria, which in the case of nanomaterial product development have historically been their size, charge and surface properties. The diverse physiological barriers presented by primary tumors, organs affected by metastasis, and tumor interstitium prevent universal design considerations. As such, nanoscale therapeutics for cancer therapy face unique challenges in that they must integrate features to propagate across diverse physiological barriers and cater to changing disease states, expression levels of molecular targets, and vasculature, in a scalable and economical manner. Here is a review of recent work in the development of nanoscale therapeutics for cancer therapy with a specific focus on delivery to primary, metastatic, and multi-drug resistant cancers.

Literature is abound in research highlighting the successful implementation of engineered nanomaterials for cancer treatment, despite modest overall survival benefits. Marginal improvements arising from nanotechnological solutions, have raised concerns emphasizes the need to reflect back on the chemical and molecular design of materials led by recent reveals of

primary tumor and metastatic cancer physiology. Elegance in design criteria that may appear to simplify nanomaterial product development, has been offset by the challenges that are concomitant with a diverse target range of physiochemical barriers presented in myriad cancers, organs, and cell lines. Hence, here are some of the recent efforts to understand the impact of chemical and molecular design on the ultimate biological fate of engineered nanomaterials to enable engineers to develop more potent and clinically efficacious nanoscale formulations. It is important to note that just as one therapeutic may not be effective against all cancers; one nanoparticle design may not be suitable to treat all cancer types. Chemical and molecular engineering of nanoformulations should reflect on and learn from reveals in the knowledge of tumor cell, tissue and microenvironment related biochemical features and entities.

5.2. CURRENT STANDARD OF CARE

Nanotechnology has been chiefly leveraged to compliment chemotherapeutic treatment that ensues surgical resection of tumor and/or radiotherapy. The likelihood of two therapeutic events is facilitated by nanotechnology- passively funneling to disease site/ targeting (based on size/epr) and active targeting (physiological goals based on organ-specific, cellular, or subcellular targets). Identification of molecular targets has advanced the development of nanomedicine design through established drugs/more potent drugs/peptides/RNA molecules/biologics). Newer nanoparticles are being developed and investigated to Emerging research in nanotechnology aims at developing novel platforms that can improve the efficacy of such potent drugs/biologics by specifically transporting them to the site of action. NCI intitiative recently highlighted some of the progress that has been made in conjunction with associated researchers. Recent approaches in nanotechnology rely on passive targeting to accumulate within the tumor area, and exploit active targeting of molecular targets to achieve drug delivery to the

site of action. Successful formulations will need to sustain relevant circulation concentration, navigate to the tumor tissue area based on physicochemical properties, and finally effect delivery under specific conditions.

Reaching the tumor tissue subsequent to circulation in the blood, is largely a passive process unless the nanoparticle is designed to be targeted to the specific tumor vasculature. This process is dependent chiefly on the size of the nanoparticles so that it avoids clearance prior to accumulation within tumor tissue by enhanced permeation and retention effect (EPR). It is also possible to elongate circulation time by minimizing interaction of the formulation with blood constituents. This can be done reducing surface charge by using PEG tethers thereby avoiding opsonization. Active targeting is of immense relevance once the nanoparticle has extravasated into tumor tissue. Such targeting is based on the principal that extravsated nanoparticles can be induced into anti-cancer action upon activation by tumor microenvironment or external triggering.

One unique challenge is manufacturing nanoparticle platforms that can integrate features to propagate successfully through the diverse physiological barriers to cater to changing disease states, expression levels of molecular targets, and vasculature, in a scalable and economical manner.

5.2. NANOMATERIALS USED IN CANCER THERAPY

Nanomaterials for use in therapeutic applications must be designed to navigate the challenges presented by cancer physiology. The most commonly employed nanomaterials in research for cancer therapy are polymers, inorganic nanoparticles such as gold, iron oxide and mesoporous silica, and carbon based materials such as carbon nanotubes or graphene. Polymer nanoparticles have been researched extensively for various drug delivery applications and have

well characterized synthesis methods including solvent evaporation, nanoprecipitation, emulsion polymerization, and controlled/living radical polymerizations as shown in Fig. 1.[1],[2] Both degradable and non-degradable nanoparticles have been utilized for cancer therapies, with the most commonly employed polymeric material being PLGA due to relatively non-toxic degradation products and FDA approval [3, 4]. Gold and iron oxide nanoparticles have been of great interest as nanomaterials for cancer therapy because of their ability to be remotely heated by IR light and magnetic fields respectively [5, 6]. In the past decade, mesoporous silica based nanotherapeutics for cancer have increased in popularity because of the ability to tailor surface functionality and load drugs into pores [7-9]. Carbon based materials such as carbon nanotubes and graphene have also emerged as promising candidates for cancer therapy due to high surface area and ability to be used in photothermal therapies [10, 11].

5.3.1 Size

Based upon current knowledge of cancer physiology, nanomaterials in the range of 100-200nm have the highest chance of reaching cancerous tissues through passive targeting methods. However, many variables can influence the ability of a drug delivery system to reach these tumor cells. A single step assembly of PLGA-lecithin-PEG nanoparticles loaded with doxorubicin and indocyanine green for a chemotherapy photothermal combination therapy for cancer by a single step sonication method was recently reported by Zheng et al. Loaded particles had a hydrodynamic radius 97.6nm and demonstrated a synergistic effect compared to monotherapies in inducing apoptosis in both doxorubicin sensitive and doxorubicin resistant MCF-7 cell lines in vitro while suppressing tumor growth in vivo [12]. Mitragotri and colleagues recently demonstrated that rod shaped nanoparticles conjugated with the targeting antibody trastuzumab demonstrated higher specific uptake and decreased nonspecific uptake in a series of breast cancer

cell lines in comparison to spherical nanoparticles [13]. In addition, the antibody conjugated rod-shaped nanoparticles demonstrated an enhanced ability to inhibit growth BT-474 breast cancer cells in-vitro.

5.3.2 Charge

The charge on polymeric nanomaterials is a result of functional groups incorporated during polymerization. Cationic polymers result from the incorporation of amine containing monomers, while anionic polymers typically result from acid containing monomers. New advances controlled/living radical polymerization by Matyjaszewski and colleagues, have allowed for enhacned control over polymer architecture with a reduction in catalyst required with techniques by ARGET ATRP [14-16]. Forbes et al. recently employed an ARGET ATRP emulsion polymerization technique to synthesize cationic nanogels composed of diethylaminoethyl methacrylate with poly(ethylene glycol) tethers that could be complexed with siRNA and loaded with a small molecule drug. Particle sizes were 120nm with pH dependent drug release, and have potential for local delivery to colon cancer or to multi-drug resistant cancer cells by intravenous injection [17].

5.3.3 Functionality

Graphene and graphene oxide have recently surfaced in the field of intelligent drug delivery as drug and gene carriers. One such carrier is a nanosized chitosan-functionalized graphene oxide, which served to enhance biocompatibility and solubility. Further, the authors demonstrated the ability to effectively load camptothecin as a result of pi-pi stacking and hydrophobic interaction and transfect HeLa cells using luciferase as a gene reporter [18]. Liu et al. synthesized polyion complexes with passive and active targeting, cell membrane

translocation, pH dependent drug release, and co-delivery capabilities. TAT was conjugated to the distal end of PEG in poly(ethylene imine)-poly(ethylene)glycol copolymers, and doxorubicin was chemically conjugated to amino group of the PEI with a hydrazone linkage. Electrostatic interactions were then used to bind DNA to the PEI backbone, and a NGR functionalized virus mimetic shell to the surface of the polyion complex [19].

5.4 DELIVERY TO PRIMARY CANCERS

Primary cancers can be described as tumors that have not shown growth of carcinogenic entities in sites other than the organ of origin. For most primary cancers, surgical resection of tissue remains as the first mode of therapeutic action, especially in colon cancer. This is usually followed by radiation therapy and chemotherapy to ensure complete elimination of cancerous cells and possible metastases. Both these treatments are not without undesirable side effects. Hence, considerable research focus has been devoted to minimizing off-target effects and making treatment more targeted to cancerous cells and tissues. Examples of targeted radiation therapy include. Approaches modulating particle size, charge and active targeting continue to dominate targeted therapy in primary cancer treatment.

Primary tumors usually vary in size and microenvironmental characteristics depending on progression of growth, thereby presenting unique challenges for delivery of therapy. On the basis of steps taken to accomplish intracellular delivery of therapeutics, the following barriers are exhibited in the case of primary cancers – (1) Blood vessels and the circulatory system (as the therapeutic is transported through blood flow to the region of therapeutic action) (2) Tumor interstitium (Upon penetration through blood vessel wall, the therapeutic will encounter the interstitial space or extracellular matrix filling the blood vessel margin and cancer cells, (3) Target cancer cells [20]. Complex, multilayered problems are presented by the metastatic version

of cancer, expanding the target area of therapy to organs other than the primary site of disease, along with the possible presence of metastases in the blood or lymph. Furthermore, multidrug resistance occurs in cancer cells when cells develop mechanisms to resist chemotherapeutic agents [19]. Each step presents its own unique set of challenges that have informed design considerations in cancer nanomedicine. To demonstrate efficacy, most anti-cancer drugs have to be present in the correct dosage and appropriate activity level, within the nucleus of the cancer cells, and in the case of monoclonal antibodies, sometime to the cell surface receptors. Loss or inability of active pharmaceutical ingredients to reach their final destination results in ineffective treatment, or sometimes worse- off-target side effects. Understanding the physiochemical intricacies of each environment is crucial to achieve this. Here is a review of the most recent findings that may inform rational design of nanomedicine, or highlight work that has demonstrated successful delivery *in vitro* or *in vivo*.

Nanoscale therapeutics are typically administered intravenously, and spends most of its biological presence traversing through thse blood circulation. This presents the most challenges to the delivery efficacy, which if not addressed, could lead to rapid and significant clearance of the therapeutic before it can even reach the relevant site. Fortunately, design considerations to evade circulatory clearance have received tremendous, well-deserved attention.

Size is an important consideration post interstitial/ intravenous administration of nanotherapeutics, as the appropriate size can enable preferential uptake in the lymph and avoid drainage back into the blood. Experimental evidence shows that particles with size <10nm are uptaken rapidly by lymph nodes, but are at higher risk of resorption back into the blood flow [20, 21]. On the other hand, particles >100nm may remain accumulated at the injection site instead of being transferred into the lymphatic circulation [22, 23]. In general, smaller nanoparticles have

faster clearance kinetics from the blood as well as the lymphatic system. Renal clearance occurs if the size of the nanomedicine is smaller than 10 nm [3]. On the other end of the scale, however, if the size is increased beyond a certain threshold, the nanoscale entity can more readily adsorb proteins and undergo opsonization in blood flow, subsequently becoming vulnerable to uptake by macrophages and reticuloendothelial clearance [4].

Studies investigating surface charge effects show that the uptake of neutral or positively charged nanoparticles by macrophages/lymphocytic bodies is drastically low as compared to negatively charged nanoparticles. While modulating surface charge has not demonstrated any relief from renal/hepatobiliary clearance, neutral or positively charged particles are known to avoid uptake by macrophages/lymphocytic bodies. Similarly, the influential role played by poly(ethylene glycol) (PEG) in avoiding non-specific protein adsorption and thus improving circulation time, has driven numerous preclinical studies and engendered the widely accepted DOXIL- a PEGylated liposomal formulation of doxorubicin.

Other surface coatings that hold immense promise in masking nanotherapeutics from the typical clearance mechanisms in the body are red blood cells/erythrocytes themselves and polysaccharides such as cyclodextrin, heparosan and hyaluronic acid owing to properties such as biocompatibility, biodegradability, and ability to be chemically modified. There is a growing body of work enunciating the exemplary effects of coating nanoparticles with erythrocytes to enhance circulation time, as well as improve intracellular concentration of drugs. Self-assembly micelles based on heparosan and deoxycholic acid conjugate have been reported to show superior DOX loading (into the hydrophobic deoxycholic acid core) and release, and enhanced cellular uptake in HeLa cells [24]. One reason to seek other surface modification alternatives over PEG is the reported activation of the complement immune pathway by PEGylated

liposomes. Negatively charged heparosan avoided adsorption of serum protein components and extended intravenous circulation time of the formulation, and could be a potential substitute for the popular alternative PEG. The use of PEG has also been reported to create several problems such as reduced cellular uptake (due to the hydrophilicity of PEG) and poor endosomal escape subsequent to endocytosis (due to minimal interaction with endosomal lipids) [25]. Neutral or negatively charged nanoparticles seeking access to the lymphatics avoid electrostatic interaction with negatively charged glycosaminoglycans, and are able to enter the lymphatic system more readily. Cationic nanoparticles can form high molecular weight aggregates with interacting proteins precluding absorption from the injection site. Lymph node retention of drug delivery devices is commonly increased by using an increased size (physical filtration) or increased hydrophobicity/receptor interactions. By contrast, drainage into the lymphatics from the blood necessitates opposing properties [26].

Solving the problem of short circulation times, leads us to our next challenge; permeating the blood vessel at the appropriate location and entering the tumor interstitial matrix. While this seems rather intuitive and easy, the complexity of myriad tumors and the high interstitial pressure in the surrounding microenvironment makes this a force to reckon with. Research suggests that small molecules and particles, will prominently extravasate in normal tissues instead of the tumor tissues, owing to relatively higher interstitial fluid pressures in tumors [27]. Pores in normal vessels have an average cross-section of, while that in tumor associated vessels are. Evidence also indicates that increasing the size above may exclude extravasation into tumor interstitium surrounded by the lower threshold of blood vessel pore diameter, and negate the gain in selectivity. Particle size will have to be balanced and optimized to cater to individual tumor and microenvironments. Even if penetration into the interstitial space is achieved, the tumor

environment itself is spatially heterogeneous, further impeding transport of particles of certain size. Furthermore, surface charge and shape of nanoparticles can also influence extravasation and interstitial transport. Jain et al. have revealed that cationic particles permeate better through tumor endothelial cells and blood vessel in relation to neutral or anionic particles. But, there is no doubt that neutral particles undergo minimal interaction with components of the interstitial matrix and diffuse faster through the interstitium than cationic or anionic particles. Linear, polymeric particles are supposed to diffuse faster than spherical, rigid particles although there is no consensus on the reason behind this observation.

One reason to seek other surface modification alternatives over PEG is the reported activation of the complement immune pathway by PEGylated liposomes. Drawing inspiration from LDL receptors that dissociate in response to the intracellular environment, PEGylated nanocarriers can be designed to respond to stimuli such as pH, reducing agents, cathepsins, esterases or matrix metalloproteinases to shed/dissociate the PEG coating entailing biodistribution in the tumor site [28-32].

Strategies relying on the EPR effect typically involve a hydrophobic core and a coating with PEG polymer for biocompatibility, which is good for small molecule hydrophobic drugs which otherwise exhibit a dismal pharmacokinetic profile. Fig. 2 illustrates the intravenous administration of nanotherapeutics that utilize the EPR for passive targeting to tumor tissues. An emerging class of nanomaterials is being constructed using single-walled carbon nanotubes with the overarching aim of improving tumor uptake in intravenously injected nanoparticles by means of the EPR effect. To gain a deeper understanding of how SWNTs may be internalized by cells, Smith et al. performed in vivo studies in mice and compared internalization of SWNT by blood cells to that of PEG, and found that SWNTs were rapidly internalized by cells [33]. Conversely,

SWNTs were not uptaken by phagocytic cells, in addition to not activating monocytes 6 hours past uptake. Intriguingly, monocytes containing SWNTs were found to increasingly penetrate the tumor interstitium and vasculature as compared to other circulating monocytes. This leads into insight indicating that SWNTs may further infiltrate the tumor interstitium by entering circulatory cells employing a "Trojan Horse mechanism", in addition to the EPR effect.

In contrast to passive targeting, active targeting approaches can be used to further improve effectiveness and minimize off-target effects. Because of their specificity, peptides are a natural choice for use as targeting ligands [34]. It has been a long standing obstacle to deliver nanocarriers with peptidic ligands that may be susceptible to enzymatic degradation and lower affinity compared to antibodies. This can be resolved by introducing D-amino acids or multivalent sequences into the peptide sequence. Most commonly used peptidic sequences include cyclic RGD sequences that recognize $\alpha_v\beta_3$ integrin receptors, CSNIDARAC peptides for lung tumors, EPPT peptides for tumor-specific antigen underglycosylated mucin-1, F3 peptides that target endothelial cells lining the tumor vasculature, and also a wide range of membrane receptors for cholecystokinin, GRP and somatostatin [35].

Aptamers have gained considerable popularity as targeting ligands because of their high specificity, low cost, lower toxicity and immunogenicity, and smaller size. Development of aptamers by the systematic evolution of ligands through exponential enrichment allows for an elegant way to produce a more robust group of targeting biomolecules as opposed to protein-based ones [36]. So far, aptamer ligands have been prepared for IgG receptors, tyrosine kinase receptors, E-selectin, nucleolin, and other tumor molecules and cells.

To demonstrate efficacy in treatment of primary cancers, most anti-cancer drugs have to be present in the correct dosage and appropriate activity level, inside the cancer cells, or in the

case of monoclonal antibodies, at the cell surface. Loss or inability of active pharmaceutical ingredients to reach their final destination results in ineffective treatment, or sometimes worse-off-target side effects.

The facility to selectively compartmentalize drug molecules makes liposomes, vesicles, and micelles lucrative from a drug delivery standpoint. Such nanocarriers are constructed with a precise control over the molecular architecture, permitting loading of a variety of anticancer drugs such as hydrophobic small molecules, proteins, siRNAs, and even plasmids [29]. Sequential addition of individual layers complemented with external triggers based on pH, light, and temperature can release drugs in a site-specific manner. Of noteworthy mention is the use of PEG as the outermost layer of such multi-layered nanoformulations, primarily for achieving the benefit of biocompatibility and minimization of non-specific interactions upon intravenous administration.

Block copolymers have traditionally been the synthetic constructs/building blocks of these composite nanocarriers. Block copolymers have traditionally been the synthetic constructs/building blocks of these composite nanocarriers and have been reviewed elsewhere [37]. Of notable mention, is the recent use of polyion complex vesicles (PICsomes) synthesized from block copolymers, with the aim of delivering hydrophobic as well as hydrophilic anticancer drugs. Kishimura and group mixed oppositely charged diblock copolymers to attain self-assembly of PICsomes [38]. One unit of PICsome (uPICsome) was made from a block of PEG and a segment of charged poly(amino acid)s for the diblock copolymer uPICsome. Modulating the concentration of uPICsomes allowed for tunability of size and drug release kinetics.

For selective delivery of plasmid DNA (pDNA) to tumor cell nuclei, Nomoto et al. synthesized PEG-PAsp(DET)-PLys triblock copolymers and added them to a pDNA solution to

fabricate self-assembled three-layered polyplex micelles in a bottom-up fashion [39]. Longer circulation times, a prerequisite for effective intravenous anticancer therapy, were achieved through the use of a PEG shell compartment. Selectivity was obtained by including a photosensitizer in the design, which allowed intracellular gene delivery only after infrared irradiation subsequent to accumulation of micelles within the tumor. Inactivation of the pDNA by oxidative damage from the photosensitizer – a major hurdle in this scheme, in addition to enzymatic degradation – was largely avoided by spatially compartmentalizing pDNA within the core PLys (condensation of pDNA with anionic PLys), and complexing the photosensitizer with the cationic PAsp(DET). In-vivo success with this light-sensitive gene transfer scheme was 6-fold in photoirradiated tumors vs non-photoirradiated ones. Despite the promising selective gene transfection results within tumor cells, it is important to note that the roughly 100nm long nanocarriers, also accumulated in other highly vascularized normal organs like lungs, liver, spleen, and kidney, resulting in off-target gene expression.

Another approach exploiting the compartmentalization ability of polymeric micelles, was illustrated by Synatschke and associates, who used interpolyelectrolyte complexation between positively charged PLL-b-PEG and negatively charged BVqMAA to yield a neutral multicompartmental core-shell-corona structure [40]. By orchestrating a PEG corona, they were able to observe longer circulation times and improved tumor accumulation in vivo, while the polybutadiene core was able to preferentially load a hydrophobic model drug.

Uncontrolled, off-target drug release from Pegylated liposomal formulations such as DOXIL can be surmounted by externally-triggered drug release as demonstrated by thermoresponsive phosphatidylcholine-based liposomal carriers that rely on gel-to-liquid phase transitions, such as ThermoDox (dipalmitoylphosphatiylcholine (DPPC):

monostearoylphosphatidylcholine (MSPC)/PEG 2000- distearoylphosphatidylethanolamine (DSPE)=90:10:4 molar ratio) [41]. These 150 nm size lysolipid formulations respond specifically to mild hyperthermia, but suffer from relatively poor stability in blood plasma subsequent to intravenous administration. Chen et al. recently re-engineered this liposomal formulation, by encapsulating ammonium bicarbonate within the core leading to generation of CO_2 bubbles in response to a mild hyperthermia trigger (~41^{o}C), thereby opening up pores to enable fast, tumor-specific DOX release [41].

In another recent study, degradable DNA cages were complexed with hydrophobic drugs for intracellular delivery. Single DNA strands are complexed with smaller strands to create unique structures with sites available for attaching functional groups/targeting agents/biomolecules [42]. Formation of DOX-DNA complexes is rather intuitive given the planar structure of DOX allows efficient intercalation within the DNA molecules. In studies performed in nude nice with a human orthotopic breast tumor, triangular structures with 120 nm long sides, endocytosed within tumor cells, and were transferred into lysosomes providing sustained delivery and tumor reduction.

5.4 DELIVERY TO METASTATIC CANCERS

A large unmet need in the treatment of cancer that has metastasized, is the lack of chemotherapeutic options for bone metastases, which conduce an aggressive form of cancer typically conferred with a selective advantage [43]. Complex problems are especially presented by the metastatic version of cancer, as they expand the target area of therapy to organs other than the primary site of disease, along with the possible presence of metastases in the blood or lymph. As a result, significant co-operation is necessary from clinicians, and may rely heavily on the ability to elucidate the organs to which the metastases have spread to. Tackling metastatic cancer

with the aid of the nanotechnological toolbox has been reviewed in remarkable detail by Schroeder et al [44]. Researchers designing nanomaterials for treating metastatic cancers must consider delivering to a wide range of physiology based on the organs the cancer has metastasized to, in addition to ensuring delivery to the cancer cell/ subcellular organelle. While design considerations remain similar, physiological heterogeneity of the organs may exclude the use of a single nanoparticle and may necessitate utilization of a variety of diverse nanomaterials to individually tackle metastases in each organ and changing tumor landscape, based on the stage of development.

One approach that can be readily used for targeted delivery to bone/skeletal tissue, a common site of metastasis, utilizes high affinity apatite binding molecules like bisphosphonates and oligopeptides. Unfortunately, the negative charge conferred by these targeting moieties can exclude the nanocarriers from the negatively charged cell membranes/cytosol [45]. Solid phase synthesis of peptides allows for rational design of multifunctional peptides that allow for inclusion of diversely charged elements in the same targeting moiety. Applying this method, Wang et al. generated a custom trifunctional peptide that consisted of an anionic targeting element (for apatite targeting), a cathepsin-cleavable linker (to respond to a metastatic microenvironment), and a cationic element (for supporting cellular uptake). The peptide-b-PEG-PTMC (poly(trimethylene carbonate)) polymer self-assembles into nanomicelles that demonstrated up to 90% DOX loading efficiencies into the PTMC hydrophobic core [46]. Further, the 75 nm nanoparticles were able to avoid clearance owing to the presence of PEG, selectively targeted to bone metastases and even displayed a prolonged survival rate in mice compared to control groups, thereby highlighting the overall attractiveness of this approach.

Another hotspot for the accumulation of metastases is the lymph nodes. Poorly developed lymphatic vessels surround metastasizing cancers, and expose gaping holes between adjacent lymphatic cells that eventually facilitate invasive spread of cancer cells. In fact, the excessively permeable network of lymphatic vessels is touted to be the primary means of cancer metastasis [47]. Surgical and radiological treatments for lymph node metastases are accompanied with side effects and inefficiencies as well, presenting another urgent need that can be treated with nanotechnology. To target and inhibit cancer cells that have gained access to lymph nodes would require the use of nanoparticles that can also circulate in the lymph nodes and empower drugs to exert their therapeutic effect.

Understanding what triggers and supports lymph node metastasis can enable development of appropriate nanomedicine. Spread of cancer cells via lymph nodes typically advances through vascular endothelial growth factors- C and –D (VEGF-C and VEGF-D) [43] [31,34] and integrin $\alpha_v\beta_3$ levels [57,58], and consequentially, VEGF inhibitors are good targeting moieties for halting metastatic spread. Chemokine receptor expression-level is another determinant of the site of metastasis, and potential receptor targets include chemokine receptors CXCR4 and CCR7 [44]. PLGA Nanocapsules with size ~300nm and a negative charge, containing docetaxel at >95% nanocapsulation efficiency were largely distributed in the mesenteric lymph node [45]. While the precise mechanism by which this happens remains largely unknown, it is believed that nanoparticles were coated with apoproteins and phospholipids, thereby facilitating delivery to the lymphatic system.

Size is an important consideration post interstitial/ intravenous administration of nanotherapeutics, as the appropriate size can enable preferential uptake in the lymph and avoid drainage back into the blood. Experimental evidence shows that particles with size <10nm are

uptaken rapidly by lymph nodes, but are at higher risk of resorption back into the blood flow [20, 21]. On the other hand, particles >100nm may remain accumulated at the injection site instead of being transferred into the lymphatic circulation [22, 23]. In general, smaller nanoparticles have faster clearance kinetics from the blood as well as the lymphatic system. Neutral or negatively charged nanoparticles seeking access to the lymphatics avoid electrostatic interaction with negatively charged glycosaminoglycans, and are able to enter the lymphatic system more readily. Cationic nanoparticles can form high molecular weight aggregates with interacting proteins precluding absorption from the injection site. By subcutaneously delivering a polycationic dextran with their liposomal formulation, Feng et al. were able to increase interstitial pressure as the positively charged dextran bound to the interstitium and the increased pressure was able to drive their liposomal DOX formulation into the lymphatics. Lymph node retention of drug delivery devices is commonly increased by using an increased size (physical filtration) or increased hydrophobicity/receptor interactions. By contrast, drainage into the lymphatics from the blood necessitates opposing properties [9]. In particular, PEG which is coated on most nanocarriers to increase hydrophilicity, blood retention time, and avoid opsonisation and phagocytosis, drains rapidly from the blood into the lymphatics, but is not retained within the lymphatics owing to its hydrophilicity and minimal phagocytic engulfment.

Newer strategies to ascertain chemotherapeutic delivery within cancer cells include the use of ATP triggered nanoparticles. To achieve increased accumulation within the tumor mass, Mo et al. leveraged an anionic hyaluronic acid coating/shell that remains stable in blood circulation and allows functionalization with targeting moieties, and undergoes degradation only in the presence of tumor extracellular matrices and tumor cellular endocytic vesicles/endolysosomes [34-36]. Within the HA shell, they used the cationic protein protamine,

which enables active cellular uptake, endosomal escape, and nuclear targeting [33]. Protamine is complexed with an ATP-responsive DNA motif that is itself complexed with DOX, a planar molecule and model chemotherapeutic drug. DOX is released in the vicinity of ATP because the DNA motif forms a complex structure with the ATP, dissociating the intercalated DOX. Concentration differences between extracellular ATP (<0.4 mM) and intracellular ATP (1-10mM) displayed selective release of DOX within the cytosol, both in vivo and in vitro.

Remodeling the tumor microenvironment to essentially discourage cancer cells from proliferating has been the focus of several anti-cancer combination therapies. Nanomedicine can play a pivotal role in this by encapsulating multiple drugs in appropriate dosage ratios. By inhibiting antiangiogenic activity in a xenograft tumor model, Leaf Huang and group revalidate this attractive strategy to halt the metastatic spread of cancer cells [48]. By loading DOPA-cisplatin cores into PLGA nanoparticles, they increased the core hydrophobicity of PLGA, further facilitating improved loading of the hydrophobic anti-angiogenic drug - rapamycin (a VEGF and Tumor associated fibroblasts inhibitor). Co-encapsulation within the same nanoparticle is crucial as it can help maintain the desired dose ratio, giving better control over the release and synergistic therapeutic effect; while ensuring a lower IC_{50} value than co-treatment of rapamycin and cisplatin as a result of distinct *in vivo* pharmacokinetics and biodistribution.

Because anti-angiogenic therapy can normalize tumor vasculature and improve drug delivery to metastasizing cancers, researchers have delivered siRNA to vascular endothelial cells in metastatic lung cancer models [49]. An epoxide-terminated lipid was reacted with PEI_{600} , a commonly used siRNA delivery agent, to tune size and charge for efficient particle uptake by target endothelial cells, reduce particle accumulation and subsequent undesirable gene

expression in the liver, along with the achieving the overarching goal of multi-gene silencing in vivo. The lipid formulation called 7C1 forms multilamellar vesicles having a size range of 35-60 nm and has a neutral charge at pH 7.4. Carrying a neutral or slightly lower cationic surface charge at pH 7.4 is a desirable property to ensure appropriate biodistribution and endosomal escape [50]. While the exact mechanism by which 7C1 succeeds at targeted delivery to endothelial cells remains unknown, it is believed to promote delivery to endothelial cells by favorably interacting with serum proteins.

Strictly speaking, the central core of a tumor that is metastasizing has immense interstitial pressure that can drive nanoparticles out before a desired therapeutic outcome is achieved using the popular EPR effect. To combat this vascular permeability issue, nanoparticles are usually targeted to be delivered directly to the tumor site, or co-delivered with biomolecules (VEGF, TGFβ inhibitors) that normalize the vasculature [47]. Improved biocompatibility confers these particles with a prolonged half-life that has extend the elimination half-life of drugs like doectaxel from 2.2-4.5h in normal tissue to 22h in tumors. It is important to note, however, that PEGylated nanoparticles that simply rely on EPR effect are most likely to release their payload outside the cancer cell/extraceullarly, owing to poorer cellular uptake arising from steric hindrance/ hydrophilicity due to PEG. Extracelullar delivery is desirable for treatment of metastasizing tumors/ micrometastases since modulating the tumor microenvironment can substantially improve accompanying chemotherapy. Interestingly, improved circulation and biodistribution had also been suggested to explain the success of Abraxane (albumin bound paclitaxel) – the first-ever FDA approved intravenous, passive nanomedicinal treatment of metastatic breast cancer. However, albumin lipid nanoparticle technology did not significantly improve drug pharmacokinetics. In fact, it is suggested that simply using albumin instead of

cremophor EL, the toxic excipient previously used to formulate paclitaxel for the treatment, can lead an increase in the therapeutic index and maximum tolerated dose of Paclitaxel owing to lowered systemic toxicity in the absence of cremophor EL.

PEGylated formulations that make use of block compolymer chemistry yield micelles that have been carefully tailored to modulate drug loading and release profile. PEG-PLA nanoparticles have especially received widespread attention, and Genexol-PM formulation is currently undergoing Phase II clinical trials in the USA for treatment of metastatic cancer. Better control over characteristics of PEGylated block copolymers can overcome current immunogenic limitations associated with PEG [51], burst release related issues, and even extracellular anti-cancer drug release within the tumor microenvironment instead of cell interior.

Similarly, albumin-manganese dioxide nanoparticles have been used to regulate the tumor microenvironment with the aim of improving prognosis with radiation therapy [48]. MnO_2 nanoparticles can specifically catalyzed and reacted with hydrogen peroxide produced in a growing tumor microenvironment to sustainably generate oxygen to counteract hypoxia and improve cytotoxic effect of radiation, in addition to increase the acidic extracellular pH in a responsive manner. The core MnO_2 was coated with the cationic polyelectrolyte poly(allylamine hydrochloride), followed by conjugation with bovine serum albumin to produce ~50nm particles, which can be delivered locally and displayed excellent retention in tumors. Polyelectrolyte complexes like these can resist enzymatic degradation by proteases, and undergo endocytotic uptake by cells [52].

Leaf Huang and group have also examined the utility of nanomedicine enabled cancer immunotherapy to combat metastatic disease [49]. Most combination therapies rely on loading multiple therapeutics within the same nanomaterial to better modulate the tumor

microenvironment and cytotoxicity. In the aforementioned study, the antigen-specific response of a therapeutic vaccine against melanoma was boosted by the use of a separately delivered siRNA that reversed the immunosuppressive microenvironment found in an advanced melanoma mouse model. To elicit an immune response, immunogenic self-antigen tyrosinase-related protein 2 (Trp2) peptide was encapsulated within mannose-modified lipid-calcium phosphate nanoparticles having a size of 30 nm as observed under electron microscopy. As an adjuvant, CpG oligonucleotides were loaded into the same nanoparticle to evoke a strong immunogenic response from the cytotoxic T lymphocyte (CTL) towards the tumor. In order to address the microenvironmental changes concomitant with metastasis, a separately delivered TNF β siRNA nanoformulation performed the task of normalizing the tumor microenvironment and enabling improved vaccine performance. For siRNA delivery, considerations for design were slightly different requiring another nanocarrier. Firstly, a cationic liposome coated with PEG was used to overcome challenges associated with biodistribution and opsonization. Then, anisamide, a ligand targeting the sigma receptor in cancer cells was conjugated to the cationic lipsome. Finally, siRNA and hyaluronic acid were condensed together to yield a negatively charged complex that is coated on the cationic liposomes via electrostatic interactions.

5.5 DELIVERY FOR ANTI-ANGIOGENIC THERAPY

5.5.1 Introduction

Angiogenesis is a biological phenomenon that promotes formation of blood vessels (hemoangiogenesis) and lymphatic vessels (lymphangiogenesis) from pre-existant vessels [53]. Angiogenesis entails the outgrowth of new capillaries from the prevailing endothelial cells in blood vessels in order to nourish the primary tumor [54]. When a tumor reaches 2mm in

diameter, oxygen is unable to diffuse throughout all cancer cells within the tumor [55]. Hypoxic cancer cells start a pro-angiogenic signaling process that ultimately translates into secretion of growth factors and extracellular matrix components (ECM) that induce the angiogenic process [56]. Angiogenesis sustains the continued growth of malignant tumors by providing oxygen and nutrients and disposing of waste products over the period of disease progression. These newly formed small blood vessels are critical for the survival and metastasis of the primary tumor to other organs of the body, spreading the malignancy and advancing the stage of the disease. Compelling evidence in numerous mouse models of inhibition of the customary "angiogenic switch" that triggers the resilient foray of primary tumor cells to other body organs, has indicated halt of tumor growth and metastatic spread [57-59]. The process of angiogenesis is as complex as cancer itself, comprising of several steps and ancillary diffusible factors that facilitate the development of a supportive vascular network. Cancer cells are equipped to escalate the production of proangiogenic factors and downregulate angiogenesis inhibitors, thus thwarting the natural balance of angiogenic factors. The initiation of angiogenesis involves extravasation of plasma proteins, degradation of extracellular matrix to allow migration of cells, followed by actual endothelial cell proliferation and migration, and capillary tube formation.

5.5.1.1 Proangiogenic factors

Among proangiogenic factors there are several types of growth factors, such as Vascular Endothelial Growth Factor (VEGF), Platelet Derived Growth Factor (PDGF), Epidermal Growth Factor (EGF), Fibroblast Growth Factor (FGFs), and extracellular matrix (ECM) components such as adhesion molecules [60-62].

5.5.2.1 Growth factor related proangiogenic factors

5.5.2.1.1 VEGF or VPF(Vascular Endothelial Growth Factor or Vascular Permeability Factor)

Most notable of the army of proangiogenic signals that aid in the spread of tumor cells is the Vascular Endothelial Growth Factor. VEGF is programmed to be released by an oxygen-deprived tumor cell for adjusting the vessel blood flow to fulfill its higher oxygen demands for rapid growth and proliferation [mo. The VEGF signal causes the endothelial cells of the said blood vessel to loosen their junctions, thereby allowing increased blood flow through the vessel as a consequence of vessel dilation. VEGF also enhances the permeability of the endothelial cell layer previously covered by the now liberated pericytes. This increased permeability enables plasma proteins from the endothelial cell layer to extravasate and form an extracellular matrix scaffold that can eventually house endothelial cells migrating as a result of integrin signaling. This is a stepping-stone in the crucial process of migration of endothelial cells to from a well-developed vascular network that can abet the malicious interests of tumor cells.

The molecular members of the VEGF family include the angiogenesis stimulators VEGF A, VEGF B, VEGF C and PlGF (Placental Growth Factor); the growth factor receptors VEGFR-1 ,VEGFR-2 and, and co-receptors NRP1 and NRP2. Table 1 summarizes their roles in the intricate angiogenesis mechanism.

Molecule	Class	Function	References
VEGF A	Stimulator	(a) Predominates activation of angiogenesis in abnormal/diseased cases as well as during regular vascularization in the event of injury (b) Maintains vascular homeostasis if secreted by endothelial cells (c) Increases vessel branching and promotes	[63-65]

		abnormal vessel formation if secreted by tumor, myeloid and stromal cells	
VEGF B	Stimulator	(a) Promotes growth of cardiac vessels (b) Supports neuronal survival (c) Induces metabolic effects	[66, 67]
VEGF C	Stimulator	Stimulates "blood-vessel tip cells" that precede the endothelial cells forming new blood vessels	[68]
PlGF	Stimulator	(a) Cytokine that activates tumor cells in disease but remains inactive during regular vascular functioning (b) Creates favorable microenvironment for replication and migration of tumor cells by activating the bone-marrow-based EPC, myeloid cells, stromal cells (c) Decreases population of tumor-associated macrophages and opposes benefits offered by chemotherapy	[66, 69, 70]
VEGFR-1	Receptor	(a) Regulates amount of VEGF A available to stimulate angiogenesis (b) Angiogenesis caused if signaled from intracellular components in angiogenic endothelial, stromal and myeloid cells	[66, 71-74]

		(c) Signaling promotes growth of VEGFR-1^{+} tumor cells in response to VEGF A produced by endothelial cells	
VEGFR-2	Receptor	(a) Receptor for VEGF A and C (b) Arterial morphogenesis caused if signaled from intracellular components (c) Causes vascular tumors, genetic polymorphisms leading to angiogenesis if VEGFR-2 mutation is activated	[75-77]
VEGFR-3	Receptor	(d) Receptor for VEGF C (e) aids formation of blood vasculature formation during early embryogenesis (f) Forms new lymphatic vessels from pre-existing ones	[78]
NRP1	Co-receptor	Enhance activity of VEGFR-2	[79]
NRP2	Co-receptor	Enhance activity of VEGFR-2	[79]

Table 1. Molecular members of the VEGF family and their role in the angiogenesis mechanism.

5.5.1.1.2 Platelet-Derived Growth Factor

While VEGF takes the lead in forming new blood capillaries, PDGF comes to the fore in order to help these neophytes become mature. The small blood vessels comprising of endothelial cells lack pericytic membrane coverage resulting in vessel leakage, tortuosity of blood flow,

microaneurysm formation and bleeding. Endothelial cell release PDGF-B which "chemoattracts" PDGF receptor-β (PDGFR- β)$^{+}$ pericytes as well perivascular pericyte progenitor cells from the bone marrow, thereby, fortifying these frail, tumor-supporting vessels [mol. Mech jain]. PDGF-B released by tumor cells indirectly assists increasing the endothelial cell coverage of pericytes by upregulating stromal-cell-derived factor-1α. Preliminary studies with PDGF-B based pericyte recruitment certainly point towards PDGFR- β as a promising candidate for receptor inhibition [80]. It is important to note that blocking the PDGF-B angiogenic mechanism is effective only if the pericytes covering the endothelial cells are themselves releasing VEGF for further growth; implying a combination therapy of anti-VEGF and anti-PDGF drugs will achieve the same goal of arresting stabilization of newly formed tumor vessels by depleting their pericyte cell coverage. Apart from no additional advantages bestowed by the inhibition PDGF receptors over anti-VEGF therapy, there is also a sizeable amount of contradictory opinions in the literature regarding the efficacy of such a blockade in preventing tumor metastasis. It is a well-known fact that tumor vessels are leaky in nature. It is this leaky, tortuous nature that renders anti-cancer drugs ineffective in advanced tumors owing to poor drug delivery conditions. In fact, presence of extremely leaky blood vessels due to lack of perciytes due to PDGF-receptor inhibition can cause exacerbate tumor metastasis instead of preventing it. While stabilization and maturation of tumor vessels by other PDGF family members like PDGF-CC is known to diminish the effectiveness of anti-VEGF drugs, overexpression of PDGF-DD results in improved delivery of anti-VEGF drugs by normalizing tumor blood vessels.

5.5.1.1.3 Fibroblast Growth Factor

Both the acidic and the basic Fibroblast Growth Factors (aFGF and bFGF) play influential roles in the entire breadth of angiogenic activities: from the proliferation and migration of endothelial

cells to the upregulation of other growth factors that endorse the same angiogenic cause. These multi-faceted growth factors (especially FGFs 1,2 and 4) successfully execute the operation of endothelial cell proliferation by acting as mitogens, strongly binding to tyrosine kinase receptors (FGFRs 1 and 2) on the endothelial cell surface, thereby, stimulating the MAPK signaling pathway [81, 82]. To achieve the same end, VEGF and VEGFR-2 expression is upregulated by FGF2 [75].

In addition to proliferation of endothelial cells, FGF 1,2 and 4 also help accomplish the vital task of enabling the migration of endothelial cells by way of degradation of extracellular matrix proteins such as fibrin, which hinder the movement of endothelial cells. Urokinase-type plasminogen activator (uPA), a protein that has been identified for being instrumental in degradation of the ECM along with matrix metalloproteinases, is upregulated in endothelial cells by the activity of FGFs along with the upregulation of MMPs and uPA receptors [83]. Moreover, the existing blood vessels that sprouted during angiogenesis are further reinforced by FGFs, preventing vessel disintegration [43].

5.5.1.1.4 Angiopoietins

Unlike the FGFs, angiopoietins are more involved in the upkeep of blood vessels spawned by the proangiogenic effect of other growth factors rather than inducing endothelial cell proliferation itself. The ANG-TIE angiogenic system comprises of mural and tumor-cell secreted proteins ANG 1,2 and 4, which act as ligands for the TIE-2 tyrosine kinase receptors on endothelial cells. ANG 1, in the presence of reactive oxygen species, cements integrity of angiogenically sprouted blood vessels by inducing TIE-2 clustering at endothelial cell-cell junctions. The result is a more stable, mature, normalized and tight vascular network capable of ensuring endothelial cell survival and tumor nourishment. Contradictory to the proangiogenic role of ANG 1, ANG 2 and

Tie-2 signalling is purported to make the vasculature leaky by enhancing vessel permeability and detachment of pericytes, which may be more detrimental to the delivery of drugs to solid tumors than it is advantageous for tumor undernourishment [43]. Moreover, despite countering the vessel stabilization effects of ANG 1, ANG 2 released from blood-vessel tip cells, stimulates endothelial cell growth and sprouting of new blood vessels, while eliciting decay of the existing ones. In tumors, ANG 2 secures the future growth of the newly sprouting vessels by recruiting pro-angiogenic TIE-2 expressing monocytes from the bone marrow. Tumor angiogenesis employs a favorable balance of ANG 1 and ANG 2 to obtain the desired effect, which is hypothesized to be disrupted by inhibiting ANG 2 or TIE-2 receptors, for more favorable anti-angiogenic outcomes.

5.5.1.1.5 Transforming Growth Factor-β

Transforming growth factor-βs (TGF-β) such as TGF- β1 are cytokines which recruit other cells to fulfill the communal objective of stimulating angiogenesis. It is believed that receptors like activin receptor-like kinase (ALK) and endoglin (ENG) play a key part in the angiogenic ways of TGF-β1 [80]. As in the case of angiopoietins, there is a balance of the pro- and anti-effects TGF-βs depending upon the extent of TGF-β1 production. The effect exerted by TGF-β1 is proangiogenic at low concentrations by attracting cells like macrophages which then release angiogenic factors. On the other hand, at higher concentrations TGF-β1 undertakes the task of vessel maturation instead of vessel sprouting or endothelial cell proliferation. This results in the production of mural cells, differentiation and recruitment of smooth muscle cells. Thus, the use of drugs that can inhibit ENG and ALK receptors stand to be encouraging candidates for anti-angiogenic therapy.

5.5.1.1.6 Epidermal Growth Factor-related receptors

The diversity of the epidermal growth factor-like peptides such as TGF-α, amphiregulin, heparin-binding EGF, epiregulin, heregulins, neuregulins, and betacellulin and their equally manifold receptors, only add to the complexity of the pathways that can potentially be inhibited. In the event of an epidermal growth factor binding to a tyrosine kinase receptor presenting itself on the extracellular side of the cell, the EGF receptor undergoes dimerization with itself or any of its homologous ErbB receptor family members [80]. This dimerization guides autophosphorylation from ATP, which in turn, culminates into upregulation of cellular proliferation, survival in addition to angiogenesis, invasion and metastasis.

The concept of using EGFR inhibitors that bind to the ErbB receptor family is fundamentally similar to that of a particular antibody binding to a specific antigen on a cell surface. Appreciation of the ramifications of introducing EGFR inhibitors to compete with ATP molecules for intracellular catalytic sites of the EGF receptor led to the development of these tyrosine kinase inhibitors. The binding of tyrosine kinase inhibitors to EGF receptors blocks the catalytic site required for the autophosphorylation-motivated intracellular signal stimulation, thereby precluding the possibility of exacerbating tumor growth and development. The efficacy of such drugs has been theorized to be bolstered on the molecular scale by utilizing an irreversible tyrosine kinase inhibitor over a reversible inhibitor or an inhibitor that binds tightly to the target receptor [84].

5.5.1.1.7 Other soluble and membrane-bound factors

A broader perspective of the role of growth factors in other neoplasia promoting processes such as inflammation indicates a link between inflammation and tumor growth that has been epidemiologically verified. This idea germinated further study into the mechanism of action of some soluble factors found in the ECM which eventually led to the recognition of their

angiogenic faculties. Tumor Necrosis Factor-α (TNF- α), secreted by macrophages that may have been activated by other proangiogenic factors, has been implicated for bringing new blood capillary formation. While TNF- α may not be directly culpable for tumor growth and metastasis, it is certainly responsible for the intensification of the initial angiogenic effect produced by other growth factors [80]. Similarly, cellular adhesion regulating entities E-selectin and vascular cellular adhesion molecule – 1 are also deemed to be indirectly contributory to the cause of angiogenesis. E-selectin and VCAM-1 produced in activated endothelial cells, pass the torch of propagating angiogenesis to other endothelial cells by binding to the receptors for sialyl Lewis-X and VLA-4 ligands; thereby, wielding their angiogenic capabilities. Apart from directly actuating the proliferation and migration of endothelial cells, the aforementioned inflammatory cytokines can also activate nuclear factor-KB (NF-KB) in cancel cells, boosting their invasive tendencies. Nuclear factor-KB, which is also stimulated in necrotic cancer cells soliciting angiogenesis for survival, upregulates expression of genes coding for interleukin-8, matrix metalloproteinase-9, TNF-α and VEGF and promotes tumor development and advancement..

5.5.1.2. Extracellular Matrix Component related proangiogenic factors

The extracellular matrix (ECM) is a network of macromolecules that includes the interstitial matrix, made by stromal cells, and the basement membrane, made by epithelial, endothelium and stromal cells, to separate epithelium and endothelium from the interstitial matrix [85]. The extracellular matrix is mostly composed of proteoglycans, hyaluronic acid, collagen, elastin, laminins, fibronectin, and other proteins that contribute to the biochemical, physical and mechanical properties of the ECM [86]. For instance, some of the physical and mechanical properties are rigidity, porosity, insolubility, topography, elasticity, barrier, anchorage site, and movement track that regulate cell behavior and play an essential role in differentiation and in

cell migration [87, 88]. The biochemical properties encompass the ability of the ECM to regulate intercellular communication by controlling the diffusion rate and accessibility of ligands and other molecules to its receptors or target sites and by directly initiating signaling events. ECM is a highly dynamic structure, constantly under transformation, where cell interaction is a reciprocal and an essential constituent to the development of the ECM interconnected properties. Components of the ECM such as fragments of collagens type IV and XVIII are involved in regulation of angiogenesis, in collaboration with other factors such as VEGF. Stiffening of the ECM due to hypoxia causes blood vessels to branch resulting in sprouting angiogenesis. ECM components are also involved in vessel lumen formation and tubulogenesis through cellular morphogenesis [89, 90].

Two important components that can modify the ECM and are highly involved in angiogenesis are matrix metalloproteases (MMPs) and Integrins.

5.5.1.2.1 Matrix Metalloproteases

Matrix metalloproteases (MMPs) are zinc-dependent endoproteinases that can break peptide bonds of specific non terminal aminoacids. The overexpression of MMPs can change the dynamics of the ECM and compromise the integrity of the basement membrane, which loses its function as a barrier. This loss of functionality affects permeability through the basement membrane, allowing migration and infiltration of cells. This increases the risks of penetration of cancer cells to the blood vessels to undergo metastasis. It also allows endothelial leading tip cells from the blood vessels to infiltrate the interstitial matrix and initiate the formation of new blood vessels [91].

5.5.1.2.2 Integrins

Integrins are adhesion receptors known to regulate the angiogenic process (Hocivala-Dilke 2008). Integrins are transmembrane glycoproteins composed of one alpha (α) and one beta (β) chain that, upon ligand activation, start a signaling cascade that can either occur intra or extracellularly [92]. There are several known mammalian integrins and their expression is cell type specific. Endothelial cells, which more cancers arose from, express αvβ3, αvβ5, α4β1, α5β1, α1β1, α2β1, α3β1, α6β1, α6β4, and α9β1 integrins. Integrin receptors can be classified depending on its ligand. For example, Vitronectin binds to αvβ3 and αvβ5, while fibronectin binds to α4β1 and α5β1 [93]. Integrins provide mechanical traction for cell motility, migration and invasion. They are involved in the modification of the ECM. They contribute to cell proliferation in a ligand dependent and ligand independent manner. Overall, integrins may increase the malignancy of the tumor. Integrins are often overexpressed in many endothelial originated tumor cells, being αvβ3 one of the most studied integrin. Integrins are also expressed in angiogenic endothelial cells. The role of integrins in angiogenesis seems to differ depending on its type. For example, αvβ3 is involved in downstream activation of epidermal growth factor (EGFR) after fibroblast growth factor (FGF) binding. Meanwhile, αvβ5 promotes VEGF-induced angiogenesis upon interaction with VEGFR2. The integrin αvβ1, overexpressed in the endothelial vascular cells of angiogenic vessels interacts with vascular cell adhesion molecule 1 (VCAM1) present on pericytes for vessel stabilization [94].

5.5.2. Antiangiogenic therapy for cancer treatment

There are several molecular entities and signaling pathways, both in cancer cells and endothelial cells, involved with the complex process of angiogenesis. Antiangiogenic therapy is mostly based on the fact that the inhibition of pro-angiogenics factors reduces angiogenesis. Due to the variety of entities involved in angiogenesis, there is a wide variety of antiangiogenesis strategies.

For example, the use of gene and antisense therapy to modulate the activation or inhibition of proteins involved in angiogenesis translates in a decrease in angiogenesis and hence, tumor growth. Specific signaling pathways can be obstructed by using anti-angiogenic drugs that can prevent, inhibit or decrease activation of tyrosine kinases on tumor cells/endothelial cells stemming out of primary tumor vasculature; thus, safeguarding judicious destruction of tumor cells over healthy cells. Tyrosine kinases are enzymes that can either be transmembrane (receptor tyrosine kinases, such as VEGFR) or cytosolic (non-receptor tyrosine kinases). Binding of a ligand to the extracellular end of the receptor tyrosine kinase commences a cascade of reactions through its carboxyl-terminated cytosolic end, catalyzing transfer of a γ phosphate group from adenosine triphosphate to target proteins within the cytoplasm. Realization of the kinase activity subsequently activates intracellular signaling cascades like Ras/Raf MAPK pathway, P3k/Akt pathway, STAT3 pathway, and the protein kinase C pathway [95, 96]. Not only does activation of these signaling pathways alter the proliferative tendencies of the particular tumor cell, but they also induce genetic alterations so as to propagate aggressive growth and angiogenic predilections across generations. Inhibition of the tyrosine kinase enzyme either by bloking the extracellular domain using antibodies or blocking the intracellular domain using tyrosine kinase inhibitor (TKI), have shown to be effective in antiangiogenesis therapy.

5.5.2.1 Monoclonal Antibodies

Antibodies belong to an important class of compounds that can specifically target cells and molecules revealed to play crucial roles in angiogenesis. A superior understanding of the series of events leading up to angiogenesis, and the cellular and extracellular components involved in the proceedings, have created a niche that therapeutic antibody agents can target. Thus far, antibodies have been engineered to specifically target a cell surface receptors or extracellular

molecules implicated for their involvement in angiogenesis. These miscreant molecular targets are typically over-expressed in a vast majority of cancers that are metastasizing or have metastasized, and present an opportunity for the antibodies to latch on to. As a result of the potential of such a therapy, substantial research has been directed towards developing antibodies that can attach to receptors on endothelial cells or soluble molecules that interact with endothelial cells [97]. The ultimate goal of research in this area has been to thwart the mitogen-based signaling cascade that instigates endothelial cell multiplication, migration and proliferation, which is now known to be an intrinsic step in tumor angiogenesis. Further, developments in comprehending new biological mechanisms that could possibly underpin the development of blood vessels supplying nutrition to starving tumor cells continue to drive research in this area.

Antibodies having the potential to perturb intracellular signaling pathways can either target endothelial cell growth directly or can aim to halt endothelial cell adhesion and migration. Endothelial cell surface receptors that bind to growth factors stimulating enhanced cell multiplication include the vascular endothelial growth factors VEGFR-1, VEGFR-2, and VEGFR-3, and the epidermal growth factor receptors HER-1 and HER-2, as previously discussed [98, 99]. Antibodies developed to target these receptors exclusively, evidenced to have been over-expressed in a number of tumors, can foil the signaling cascade resulting from growth factor binding. Anti-VEGFR and Anti-EGFR antibodies had demonstrated their ability to successfully compete with VEGF ligands and EGF or TGF-α, for binding to the extracellular domains of such tyrosine kinase receptors. Inhibition of this growth factor attachment averts dimerization of the receptor, a key step occurring prior to intracellular signal transduction in endothelial cells. Eventually, this results in receptor internalization and proteosomal degradation,

thereby preventing any further possibility of ligand-receptor binding for the rapid replication of endothelial cells. Similarly, FGFR activity can also be inhibited in similar fashion [100].

Endothelial cell migration pathways can be targeted by use of antibodies that inhibit the activity of integrins, VE-cadherins and angiogenins (DDT). Anti-integrin antibodies have demonstrated great efficacy in hindering the integrin receptor sites on endothelial cells that are essential for adhering to extracellular matrix components for the purpose of migration [101, 102]. Similarly, VE-cadherins and angiogenins participate in cell-cell interactions and cell-matrix interactions during endothelial cell adhesion and migration. Their action can be inhibited by use of antibodies that bind to the respective receptors instead of the cadherins and angiogenins, thus, eradicating their presence in the angiogenic mechanism [103].

Some shortcomings that may impair the therapeutic efficacy of antibodies developed for cancer therapy include rapid renal clearance, lack of stability against proteolysis in the serum, possible threat of immunogenicity (especially for chimeric antibodies) or even interaction with healthy tissues, and most importantly, effective entry into tumor masses and high specificity and efficacy of binding to cell surface receptors or soluble cytokines [104]. Delivery mechanisms utilizing the wide array of carriers offered by progress made in the field of nanotechnology could perhaps help circumvent some if not most of the aforementioned shortcomings.

5.5.2.2 Aptamers and proteins

A vast body of research indicating the influential role of the Arg-Gly-Asp (RGD) peptide sequence, has been instrumental in helping midwife another class of molecules with anti-angiogenic potential. It is known that the RGD sequence can exquisitely antagonize the $\alpha_V\beta_3$ integrin; proving to be a hindrance to angiogenic cell-extracellular matrix interactions [105]. RGD motifs capable of homing molecules to tumors, can be incorporated into human/chimeric

protein based therapeutics such as bacteriophage peptides and immunoglobulin antibodies, by covalent coupling with side chain amino acids on the protein [106]. This conjugation ability of RGD sequences opens up new avenues not just for therapeutics, but also for diagnostic tools.

Notably, in this regard, cyclic RGD peptides have demonstrated their superior antagonistic ability to deter angiogenesis, tumor growth and metastasis in melanoma-afflicted animal models [107]. Another conjugate, which echoes the success that can be achieved by use of cyclic RGD peptides, is the cyclic RGD-heparin bile acid derivative. The RGD sequence is believed to target the quickly dividing endothelial cells, while the heparin exerts its adverse effects on blood vessel development and angiogenesis.

Initial success with RGD sequences that inhibit integrins spawned the search for other such potent peptidic domains, which could presumably bind to cell surface receptors culpable for tumor angiogenesis. Utilization of peptide libraries led to the discovery of peptides such as Gly-Asn-Gln-Trp-Phe-Ile (GNQWF1 or anti-Flt1) capable of selectively inhibiting VEGFR1. On similar lines, single/double stranded short DNA/RNA molecules called aptamers, are capable of binding to specific molecules such as enzymes/receptors [108, 109]. They are typically segregated with peptides owing to comparable molecular weights (8-25 kDa). Aptamers enjoy the same advantages as small peptide sequences such as increased solubility and tissue penetrability, and steer clear of the drawbacks characteristic of antibodies like reduced immunogenicity and blood circulation times [110]. The short length of aptamers make them suitable for targeting purposes in therapeutic and diagnostic applications alike.

5.5.2.3 Antisense and gene therapy

Gene therapy encompasses the introduction of DNA into the cell nucleolus in an attempt to restore the loss of a gene. Cancer cells present mutations and alterations in their genes that

translate into the loss of proteins that are involved in the normal cell cycle. The loss of these proteins leads to an increase in proliferation, inability to properly regulate the cell cycle, and gained ability to metastases. Healthy cells can also present aberrant behavior due to paracrine manipulation from cancer cells. This is the case for endothelial cells, located near tumors, which respond to pro-angiogenic signals from the cancer cells within the tumor. By restoring the ability to synthesize anti-apoptotic proteins in both endothelial cells and cancer cells, the angiogenesis process can be considerably minimized. The most common genes delivered and transfected for anti-angiogenesis therapy are those encoding the endogenous anti-angiogenic proteins interferons, angiostatin,endostatin, and vasostatin [111].

Interferon alpha (IFN-α) is a glycoprotein that has been used in anti-angiogenic cancer therapy because it down-regulates bFGF and VEGF (Singh 95). Preclinical studies using IFN- α have shown inhibition of angiogenesis in Kaposis' sarcoma, glioma, renal, and ovarian cancer, among others. Angiostatin is a plasminogen fragment that inhibits endothelial cell proliferation and migration and suppresses tumor growth and metastases. Angiogenesis gene therapy showed delay in tumor growth in melanoma xenografted mice after intratumoral injection. Similar results were found in lymphoma tumors in mice livers after portal vein injection and in human glioma in mice after intramuscular injection. Endostatin is a collagen fragment that inhibits endothelial cells functions by binding to the α5β1 integrin receptor [112]. Endostatin also inhibits cyclin D1 and attenuate[112-114]s VEGFR signaling [114]. It has been used for anti-angiogenesis therapy but it appears to be tumor specific, as reported by heteregenous results in tumor growth. Vasostatin is a peptide that showed inhibition of endothelial cell proliferation in vitro and tumor growth in vivo [113]. Gene therapy involving vasostatin showed both inhibition and enhancement of tumor growth.

Antisense therapy comprises the use of oligonucleotides to prevent messenger RNA (mRNA) transcribed from a specific gene to be translated into proteins. Small interference RNA (siRNA) has been widely used in antisense therapy to disrupt cellular pathways by knocking down genes, opening the door for new treatments of diseases caused by aberrant gene expression [115, 116]. A great variety of siRNA to knockdown different genes encoding for proteins involved in angiogenesis have been used to reveal the function of cellular signaling factors, cytokines, receptors, matrix proteins, and adhesion molecules involved in the formation of new blood vessels. The use of siRNA for antiangiogenic purposed has been widely used to elucidate the mechanisms of angiogenesis. In recent years, there has been an increasing interest in using siRNA as a therapeutic agent for antiangiogenesis therapy.

For instance, Hanze et al. (Hnze 2003, Biochem. Biophys.research commu.) used siRNA against the hypoxia induction factor (siHIF-1) which inhibited its downstream signaling . This correlated with a decrease in VEGF expression that affected cellular proliferation. It has been demonstrated that an increase in Progesteron B (PR-B) in breast cancer cells correlates with an increase in VEGF. By treating human breast cancer with siPR-B, Wu et al. (Wu 2004, cancer research) observed a significant decrease in expression levels of VEGF. The intratumoral injection of siVEGF in MCF-7 breast tumor models xenografted in mice, reduced significantly tumor gowth (Kurenova 2009). The same observations were found in PC-3 prostate cancer xenografts in mice. The in vitro studies with PC-3 prostate cells showed almost a complete inhibition of VEGF (Takei 2004 Cancer research). The use of siVEGF in a neuroblastoma synergic tumor model also reduced significantly tumor growth (Schiffelers 2004, Nucleaic acid research). It has been reported that VEGF inhibits the protein Thrombospondin-1 (TSP1), which

regulated vascularization and tumor growth. The use of siVEGF in a fibrosarcoma tumor model in mice, restore the ability of TSP1 to reduce vascularization and tumor growth.

The use of siRNA as an antisense antiangiogenic therapy for cancer treatment, has shown very promising results in vitro and in vivo. However, poor cellular uptake, low selectivity for the desired tissue, and rapid systemic clearance of siRNA through the renal system have been reported for intravenous injection of siRNA. Moreover, when injected intravenously, siRNA chains exhibit a short half-life due to intravascular degradation by the catalytic activity of Ribonuclease (RNase) enzymes present in the bloodstream (Chen 11 from co-delivery). The use of nanocarriers as siRNA delivery systems can prevent both renal clearance and RNase degradation, effectively increasing the siRNA half-life in blood (aliabadi 2011, Singha 2011).

5.5.3 Delivery systems

The overall survival rate of cancer patients depends largely on the extent of dissemination of tumorous cells in the body. One way of improving the chances of patient survival is the use of antiangiogenic therapy. Several entities for antiangiogenic therapy, such as small drugs, siRNA, peptides, etc. aspire to inhibit the spread of cancer by reducing oxygen supply to the tumor mass. Poor solubitlity of small drugs, degradation, poor tumor uptake, and low selectivity towards cancer cells are some of the challenges that antiangiogenic agents present. The existence of a variety of antiangogienic agents requires the development of an equal variety of delivery systems to overcome the limitations of the aforementioned agents.

5.5.3.1 Small drug delivery systems

The matrix metalloproteinase is another target for antiangiogenic therapy as it degrades the ECM paving the way for migration of tumor cells to distant parts of the body. TNP-470 is a

small molecule angiogenic inhibitor that binds to and incapacitates the MMP in addition to halting replication of vascular endothelial cells. However, TNP-470 is a highly hydrophobic molecule making intravenous administration an issue. Moreover, TNP-470 has been shown to be degraded due to a hydrophilic environment when delivered intravenously. This warrants the need to develop novel drug delivery systems that can circumvent the problems facing delivery of an antiangiogenic inhibitor alone.

PLA (Poly-lactic acid) based biodegradable systems offer great promise when it comes to enhancing intravenous delivery of drugs. However, the hydrophobic nature of TNP-470 requires the presence of a hydrophobic moiety within the conventional PLA system that can associate preferentially with hydrophobic drugs. Kakinoki et al. [preparation of poly-lactic acid micro] have used medium chain tri-glyceride to form oily domains within PLA microparticles that can enhance encapsulation of TNP-470 by the microparticles. The TNP-470 released from such a composite microparticle drug delivery system was observed to be more stable in vitro, thereby suggesting an influential role could be played by PLA microparticles in improving the therapeutic effect of TNP-470.

5.5.3.2 Monoclonal Antibody-based delivery systems

More popular in targeting studies, is the use of monoclonal antibodies to home on to VEGFR2, and release a cytotoxic drug such as docetaxel or paclitaxel. Lecithin based lipid nanoparticles targeted to VEGFR2 used by Liu et al. have demonstrated increased accumulation in tumor vasculature owing to antiangiogenic targeting [117].

Sequential delivery of antiangiogenic drugs followed by an anticancer drug is supposed to reduce tumor vasculature and further enhance the delivery of chemotherapeutics to the diseased area. Sengupta et al. formulated a nanocapsule made up of inner coating (containing an anticancer

drug) and an outer coating (containing an antiangiogenic drug combretastatin A4) to allow for temporal release of drugs and to increase the efficacy of the therapeutic treatment [118]. Pegylated-phospholipid block copolymers containing PLGA. On the other hand, Wang et al. conjugated paclitaxel to PLA in order to permit timely release of paclitaxel only within the tumor vasculature.

Instead of releasing drugs or therapeutic agents of any kind, Kalishwaralal et al. have researched the potential of silver nanoparticles in the size range of 100-500 nm alone, in blocking the binding of VEGF to receptors and calling off the mitogen-based progression of angiogenesis [119]. Silver nanoparticles are hypothesized to prevent the phosphorylation of Akt, a crucial step of the Protein kinase B/Akt pathway.

5.5.3.3 Aptamers and proteins delivery systems

Peptides synthesized from polyamino acidic groups are rapidly being developed mainly due to their abilities to cater to specific biological targets. These peptides are believed to interfere with the proliferative abilities of VEGF and bFGF, thereby proving to be an impediment to microvessel formation. However, their specificity makes them extremely susceptible to loss of activity through degradation and require vehicles that can transport and release them with great efficacy. PLGA (Poly(lactic-co-glycolic acid)), a highly researched biodegradable carrier, seemed like a suitable candidate for this job. However, degradation of PLGA causes formation of acidic oligomers that decrease the pH of the environment around the peptide, resulting in degradation. Loss of functionality of these peptides implies loss of antiangiogenic action. I d'Angelo et al. blended PLGA with poloxamers to minimize accumulation of PLGA aligomers in the presence of proteins, thereby preserving the biodegradable nature of the carriers as well the specificity of the peptides. Poloxamers are triblock copolymers consisting of a hydrophobic

(polyoxypropylene) chain in the middle, flanked by two hydrophilic (polyoxyethylene) chains at the end. PLGA-poloxamer blended nanocarriers and microcarriers showed great efficacy in vitro in the loading and release of JS-2892b, a polyaminoacid based peptide.

Use of polysaccharide molecules, such as chitosan and dextran sulfate blends, has also shown to produce positive results for delivering peptides. Chen et al. demonstrated 75% entrapment efficiency of ARH protein in chitosan-dextran sulfate nanoparticles formed by coacervation. However, any in vivo/cell based studies illustrating the ability of this system to inhibit growth of VEGF in metastasizing vascular endothelial cells was lacking.

Integrins such as $\alpha_V\beta_3$, $\alpha_V\beta_3$, and $\alpha_5\beta_1$ play a crucial role in the dissemination and growth of tumor cells by modulating cell-cell adhesion and cell-ECM adhesion. As a result, molecules that inhibit the action of these integrins offer great potential for anti-angiogenic therapy. Cyclic RGD peptides developed by Kessler et al. [In vitro and in vivo evaluation paper] have demonstrated their antiangiogenic efficacy in preclinical tumor models. However, their therapeutic potential has been severely limited by shortcomings such as poor bioavailability, shorter half-life, and most importantly inherently weak lethal effect on endothelial cells. RGD peptides have always been known for their ability to bind to integrins and this makes them a suitable candidate for targeting purposes. Ryppa et al. have conjugated paclitaxel to RGD peptides in order to compliment/boost the antiangiogenic potential of RGD peptides alone. Paclitaxel albumin-cyclopeptide conjugates were developed using EDC-NHS chemistry. RGD peptides act as antagonists to the integrins central to angiogenesis homing the conjugate to the area of interest. Upon attaching to integrins, the ester bond connecting paclitaxel to the RGD peptide can be cleaved to release paclitaxel and bring about endothelial cell death. This method was shown to inhibit endothelial cell migration and proliferation in xenograft models in vitro as

well as mice in vivo. Instead of using Paclitaxel conjugated cyclopeptide alone, Eldar-Boock et al. used PGA-Paclitaxel conjugated cyclopeptide to deliver paclitaxel by targeting integrins. PGA being biocompatible, non-immunogenic, and biodegradable by cathepsin B expressed strongly in tumor cells is believed to provide a safer route for paclitaxel delivery.

5.5.3.4 Antisense and gene delivery systems

Antiangiogenic gene and antisense therapy involve transfection of DNA and siRNA respectively, into human cells tailoring the cellular interaction and replication at a genetic level. Transfection of specific DNA or siRNA can be used to restore natural antiangiogenic or knockdown proangiogenic gene expression of cancer cells. DNA and siRNA are highly degradable if injected systemically due to nucleases and other enzimes present in the blood stream. It is primordial to keep the integrity of both DNA and siRNA to increase treatment efficiency. Nucleotides delivery can be achieved in two ways- using viral vectors and non-viral vectors. Viral vectors are extremely efficacious in transfecting nucleotides into cells but are limited by shortcomings such as low loading capacity, chances of infection and increased risk to cancer due to viral infection. Non-viral vectors have recently been looked into to bypass some of these shortcomings. Nanoparticles offer desirable properties to deliver nucleotides: high solubility, easy to modify, and with a great surface/volume ratio that provides large complexation surface. However, non-viral vehicles present lower transfection efficiency and cell toxicity. This is mostly due to the positive charge present in the nanoparticle surface that allows negatively charged nucleotides to complex on the surface and also improves transfection efficiency. Different strategies have been used to achieve high transfection efficiency and low toxicity nanoparticles formed by lipids, dendrimers, silica, and a variety of polymers.

The use of lipidic nanoparticles for different biomedical and pharmaceutical applications has been widely spread among the scientific community, (Garcia Fuentes 05) specially for transfection efficiencies since the liposome Lipofectamine ® became the commercial standard for nucleotide transfection. Other liposomes and lipid bases nanoparticles are being investigated as transfection vehicles. For example Saad et al. (Saad 08) synthesized a liposome using 1,2-dioleoyl-3-trimethylammonium-propane (DOTAP) and complexed siRNA through electrostatic interactions. Chen et al. (Chen 2010) synthesized cationic liposome-DNA (LPD) using the guanidine containing cationic lipid N,N-distearyl-N-methyl-N-2-(N-arginyl) aminoethyl ammonium chloride (DSAA)(Chen 2010). siVEGF was complexed onto the liposome surface. Yu et al. (Yu 11) synthesized high transfection cationic nanoparticles using 1,2-Dioleoyl-sn-glycero-3-ethylphosphocholine (EDOPC) and then complexed siRNA on the surface. Li et al. (Li 2012) tested different formulations and concluded that the use of the stable nucleic acid lipid particle (SNALP), *a* d*istearylphosphatidylcholine (DSPC)* based liposome, performed the best in transfection efficiency in vitro, but it was effective only in highly vascularized in vivo tumor models (Li 12).

Dendrimers, such as polyamidoamine dendrimer (PAMA) , can be use to confer a positive charge to silica nanoparticles, to complex siRNA and serve as delivery vehicles. (Chen 2009). Dendritic polyamines conjugated to β-cyclodextrin and complexed to siRNA against EGFR offered also a vehicle system for nucleotide delivery. (Kim 11)

Green et al. have recently studied the use of poly(β-amino esters) to deliver DNA to HUVECs, a genetically stable and prominently refractory class of endothelial cells. Key findings have suggested that poly(β-amino esters) nanoparticles may be efficacious in delivering DNA to

HUVECs due to their ability to condense DNA into the nanoparticles. Poly(β-amino esters) are able to buffer endosome and they are biodegradable.

While polymeric and biopolymeric particles constitute the majority of this kind of vectors, they are far from being applied in a clinical setting owing to their lack of biocompatibility or even biodegradability. Great effort is being made to synthesize polymeric nanoparticles with high complexation, high transfection, lox toxicity, and high degradability. For example, Zhu et al. (Zhu 2010) modified the toxic and highly transfection efficiency polymer poly (2-(N,N-dimethyl aminoethyl) methacrylate) P((DMAEMA) with poly(ε-caprolactone) (PCL) a biodegradable and biocompatible polymer. The resulting block co-polymer 2-(N,N-dimethyl aminoethyl) methacrylate-b- poly(ε-caprolactone)-b 2-(N,N-dimethyl aminoethyl) methacrylate (PDMAEMA–PCL–PDMAEMA) was assembled in biodegradable cationic micelles that had great transfection efficiency and biocompatibility.

5.6 DELIVERY TO MULTIDRUG-RESISTANT CANCERS

Multidrug resistance in cancer cells, a condition which accompanies metastatic cancer, is also responsible for a majority of cancer-related deaths and lack of potent treatment options [50]. Sequence-specific gene silencing has been explored extensively in this regard to favorably sensitize refractory cancer cells to conventional chemotherapy [120, 121]. A wide range of strategies have been developed for improving biodistribution of nanoparticles at the tumor site, however, recently, schemes to increase intracellular concentration of chemotherapeutics within multidrug resistant cancer cells is gaining importance. The advent of RNAi based therapeutics has led the charge in this area, by opening up otherwise insensitive cancer cells to the cytotoxic effects of chemotherapeutics. Especially because, multidrug resistance is manifested by

genetically engineering cancer cells to rapidly expel anti-cancer drugs that are subsequently recycled back into the bloodstream.

From a material design perspective, hyaluronan (HA), a major ligand of CD44 is a suitable active targeting ligand for most types of cancerous cells, as HA receptors are largely upregulated in these cells. As previously mentioned, HA also promotes long circulation owing to its non-immunogenicity and hydrophilicity. Cohen et al. have used HA-coated phospholipid nanoparticles to encapsulate DOX and PTX, both of which are substrates for P-gp receptors overexpressed in cancer cells [53]. They demonstrated increased cytotoxicity and reduced IC_{50} values in an NCI/ADR-Res ovarian cancer cell model that was derived by continuous exposure to increasing DOX concentrations in cell culture. Internalization of the ~500 nm drug loaded particles led to evasion of the drug efflux mechanism, and subsequent surge in intracellular DOX concentration in otherwise DOX-resistant cells.

In a recent study, Kim et al. surmounted two key challenges with one nanomedicine platform, by gaining access across the blood-brain barrier and sensitizing refractory glioblastoma cells to temozolomide (TMZ), which acts a substrate for the O^6 –methylguanine-DNA methyltransferase (MGMT) enzyme [54]. Incorporation of a wild-type p53 plasmid DNA within a cationic liposome, and separate administration of TMZ was shown to have appreciable cytotoxic effect in both in vitro and in vivo models.

Researchers seek to utilize the considerable surface area of carbon nanotubes (up to ~2600 m^2/g) and strong optical absorption leading to compatibility with photodynamic therapy, for the development of potent nanoformulations [122],[123]. It is evident that liposomes continue to be the nanomedicine of choice for cases requiring cellular uptake or gene therapy. To tackle this problem from another perspective, Bhirde et al. engineered a semiconducting single-walled

carbon nanotube (sSWCNT) drug delivery system that showed it is possible to achieve more effectiveness in killing cancer cells by wrapping nanoparticles with hyaluronic acid rather than PEG [57]. Cholanic acid-derivatized hyaluronic acid (CAHA) biopolymer is coated on sSWCNT to leverage the substantial affinity of hyaluronic acid to CD44 receptors that are over-expressed in metastatic cancer cells. The combined π- π stacking resulted in greater DOX encapsulation; while, rapid intracellular trafficking of CAHA-sSWCNTs occurs with ease owing to their small size (2-4 nm), especially in drug-resistant OVCAR8/ADR cells that overexpress CD44 receptors and tumor bearing mice xenograft models. Additionally, viscoelastic response of drug-resistant cancer cells was also analyzed to show that higher uptake with CAHA-sSWCNT caused an increase in energy dissipation, suggesting a decrease in the rigidity of refractory cells.

Choi and others investigated the role of Zn(II)-DPA and a Calcium Phosphate coating to load RNAi-based therapeutics to accompany small molecule drugs for sensitizing OVCAR8/ADR tumor cells in vitro and in vivo [58]. These dual-responsive nanoparticles were also coated with hyaluronic acid to establish tumor-specific biodistribution subsequent to intravenous administration. Their "nanoformula" is described as a versatile platform that can simultaneously deliver a wide range of therapeutics in one formulation.

Developing nanoformulations that can release multiple therapeutics holds tremendous potential for combination cancer therapy. One such approach, established by Liao and colleagues, orchestrated the loading and release of small molecule drugs encapsulated within the same nanoparticle in a precise, controlled manner. Although multidrug delivery approaches are typically limited by overlapping toxicity profile, these hurdles can be overcome by a judicious choice of drug solutes and their molar ratios within the same particle. Ensuring rational design of synthesis and encapsulation techniques is another challenge that needs to be addressed here. To

enable differential release of multiple drugs encapsulated within the same nanoparticles, Liao et al. prepared nanoscopic brush-arm star polymers (BASPs) using a ring-opening metathesis polymerization method (ROMP) [124]. Drug-macromonomer conjugates were developed to allow for improved solubility and responsiveness to environmental stimuli. To enable controlled release for each of the three drugs, drug conjugates were synthesized to respond to three different stimuli. DOX and CPT were conjugated to a PEGylated-norbornene macromonomer using a graft-through ROMP synthesis [125]. DOX conjugate were shown to respond to a photo-trigger such as long-wavelenght UV (UVA). Cisplatin was conjugated to Pt(IV) diester derivative that released the cytotoxic ingredient Pt(II) upon reduction in the presence of intracellular glutathione. Another method of linking camptothecin involved covalently conjugation to zwitterionic polyMPC (poly(methacryloyloxyethyl phosphorylcholine)) using an ATRP-"click" bioconjugation strategy. Herein, conjugation was achieved through an esteric linker that underwent hydrolysis in a manner dependent upon the length and steric hindrance around the linkage. The triple drug combination therapy demonstrated effectiveness against an otherwise camptothecin-resistant OVCAR3 (human ovarian carcinoma cell line).

Targeting the lysosomal cell death pathway is another premise that holds immense promise for nanomedicine-mediated treatment of multidrug resistant cancers and especially apoptosis-resistant cancers. In refractory cancers that resist apoptosis by conventional chemotherapy, lysosomal membrane permeabilization can stimulate release of cathepsins and proteolases, engendering cytosolic protein digestion and induction of apoptosis [61]. The obvious challenge is to specifically deliver to the subcellular target – lysosomes. In a recent investigation, Sanchez et al. accomplish induction of apoptosis and cell death by activation of the lysosomal death pathway by means of iron oxide nanoparticles grafted with peptidic ligands for

targeted delivery to cancer cells [62]. Functionalization of an iron oxide nanocrystal with gastrin, a peptidic ligand for the cholecystokinin-2 receptor (a G-protein couple receptor) resulted in strong binding and internalization of the composite nanoparticles. Unlike other magnetic stimuli-based approaches, cell death was incurred through lysosomal internalization subsequent to endocytosis instead of hyperthermia. The method demonstrated that particles accumulated within the lysosome induced cell death in HEK293 and CCKR2 over-expressing endocrine tumor cells upon application of an alternating magnetic field that possibly, triggered lysosomal membrane permeabilization and production of reactive oxygen species, leading to highly selective tumor cell demise.

5.7 CONCLUSION

Nanoscale therapeutics for cancer therapy represent a promising strategy to enhance therapeutic outcomes by reducing off-target side effects compared to intravenously administered chemotherapeutics. Polymer based nanotherapeutics have received the most attention from researchers, but there is a wealth of promising research on inorganic nanomaterials which is primarily focused upon photothermal therapy and co-delivery. With respect to the design of these systems, nanomaterials with a size on the order of 100nm of various morphologies have become the most prominent. The desired charge of the system depends largely on the application. Recently, increased attention has been focused on the development of cationic nanotherapetuics for the purpose of co-delivery of chemotherapeutics and interfering RNA. Surface functionalizations for many nanotherpaetuics has been primarily focused upon using PEG to enhance circulation time and thereby the localization of the nanomaterials to the tumor by the EPR effect. However, recent literature has shown that reliance solely on the EPR effect is insufficient for many nanotherapeutic to penetrate the tumor intersitium, and as a result the use

of active targeting agents has become increasingly compulsory. Finally, with the prominence of drug-resistant cancers, there is an increasing need to design therapeutic agents with the ability to sensitize or synergistically target cancerous cells over healthy cells to effectively reduce off-target effects.

5.8 REFERENCES

[1] Rao JP, Geckeler KE. Polymer nanoparticles: Preparation techniques and size-control parameters. Progress in Polymer Science 2011; 36:887-913.

[2] Matyjaszewski K. Atom Transfer Radical Polymerization (ATRP): Current Status and Future Perspectives. Macromolecules 2012; 45:4015-4039.

[3] Brannon-Peppas L, Blanchette JO. Nanoparticle and targeted systems for cancer therapy. Advanced Drug Delivery Reviews 2004; 56:1649-1659.

[4] Astete CE, Sabliov CM. Synthesis and characterization of PLGA nanoparticles. Journal of Biomaterials Science-Polymer Edition 2006; 17:247-289.

[5] Huang XH, El-Sayed IH, Qian W, El-Sayed MA. Cancer cell imaging and photothermal therapy in the near-infrared region by using gold nanorods. Journal of the American Chemical Society 2006; 128:2115-2120.

[6] Gupta AK, Gupta M. Synthesis and surface engineering of iron oxide nanoparticles for biomedical applications. Biomaterials 2005; 26:3995-4021.

[7] Li ZX, Barnes JC, Bosoy A, Stoddart JF, Zink JI. Mesoporous silica nanoparticles in biomedical applications. Chemical Society Reviews 2012; 41:2590-2605.

[8] Tang F, Li L, Chen D. Mesoporous Silica Nanoparticles: Synthesis, Biocompatibility and Drug Delivery. Advanced Materials 2012; 24:1504-1534.

[9] Vivero-Escoto JL, Slowing II, Trewyn BG, Lin VSY. Mesoporous Silica Nanoparticles for Intracellular Controlled Drug Delivery. Small 2010; 6:1952-1967.

[10] Kam NWS, O'Connell M, Wisdom JA, Dai HJ. Carbon nanotubes as multifunctional biological transporters and near-infrared agents for selective cancer cell destruction. Proceedings of the National Academy of Sciences of the United States of America 2005; 102:11600-11605.

[11] Liu Z, Robinson JT, Sun X, Dai H. PEGylated nanographene oxide for delivery of water-insoluble cancer drugs. Journal of the American Chemical Society 2008; 130:10876-+.

[12] Zheng MB, Yue CX, Ma YF, Gong P, Zhao PF, Zheng CF, Sheng ZH, Zhang PF, Wang ZH, Cai LT. Single-Step Assembly of DOX/ICG Loaded Lipid-Polymer Nanoparticles for Highly Effective Chemo-photothermal Combination Therapy. Acs Nano 2013; 7:2056-2067.

[13] Barua S, Yoo JW, Kolhar P, Wakankar A, Gokarn YR, Mitragotri S. Particle shape enhances specificity of antibody-displaying nanoparticles. Proceedings of the National Academy of Sciences of the United States of America 2013; 110:3270-3275.

[14] Jakubowski W, Min K, Matyjaszewski K. Activators regenerated by electron transfer for atom transfer radical polymerization of styrene. Macromolecules 2006; 39:39-45.

[15] Jakubowski W, Matyjaszewski K. Activators regenerated by electron transfer for atom-transfer radical polymerization of (meth)acrylates and related block copolymers. Angewandte Chemie-International Edition 2006; 45:4482-4486.

[16] Siegwart DJ, Oh JK, Matyjaszewski K. ATRP in the design of functional materials for biomedical applications. Progress in Polymer Science 2012; 37:18-37.

[17] Forbes DC, Creixell M, Frizzell H, Peppas NA. Polycationic nanoparticles synthesized using ARGET ATRP for drug delivery. European Journal of Pharmaceutics and Biopharmaceutics 2013; 84:472-478.

[18] Bao HQ, Pan YZ, Ping Y, Sahoo NG, Wu TF, Li L, Li J, Gan LH. Chitosan-Functionalized Graphene Oxide as a Nanocarrier for Drug and Gene Delivery. Small 2011; 7:1569-1578.

[19] Liu CX, Liu FX, Feng LX, Li M, Zhang J, Zhang N. The targeted co-delivery of DNA and doxorubicin to tumor cells via multifunctional PEI-PEG based nanoparticles. Biomaterials 2013; 34:2547-2564.

[20] Reddy ST, Rehor A, Schmoekel HG, Hubbell JA, Swartz MA. In vivo targeting of dendritic cells in lymph nodes with poly(propylene sulfide) nanoparticles. Journal of Controlled Release 2006; 112:26-34.

[21] Hawley AE, Davis SS, Illum L. TARGETING OF COLLOIDS TO LYMPH-NODES - INFLUENCE OF LYMPHATIC PHYSIOLOGY AND COLLOIDAL CHARACTERISTICS. Advanced Drug Delivery Reviews 1995; 17:129-148.

[22] Khullar OV, Griset AP, Gibbs-Strauss SL, Chirieac LR, Zubris KAV, Frangioni JV, Grinstaff MW, Colson YL. Nanoparticle Migration and Delivery of Paclitaxel to Regional Lymph Nodes in a Large Animal Model. Journal of the American College of Surgeons 2012; 214:328-337.

[23] Oussoren C, Zuidema J, Crommelin DJA, Storm G. Lymphatic uptake and biodistribution of liposomes after subcutaneous injection .2. Influence of liposomal size, lipid composition and lipid dose. Biochimica Et Biophysica Acta-Biomembranes 1997; 1328:261-272.

[24] Chen J-X, Zhang M, Liu W, Lu G-Z, Chen J-H. Construction of serum resistant micelles based on heparosan for targeted cancer therapy. Carbohydrate Polymers 2014; 110:135-141.

[25] Hatakeyama H, Akita H, Harashima H. A multifunctional envelope type nano device (MEND) for gene delivery to tumours based on the EPR effect: A strategy for overcoming the PEG dilemma. Advanced Drug Delivery Reviews 2011; 63:152-160.

[26] Moghimi SM, Hawley AE, Christy NM, Gray T, Illum L, Davis SS. SURFACE ENGINEERED NANOSPHERES WITH ENHANCED DRAINAGE INTO LYMPHATICS AND UPTAKE BY MACROPHAGES OF THE REGIONAL LYMPH-NODES. Febs Letters 1994; 344:25-30.

[27] Jain RK, Stylianopoulos T. Delivering nanomedicine to solid tumors. Nature Reviews Clinical Oncology 2010; 7:653-664.

[28] Zhu L, Wang T, Perche F, Taigind A, Torchilin VP. Enhanced anticancer activity of nanopreparation containing an MMP2-sensitive PEG-drug conjugate and cell-penetrating moiety. Proceedings of the National Academy of Sciences 2013; 110:17047-17052.

[29] Li J, Ge Z, Liu S. PEG-sheddable polyplex micelles as smart gene carriers based on MMP-cleavable peptide-linked block copolymers. Chemical Communications 2013; 49:6974-6976.

[30] Xu H, Deng Y, Chen D, Hong W, Lu Y, Dong X. Esterase-catalyzed dePEGylation of pH-sensitive vesicles modified with cleavable PEG-lipid derivatives. Journal of Controlled Release 2008; 130:238-245.

[31] Zhang JX, Zalipsky S, Mullah N, Pechar M, Allen TM. Pharmaco attributes of dioleoylphosphatidylethanolamine/cholesterylhemisuccinate liposomes containing different types of cleavable lipopolymers. Pharmacological Research 2004; 49:185-198.

[32] Shin J, Shum P, Thompson DH. Acid-triggered release via dePEGylation of DOPE liposomes containing acid-labile vinyl ether PEG–lipids. Journal of Controlled Release 2003; 91:187-200.

[33] Smith BR, Ghosn EEB, Rallapalli H, Prescher JA, Larson T, Herzenberg LA, Gambhir SS. Selective uptake of single-walled carbon nanotubes by circulating monocytes for enhanced tumour delivery. Nature Nanotechnology 2014; 9:481-487.

[34] Steichen SD, Caldorera-Moore M, Peppas NA. A review of current nanoparticle and targeting moieties for the delivery of cancer therapeutics. European Journal of Pharmaceutical Sciences 2013; 48:416-427.

[35] Accardo A, Tesauro D, Morelli G. Peptide-based targeting strategies for simultaneous imaging and therapy with nanovectors. Polymer Journal 2013; 45:481-493.

[36] Liu Q, Jin C, Wang Y, Fang X, Zhang X, Chen Z, Tan W. Aptamer-conjugated nanomaterials for specific cancer cell recognition and targeted cancer therapy. Npg Asia Materials 2014; 6.

[37] Liechty WB, Peppas NA. Expert opinion: Responsive polymer nanoparticles in cancer therapy. European Journal of Pharmaceutics and Biopharmaceutics 2012; 80:241-246.

[38] Kishimura A. Development of polyion complex vesicles (PICsomes) from block copolymers for biomedical applications. Polymer Journal 2013; 45:892-897.

[39] Nomoto T, Fukushima S, Kumagai M, Machitani K, Arnida, Matsumoto Y, Oba M, Miyata K, Osada K, Nishiyama N, Kataoka K. Three-layered polyplex micelle as a multifunctional nanocarrier platform for light-induced systemic gene transfer. Nat Commun 2014; 5.

[40] Synatschke CV, Nomoto T, Cabral H, Förtsch M, Toh K, Matsumoto Y, Miyazaki K, Hanisch A, Schacher FH, Kishimura A, Nishiyama N, Müller AHE, Kataoka K. Multicompartment Micelles with Adjustable Poly(ethylene glycol) Shell for Efficient in Vivo Photodynamic Therapy. ACS Nano 2014; 8:1161-1172.

[41] Chen K-J, Chaung E-Y, Wey S-P, Lin K-J, Cheng F, Lin C-C, Liu H-L, Tseng H-W, Liu C-P, Wei M-C, Liu C-M, Sung H-W. Hyperthermia-Mediated Local Drug Delivery by a Bubble-Generating Liposomal System for Tumor-Specific Chemotherapy. ACS Nano 2014; 8:5105-5115.

[42] Zhang Q, Jiang Q, Li N, Dai L, Liu Q, Song L, Wang J, Li Y, Tian J, Ding B, Du Y. DNA Origami as an In Vivo Drug Delivery Vehicle for Cancer Therapy. ACS Nano 2014; 8:6633-6643.

[43] Nguyen DX, Massague J. Genetic determinants of cancer metastasis. Nature Reviews Genetics 2007; 8:341-352.

[44] Schroeder A, Heller DA, Winslow MM, Dahlman JE, Pratt GW, Langer R, Jacks T, Anderson DG. Treating metastatic cancer with nanotechnology. Nature Reviews Cancer 2012; 12:39-50.

[45] Goldenberg NM, Steinberg BE. Surface Charge: A Key Determinant of Protein Localization and Function. Cancer Research 2010; 70:1277-1280.

[46] Wang X, Yang Y, Jia H, Jia W, Miller S, Bowman B, Feng J, Zhan F. Peptide decoration of nanovehicles to achieve active targeting and pathology-responsive cellular uptake for bone metastasis chemotherapy. Biomaterials Science 2014; 2:961-971.

[47] Ryan GM, Kaminskas LM, Porter CJH. Nano-chemotherapeutics: Maximising lymphatic drug exposure to improve the treatment of lymph-metastatic cancers. Journal of Controlled Release.

[48] Guo S, Lin CM, Xu Z, Miao L, Wang Y, Huang L. Co-delivery of Cisplatin and Rapamycin for Enhanced Anticancer Therapy through Synergistic Effects and Microenvironment Modulation. ACS Nano 2014; 8:4996-5009.

[49] Dahlman JE, Barnes C, Khan OF, Thiriot A, Jhunjunwala S, Shaw TE, Xing Y, Sager HB, Sahay G, Speciner L, Bader A, Bogorad RL, Yin H, Racie T, Dong Y, Jiang S, Seedorf D, Dave A, Sandhu KS, Webber MJ, Novobrantseva T, Ruda VM, Lytton-Jean AKR, Levins CG, Kalish B, Mudge DK, Perez M, Abezgauz L, Dutta P, Smith L, Charisse K, Kieran MW, Fitzgerald K, Nahrendorf M, Danino D, Tuder RM, von Andrian UH, Akinc A, Panigrahy D, Schroeder A, Koteliansky V, Langer R, Anderson DG. In vivo endothelial siRNA delivery using polymeric nanoparticles with low molecular weight. Nature Nanotechnology 2014; 9:648-655.

[50] Semple SC, Akinc A, Chen J, Sandhu AP, Mui BL, Cho CK, Sah DWY, Stebbing D, Crosley EJ, Yaworski E, Hafez IM, Dorkin JR, Qin J, Lam K, Rajeev KG, Wong KF, Jeffs LB,

Nechev L, Eisenhardt ML, Jayaraman M, Kazem M, Maier MA, Srinivasulu M, Weinstein MJ, Chen Q, Alvarez R, Barros SA, De S, Klimuk SK, Borland T, Kosovrasti V, Cantley WL, Tam YK, Manoharan M, Ciufolini MA, Tracy MA, de Fougerolles A, MacLachlan I, Cullis PR, Madden TD, Hope MJ. Rational design of cationic lipids for siRNA delivery. Nat Biotech 2010; 28:172-176.

[51] Hatakeyama H, Akita H, Kogure K, Oishi M, Nagasaki Y, Kihira Y, Ueno M, Kobayashi H, Kikuchi H, Harashima H. Development of a novel systemic gene delivery system for cancer therapy with a tumor-specific cleavable PEG-lipid. Gene Ther 2006; 14:68-77.

[52] Rivera-Gil P, De Koker S, De Geest BG, Parak WJ. Intracellular Processing of Proteins Mediated by Biodegradable Polyelectrolyte Capsules. Nano Letters 2009; 9:4398-4402.

[53] STACKER SA, BALDWIN ME, ACHEN MG. The role of tumor lymphangiogenesis in metastatic spread. The FASEB Journal 2002; 16:922-934.

[54] Folkman J. Tumor Angiogenesis: Therapeutic Implications. New England Journal of Medicine 1971; 285:1182-1186.

[55] Folkman J. Tumor Angiogenesis Factor. Cancer Research 1974; 34:2109-2113.

[56] Phelps EA, Garcia AJ. Update on therapeutic vascularization strategies. Regenerative Medicine 2008; 4:65-80.

[57] Folkman J. Role of angiogenesis in tumor growth and metastasis. Seminars in Oncology 2002; 29:15-18.

[58] Hanahan D, Folkman J. Patterns and Emerging Mechanisms of the Angiogenic Switch during Tumorigenesis. Cell 1996; 86:353-364.

[59] O'Reilly MS, Holmgren L, Shing Y, Chen C, Rosenthal RA, Moses M, Lane WS, Cao Y, Sage EH, Folkman J. Angiostatin: A novel angiogenesis inhibitor that mediates the suppression of metastases by a lewis lung carcinoma. Cell 1994; 79:315-328.

[60] Bergers G, Song S, Meyer-Morse N, Bergsland E, Hanahan D. Benefits of targeting both pericytes and endothelial cells in the tumor vasculature with kinase inhibitors. The Journal of Clinical Investigation 2003; 111:1287-1295.

[61] Bergers G, Coussens LM. Extrinsic regulators of epithelial tumor progression: metalloproteinases. Current Opinion in Genetics & Development 2000; 10:120-127.

[62] Berger AP, Kofler K, Bektic J, Rogatsch H, Steiner H, Bartsch G, Klocker H. Increased growth factor production in a human prostatic stromal cell culture model caused by hypoxia. The Prostate 2003; 57:57-65.

[63] Phng LK, Gerhardt H. Angiogenesis: a team effort coordinated by notch. Developmental cell 2009; 16:196-208.

[64] Stockmann C, Doedens A, Weidemann A, Zhang N, Takeda N, Greenberg JI, Cheresh DA, Johnson RS. Deletion of vascular endothelial growth factor in myeloid cells accelerates tumorigenesis. Nature 2008; 456:814-818.

[65] Lee S, Chen TT, Barber CL, Jordan MC, Murdock J, Desai S, Ferrara N, Nagy A, Roos KP, Iruela-Arispe ML. Autocrine VEGF signaling is required for vascular homeostasis. Cell 2007; 130:691-703.

[66] Fischer C, Mazzone M, Jonckx B, Carmeliet P. FLT1 and its ligands VEGFB and PlGF: drug targets for anti-angiogenic therapy? Nat Rev Cancer 2008; 8:942-956.

[67] Hagberg CE, Falkevall A, Wang X, Larsson E, Huusko J, Nilsson I, van Meeteren LA, Samen E, Lu L, Vanwildemeersch M, Klar J, Genove G, Pietras K, Stone-Elander S, Claesson-

Welsh L, Yla-Herttuala S, Lindahl P, Eriksson U. Vascular endothelial growth factor B controls endothelial fatty acid uptake. Nature 2010; 464:917-921.

[68] Tvorogov D, Anisimov A, Zheng W, Leppänen V-M, Tammela T, Laurinavicius S, Holnthoner W, Heloterä H, Holopainen T, Jeltsch M, Kalkkinen N, Lankinen H, Ojala PM, Alitalo K. Effective Suppression of Vascular Network Formation by Combination of Antibodies Blocking VEGFR Ligand Binding and Receptor Dimerization. Cancer Cell 2010; 18:630-640.

[69] Rolny C, Mazzone M, Tugues S, Laoui D, Johansson I, Coulon C, Squadrito ML, Segura I, Li X, Knevels E, Costa S, Vinckier S, Dresselaer T, Åkerud P, De Mol M, Salomäki H, Phillipson M, Wyns S, Larsson E, Buysschaert I, Botling J, Himmelreich U, Van Ginderachter JA, De Palma M, Dewerchin M, Claesson-Welsh L, Carmeliet P. HRG Inhibits Tumor Growth and Metastasis by Inducing Macrophage Polarization and Vessel Normalization through Downregulation of PlGF. Cancer Cell 2011; 19:31-44.

[70] Carmeliet P, Moons L, Luttun A, Vincenti V, Compernolle V, De Mol M, Wu Y, Bono F, Devy L, Beck H, Scholz D, Acker T, DiPalma T, Dewerchin M, Noel A, Stalmans I, Barra A, Blacher S, Vandendriessche T, Ponten A, Eriksson U, Plate KH, Foidart J-M, Schaper W, Charnock-Jones DS, Hicklin DJ, Herbert J-M, Collen D, Persico MG. Synergism between vascular endothelial growth factor and placental growth factor contributes to angiogenesis and plasma extravasation in pathological conditions. Nat Med 2001; 7:575-583.

[71] Duda DG, Jain RK. Premetastatic lung "niche": is vascular endothelial growth factor receptor 1 activation required? Cancer research 2010; 70:5670-5673.

[72] Kaplan RN, Riba RD, Zacharoulis S, Bramley AH, Vincent L, Costa C, MacDonald DD, Jin DK, Shido K, Kerns SA, Zhu Z, Hicklin D, Wu Y, Port JL, Altorki N, Port ER, Ruggero D,

Shmelkov SV, Jensen KK, Rafii S, Lyden D. VEGFR1-positive haematopoietic bone marrow progenitors initiate the pre-metastatic niche. Nature 2005; 438:820-827.

[73] Lichtenberger BM, Tan PK, Niederleithner H, Ferrara N, Petzelbauer P, Sibilia M. Autocrine VEGF Signaling Synergizes with EGFR in Tumor Cells to Promote Epithelial Cancer Development. Cell 2010; 140:268-279.

[74] Schwartz JD, Rowinsky EK, Youssoufian H, Pytowski B, Wu Y. Vascular endothelial growth factor receptor-1 in human cancer. Cancer 2010; 116:1027-1032.

[75] Buysschaert I, Schmidt T, Roncal C, Carmeliet P, Lambrechts D. Genetics, epigenetics and pharmaco-(epi)genomics in angiogenesis. Journal of cellular and molecular medicine 2008; 12:2533-2551.

[76] Jain RK, Duda DG, Willett CG, Sahani DV, Zhu AX, Loeffler JS, Batchelor TT, Sorensen AG. Biomarkers of response and resistance to antiangiogenic therapy. Nat Rev Clin Oncol 2009; 6:327-338.

[77] Lanahan AA, Hermans K, Claes F, Kerley-Hamilton JS, Zhuang ZW, Giordano FJ, Carmeliet P, Simons M. VEGF Receptor 2 Endocytic Trafficking Regulates Arterial Morphogenesis. Developmental cell 2010; 18:713-724.

[78] Tammela T, Alitalo K. Lymphangiogenesis: Molecular Mechanisms and Future Promise. Cell 140:460-476.

[79] Neufeld G, Kessler O. The semaphorins: versatile regulators of tumour progression and tumour angiogenesis. Nat Rev Cancer 2008; 8:632-645.

[80] Carmeliet P, Jain RK. Molecular mechanisms and clinical applications of angiogenesis. Nature 2011; 473:298-307.

[81] Cross MJ, Claesson-Welsh L. FGF and VEGF function in angiogenesis: signalling pathways, biological responses and therapeutic inhibition. Trends in Pharmacological Sciences 2001; 22:201-207.

[82] Presta M, Tiberio L, Rusnati M, Dell'Era P, Ragnotti G. Basic fibroblast growth factor requires a long-lasting activation of protein kinase C to induce cell proliferation in transformed fetal bovine aortic endothelial cells. Cell Regul 1991; 2:719-726.

[83] Otrock ZK, Mahfouz RA, Makarem JA, Shamseddine AI. Understanding the biology of angiogenesis: review of the most important molecular mechanisms. Blood cells, molecules & diseases 2007; 39:212-220.

[84] McNeil C. Two targets, one drug for new EGFR inhibitors. Journal of the National Cancer Institute 2006; 98:1102-1103.

[85] Lu P, Weaver VM, Werb Z. The extracellular matrix: a dynamic niche in cancer progression. The Journal of cell biology 2012; 196:395-406.

[86] Mouw JK, Ou G, Weaver VM. Extracellular matrix assembly: a multiscale deconstruction. Nat Rev Mol Cell Biol 2014; 15:771-785.

[87] DuFort CC, Paszek MJ, Weaver VM. Balancing forces: architectural control of mechanotransduction. Nat Rev Mol Cell Biol 2011; 12:308-319.

[88] Solon J, Kaya-Çopur A, Colombelli J, Brunner D. Pulsed Forces Timed by a Ratchet-like Mechanism Drive Directed Tissue Movement during Dorsal Closure. Cell 2009; 137:1331-1342.

[89] Davis GE, Senger DR. Endothelial extracellular matrix: biosynthesis, remodeling, and functions during vascular morphogenesis and neovessel stabilization. Circulation research 2005; 97:1093-1107.

[90] Newman AC, Nakatsu MN, Chou W, Gershon PD, Hughes CC. The requirement for fibroblasts in angiogenesis: fibroblast-derived matrix proteins are essential for endothelial cell lumen formation. Molecular biology of the cell 2011; 22:3791-3800.

[91] Genis L, Gonzalo P, Tutor AS, Galvez BG, Martinez-Ruiz A, Zaragoza C, Lamas S, Tryggvason K, Apte SS, Arroyo AG. Functional interplay between endothelial nitric oxide synthase and membrane type 1 matrix metalloproteinase in migrating endothelial cells. Blood 2007; 110:2916-2923.

[92] Hynes RO. The Extracellular Matrix: Not Just Pretty Fibrils. Science 2009; 326:1216-1219.

[93] Hodivala-Dilke KM, Reynolds AR, Reynolds LE. Integrins in angiogenesis: multitalented molecules in a balancing act. Cell and tissue research 2003; 314:131-144.

[94] Garmy-Susini B, Jin H, Zhu Y, Sung RJ, Hwang R, Varner J. Integrin alpha4beta1-VCAM-1-mediated adhesion between endothelial and mural cells is required for blood vessel maturation. The Journal of clinical investigation 2005; 115:1542-1551.

[95] Schlessinger J. Cell Signaling by Receptor Tyrosine Kinases. Cell 2000; 103:211-225.

[96] Bogdan S, Klämbt C. Epidermal growth factor receptor signaling. Current Biology 2001; 11:R292-R295.

[97] Hicklin DJ, Witte L, Zhu Z, Liao F, Wu Y, Li Y, Bohlen P. Monoclonal antibody strategies to block angiogenesis. Drug discovery today 2001; 6:517-528.

[98] Ferrara N. Role of vascular endothelial growth factor in the regulation of angiogenesis. Kidney international 1999; 56:794-814.

[99] Kerbel RS, Viloria-Petit A, Klement G, Rak J. 'Accidental' anti-angiogenic drugs. anti-oncogene directed signal transduction inhibitors and conventional chemotherapeutic agents as examples. European journal of cancer (Oxford, England : 1990) 2000; 36:1248-1257.

[100] Reilly JF, Maher PA. Importin beta-mediated nuclear import of fibroblast growth factor receptor: role in cell proliferation. The Journal of cell biology 2001; 152:1307-1312.

[101] Brooks PC, Montgomery AMP, Rosenfeld M, Reisfeld RA, Hu T, Klier G, Cheresh DA.

[102] Brooks PC, Str, xF, mblad S, Klemke R, Visscher D, Sarkar FH, Cheresh DA.

[103] Liao F, Doody JF, Overholser J, Finnerty B, Bassi R, Wu Y, Dejana E, Kussie P, Bohlen P, Hicklin DJ. Selective Targeting of Angiogenic Tumor Vasculature by Vascular Endothelial-cadherin Antibody Inhibits Tumor Growth without Affecting Vascular Permeability. Cancer research 2002; 62:2567-2575.

[104] Boder ET, Jiang W. Engineering antibodies for cancer therapy. Annual review of chemical and biomolecular engineering 2011; 2:53-75.

[105] Ruoslahti E, Pierschbacher MD. New perspectives in cell adhesion: RGD and integrins. Science 1987; 238:491-497.

[106] Pasqualini R, Koivunen E, Ruoslahti E. Alpha v integrins as receptors for tumor targeting by circulating ligands. Nature biotechnology 1997; 15:542-546.

[107] Buerkle MA, Pahernik SA, Sutter A, Jonczyk A, Messmer K, Dellian M. Inhibition of the alpha-[nu] integrins with a cyclic RGD peptide impairs angiogenesis, growth and metastasis of solid tumours in vivo. Br J Cancer 2002; 86:788-795.

[108] Famulok M, Mayer G. Aptamers as tools in molecular biology and immunology.

[109] Osborne SE, Matsumura I, Ellington AD. Aptamers as therapeutic and diagnostic reagents: problems and prospects. Current opinion in chemical biology 1997; 1:5-9.

[110] Jellinek D, Green LS, Bell C, Lynott CK, Gill N, Vargeese C, Kirschenheuter G, McGee DPC, Abesinghe P. Potent 2'-Amino-2'-deoxypyrimidine RNA Inhibitors of Basic Fibroblast Growth Factor. Biochemistry 1995; 34:11363-11372.

[111] Persano L, Crescenzi M, Indraccolo S. Anti-angiogenic gene therapy of cancer: Current status and future prospects. Molecular Aspects of Medicine 2007; 28:87-114.

[112] Sudhakar A, Sugimoto H, Yang C, Lively J, Zeisberg M, Kalluri R. Human tumstatin and human endostatin exhibit distinct antiangiogenic activities mediated by alpha v beta 3 and alpha 5 beta 1 integrins. Proceedings of the National Academy of Sciences of the United States of America 2003; 100:4766-4771.

[113] Hynes RO, Lively JC, McCarty JH, Taverna D, Francis SE, Hodivala-Dilke K, Xiao Q. The diverse roles of integrins and their ligands in angiogenesis. Cold Spring Harbor symposia on quantitative biology 2002; 67:143-153.

[114] Kim S, Bell K, Mousa SA, Varner JA. Regulation of angiogenesis in vivo by ligation of integrin alpha5beta1 with the central cell-binding domain of fibronectin. The American journal of pathology 2000; 156:1345-1362.

[115] Burnett John C, Rossi John J. RNA-Based Therapeutics: Current Progress and Future Prospects. Chemistry & Biology 2012; 19:60-71.

[116] Chen S-H, Zhaori G. Potential clinical applications of siRNA technique: benefits and limitations. European Journal of Clinical Investigation 2011; 41:221-232.

[117] Liu D, Liu F Fau - Liu Z, Liu Z Fau - Wang L, Wang L Fau - Zhang N, Zhang N. Tumor specific delivery and therapy by double-targeted nanostructured lipid carriers with anti-VEGFR-2 antibody.

[118] Sengupta S, Eavarone D, Capila I, Zhao G, Watson N, Kiziltepe T, Sasisekharan R. Temporal targeting of tumour cells and neovasculature with a nanoscale delivery system. Nature 2005; 436:568-572.

[119] Sheikpranbabu S, Kalishwaralal K Fau - Venkataraman D, Venkataraman D Fau - Eom SH, Eom Sh Fau - Park J, Park J Fau - Gurunathan S, Gurunathan S. Silver nanoparticles inhibit VEGF-and IL-1beta-induced vascular permeability via Src dependent pathway in porcine retinal endothelial cells.

[120] Elbashir SM, Harborth J, Lendeckel W, Yalcin A, Weber K, Tuschl T. Duplexes of 21-nucleotide RNAs mediate RNA interference in cultured mammalian cells. Nature 2001; 411:494-498.

[121] de Fougerolles A, Vornlocher H-P, Maraganore J, Lieberman J. Interfering with disease: a progress report on siRNA-based therapeutics. Nature Reviews Drug Discovery 2007; 6:443-453.

[122] Bianco A, Kostarelos K, Prato M. Opportunities and challenges of carbon-based nanomaterials for cancer therapy. Expert Opinion on Drug Delivery 2008; 5:331-342.

[123] Liu Z, Chen K, Davis C, Sherlock S, Cao Q, Chen X, Dai H. Drug delivery with carbon nanotubes for in vivo cancer treatment. Cancer Research 2008; 68:6652-6660.

[124] Liao L, Liu J, Dreaden EC, Morton SW, Shopsowitz KE, Hammond PT, Johnson JA. A Convergent Synthetic Platform for Single-Nanoparticle Combination Cancer Therapy: Ratiometric Loading and Controlled Release of Cisplatin, Doxorubicin, and Camptothecin. Journal of the American Chemical Society 2014; 136:5896-5899.

[125] Johnson JA, Lu YY, Burts AO, Xia Y, Durrell AC, Tirrell DA, Grubbs RH. Drug-Loaded, Bivalent-Bottle-Brush Polymers by Graft-through ROMP. Macromolecules 2010; 43:10326-10335.

Chapter 6: Synthesis and Characterization of pH-Responsive Nanoscale Hydrogels for Oral Delivery of Hydrophobic Therapeutics

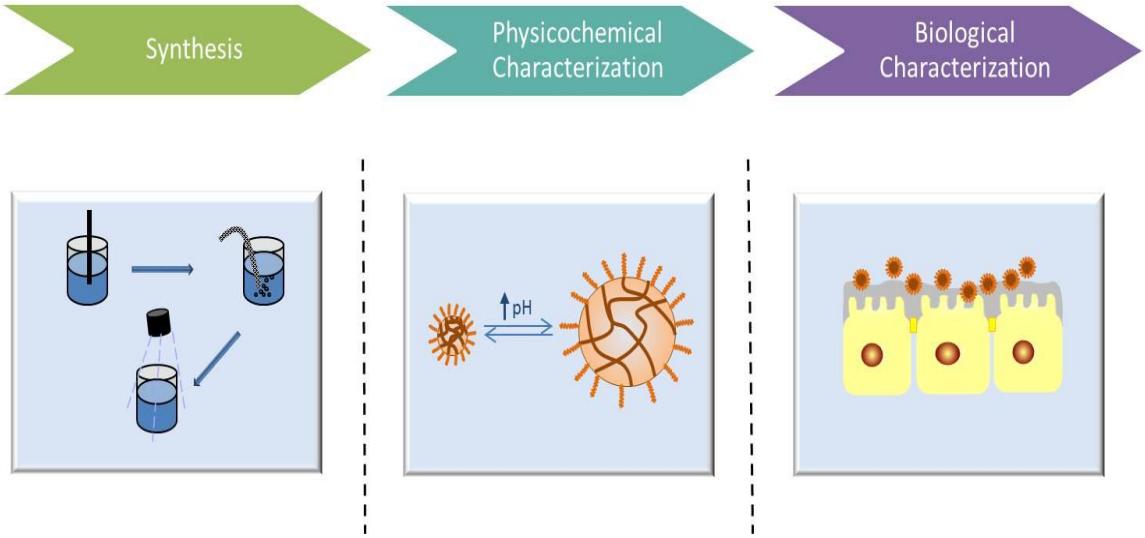

- Nanoscale hydrogels were synthesized for oral delivery of hydrophobic therapeutics
- Interplay exists between factors such as selection of hydrophobic monomer component of and physicochemical and biological characteristics providing a basis for optimization
- Physicochemical characterization of hydrogels was conducted to analyze and compare swelling properties and cellular cytotoxicity, alongside validation of composition using FTIR and NMR.
- Other relevant properties such as mucoadhesion and uptake by macrophages were also considered

6.1 INTRODUCTION

Oral delivery of hydrophobic therapeutics using polymer-based nanomaterials relies on the rational design of carriers with respect to size, charge, and surface properties so that they can effectively mediate diverse physicochemical and physiological barriers encountered in the gastrointestinal (GI) tract [1]. An expansive review of current technologies and drug delivery carriers used to orally deliver hydrophobic drugs, as described in Chapter 4, connotes several desirable particle-design features, including the presence of a lipophilic element that associates preferentially with the payload. Other performance criteria expected involve releasing the drug at the location of the small intestine, improved mucoadhesiveness to allow more time for the drug to cross over from the gastrointestinal lumen into the small intestine and finally, the ability to inhibit efflux pumps on intestinal enterocytes that recycle such drugs back into the lumen. Making carriers that meet these touchstones will improve bioavailability of hydrophobic drugs by increasing their solubility and permeability subsequent to oral intake.

We have proposed the development of nanoscale, polyanionic, pH responsive hydrogel system to overcome the physicochemical and physiological challenges of delivering hydrophobic drugs orally so as to ensure release at the site of the small intestine and facilitate transport of the hydrophobic drug across the intestinal epithelium. Stimuli-responsive hydrogels that can respond to pH changes in order to realize controlled drug release in the GI tract have been reviewed by Sharpe et al. [2]. Such pH responsive polymeric networks are designed with the aim of retaining the drug during passage through the stomach, and releasing the drug only at the site of the small intestine. Because these hydrogels contain acidic pendant groups that ionize at pH values higher than the pKa of the acid, and the subsequent ionic repulsion between the negatively charged groups leads results in swelling of the hydrogel. The polyanionic hydrogel system, shown in

Figure 3, will consist of a backbone comprised of a copolymer of methacrylic acid (MAA) and a hydrophobic monomer.

Modifying the copolymer composition to tailor polymer properties has been widely examined for a variety of biomedical applications [3-6]. In the present study, a set of four different formulations was developed using a diverse hydrophobic monomer each time. The four hydrophobic monomers selected are tert-butyl methacrylate (t-BMA), n-butyl methacrylate (nBMA), n-butyl acrylate (nBA) and methyl methacrylate (MMA). The hydrophobic monomer will form a lipophilic core that can associate preferentially with hydrophobic drugs. The copolymer backbone will be grafted with poly(ethylene glycol) tethers that confer colloidal stability to the nanoparticles in solution and also facilitate hydrogen bonding in the collapsed state in the stomach. Similarly, the presence of PEG tethers on the nanoparticle surface is believed to modulate biocompatibility and even promote mucoadhesion [7]. More importantly, PEG tethers of different molecular weights have been reported to play a role in the inhibition of efflux pumps that regulate the transport of hydrophobic drugs on the apical side of the small intestine [8]. The use of nano-sized hydrogels instead of micro-sized is believed to enhance the dissolution rate of the non-covalently linked drug owing to a higher surface area-to-volume ratio. Moreover, it has been suggested that, in order to diffuse “against” a mucus layer that is continuously being secreted or cleared, and accumulate at the intestinal epithelium in large proportions to release drugs, the size of the particles should be less than 500 nm [9].

The emulsion polymerization technique used to synthesize the nanoscale hydrogels allowed for a panel of formulations to be developed with different hydrophobic monomer components (t-BMA, n-BMA, n-BA, and MMA) in the feed. Photoemulsion polymerization conditions and relative feed monomer ratios were kept constant across the set of four formulation

variants containing different hydrophobic monomers. Formulations were evaluated for criteria commonly identified as metrics for effective oral delivery of hydrophobic drugs, such as *in vitro* cytocompatibility to intestinal epithelium model and other physicochemical characteristics, capacity for drug loading and release at *in vitro* conditions mimicking site of the intestinal epithelium within timelines relevant to the GI tract emptying and absorption (described in Chapter 7), and finally apical-to-basal transport of the drug across an *in vitro* intestinal cell model (described in Chapter 8).

The method of synthesis and purification employed in the production of nanoscale drug delivery system for controlled release is directly influenced by the nature and size of the drug to be encapsulated, the nature of comprising monomers and final polymer to be produced, mode of administration, and expected duration of drug release typically dictated by desired therapeutic range. Within each facile synthesis method, numerous parameters can be varied to yield nanoparticles that satisfy pharmacological requirements. Design parameters that affect polymeric nanoparticle physicochemical and biological properties, drug encapsulation efficiency, and drug release rate include polymer type and molecular weight, composition of copolymers, cross linking density, drug loading concentrations, type of solvent, types of surfactants, and other reaction conditions such as pH, temperature, concentration [10]. Finally, the response of polymeric nanoparticles to environmental stimuli can also be modulated to achieve favorable responses for the specific drug delivery application by tuning material properties. Material properties affecting the *in vitro*, *in vivo*, and clinical response of the nanoparticles broadly encompass physicochemical properties such as the particle size and size distribution, particle shape and surface morphology, surface chemistry and biological interactions, colloidal stability,

drug encapsulation efficiency, surface/bulk erosion/degradation, cell cytocompatibility, hemodynamic properties, and diffusion/permeability/kinetics of drug release.

Here, we present the synthesis of polymeric nanoparticles for the oral delivery of hydrophobic therapeutics. Interplay between hydrophilic monomer-hydrophobic monomer composition, and the resultant particle properties provides a basis for optimization of these nanoparticles, with the overarching goal of obtaining a favorable response to the environment these particles may be exposed to upon oral administration. For the specific application of oral delivery, it is required that the polymer nanoparticle retain the encapsulated drug as it traverses through the stomach, and that the drug be released only at the site of oral absorption i.e. the small intestine. The chief environmental condition that changes as a drug carrier travels through the stomach into the small intestine is the pH of the surrounding milieu, as it changes from a pH of ~ 2 (fasted stomach) to a pH 6.1 (small intestine). Consequently, it is expected that a cross linked hydrogel nanoparticle remain collapsed within the stomach (thereby retaining the drug) and swell only in the intestine (thus, releasing the drug at the site of absorption), as shown schematically in Figure 6.1. Another response that can be tuned is the rate at which entrapped drug diffuses out of the cross linked hydrogel. Keeping this function in mind, interplay between parameters such as polymer hydrophobic composition and cross linking density, and the resulting particle swelling response and drug encapsulation/release efficiency provides a strong basis to optimize our formulation.

6.2 PHYSICOCHEMICAL CHARACTERIZATION: MATERIALS AND METHODS

Blanchette and Peppas [11] previously investigated P(MAA-g-EG) hydrogel nanoparticles for their ability to deliver the cancer therapeutic bleomycin, which is a relatively hydrophilic drug freely soluble in water. However, the P(MAA-g-EG) nanoscale hydrogels did

not have a hydrophobic component that could associate well with hydrophobic drugs. As a result, P(MAA-g-EG) nanoparticles may be unsuitable for the purpose of delivering extremely lipophilic drugs such as doxorubicin. In this thesis, we propose the development of nanoscale hydrogel with a hydrophobic component that can preferentially associate with hydrophobic drugs. We have chosen methacrylate based hydrophobic monomers that have previously demonstrated success at forming non-covalent associations with lipophilic molecules. Inclusion of hydrophobic monomer components or hydrophobic moieties is believed to favorably impact drug loading and release by preferentially associating with the hydrophobic drug, and there are increasing reports of such a strategy for improving efficacy of intravenously administered nanoscale approaches for anticancer drug delivery [12-14]. Modulating polymer composition and the resulting polymer-solvent interactions can also affect critical phenomena involving polymer phase transitions; various reports provide examples of changes in temperature/pH at which phase transitions occur in response to varying polymer composition [15-17]. In this chapter, we describe the synthesis of these formulations using a photoemulsion polymerization method and examine the impact of changing the hydrophobic monomer component on the physicochemical and biological properties of the nanoscale formulations.

6.2.1 Synthesis of Polyanionic Nanoscale Hydrogel Systems

To synthesize the nanoscale hydrogels, we have adapted a UV-initiated free radical polymerization method developed in our lab [11]. Nanoscale polyanionic hydrogels were synthesized by UV-initiated free radical polymerization of a pre-polymer solution mixture. The pre-polymer mixture was comprised of monomers - methacrylic acid (MAA), tert-butyl methacrylate (t-BMA) or other hydrophobic monomer, poly(ethylene glycol) monomethyl ether methacrylate (PEGMMA) (molecular weight ~ 2080), and cross linking agent tetraethylene

glycol dimethacrylate (TEGDMA) at 1% mole fraction of total monomer amount. The surfactants sodium dodecyl sulfate and Brij-30® were then added to the system followed by Irgacure 2959 at 0.5 wt% of total monomer. For the formulation including methyl methacrylate as the hydrophobic monomer, sodium dodecyl sulfate was the only surfactant used as the use of Brij-30® led to destabilization of the emulsion. The mixture was mixed and emulsified using a Misonix sonicator for 10 minutes. Nitrogen was bubbled into the mixture for 20 minutes to eliminate any oxygen that may scavenge free radicals participating in the polymerization. Finally, polymerization was initiated with a Dymax BlueWave® 200 UV (Dymax, Torrington, CT) point source for 2.5 hours at 100 mW/cm^2 , with emulsion constantly stirring.

After polymerization, the polymeric nanoparticles were first completely swollen by addition of 1N NaOH, followed by precipitation and extraction using acetone. Purification to eliminate any residual monomers was carried out by alternate washes with 0.5 N NaOH and acetone, followed by centrifugation. The polymeric nanoparticles were then dialyzed against water for 14 days to elute any more surfactants or monomers that may be present from the polymerization process. Finally, the nanoscale hydrogels were freeze-dried/lyophilized and stored in a desiccator until further use.

Using this method, four different formulations were developed. The four formulations are as follows (with unique hydrophobic monomer component emboldened):

1. Poly (Methacrylic acid-g-poly(ethylene glycol)-co-**tert-butyl methacrylate**) or P(MAA-g-PEG-co-**tBMA**)
2. Poly (Methacrylic acid-g-poly(ethylene glycol)-co-**n-butyl methacrylate**) or P(MAA-g-PEG-co-**nBMA**)
3. Poly (Methacrylic acid-g-poly(ethylene glycol)-co-**n-butyl acrylate**) or

P(MAA-g-PEG-co-**nBA**)

4. Poly (Methacrylic acid-g-poly(ethylene glycol)-co-**methyl methacrylate**) or P(MAA-g-PEG-co-**MMA**)

Structures of the monomers used in the emulsion polymerization procedure and the four hydrophobic monomers are shown in Figure 6.2 and Figure 6.3 respectively.

After synthesis of P(MAA-co-tBMA-g-PEG), the cross linking density of the hydrogel was increased to 2% and 5% of the total monomer mole fraction. Increased cross linking density of the hydrogel offers greater resistance to swelling forces, causing an increase in the pH at which the formulation swells. This may be advantageous for ensuring that the hydrogel nanoparticles swell at a later stage (small intestine) of their GI tract transit. Similarly, changing the hydrophobic monomer content may also play a role in shifting the critical swelling pH. However, preliminary studies conducted with these increased cross linking densities suggested that increasing cross linking density of these nanoparticle formulations does not have a significant impact on physicochemical properties. For instance, it was observed that the variation in swelling behavior was not significant for increase in cross linking density from 1% to 2% of total monomer mole fraction, as shown in appendix A. Hence, for the present study, cross linking density was maintained at 1% of total monomer and focus is on observing trends across formulations containing a different hydrophobic monomer.

6.2.2 Dynamic Light Scattering Studies

The swelling behavior of P(MAA-co-tBMA-gPEG) nanoparticles is a key aspect that would characteristic of their success in responding to the contrasting pH conditions found in the stomach as opposed to the small intestine. Dynamic swelling responses exhibited by these nanoscale hydrogel formulations were studied using dynamic light scattering (DLS) at different

pH conditions. Dynamic light scattering (DLS) measurements were taken using a Malvern Zetasizer Nano ZS to determine the size and zeta potential of the nanoparticles as the pH of the solution changed.

Dynamic light scattering was used to measure the size of the nanoscale hydrogels and evaluate their swelling response to changes in pH. An aqueous suspension of the nanoparticles was prepared by resuspending lyophilized nanoparticles in 1X PBS at a concentration of 0.5 mg/ml. The DLS measurements and z-average particle diameters were collected using a Malvern Zetasizer NanoZS (Malvern Instruments, Malvern, UK). The measurements were obtained at 25^{o}C using a 633 nm laser source. The swelling response to dynamic pH was observed by varying the pH from 4.0 to 7.0 at intervals of 0.5 through the facility of a MPT-2 Autotitrator.
Samples were prepared by suspending freeze-dried nanoscale particles at a concentration of 0.5 mg/ml in 1X Phosphate Buffered Saline (PBS). Dynamic light scattering measurements were taken at increments of 0.5 pH units over the range of pH 4 (acidic, characteristic of conditions in the stomach) to pH 7 (neutral, characteristic of conditions in the small instestine). Each sample was measured with n=3 and the procedure repeated for three formulations, each possessing a different hydrophobic monomer in the polymer. Size measurements at different pH points shed light onto the swelling behavior of particles and the influence of the hydrophobic monomer on the overall swelling ability of the particles.

6.2.3 Zeta Potential Measurements

Zeta potential is an indicator of the magnitude of the polymer surface charge and is also representative of their colloidal stability. Surface zeta potential values were measured using the Malvern Zetasizer NanoZS (Malvern Instruments, Malvern, UK). Lyophilized samples were resuspended in 1X PBS (pH 7.4) and transferred into a disposable capillary cell (DTS1070) to be used with the Malvern Zetasizer NanoZS for zeta potential measurement. Electrophoretic light scattering measurements of the surface ζ-potential were collected at 25°C with nanoscale

hydrogels. Changes to the surface zeta potential were determined by varying the pH from 4.0 to 7.0 at intervals of 0.5 using a MPT-2 autotitrator.

6.2.4 Scanning Electron Microscopy

Nanoscale hydrogels were imaged using a FEI Quanta 650 FEG scanning electron microscope. Prior to imaging, freeze dried nanoparticles were suspended in ultrapure DI water and dropped onto carbon-tape covered aluminum stubs. A 12 nm Pt/Pd coating was applied to the prepared stub samples using a Cressington 208 Benchtop sputter coater. Scanning electron microscopy images were obtained using an FEI Quanta 650 FEG scanning electron microscope.

6.2.5 Fourier Transform Infrared Spectroscopy

Fourier Transform Infrared Spectroscopy was used to elucidate subtle differences in copolymer composition by comparing characteristic infrared bands of the four nanoparticle formulations. All nanoparticles were investigated using a Thermo Mattson Infinity Gold® spectrometer (Thermo Fisher Scientific, Waltham, MA). The characteristic infrared spectra were acquired by pressing freeze dried nanoparticle powder (~ 5 mg) into 195 mg KBr (Sigma-Aldrich) disks. In all cases, sample spectra were analyzed subsequent to subtracting background KBr (~ 200 mg) spectra.

6.2.6 ^{1}H-NMR Spectroscopy

^{1}H-NMR spectra were obtained to examine the composition of uncrosslinked polymer formulations using a Varian (Palo Alto, CA) DirectDrive 400 MHz nuclear magnetic resonance spectrometer fitted with an automatic sampler. Deuterium oxide (D_2O, 99.9%) was purchased from Cambridge Isotope Laboratories (Andover, MA). Prior to using the spectrometer, all relevant glassware, including NMR tubes (Wilmad Lab Glass, Vineland, NJ), Pasteur pipettes, and 3 mL sample vials were dried overnight in a vacuum oven. Freeze-dried polymer nanoparticle samples of approximately 25 mg were first weighed out directly in sample vials and

1 mL D_2O was added to achieve a final concentration of 25mg mL^{-1}. To ensure uniform dispersion of the sample in D_2O, sample solutions were sonicated in an ultrasound bath, and then transferred to NMR tubes for spectrometry. SpinWorks 3 ™ software was used to analyze the ^{1}H-NMR spectra.

6.2.6 Differential Scanning Calorimetry

Differential Scanning Calorimetry (DSC) is often performed on polymeric materials to uncover information regarding the thermal properties of the polymer by subjecting samples to a thermal cycle of heating and cooling, and gain further insight into the molecular make of the polymer. We obtained DSC thermograms for the set of four nanoparticle formulations that we have synthesized with the same hydrophilic monomers, but different hydrophobic monomers. We investigate the thermal transition temperatures across the set of nanoparticle formulations using a differential scanning calorimeter (Mettler-Toledo DSC1). For calorimetry, about 10 mg of sample of each polymer formulation was loaded tightly into an aluminum DSC pan equipped with a lid comprising a 0.1 mm hole. Prior to thermal cycling, we thoroughly dry the sample in a vacuum oven at a temperature of about 60^{o}C. Then, any reminiscent thermal history associated with the sample is removed by annealing the sample at 130^{o}C. Subsequent to annealing, we cool the samples from 130^{o}C to -65^{o}C before heating the samples to 150^{o}C. A heating rate of 10^{o}C/min and a 5^{o}C/min cooling rate were employed to operate the thermal cycles under a nitrogen gas atmosphere.

For obtaining the second set of DSC thermograms, we used about 5 mg of sample of each polymer nanoparticle formulation that was first loaded into an aluminum pan and dried by ramping up the temperature at 20^{o}C/min to 120^{o}C in a Thermogravimetric Analysis (TGA) equipment (TGA Q500, TA Instruments, Delaware, US), followed by isothermal heating at 120^{o}C to allow for removal of any moisture content. Once dried, the sample was subjected to a

heat-cool-heat cycle in a differential scanning calorimeter (DSC Q2000, TA Instruments, Delaware, US). For the first heating cycle, temperature was ramped up to 200^{o}C at a heating rate of 10^{o}C/min, followed by a cooling cycle at the rate of 10^{o}C/min to 10^{o}C. For the final heating cycle, temperature was raised once again from 10^{o}C to 200^{o}C at a rate of 10^{o}C/min. All the cycles were operated under a nitrogen gas atmosphere.

6.3 BIOLOGICAL CHARACTERIZATION: MATERIALS AND METHODS

In addition to evaluating physicochemical properties, it is crucial to understand the behavior of these nanoscale hydrogels in the presence of cells that may be encountered during the course of their drug delivery function in the GI tract. Importantly, the cytocompatibility of the polymer formulations in the presence of an intestinal cell layer model was determined *in vitro* using two different, commercially available assays. The [3-[4,5-dimethylthiazol-2-yl]-5-(3-carboxymethoxyphenyl)-2-(4-sulfophenyl)-2H-tetrazolium] (MTS) assay evaluates cellular proliferation of the intestinal cell model, while the lactate dehydrogenase (LDH) assay investigates the plasma membrane integrity of the intestinal cell model.

6.3.1 Cellular Cytocompatibility using MTS Assay

Cytocompatibility of the nanoscale hydrogel systems was evaluated by incubation with the Caco-2 human colon adenocarcinoma cells. The Caco-2 cells are popular as a model intestinal epithelial cell line.

To conduct the cytotoxicity studies, aforementioned cells were incubated with the particles for periods of two hours, in order to better simulate the time spent by the nanoparticles within the small intestine. A CellTiter 96® Aqueous One Solution Cell Proliferation Assay (Promega Corp., Madison, WI) will be used to measure cell proliferation. Cell proliferation greater than 80% is indicative of better tolerance of the cells to the polymeric nanoparticles.

Cytotoxicity studies were carried out for the four formulations with different hydrophobic monomer components, namely, P(MAA-g-PEG-co-tBMA), P(MAA-g-PEG-co-nBMA), P(MAA-g-PEG-co-nBA), and P(MAA-g-PEG-co-MMA). Each formulation was incubated with the Caco-2 monolayer at concentrations ranging from 4 mg/ml to 0.008 mg/ml. Nanoscale hydrogel formulations were added at 10 different concentrations ranging from 4 mg/mL to 0.008 mg/ml in culture medium. The negative control was a 3% (v/v) bleach solution in culture medium and the positive control was culture medium. After incubation with particles for 2 hours, the particle solution was vacuum aspirated and the cells were rinsed with culture medium once to ensure removal of particles. The cells were then incubated with the MTS assay solution for 2 hours. Subsequent to incubation with the assay solution, the absorbance of the supernatant was measured at 490 nm using a Bio-Tek Synergy™ HT multi-mode plate reader (Winooski, VT). Background absorbance measured at 690 nm was subtracted from the values to account influence from bubbles, cell debris or other anomalies.

6.3.2 Cellular Cytocompatibility using LDH Assay

A CytoTox-ONE™ Homogeneous Membrane Integrity Assay (Promega Corp., Madison, WI) was used to determine release of lactate dehydrogenase (LDH) from cells that underwent membrane damage subsequent to nanoparticle exposure. Caco-2 cells were seeded into 96-well black, fluorescence-measurement compatible plates, and polymer solutions added in aforementioned fashion. Polymer formulations were incubated with the cells for a 2 hour time period at 37^{o}C in congruence with the incubation time for the MTS assay, and roughly time potentially spent by the particles in the small intestine prior to mucocilliary clearance. The CytoTox™ Reagent solution was then added and fluorescent measurements at 530 ex/590 em taken after 10 mins of incubation with reagent solution.

6.3.2 Mucoadhesion and Macrophage Uptake

6.3.2.1 Mucoadhesion

Biological response and interaction of newly developed biomaterials with components of the GI tract can play a role in determining their fate as oral delivery agents [18]. Enterocytes and the mucus layer covering these intestinal cells can play a role in governing outcomes related to oral drug delivery system, in addition to regulating absorption and distribution of drugs. Cytotoxicity studies with Caco-2 cells are a measure of the interactions of the particles with the intestinal epithelial layer, while mucoadhesive studies help ascertain how the polymeric system interacts with the mucosal layer covering the epithelial cells. Bioavailability of hydrophobic drugs may be improved by fortifying interactions of nanoparticles with the intestinal mucosa and this interaction depends on a number of factors such as electrostatic interactions, hydrogen bonding, van der Waals interactions and even polymer chain penetration [19]. A strong interaction with the mucosa permits the nanoparticle to reside for longer times in the GI tract, thereby allowing most of the loaded drug to release and cross the intestinal epithelial layer [7].

Mucoadhesive studies with nanoparticles were completed using a Q-Sense E4 system (BiolinScientific/Q Sense, Sweden) that characterizes surfaces by quantifying mass and structural changes to molecules and films at the interface. Firstly, mucin was deposited on an oscillating quartz plate, whose frequency and energy dissipation is monitored by a quartz crystal microbalance (QCM-D). 1X PBS solution (without any polymeric nanoparticles) was then pumped through the system for 20 min as a control to reference the frequency and energy dissipation of the oscillating plate. A solution of hydrogel nanoparticles was then pumped through the same system for another 20 min. This solution was prepared by suspending freeze dried nanoparticles in 1X PBS.

6.3.2.1 Uptake by Macrophages

Another parameter that could potentially be of relevance in oral delivery considerations is the uptake of nanoparticles by intestinal M cells. M cells comprise 1% of the 200 m^2 intestinal surface area orally delivered nanoparticles may potentially encounter. As a result, the probability of uptake by M cells is quite low, but cannot be ruled out owing to the size of the nanoparticles. Uptake by M cells can lead the nanoparticles into the Peyer's patches, allowing for contact with antigen-sampling cells/macrophages [20]. As a result, it is relevant to observe the uptake of nanoparticles by macrophages to note if there is a strong chance of losing nanoparticles to the intestinal lymph nodes. From a molecular design perspective, it is reasonable to assume that polyanionic nanoparticles may be excluded from most cells owing to their negative charge. However, it has been noted that addition of hydrophobic moieties can lead to some cellular uptake.

To assess if our polyanionic nanoparticles are uptaken by macrophages, we use confocal microscopy to provide insight regarding internalization, and compare it against polycationic nanoparticles designed for cellular uptake. For the study, 1 mg/ml fluorescently tagged nanoparticles were incubated with RAW264.7 cells for 2 h. Experimental conditions and image acquisition and processing settings for both polyanionic and polycationic nanoparticle uptake study were kept consistent to compare internalization by RAW 264.7 cells. Minimal uptake by macrophages can also imply lower uptake by most other cells, since macrophages are typically more prone to uptake of nanoparticles [21].

6.4 PHYSICOCHEMICAL CHARACTERIZATION: RESULTS AND DISCUSSION

6.4.1 Synthesis of Polyanionic Nanoscale Hydrogel Systems

We use an emulsion polymerization method to prepare the nanoscale hydrogels for oral delivery of hydrophobic therapeutics. Preparation of the nanoparticles by a UV-initiated free radical polymerization is presented by a schematic diagram in Figure. The surfactant plays an important role by stabilizing and solubilizing the hydrophobic monomer through interactions with the nonpolar ends formed within the interior of the surfactant micelles. Water-soluble initiators stimulate chain growth at the polar, hydrophilic surface of the micelle confronting the solvent i.e. water. The polymerization reaction propagates and continues inside the micelle as more and more monomer droplets from the exterior aqueous solution enter the interior of the micelle upon depletion of monomer droplets already present inside. As with any free radical reaction, the polymerization process continues until it is terminated by other free radicals. In the case of a UV-initiated free radical oil-in-water emulsion polymerization technique, the nanoparticle formation and physicochemical properties is affected by the monomer concentration, stirring speed/sonication intensity for emulsification, surfactant/stabilizer type and concentration and duration/conversion of reaction. All other parameters remaining constant, changing the monomer concentration will directly influence the nanoparticle properties such as size, molecular mass, and degree of cross linking/rigidity. In this chapter, we synthesize a panel of nanoparticles containing four different hydrophobic monomers and investigate the effect on the physicochemical properties that deserve priority for oral application – namely, size and swelling response with variation of the surrounding pH, and cell cytocompatibility in the presence of an intestinal epithelial cell model. Another important property that is investigated is the hydrophobic therapeutic loading and release, and is covered in chapter 7 [22]. A combination of FTIR and NMR was used to validate the presence of functional groups and monomers in the four polymer formulations.

One way to modify core hydrophobicity of the nanoscale hydrogels is by changing the hydrophobic monomer itself. N-butyl acrylate (n-BA) and n-butyl methacrylate (n-BMA) have been studied extensively for their ability to demonstrate preferential association with lipophilic drugs as hydrophobic core components of block copolymer micelles and even hydrogels [23-25]. N-butyl acrylate is highly hydrophobic but has a lower reactivity ratio for methacrylic acid copolymers, implying greater presence of methacrylic acid in the random copolymer formed. An indirect implication of increasing the hydrophobicity of polymeric systems can be increased cytotoxicity [26]. In fact, n-butyl acrylate and n-butyl methacrylate have demonstrated significant hemolytic activity and cytotoxicity in biological membranes owing to their ability to induce injurious changes in the lipid bilayers of living cells and disrupting functionality of membrane-bound proteins [27]. Intuitively, n-butyl acrylate has even been used to coat coronary stents and induce death among smooth muscle cells with the aim of preventing restenosis [28]. As a result, an optimization of factors such as cytotoxicity (which gets top priority) and drug loading and release kinetics will eventually provide the rationale for our choice of the hydrophobic monomer in the oral delivery of lipophilic agents. Cytotoxicity of these formulations has been evaluated in Section 6.3.

An extensively employed method to theoretically predict and speculate the composition of the final polymer nanoparticle is the use of reactivity ratios, which requires Q and e values for the different monomers [29, 30]. Q and e values for the different monomers employed in synthesis, and the corresponding reactivity ratios are shown in Table 6.1 and Table 6.2 respectively. Reactivity ratio for each monomer in the copolymer was calculated assuming negligible PEG concentration since PEG is present at < 3 mol %, and thereby assuming the final

formulation to be a copolymer of hydrophilic monomer and hydrophobic monomer, instead of a terpolymer.

Reactivity ratios are given by the following equations:

$$r_1 = \frac{Q_1}{Q_2} \exp[-e_{1(}e_1 - e_{2)}] \quad (1)$$

$$r_2 = \frac{Q_2}{Q_1} \exp[-e_{2(}e_2 - e_{1)}] \quad (2)$$

6.4.2 Dynamic Light Scattering Studies

The pH responsive behavior of the particles is as shown in figure . All four formulations exhibited a critical swelling pH around pH 4.9, and underwent a size and volume phase transition to a swollen state. For the P(MAA-co-tBMA-g-PEG) nanoparticles with 1% crosslinker, the size of the particles, represented by the z-average diameter in the measurements, increased from 80 nm to around 120 nm, as the pH of the buffer increased from 4 to 8 (Figure 6.4). We next investigated the P(MAA-g-PEG-co-nBMA) nanoparticle formulation for their swelling response to changing pH, and observed a size change from about 85 nm in the collapsed state to 115 nm in the fully swollen state (Figure 6.5). The P(MAA-g-PEG-co-nBA) formulation possessed a diameter of size approximately 125 nm at the lower pHs as shown in Figure 6.6, and a diameter of 171 nm at pH 7.5 representative of the small intestinal pH. Interestingly, the P(MAA-g-PEG-co-MMA) nanoparticle formulation underwent the largest size change from a mean z-average diameter of 277.3 nm to 472.3 nm at pH 7.5 (Figure 6.7). Incorporating MMA into the polymer network resulted in a dramatic size change of the formulation, in addition to having a marked effect on the pH-responsive size change as can be seen when swelling behavior of all formulations is shown together in Figure 6.8. All samples also demonstrated increased aggregation at pH values lower than the 4, perhaps due to the lack of ionic repulsion (since the carboxylic acid anionic groups are protonated below the pKa of 4.8-4.9) to counter the forces

driving the nanoparticles out of an aqueous solution (since the nanoparticles have a hydrophobic core).

6.4.2 Zeta Potential Measurements

Zeta potential measurements for all four formulations are shown in table. The zeta potential measurement values for all the formulations lie in the range of -17.5 to 20 mV at pH 7.5 (Figure 6.9). As the pH was lowered, the zeta potential values increased with decreasing pH as can be expected due to protonation of the anionic charges on the carboxylic acid groups of the polymer network. All formulations except the P(MAA-g-PEG-co-MMA) collapsed out of solution before the zeta potential reached a perfectly neutral value, as can be anticipated based on the aggregation of these particles previously observed at a pH lower than the pKa of methacrylic acid.

The negative surface charge on the polymer nanoparticles can be attributed to the carboxylic acid groups on the polymer core surface/polymer backbone. One way of reducing particle size is to increase concentration of surfactant/stabilizing agent such as Pluronic F68 [31]. Similarly, PEG chains grafted to the core polymer surface allow for steric stabilization leading to the formation a stable, aqueous dispersion. Interestingly, surfactants/stabilizing agents used during the emulsion polymerization process can remain associated with the surface of the nanoparticles even after repeated washing. Residual surfactants affect the zeta potential of the resulting nanoparticles in a manner that is related to the charge of the surfactants themselves. For instance, neutral PVA based surfactants mask the negative charge associated with carboxylic acid groups on the polymer core, while anionic surfactants can reinforce the charge leading to a higher zeta potential [32]. Similarly, neutrally-charged, grafted PEG can mask negative charge associated with carboxylic acid groups giving a net neutral charge to the particles, which is desirable for intravenously administered particles that might otherwise by uptaken by macrophages. Increasing PEG density and length can also increase the zeta potential from

negative to zero [33] however in this case, for the application of oral delivery, a negative surface charge at pH 7 is ideal for desirable pH-responsive behavior.

6.4.3 Scanning Electron Microscopy

The micrographs in Figure 6.10 help us visualize the nanoparticles. One caveat of using SEM is that the polymeric nanoparticles are subjected to vacuum and considerable electronic charging, leading to poorer resolution and conditions dissimilar to the pH 4-7 aqueous solutions used for sizing by DLS. As a result, the SEM images may be more of a suggestive measure of consistency in morphology than particle size itself. Particle size and swelling behavior are more crucial to the determination of optimal characteristics for use in oral delivery of hydrophobic therapeutics, and we primarily use dynamic light scattering and zeta potential measurements to substantiate these crucial properties.

6.4.4 Fourier Transform Infrared Spectroscopy

The infrared spectrum of all formulations is shown in Figure 6.15. As can be expected, the infrared spectra are not on a single nanoparticle level owing to resolution limitations of infrared radiation. However, the IR spectra can reveal information of the formulation on a broader, microscopic scale representative of a group or collection of nanoscopic elements, and we qualitatively look at trends in information regarding bond formation across the panel of formulations. A recent report by Tress et al. experimentally illustrates using broadband dielectric spectroscopy that properties arising from glassy dynamics of polymer chains are bulk-like to the extent of 0.5 nm, a size characteristic of near isolated polymer chains [34]. Since the carbonyl groups are present in each formulation, broad spectral bands at about 1760 cm^{-1} suggesting the presence of carboxylic acid groups can be observed in the carbonyl stretching region (Figures 6.11- 6.14). Similarly, spectral bands that were common to all nanoparticle formulations also

include the ester linkage belonging to the acrylate groups in the 1760 – 1665 cm^{-1}. In this case, peaks at 1714.4 and 1658.5 show absorption of about 86-88% (or transmittance of 12-14%). The concurrence of bands in the 1760-1690 regions and the 3500-3200 cm^{-1} confirm the presence of carboxylic acid groups and esters. Similarly, the O-H stretch band can be seen in the 3500-3200 cm^{-1} is representative of hydrogen bonding. PEG has characteristic strong absorption peaks arising from the C-H and C-O stretching vibrations detected in all the polymer formulations. Given the presence of alkane groups (nBMA, nBA, tBMA, and MMA) we can also observe –C-H stretching vibrations in the range of 3000 and 2800 cm^{-1}. Interesting to note is the presence of –C-H- bending vibrations in the 1500-1300 cm^{-1} range that can be seen for MMA and tBMA owing to the absence of a long hydrocarbon side chain and the umbrella deformation peak from the tert-butyl group at 1370 cm^{-1} [35].

6.4.5 ^{1}H-NMR Spectroscopy

Inclusion of monomers in the polymerization was also verified using NMR. Investigation of NMR spectra was conducted using linear polymer chains of each formulations synthesized using the same UV-initiated photopolymerization method, however, broadening of some peaks suggest the presence of physical crosslinks that may have formed between the linear chains. The most prominent peak (δ=3.55 ppm) can be attributed to the incorporation of PEG grafts into the all the polymer chains (Figures 6.16 to 6.19). Inclusion of grafted PEG as demonstrated by the PEG oxyethylene protons indicates the presence of a surface brush of solvated PEG chains in D_2O. As previously stated, PEG grafted to the polymer surface, is an important constituent of our formulations owing to its role played in favorable biocompatibility, colloidal stability, possible inhibition of P-glycoprotein efflux pumps, and improved mucoadhesion; and is most solvated by the D_2O and prominently detected by the solution-state NMR spectroscope. In the case of

P(MAA-g-PEG-co-tBMA), inclusion of tert-butyl methacrylate is ascribed to the presence of the tert-butyl group (-C-$(CH_3)_3$-, δ=1.305 ppm), i.e. the alkyl side group of the alkoxy moiety of the methacrylate. The methyl/methylene group (-CH_2- or –CH_2-CH_2-) that dominates the polymer chain backbone of all nanoscopic formulations is ubiquitous across all spectra from Fig. at δ=0.8-0.9 ppm. In the spectra for P(MAA-g-PEG-co-nBMA), downfield proton peaks at δ=1.37 ppm and δ=1.67 ppm are indicative of the presence of hydrogens belonging to the n-butyl group of the alkoxy moiety. Broadening of these peaks in the P(MAA-g-PEG-co-nBMA) can be the artifact of poor incorporation of n-butyl acrylate in the polymer chain owing to the affinity of methacrylic acid to react with itself in an ideal free radical copolymerization reaction between MAA and nBA. Inclusion of the protons belonging to the group closest to the electronegative oxygen of the alkoxy moiety consistently present in all formulations can be seen further downfield at δ~3.2 ppm, especially in the case of the P(MAA-g-PEG-co-MMA) spectrum which lacks other notable peak assignments and corresponding protons in its molecular structure. Approximate experimental quantification of the constituent monomers in the actual crosslinked polymer formulations is possible can be further pursued by means of solid state NMR spectroscopy.

6.4.6 Differential Scanning Calorimetry

Differential Scanning Calorimetry (DSC) was performed on polymeric materials to uncover information regarding the thermal properties of the polymer by subjecting samples to a thermal cycle of heating and cooling. This method can help gain further insight into the molecular make of the polymer. The DSC thermograms are shown in Figure with transition temperatures annotated on the charts. In the thermograms, the most important transition we see is the glass transition temperature. The UV-initiated photopolymerization method employed is a

random, free radical polymerization method and is consistent with the blunter glass transition observed. The P(MAA-g-PEG-co-tBMA) formulation has the highest glass transition temperature and sharpest decline, a characteristic that has previously been observed with polymer networks containing tBMA (Figure 6.20) [36].

In the second set of DSC thermograms (Figures 6.21 to 6.24), melting endotherms in all formulations are observed at a temperature of and can be attributed to the melting of crystallites formed by segregation of PEG chains or grafts present in the copolymer. These PEG crystallites may especially be an artifact of the random copolymerization method used to synthesize the nanoparticle formulations leading to a more heterogeneous distribution of PEG chains, or result from crystal growth introduced during the drying method employed to eliminate the presence of moisture in the sample. Introduction of crystallinity can reduce the extent of enthalpic relaxation and restrict chain mobility leading to lower glass transition temperatures [37]. It is worthwhile to note that the melting endotherm for PEG-crystallites is at a temperature lower than that of the PEGMA polymer observed at 58^{o}C, since this is a copolymer rather than a PEG homopolymer [36, 38]. The broad endotherm at a temperature of is the melting point (T_m), subsequent to which, the sample possibly solidifies from the melt to a glassy amorphous state upon cooling, given that the melting point endotherm peak is absent in the second heating cycle. Both the lower glass transition temperature and the melting point are consistent with those observed for PEG-based copolymers [39].

To obtain an estimate of the degree of crystallinity, X_c, for the copolymer as the ratio of PEG crystallites to the total amount of PEG in the copolymer, we use the following equation, with heat of melting for PEG homopolymer, $\Delta H^0_{m,PEG} = 200\, J/g$, and are summarized in Table 6.3.

$$X_c = \frac{\Delta H_{m,copolymer}}{\Delta H^0_{m,PEG}} \times \frac{1}{\frac{m_{PEG}}{m_{copolymer}}} \quad (3)$$

The TGA curves (Figures 6.25 to 6.28) enable observation of the degradation rate of the polymer formulations upon exposure to high temperatures in air and nitrogen. This stability may be relevant if the polymer nanoparticle formulations are undergo processing strategies occasionally used in the pharmaceutical industry such as hot melt extrusion or even sterilization procedures.

6.5 BIOLOGICAL CHARACTERIZATION: RESULTS AND DISCUSSION

6.5.1 Cellular Cytocompatibility using MTS assay

To ensure that interaction of the polymer formulations with epithelial cells is not unfavorable, we ascertain a couple of key indicators of good cell health- cell proliferation and cytotoxicity. The MTS assay was used to measure and quantify the percentage of cells undergoing proliferation subsequent to incubation with the synthesized formulations. In our case, the assay was performed with Caco-2 cells, an intestinal epithelial cell monolayer model, which was incubated with each of the four nanoparticle formulations for a period of two hours.

Methods commonly used to assess cell health include determination of cellular proliferation and cell viability. Overall cell viability can be governed by the integrity of cell membranes, redox potential of the cell population or the functionality/ activity of crucial cell enzymes [40-42]. Quantitative assays representing viability of whole cell populations are generally conducted using microplate assays. Cell viability is closely associated with cell metabolic activity, and hence, high cellular reduction potential owing to mitochondrial hydrogenases that utilize NADH for reduction, is a key metric that is symptomatic of healthy, viable and proliferating cells. The MTS assay (Promega Corp., Madison, WI) probes the

reducing power of a live cell population, generating a signal that is proportionate to the amount of colored reporter and redox reaction product- formazan. Alternatively, the redox indicator resazurin signals presence of metabolic activity when it gets converted to the fluorescent and colorimetric molecule resorufin (alamarBlue®). Relative cellular proliferation based on absorbance values is calculated and normalized using the equation,

$$Relative\ cellular\ proliferation = {(A_{sample} - A_{negative\ control})}\Big/{(A_{positive\ control} - A_{negative\ control})}$$

Results (Figures 6.29 to 6.32) demonstrate that cellular incubation with the formulation resulted in no adverse cytotoxic events, and in almost all conditions mean cellular proliferation of the live cell population was above the threshold of 80%, implying 80% of the cells continued undergoing cellular proliferation with no residual effects from nanoparticle incubation. There are no significant trends across the formulations suggesting that changing the hydrophobic monomer incorporated within a polyanionic network may not greatly impact its cytotoxic effects on *in vitro* intestinal cell models for the duration of the study.

6.5.2 Cellular Cytocompatibility using LDH assay

Appraisal of cell viability independent of metabolic activity can be achieved by determining cell membrane permeability. Loss of membrane permeability is compelling evidence of cell death, additionally acting as an indicator of cytotoxicity. Lactate dehydrogenase (LDH) release is a common indicator of cell membrane damage and can be detected using an enzymatic assay that converts resazurin into resorufin subsequent to LDH release [43]. To quantify LDH release in our *in vitro* intestinal cell model upon nanoparticle incubation, the CytoTox-ONE™ assay (Promega Corp., Madison, WI) was employed to measure LDH release from damaged cells by

detecting resorufin fluorescence. Relative cellular viability based on fluorescence values is calculated and normalized using the equation,

$$Relative\ cellular\ viability = {(A_{sample} - A_{backgrd})}\Big/{(A_{\max LDH\ release} - A_{backgrd})}$$

Results (Figures 6.33 to 6.36) demonstrate that cellular incubation with the formulations resulted in no adverse cytotoxic events, and in almost all conditions membrane integrity and thus, cellular viability of the live cell population was above the threshold of 80%, implying 80% of the cells underwent no damage or residual effects from nanoparticle incubation. There are no significant trends across the formulations suggesting that changing the hydrophobic monomer incorporated within a polyanionic network may not greatly impact its cytotoxic effects on *in vitro* intestinal cell models for the duration of the study.

Other methods exist to determine if membrane integrity has been compromised involves staining cell DNA with DNA-binding fluorescent dyes that are cell-impermeant (enter only lysed cells) and fluoresce only upon binding to the nucleus. A step further, would be to compare viability levels in different cells within a population, by measuring reduction potential and esterase activity of live cells and complementing it with DNA binding data. This can be done by using two probes- for instance, one cell-impermeant probe that will undergo fluorescence excitation in dead cells, and another metabolic activity/reduction potential indicator that will clearly differentiate dead cells from live cells in a given population. However, the LDH assay is superior for applications involving quantification of cytocompatibility of polyanionic nanoparticles, while others may be more relevant for polycationinc nanoparticles intended for endosomal escape.

Since the combination of cellular proliferation and cell viability did not reveal any major cytocompatibility-related adverse effects of polymer nanoparticles on in vitro cell models, we conclude that the nanoparticle formulations are suitable for further in vitro studies with intestinal cell models.

6.5.3 Mucoadhesion Studies and Uptake of Nanoparticles by Macrophages

6.5.3.1 Mucoadhesion Studies

Hanes and group have previously demonstrated and extensively reviewed that PEGylation of nanoparticles in the size range of 100-500 nm can lead to a dramatic increase in their transport through intestinal mucus [44]. Transport through mucus trends linearly with an increase in PEGylation density. In this study, we tested our PEGylated formulation for its mucoadhesiveness. Similarly, another *in vivo* study demonstrated that nanoparticle engineered with low molecular weight PEG display good mucoadhesion. Nanoparticles with a hydrophobic core were also shown to exhibit mucoadhesiveness [45]. Formulations synthesized in this work, sport a number of properties that have previously been shown to promote mucoadhesion, including but not limited to appropriate size range, surface charge, PEGylation, and presence of a hydrophobic core. Here, we perform a proof-of-concept study to validate mucoadhesion.

Mucoadhesive interactions with the immobilized mucin were found to be substantial for a nanoparticle concentration of 0.5 mg/ml, whereas a concentration of 0.001 mg/ml showed no conclusive mucoadhesive response (Figure 6.37 (a)). At a concentration of 0.5 mg/ml, the nanoparticles adhered to the mucin on the oscillating quartz plate. As a result of this increase in mass adhering to the oscillating plate, there was a decrease in the frequency with which the plate was oscillating (Figure 6.37 (b)). Consequently, an increase in the mass and thickness of viscoelastic material on the plate surface (Figures 6.38 (a) and 6.38 (b)), led to an increase in the

energy dissipation of the oscillating plate. This can be explained by the fact that polymeric nanoparticles, being viscoelastic, are able to absorb (and thus, dissipate) the vibrational mechanical energy of the oscillating quartz plate, thereby displaying a considerable increase in the net energy dissipated.

6.5.3.2 Uptake of Nanoparticles by Macrophages

M cells account for a very small amount of total surface area of the GI tract (1% of total intestinal surface, and 5% of human follicle-associated epithelium), and nanoparticle transport by M cells for various applications such as vaccine and therapeutic delivery into Peyer's patches has remained elusive. In our case, transcytosis/phagocytosis by intestinal M cells is undesirable, since we have designed our nanoparticles to release drug at the site of the intestinal lumen, and subsequently be cleared through the GI tract. Nanoparticle uptake by M cells is largely unlikely owing to the lower amount of M cells present in the small intestine, and M cell targeting agents have been studied [46]. The approach we described for our uptake study, investigated in vitro uptake of our nanoparticles by macrophages to assess potential M-cell phaogyctotic uptake of the nanoparticle formulation. The optimum size prescribed for particle uptake by M cells is about 100 nm [20].

Confocal microscopy was used to observe internalization of the polyanionic nanoparticle formulation. Representative images are shown in Figures 6.39 to 6.42. We observe internalization of fluorescently tagged polyanionic nanoparticles in RAW 264.7 cells. Diffuse stain seen closer to the cell periphery indicates minimal uptake if any, and non-homogeneous distribution of the particles as compared with to the polycationic nanoparticle uptake study conducted separately as a reference.

6.6 CONCLUSIONS

pH-responsive, nanoscale hydrogels were developed and characterized to screen for optimal physicochemical properties for the goal of delivering hydrophobic therapeutics. Composition of the copolymer was varied by incorporating four different hydrophobic monomers, namely, tBMA, nBMA, nBA, and MMA. A combination of ^{1}H-NMR and FTIR was used to verify the copolymer composition. All four nanoparticle formulations underwent a transition in size in response to an increase in pH from 4 to 7.5 as measured by dynamic light scattering measurements. While the commencement of swelling begins at a pH of around 4.9 for all formulations, the formulations undergo size transitions that are diverse in magnitude, with the formulaiton containing MMA undergoing the largest size and volume phase transition. Depending upon the hydrophobic monomer incorporated within the polymer network, the size of the formulations ranged from about 100-500 nm at pH 7. Despite considerable changes in swelling properties with a change in the hydrophobic monomer, all formulations displayed appreciable cytocompatibility in the presence of an *in vitro* intestinal cell model. By displaying amenable physicochemical properties and agreeable cytocompatibility, the pH-responsive nanocarriers thus, exhibited the key characteristics expected from a potential oral drug delivery system.

Table 6.1 – Q, e values of monomer components

Monomer	**e**	**Q**
methacrylic acid (MAA)	0.65	2.34
tert-butyl methacrylate	-0.35	1.18
n-butyl acrylate	1.06	0.5
n-butyl methacrylate	-0.23	0.72
methyl methacrylate	0.40	0.74

Table 6.2 – Reactivity ratios for Methacrylic acid (designated as 1) and comonomers used in polymerization

Copolymer (1/2)	r_1	r_2	$r_1 r_2$
MAA/tBMA	1.035	0.355	0.3674
MAA/n-BA	6.109	0.1384	0.8454
MAA/n-BMA	1.834	0.2513	0.4609
MAA/MMA	2.6877	0.3495	0.9394

Table 6.3 – Ratio of crystalline PEG to total PEG in the nanoparticle formulations.

No.	Formulation	X_c
1	P(MAA-co-tBMA-g-PEG)	0.0097
2	P(MAA-co-nBMA-g-PEG)	0.0023
3	P(MAA-co-nBA-g-PEG)	0.0072
4	P(MAA-co-MMA-g-PEG)	0.0098

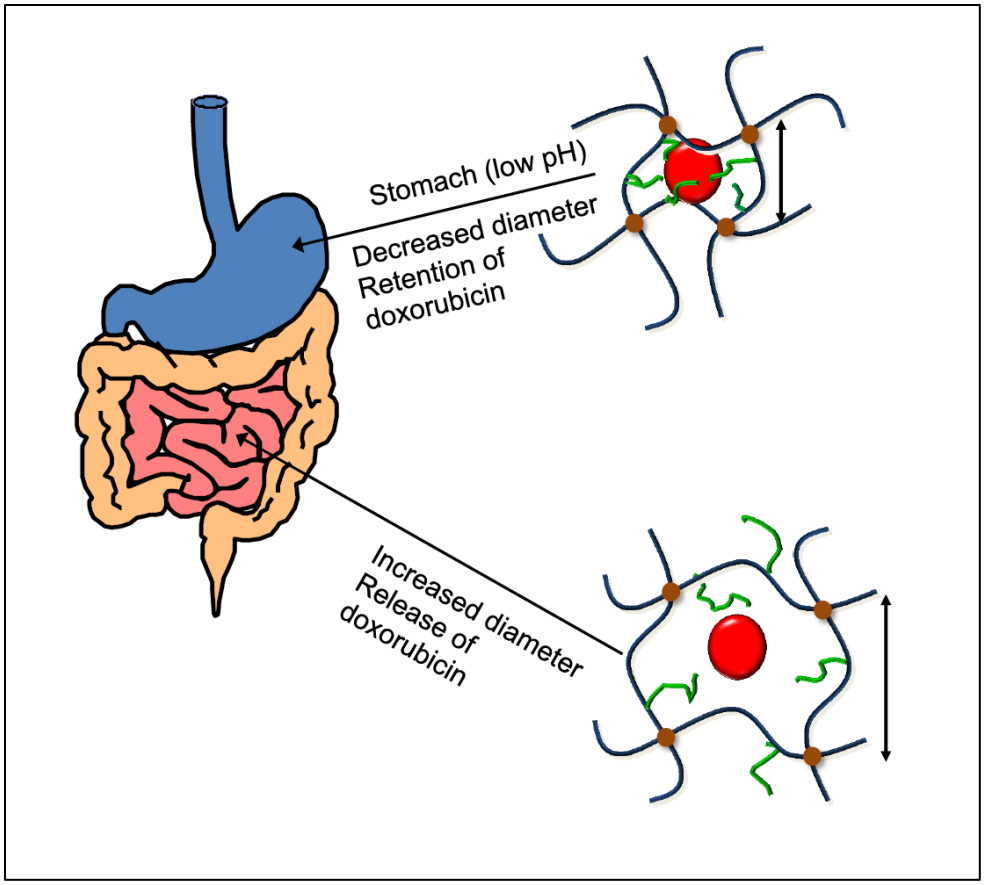

Figure 6.1 – Schematic of the swelling behavior and drug release from a pH-responsive hydrogel for the oral delivery of doxorubicin, a hydrophobic therapeutic.

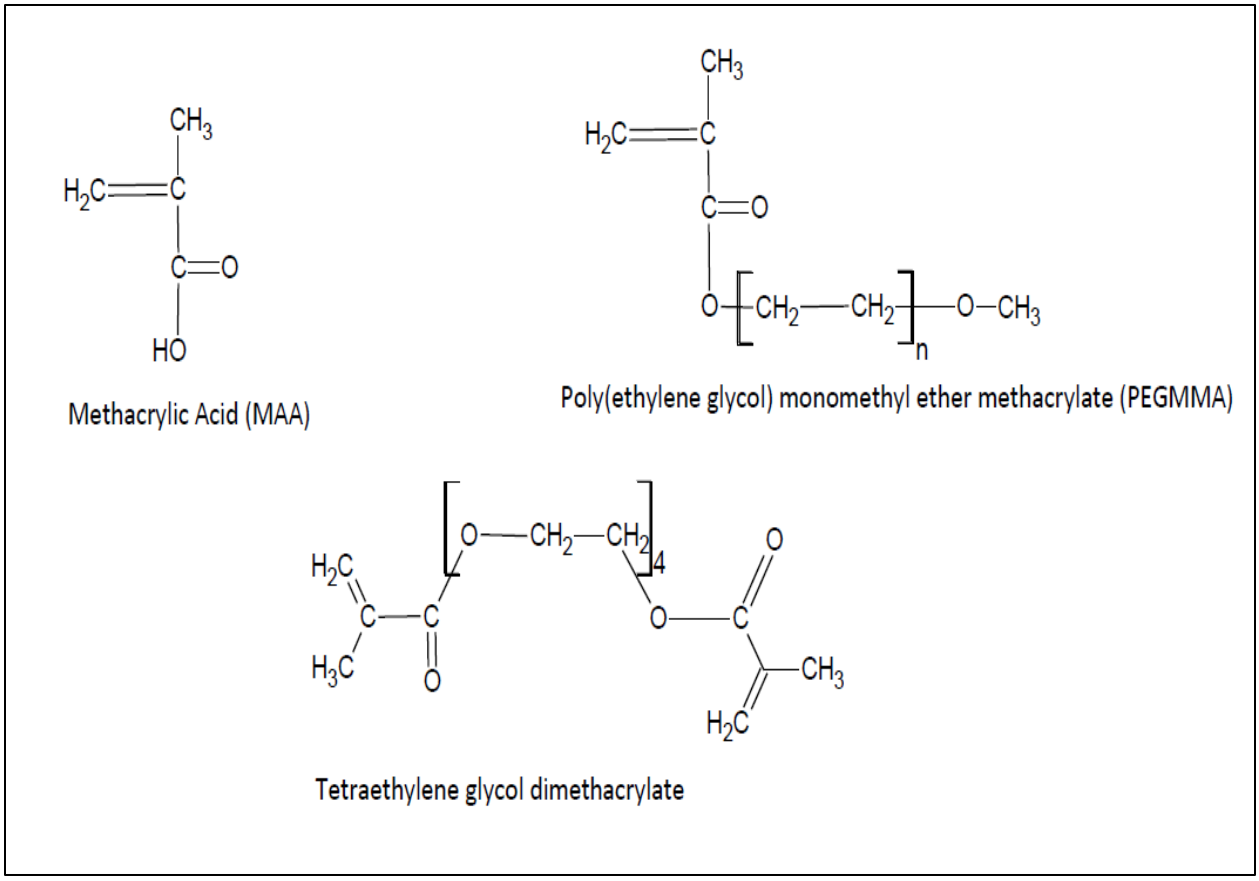

Figure 6.2 – Structures of monomers used in the emulsion polymerization procedure. MAA is the hydrophilic monomer, PEGMMA is used to form PEG grafts, and tetraethylene glycol dimethacrylate is the cross-linker. These monomers were maintained consistent for all four formulation syntheses.

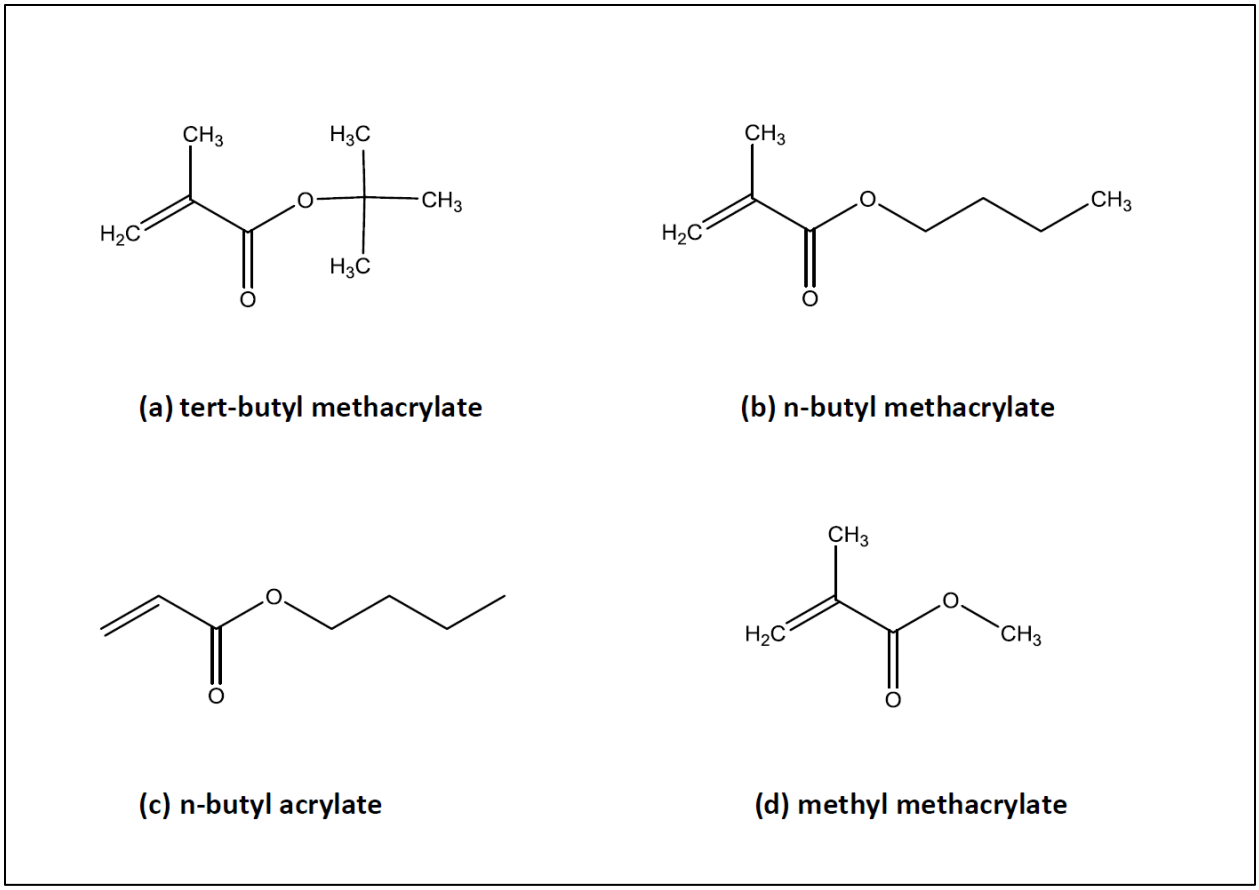

Figure 6.3 – Structures of the four hydrophobic monomers used. Formulation containing, (a) tert-butyl methacrylate is denoted as P(MAA-g-PEG-co-tBMA), (b) n-butyl methacrylate is denoted as P(MAA-g-PEG-co-nBMA), (c) n-butyl acrylate is denoted as P(MAA-g-PEG-co-nBA), and (d) methyl methacrylate is denoted as P(MAA-g-PEG-co-MMA)

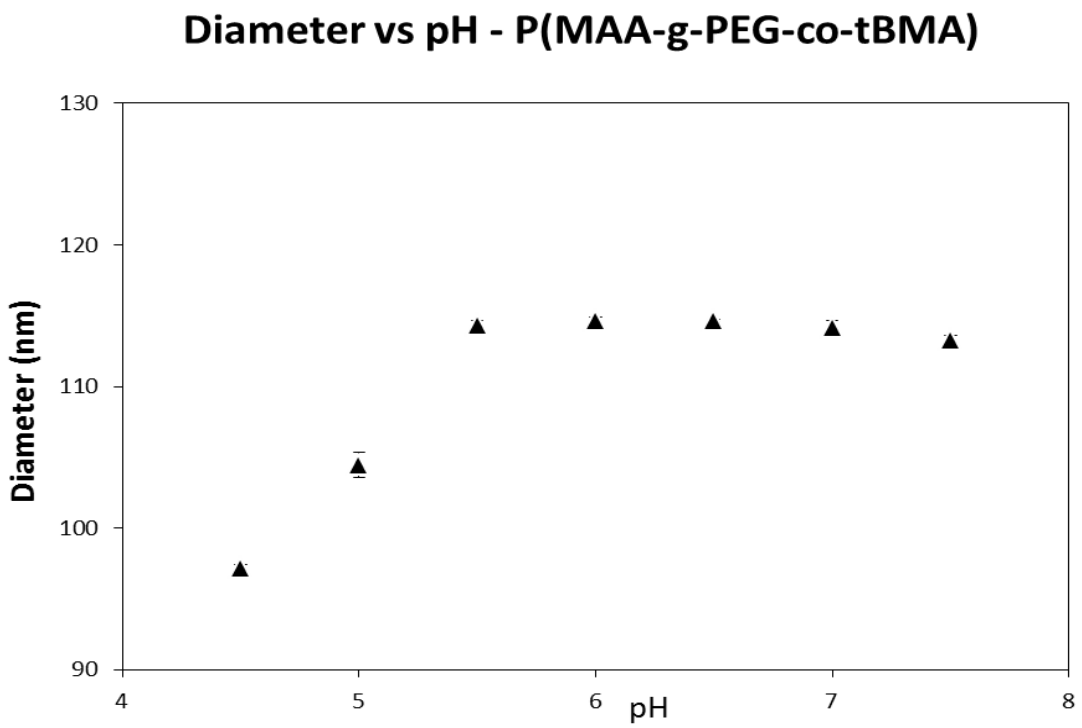

Figure 6.4 – Dynamic swelling data for P(MAA-g-PEG-co-tBMA). Data points shown are mean of measurements ± SD.

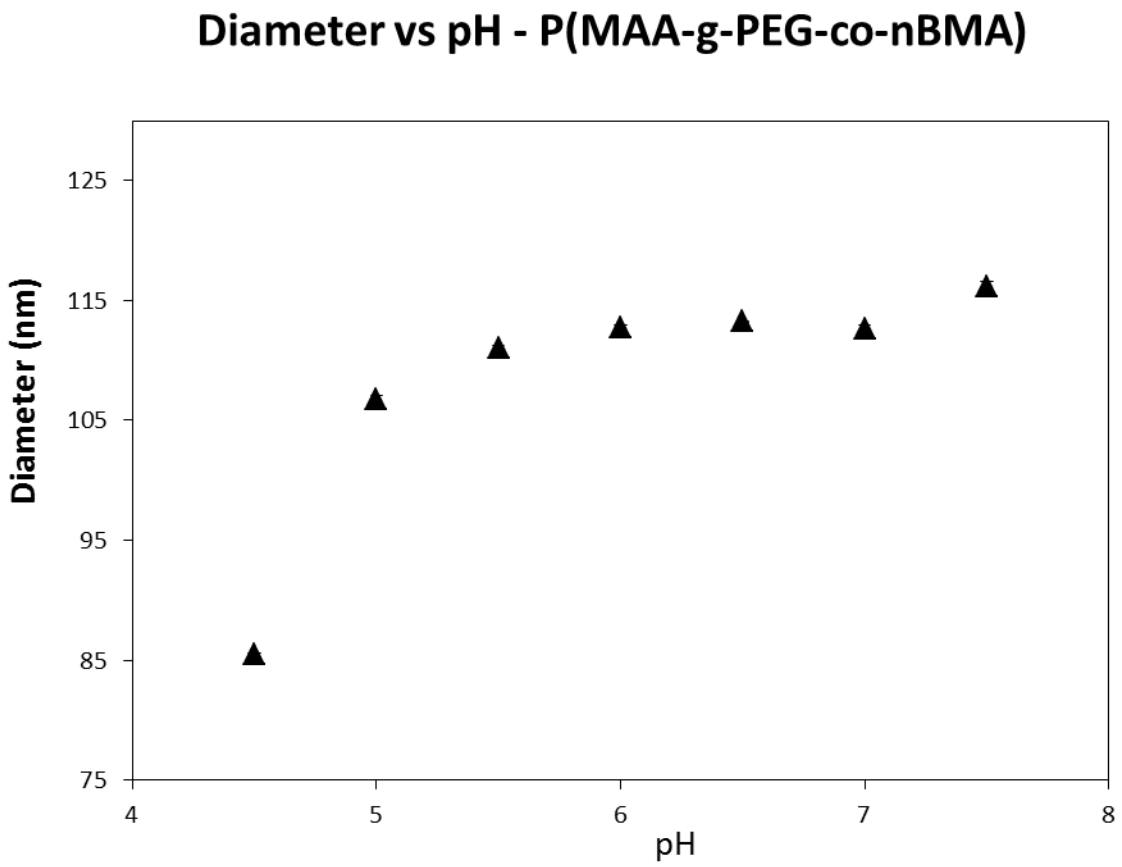

Figure 6.5 – Dynamic swelling data for P(MAA-g-PEG-co-nBMA). Data points shown are mean of measurements ± SD.

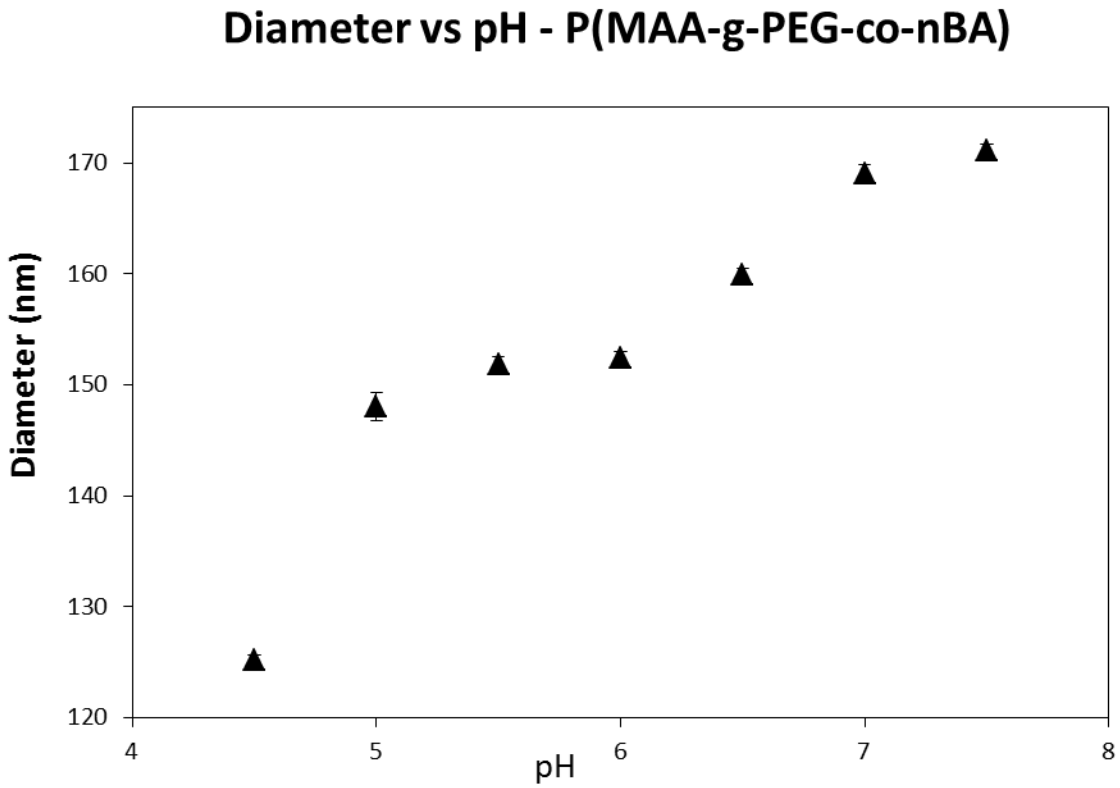

Figure 6.6 – Dynamic swelling data for P(MAA-g-PEG-co-nBMA). Data points shown are mean of measurements ± SD.

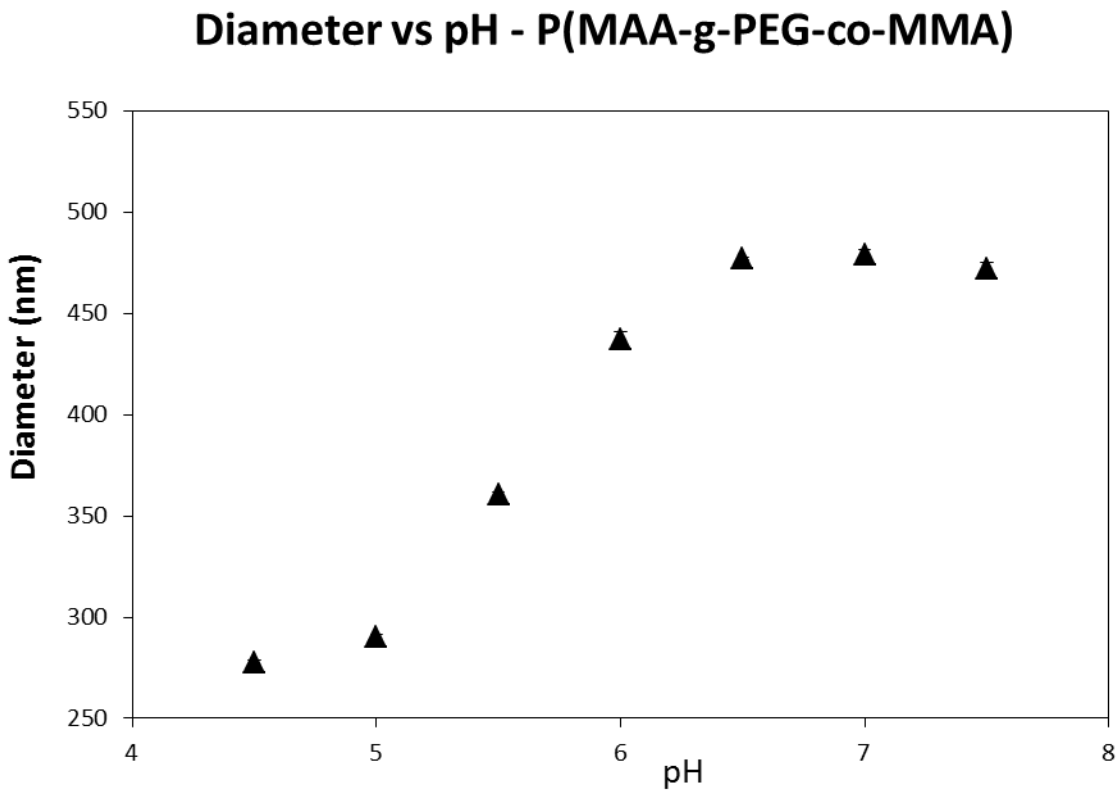

Figure 6.7 – Dynamic swelling data for P(MAA-g-PEG-co-MMA). Data points shown are mean of measurements ± SD.

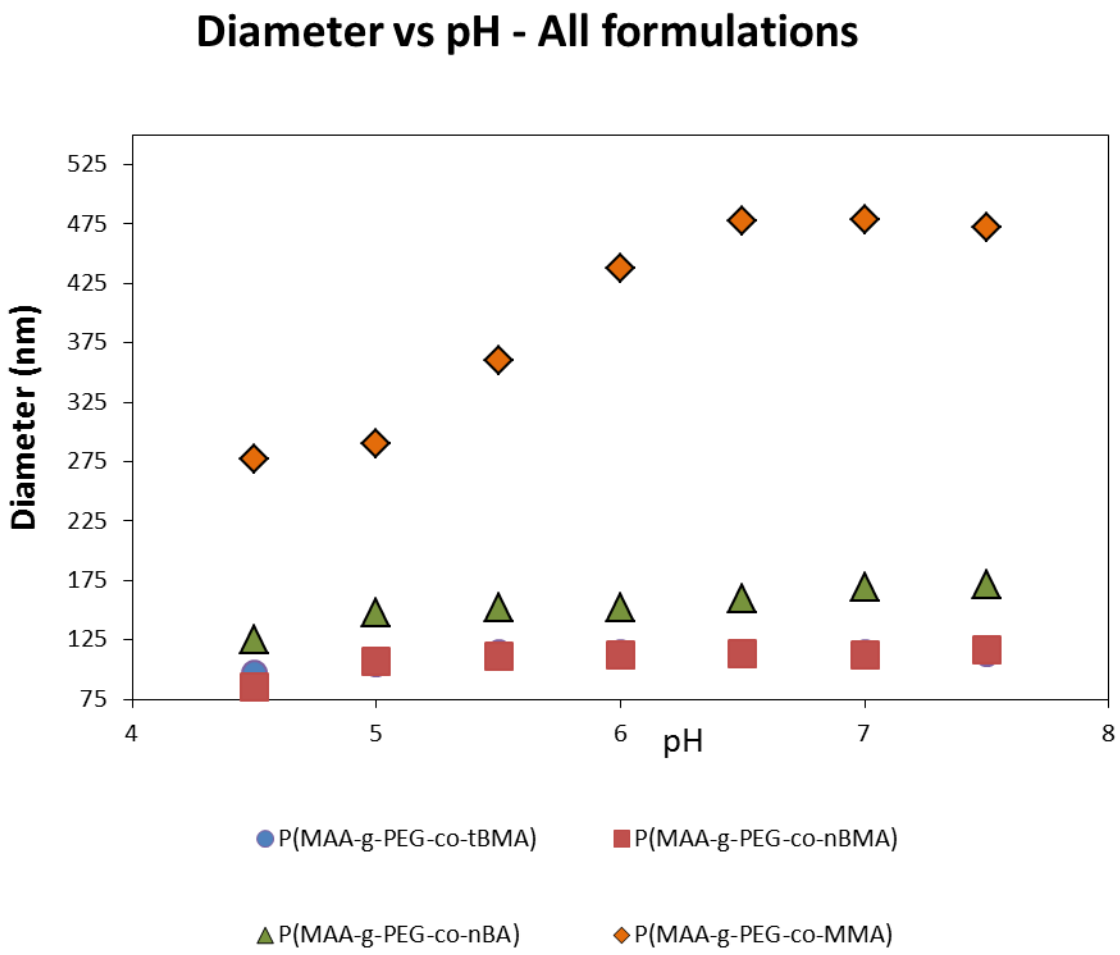

Figure 6.8 – Dynamic Swelling behavior of all formulations as measured by dynamic light scattering. P(MAA-g-PEG-co-MMA) underwent the largest size increase upon increasing pH, while P(MAA-g-PEG-co-tBMA) underwent the smallest size increase. Data points shown are mean of measurements ± SD.

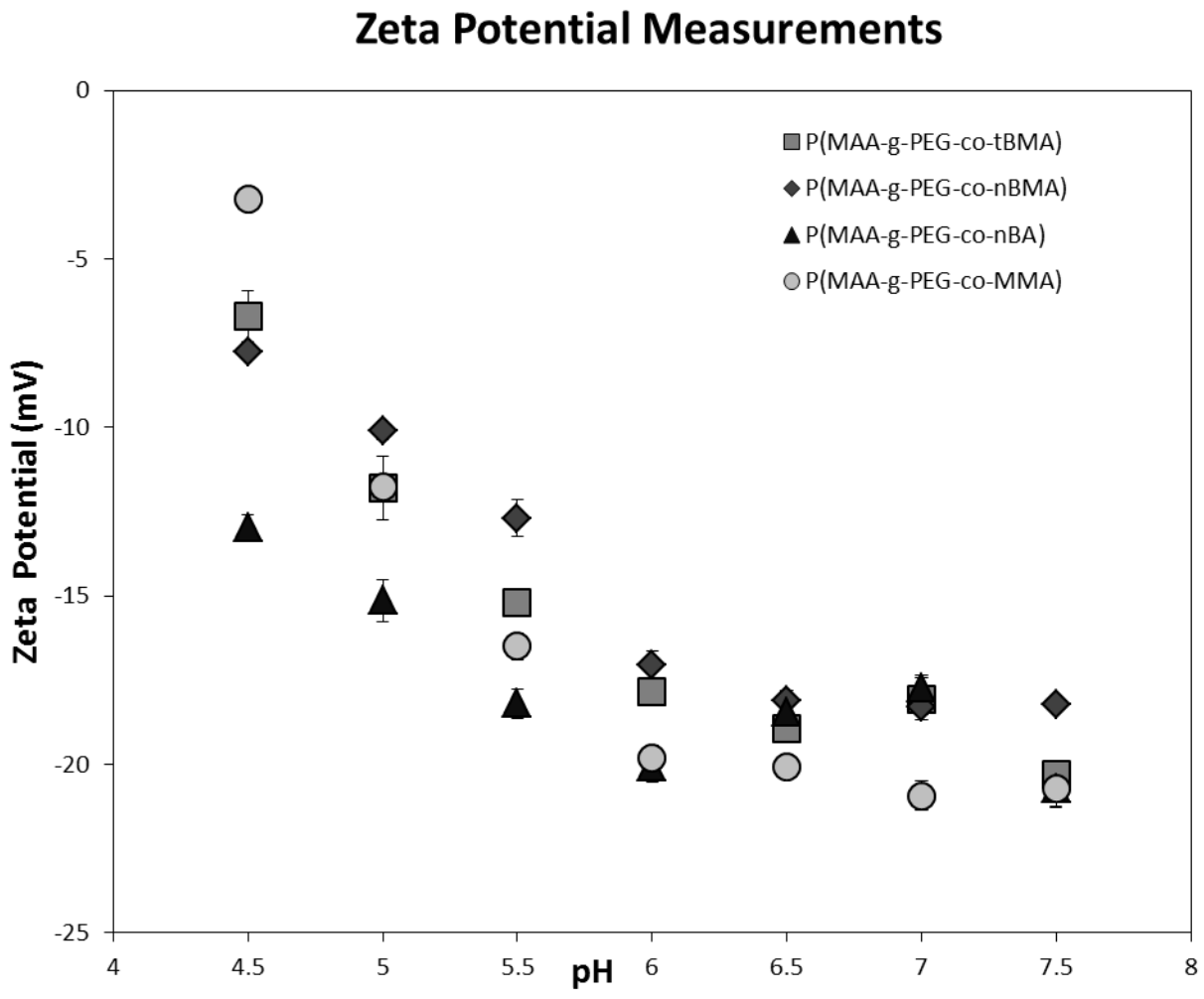

Figure 6.9 - Zeta potential measurements for all formulations. Nanoparticle surface charge typically increases from -17.5 to -20 mV at pH 7.5, to slightly less negative at lower pH. Data points shown are mean of measurements ± SD.

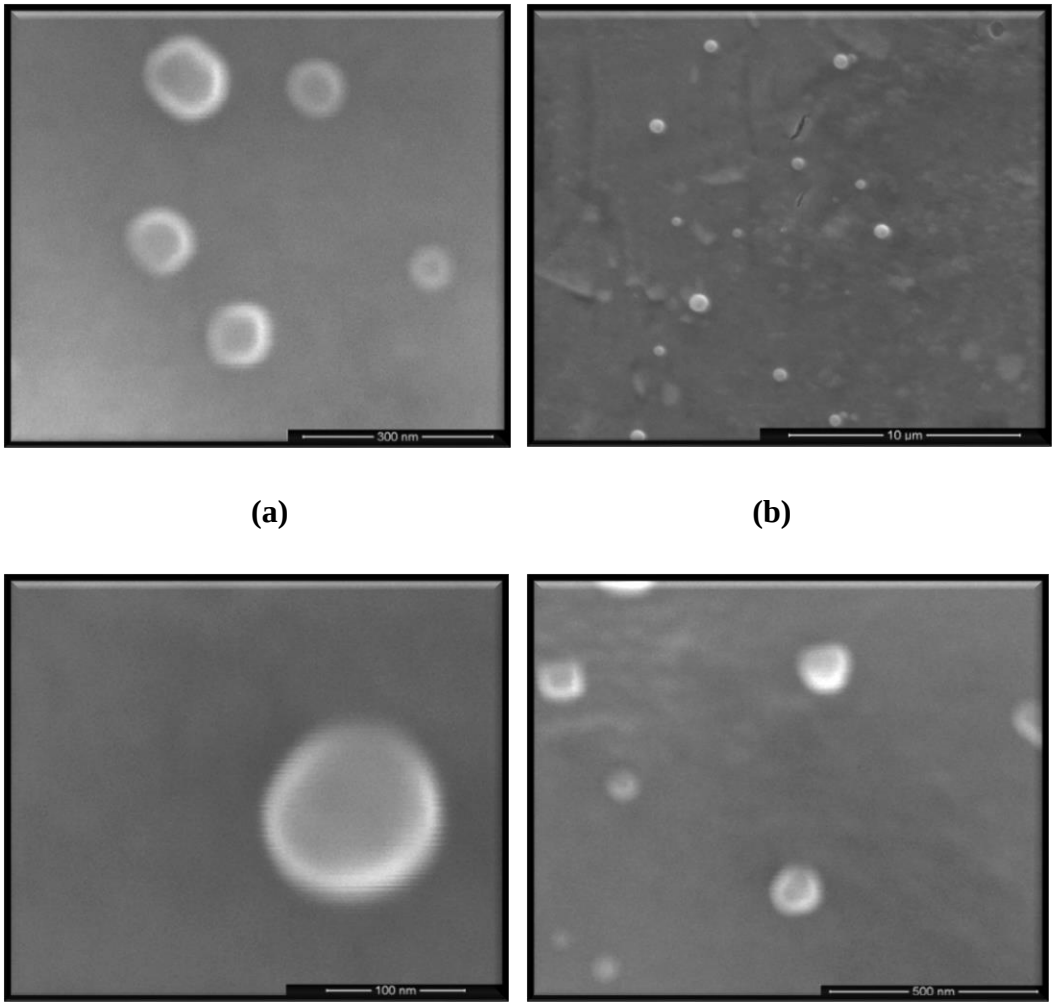

(a) **(b)**

(c) (d)

Figure 6.10 - Representative scanning electron micrograph images. Scale bars: (a) 300 nm, (b) 10 µm, (c) 100 nm, and (d) 500 nm

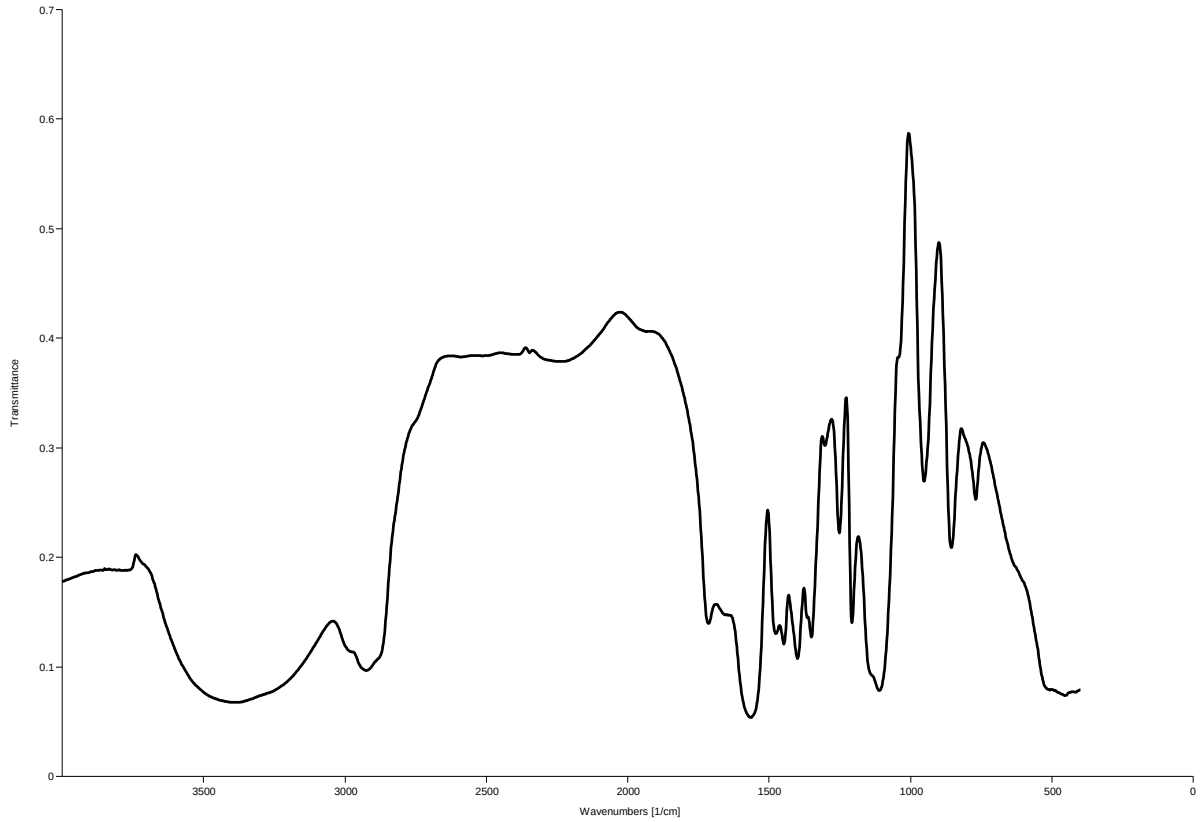

Figure 6.11 - Fourier Transform-Infrared (FTIR) spectra for P(MAA-g-PEG-co-tBMA).

Y-axis: Relative Fraction Transmittance or (1-absorbance)

X-axis: Wavenumbers (cm^{-1}), wavenumber = $1/\lambda$

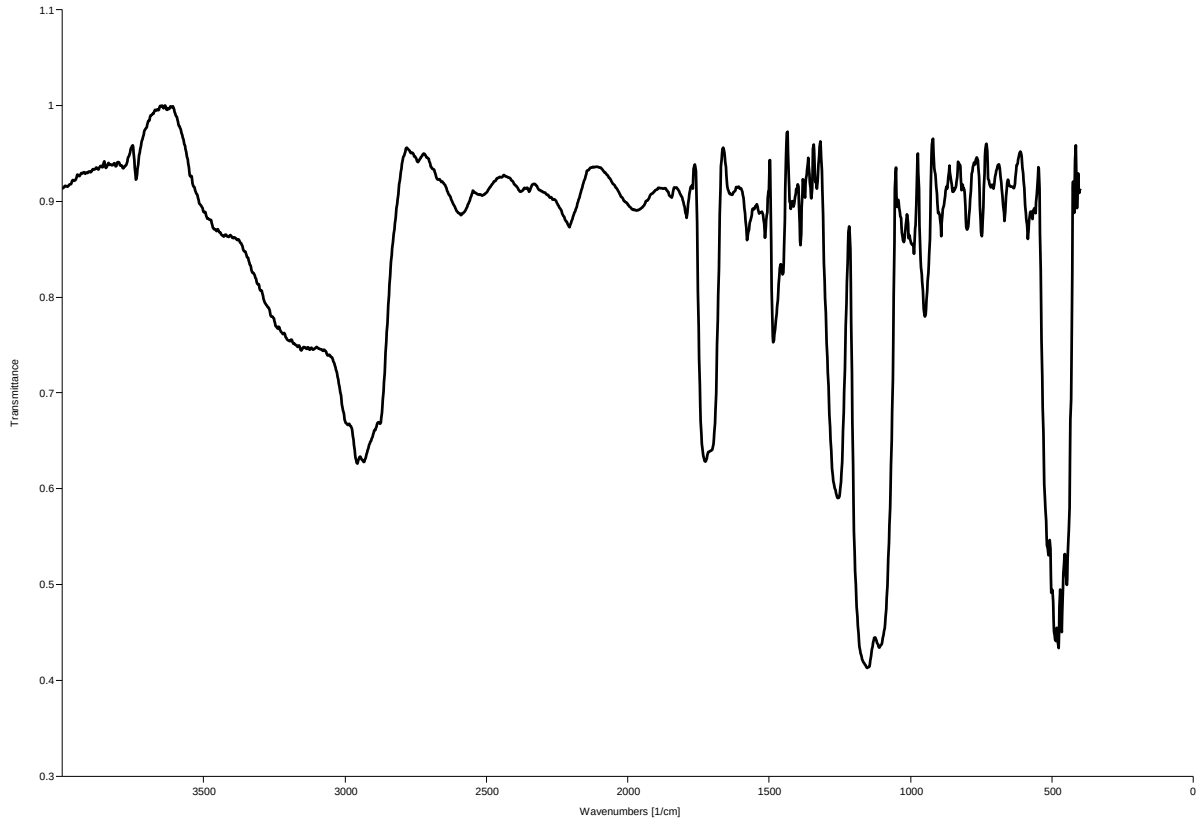

Figure 6.12: Fourier Transform-Infrared (FTIR) spectra for P(MAA-g-PEG-co-nBMA).

Y-axis: Relative Fraction Transmittance or (1-absorbance)

X-axis: Wavenumbers (cm^{-1}), wavenumber = $1/\lambda$

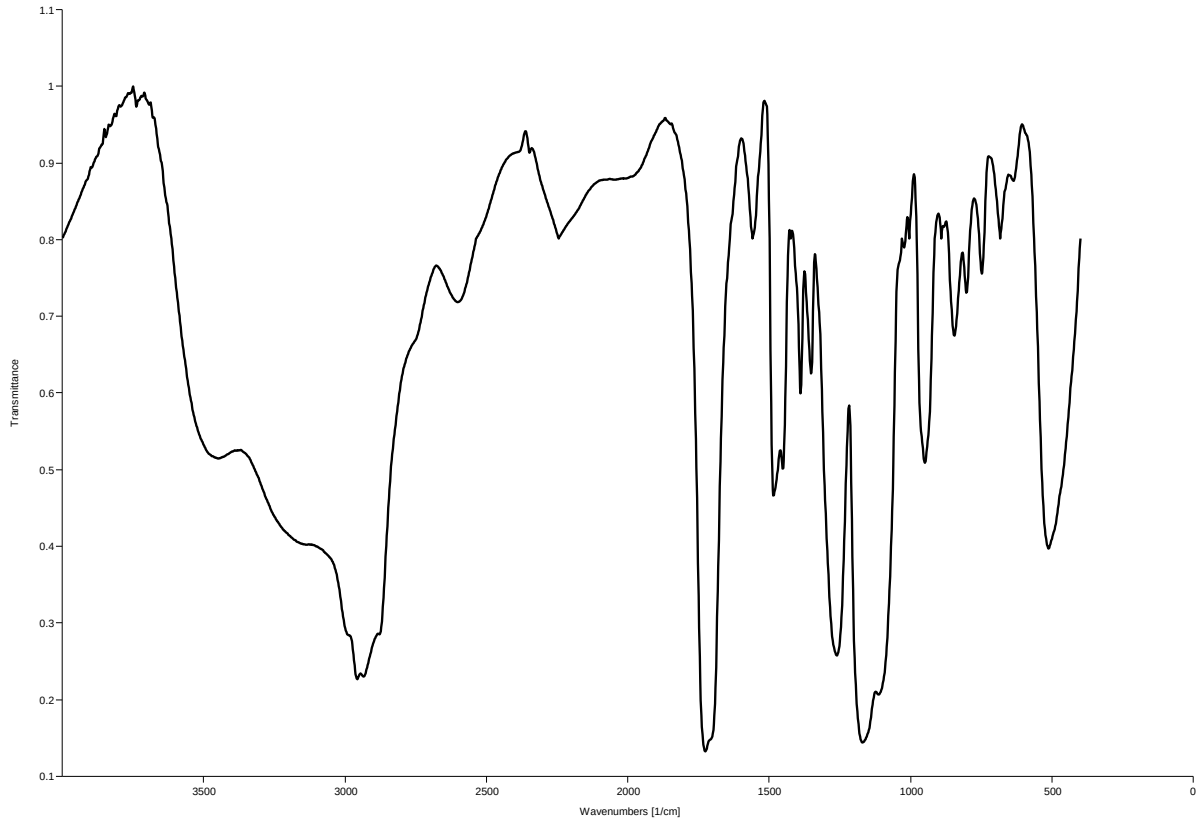

Figure 6.13: Fourier Transform-Infrared (FTIR) spectra for P(MAA-g-PEG-co-nBA).

Y-axis: Relative Fraction Transmittance or (1-absorbance)

X-axis: Wavenumbers (cm^{-1}), wavenumber = $1/\lambda$

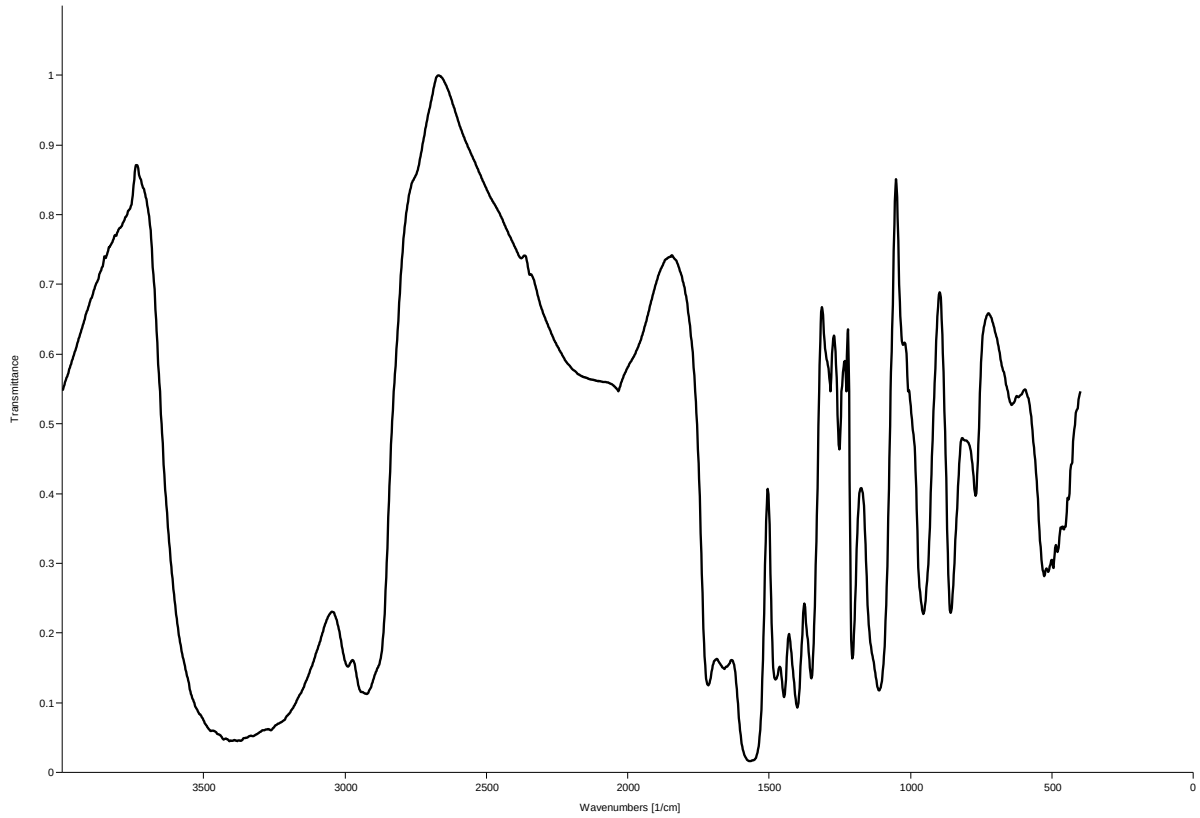

Figure 6.14: Fourier Transform-Infrared (FTIR) spectra for P(MAA-g-PEG-co-MMA).

Y-axis: Relative Fraction Transmittance or (1-absorbance)

X-axis: Wavenumbers (cm^{-1}), wavenumber = $1/\lambda$

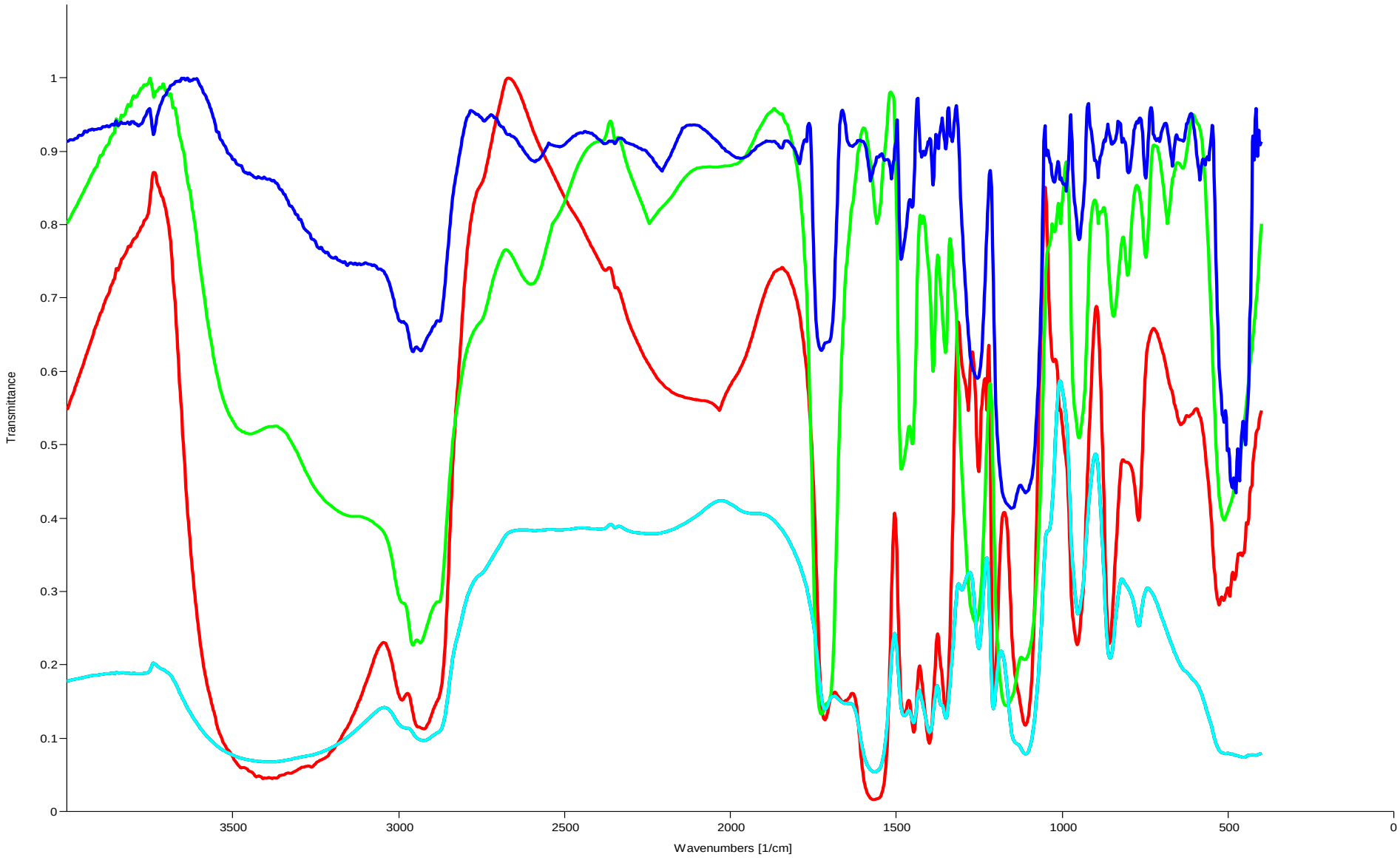

Figure 6.15 - FTIR spectra of all formulations. Light blue: P(MAA-g-PEG-co-tBMA); Red: P(MAA-g-PEG-co-MMA); Green: P(MAA-g-PEG-co-nBA); Blue:P(MAA-g-PEG-co-nBMA) ; Y axis: Fraction Transmittance

tBMA

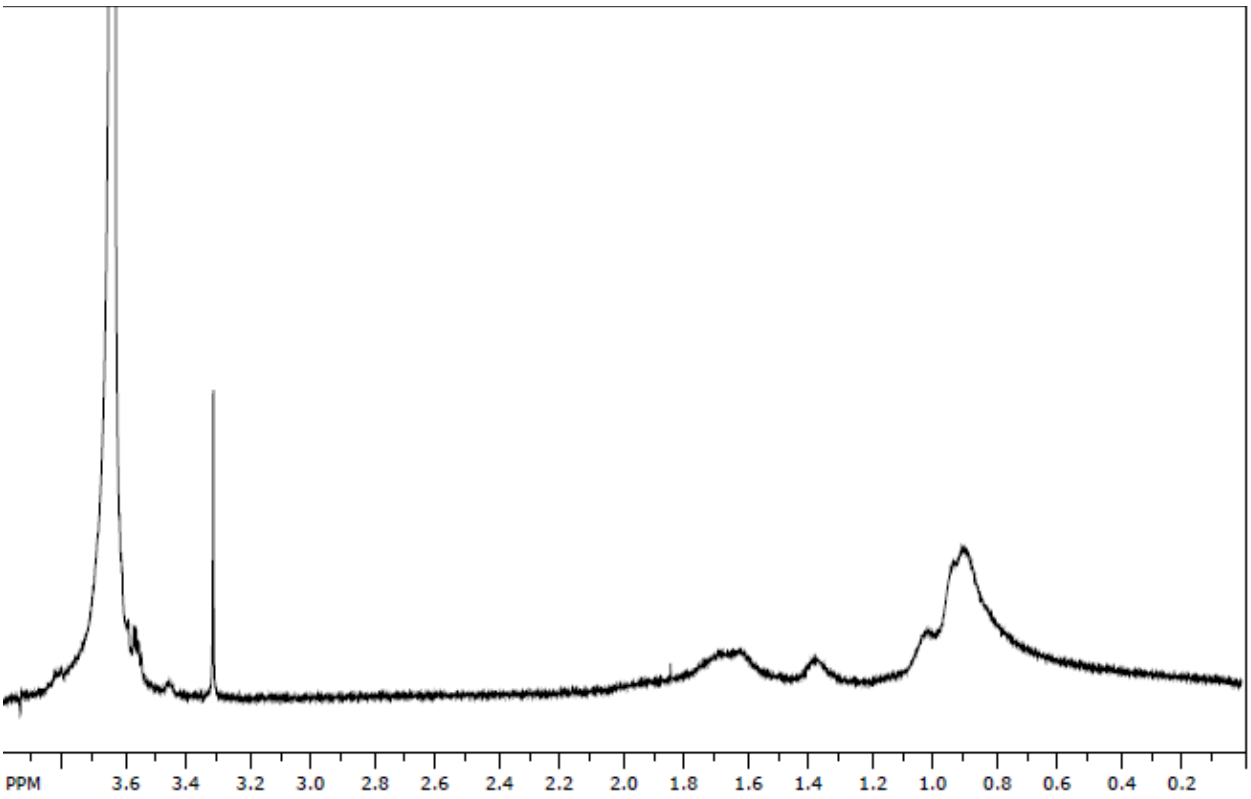

Figure 6.16 - ^{1}H-NMR spectrum of P(MAA-g-PEG-co-tBMA)

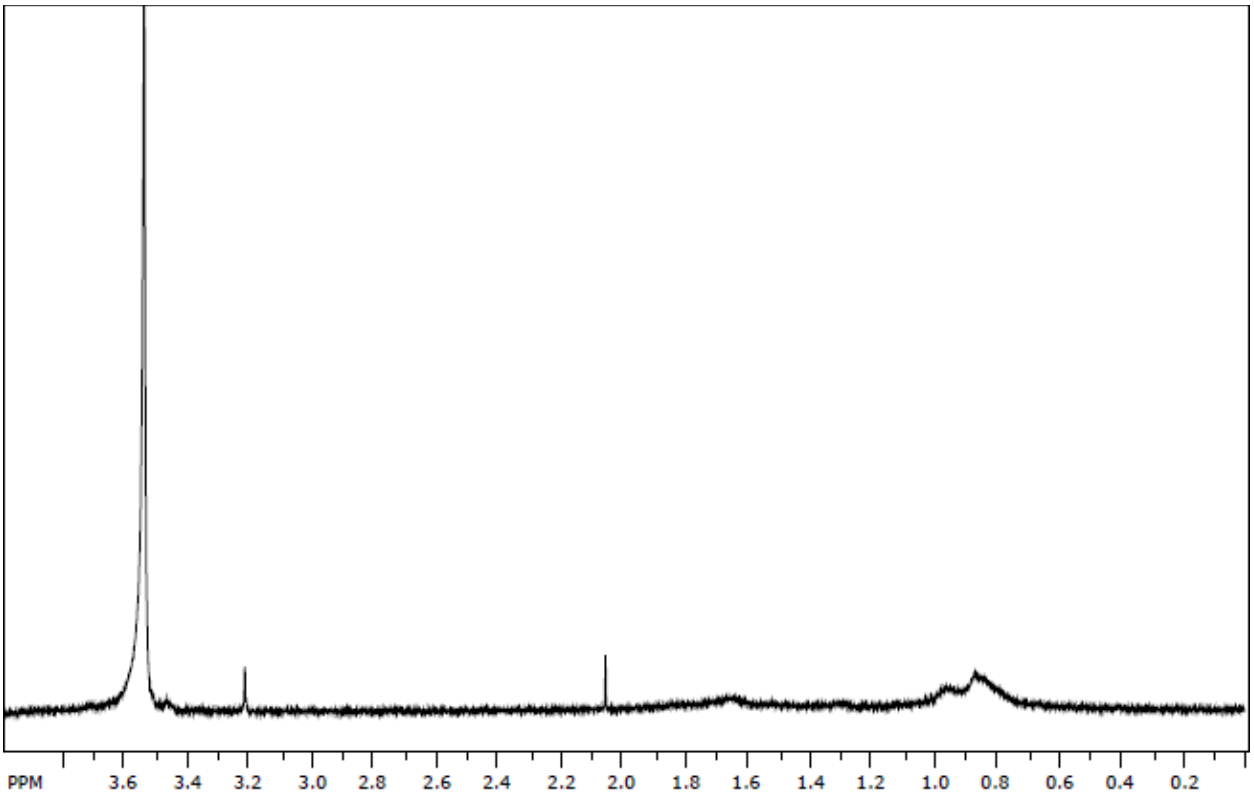

Figure 6.17 - ^{1}H-NMR spectrum of P(MAA-g-PEG-co-nBMA)

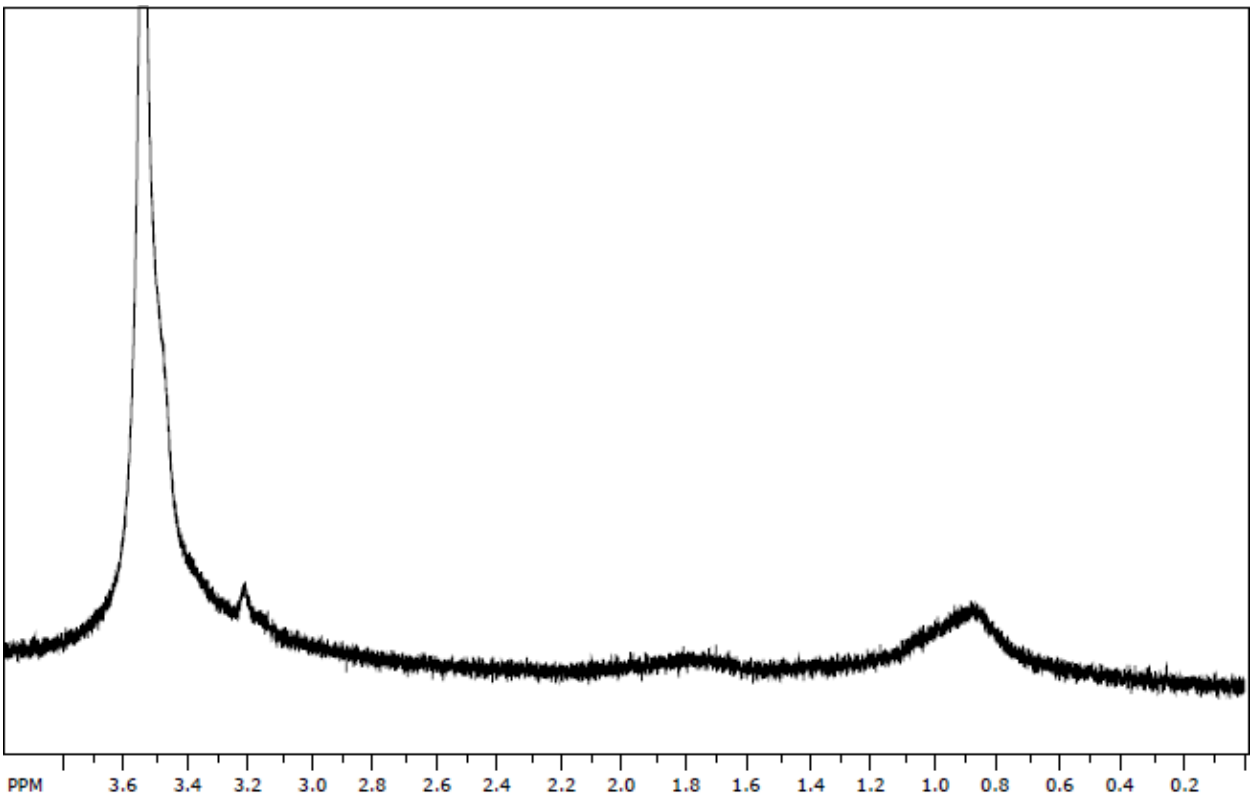

Figure 6.18 - ^{1}H-NMR spectrum of P(MAA-g-PEG-co-nBA)

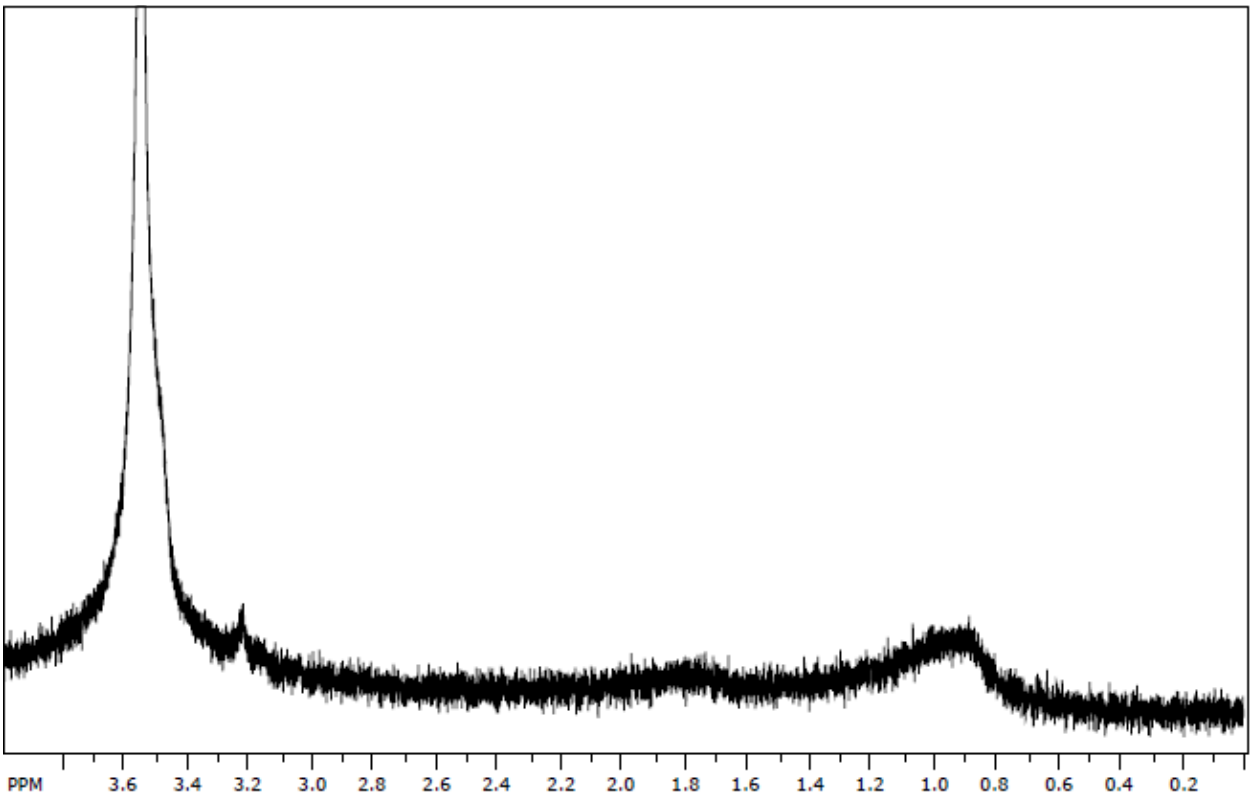

Figure 6.19 - ^{1}H-NMR spectrum of P(MAA-g-PEG-co-MMA)

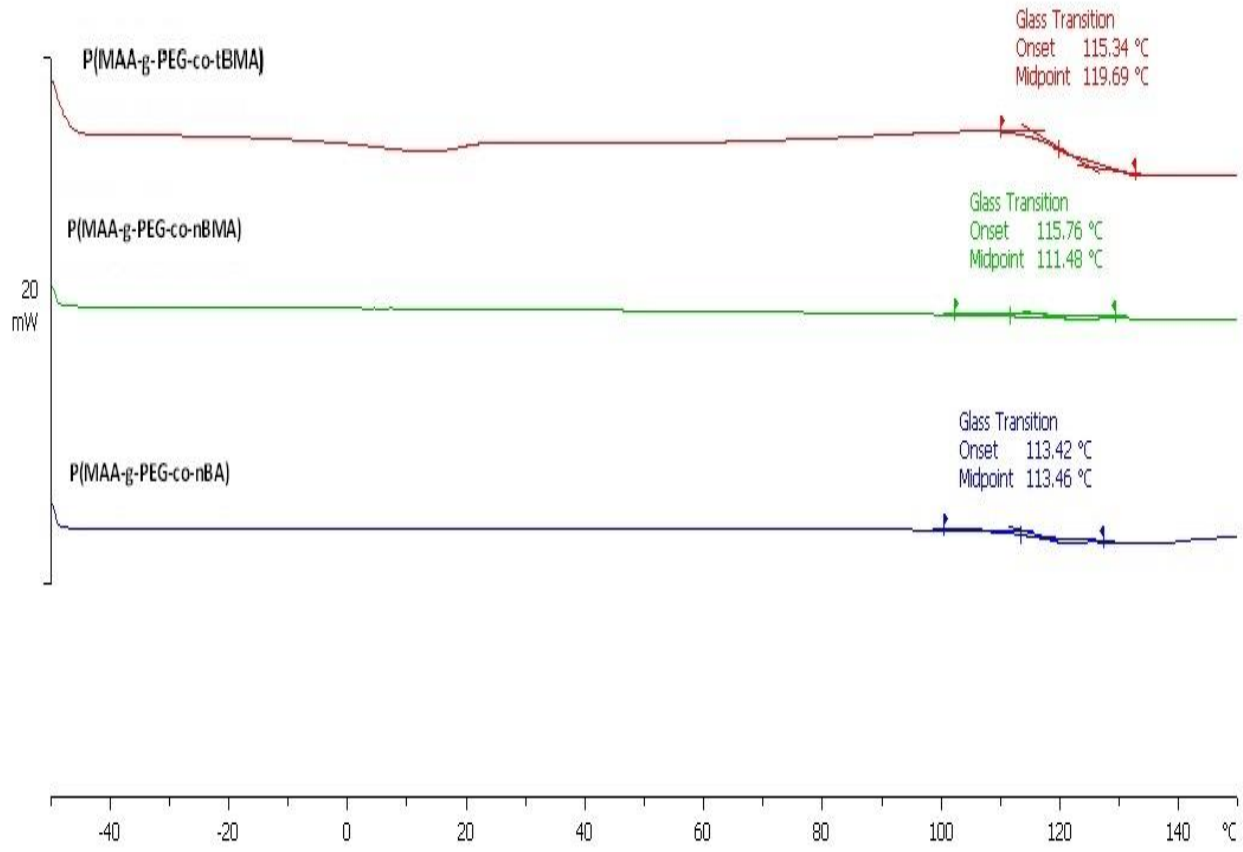

Figure 6.20 - Differential scanning calorimetry thermograms of P(MAA-co-tBMA-g-PEG) nanoparticle formulation (red), P(MAA-co-nBMA-g-PEG) nanoparticle formulation (green), P(MAA-co-nBA-g-PEG) nanoparticle formulation (red).

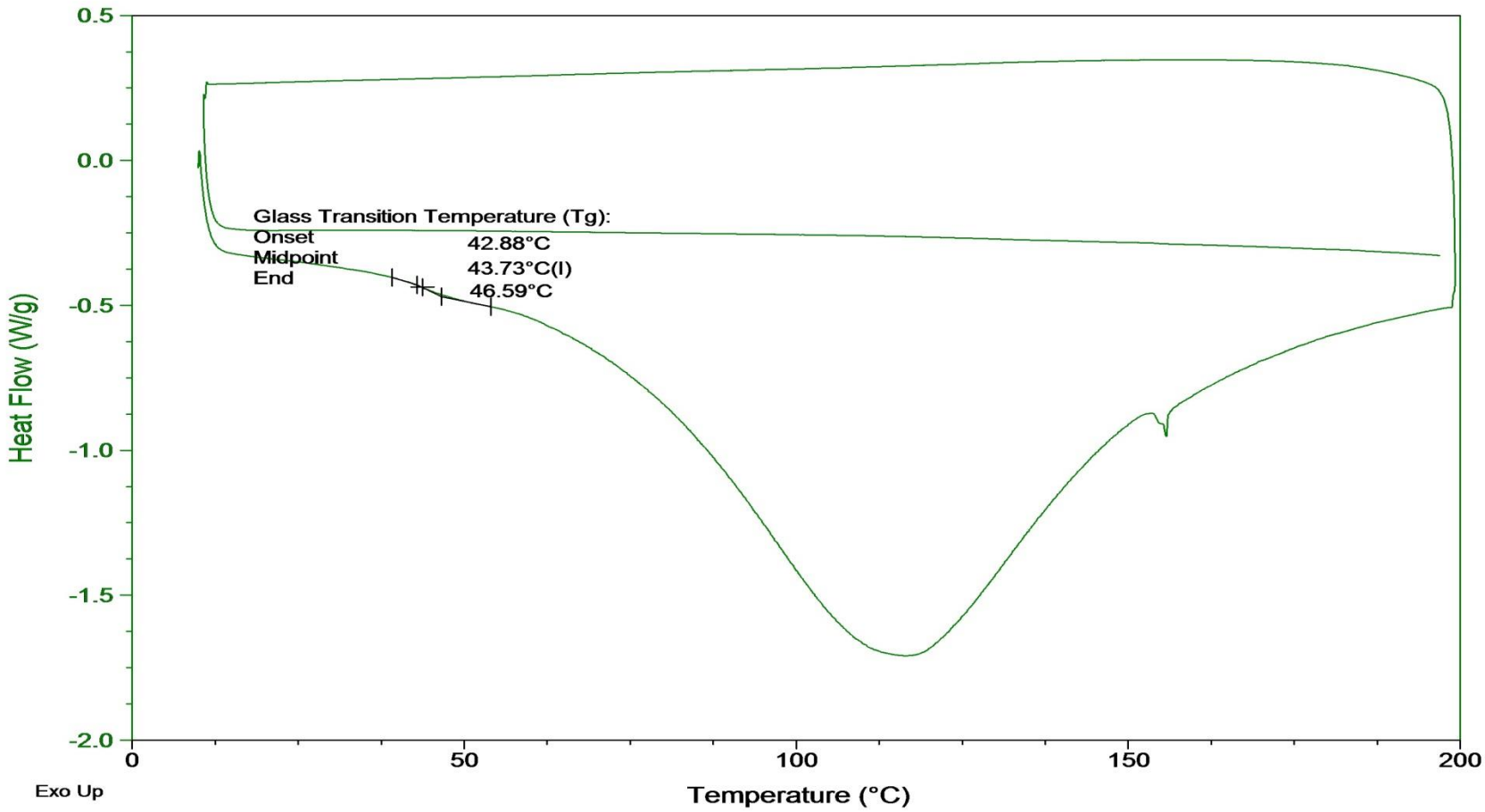

Figure 6.21 - DSC thermogram of P(MAA-co-tBMA-g-PEG) nanoparticle formulation as seen when subjected to a heat-cool-heat cycle.

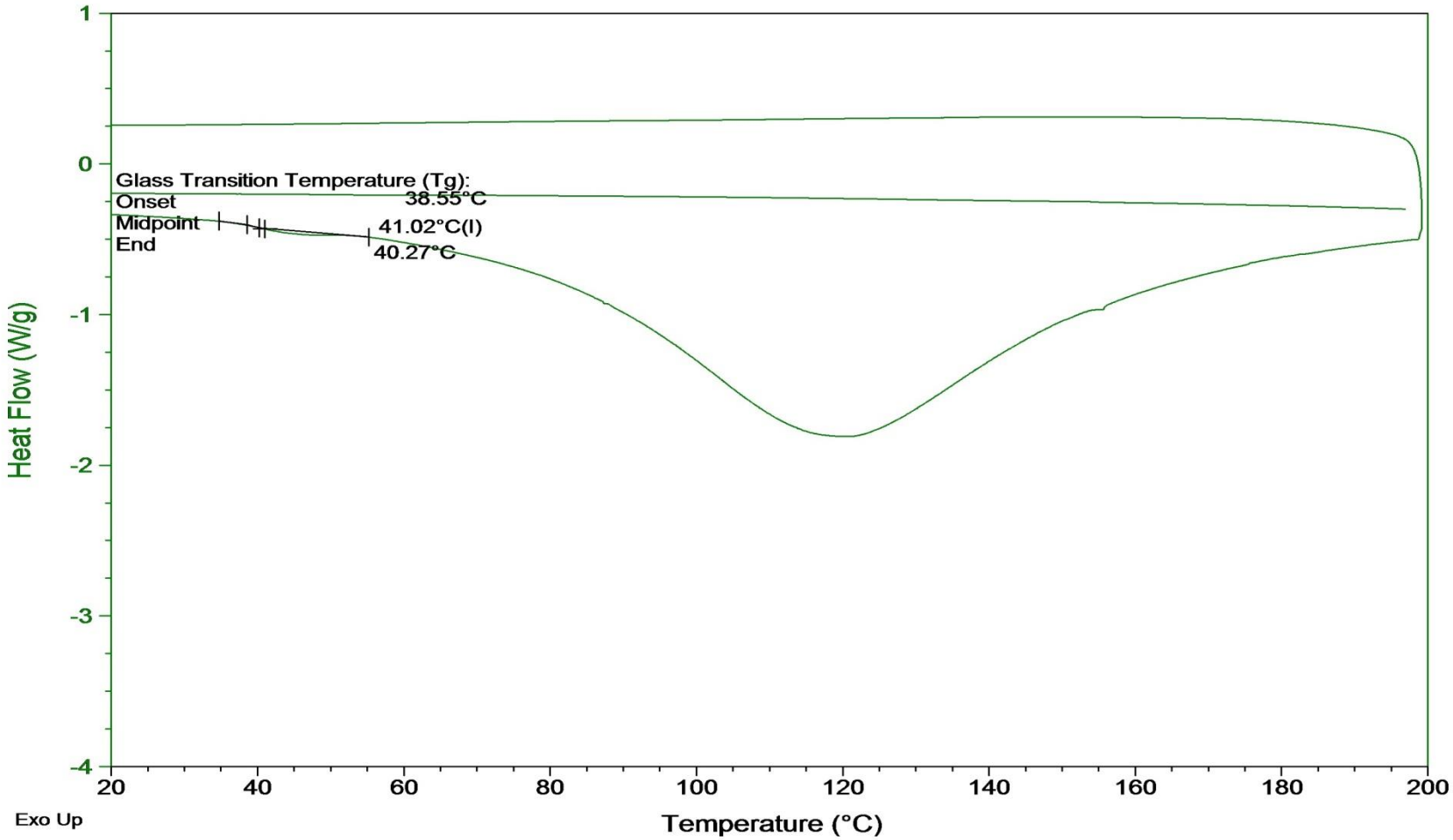

Figure 6.22 - DSC thermogram of P(MAA-co-MMA-g-PEG) nanoparticle formulation as seen when subjected to a heat-cool-heat cycle.

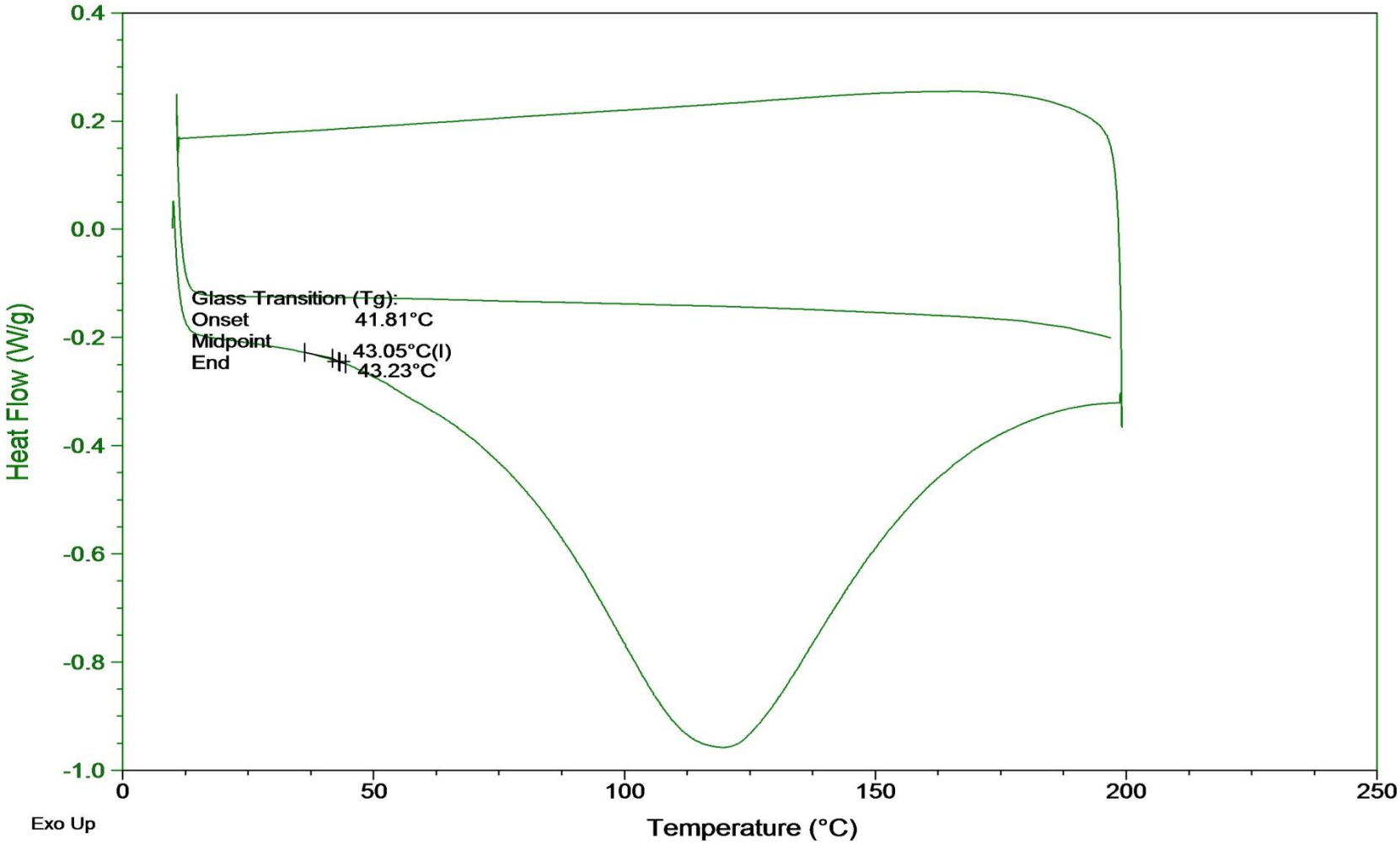

Figure 6.23 - DSC thermogram of P(MAA-co-nBMA-g-PEG) nanoparticle formulation as seen when subjected to a heat-cool-heat cycle.

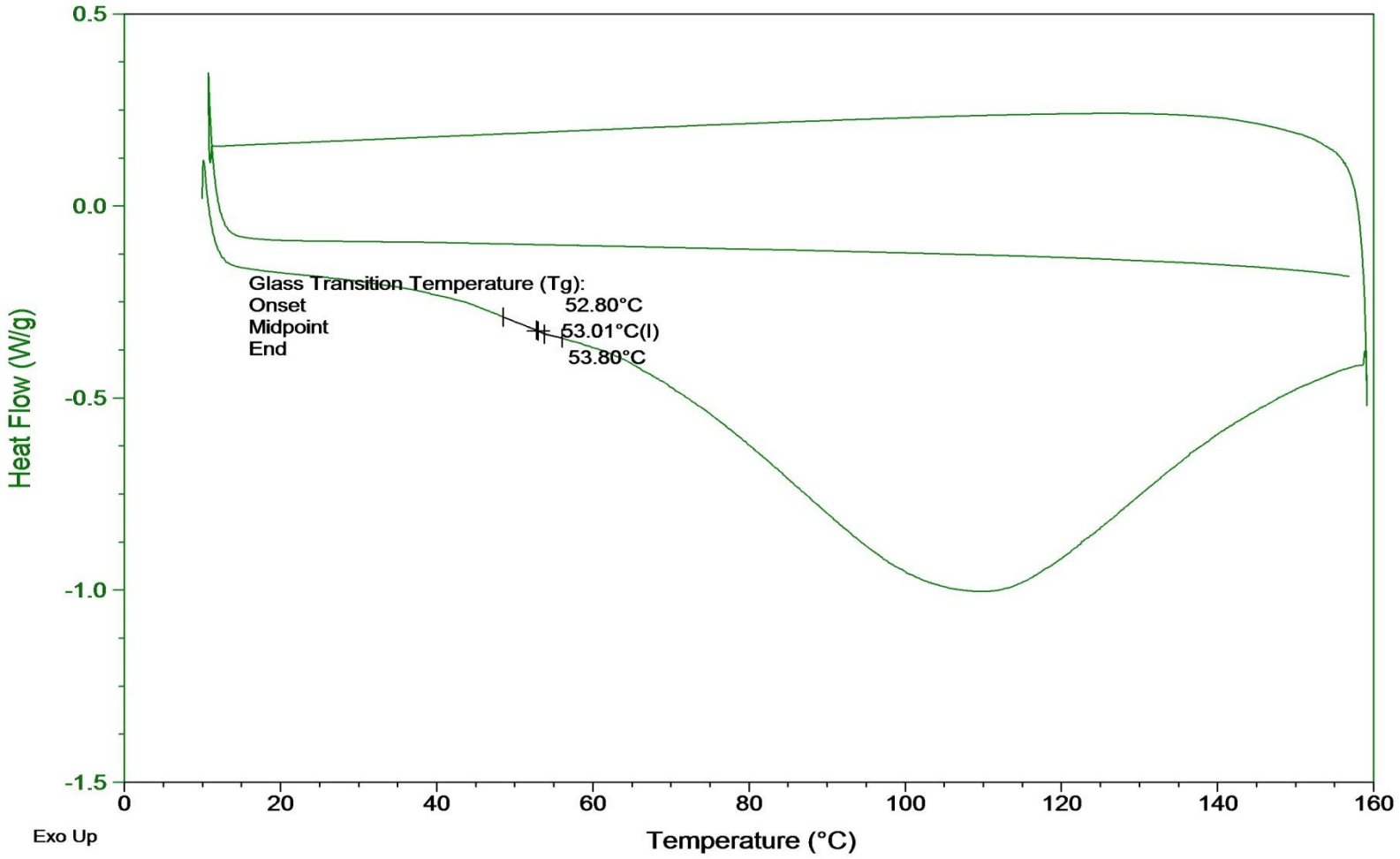

Figure 6.24 - DSC thermogram of P(MAA-co-nBA-g-PEG) nanoparticle formulation as seen when subjected to a heat-cool-heat cycle.

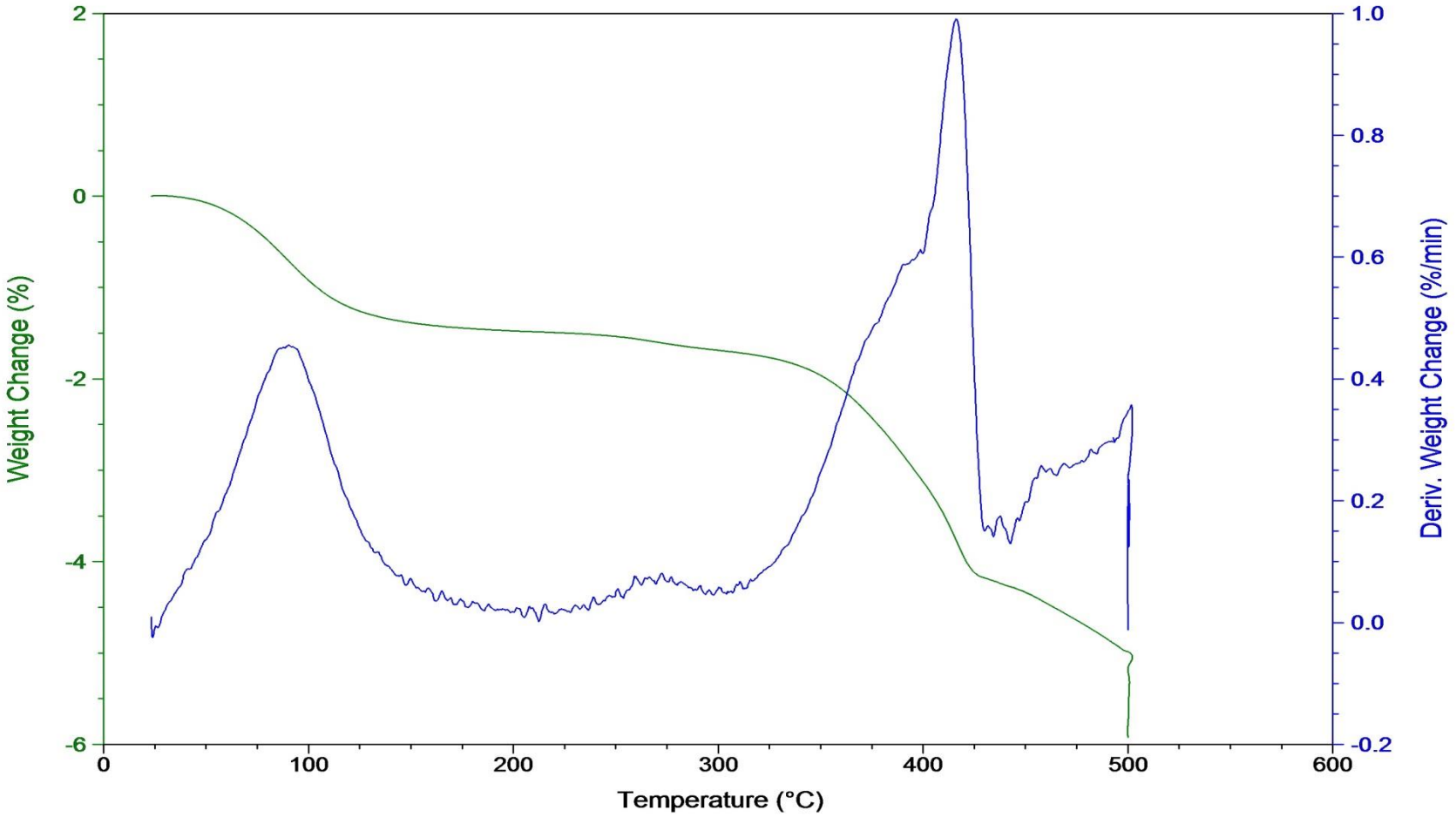

Figure 6.25 - TGA thermogram of the P(MAA-co-tBMA-g-PEG) polyanionic nanoparticles with nitrogen atmosphere. Weight Change % (green line) and derivative of Weight Change % with respect to time (blue line) are shown with increasing temperature.

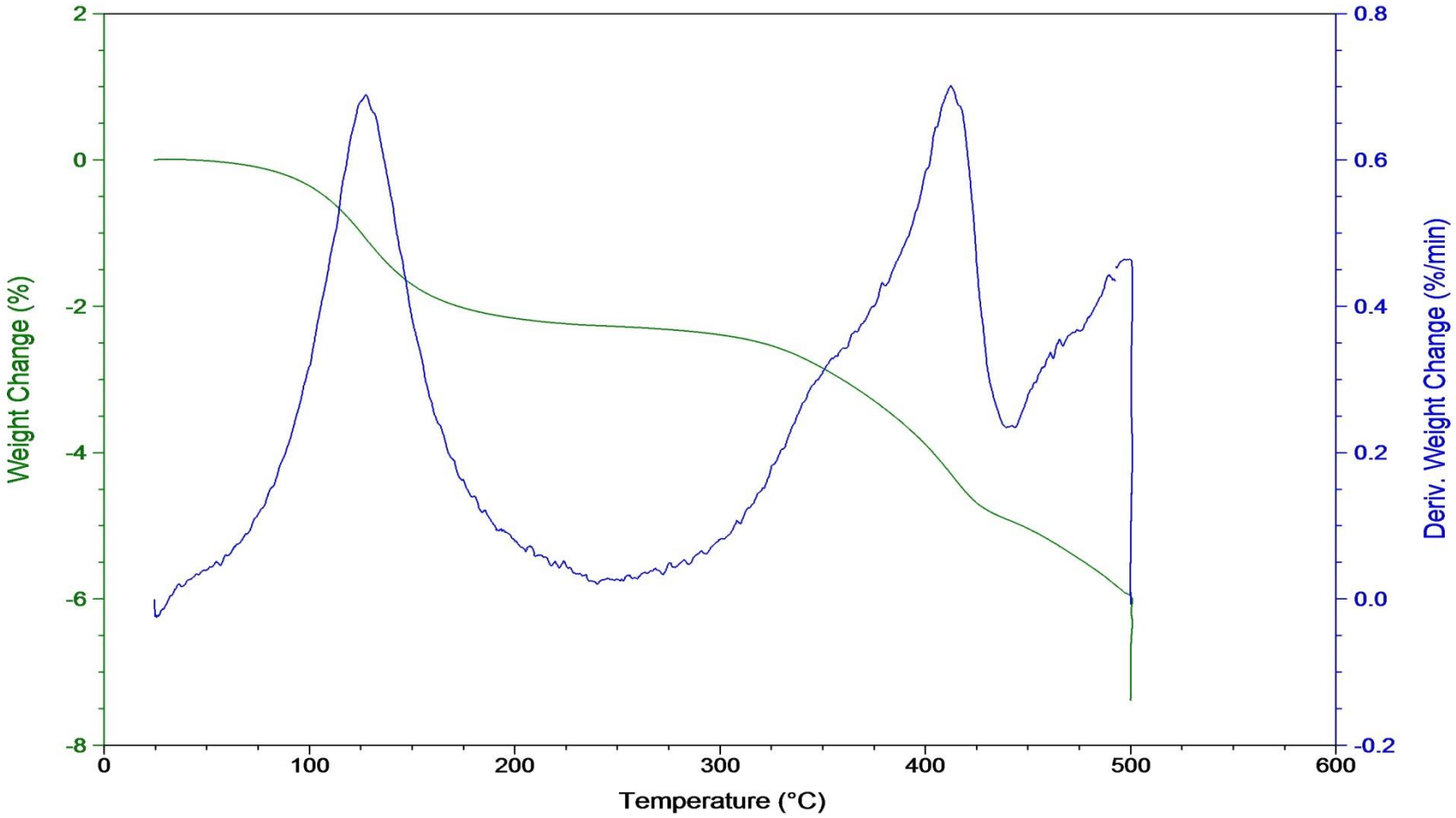

Figure 6.26 - TGA thermogram of the P(MAA-co-MMA-g-PEG) polyanionic nanoparticles with nitrogen atmosphere. Weight Change % (green line) and derivative of Weight Change % with respect to time (blue line) are shown with increasing temperature.

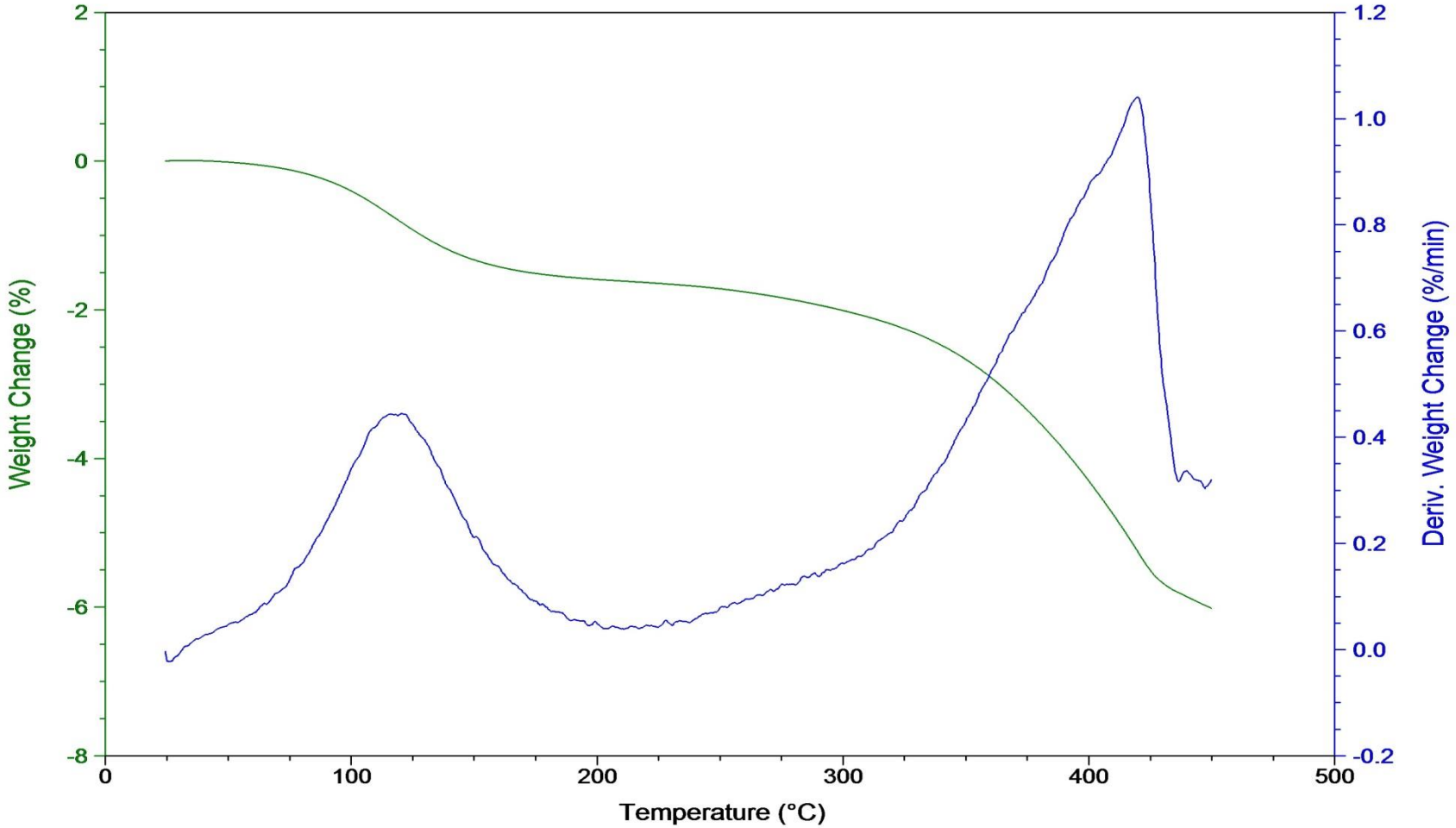

Figure 6.27 - TGA thermogram of the P(MAA-co-nBMA-g-PEG) polyanionic nanoparticles with nitrogen atmosphere. Weight Change % (green line) and derivative of Weight Change % with respect to time (blue line) are shown with increasing temperature.

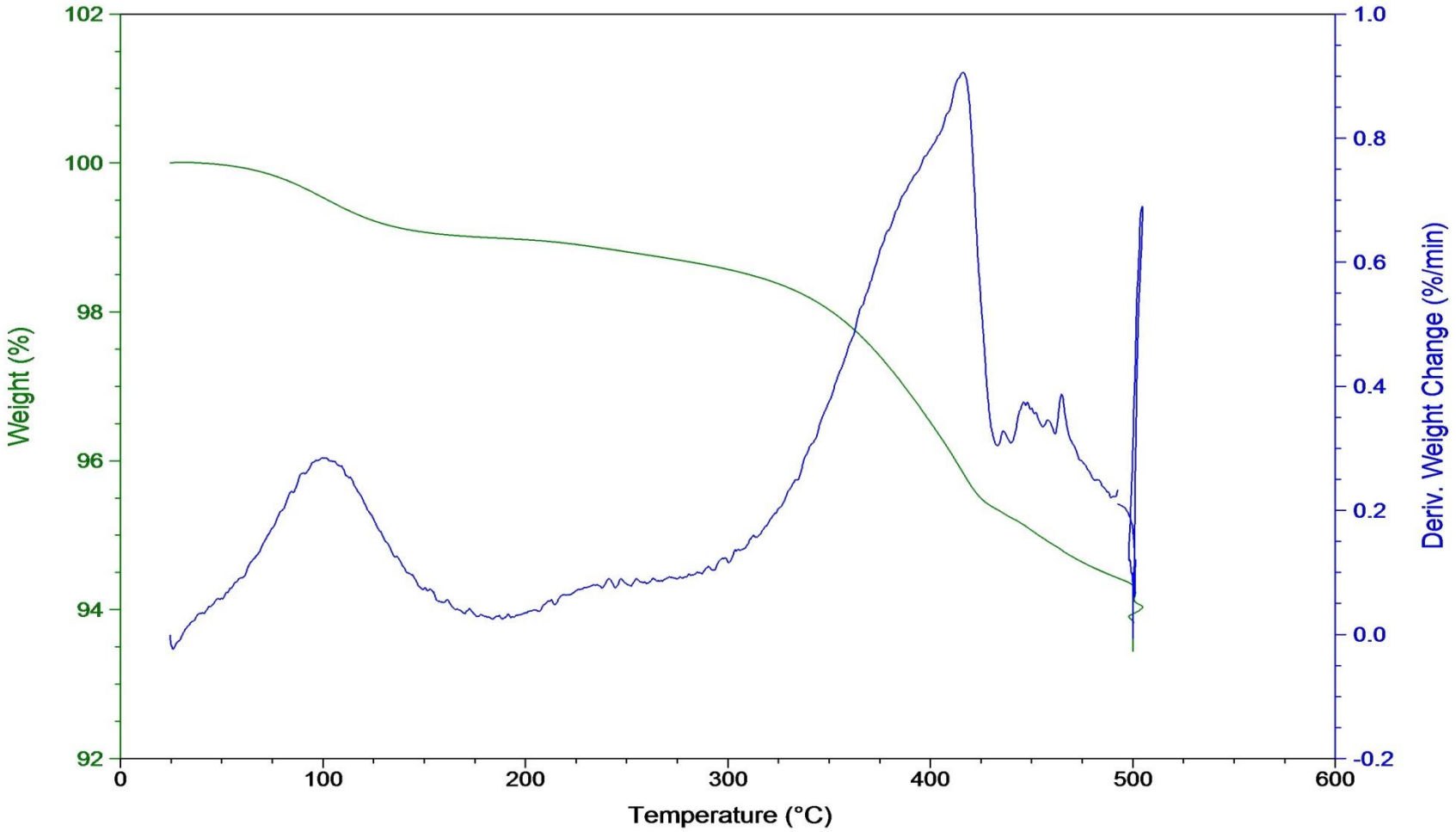

Figure 6.28 - TGA thermogram of the P(MAA-co-nBA-g-PEG) polyanionic nanoparticles with nitrogen atmosphere. Weight Change % (green line) and derivative of Weight Change % with respect to time (blue line) are shown with increasing temperature.

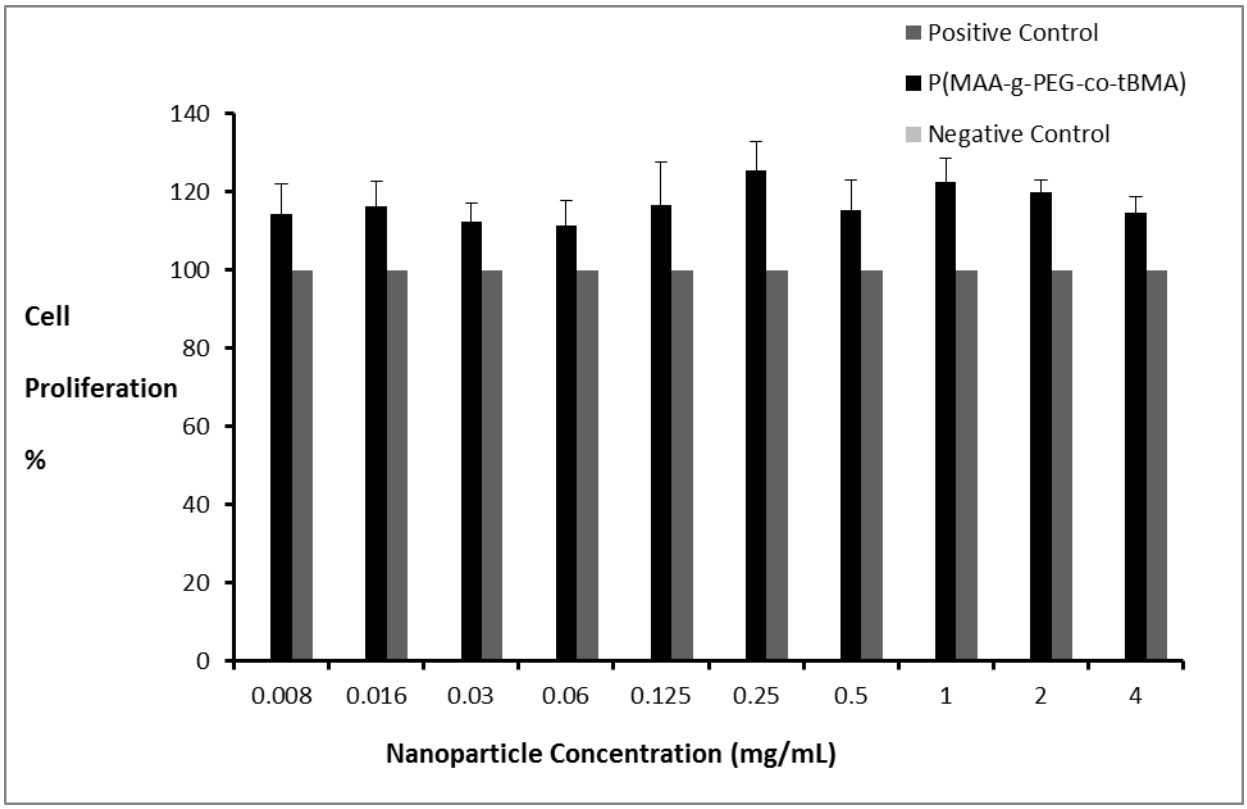

Figure 6.29 - *in vitro* cell proliferation % of evaluated by MTS assay for P(MAA-g-PEG-co-tBMA); n=4. Data are expressed as mean of measurements ± SD.

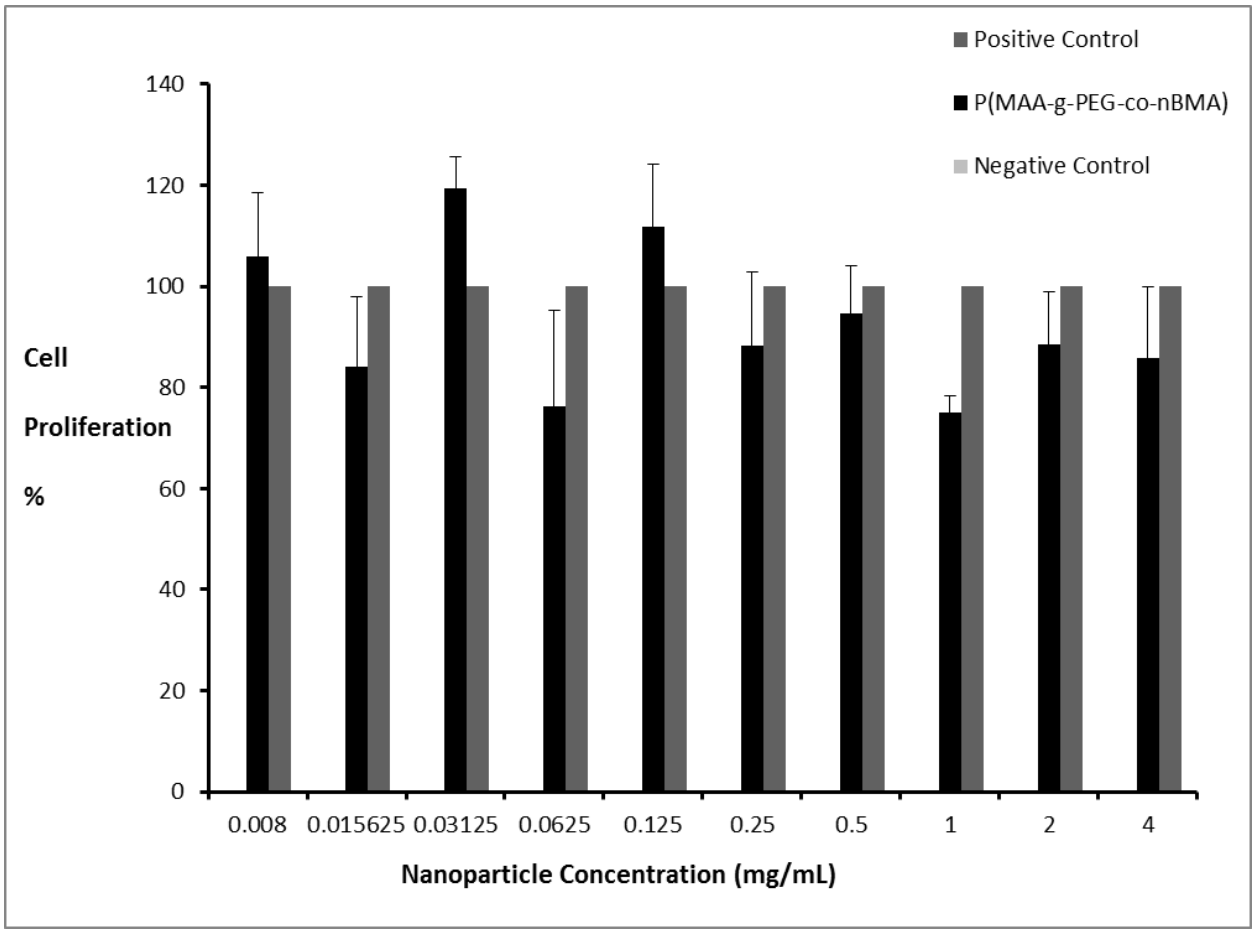

Figure 6.30 - *in vitro* cell proliferation % of evaluated by MTS assay for P(MAA-g-PEG-co-nBMA); n=4. Data are expressed as mean of measurements ± SD.

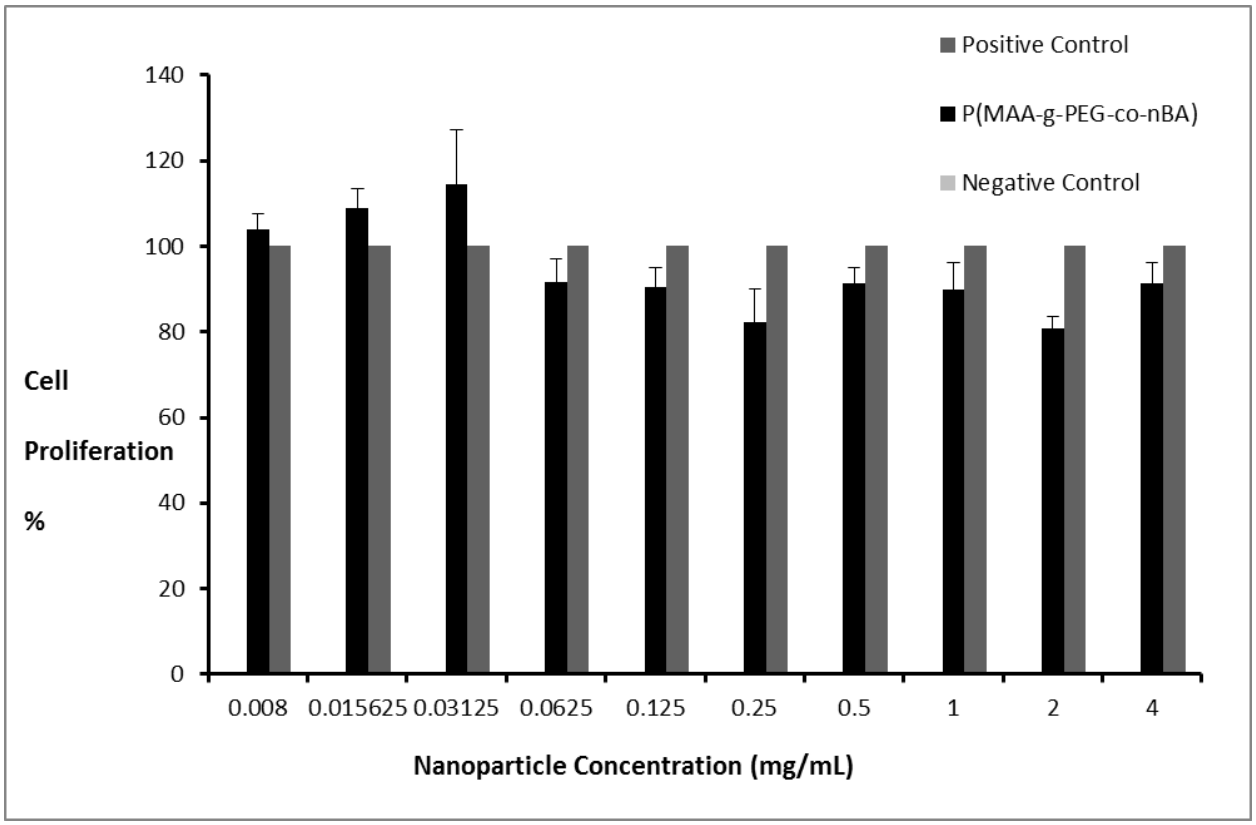

Figure 6.31 - *in vitro* cell proliferation % of evaluated by MTS assay for P(MAA-g-PEG-co-nBA); n=4. Data are expressed as mean of measurements ± SD.

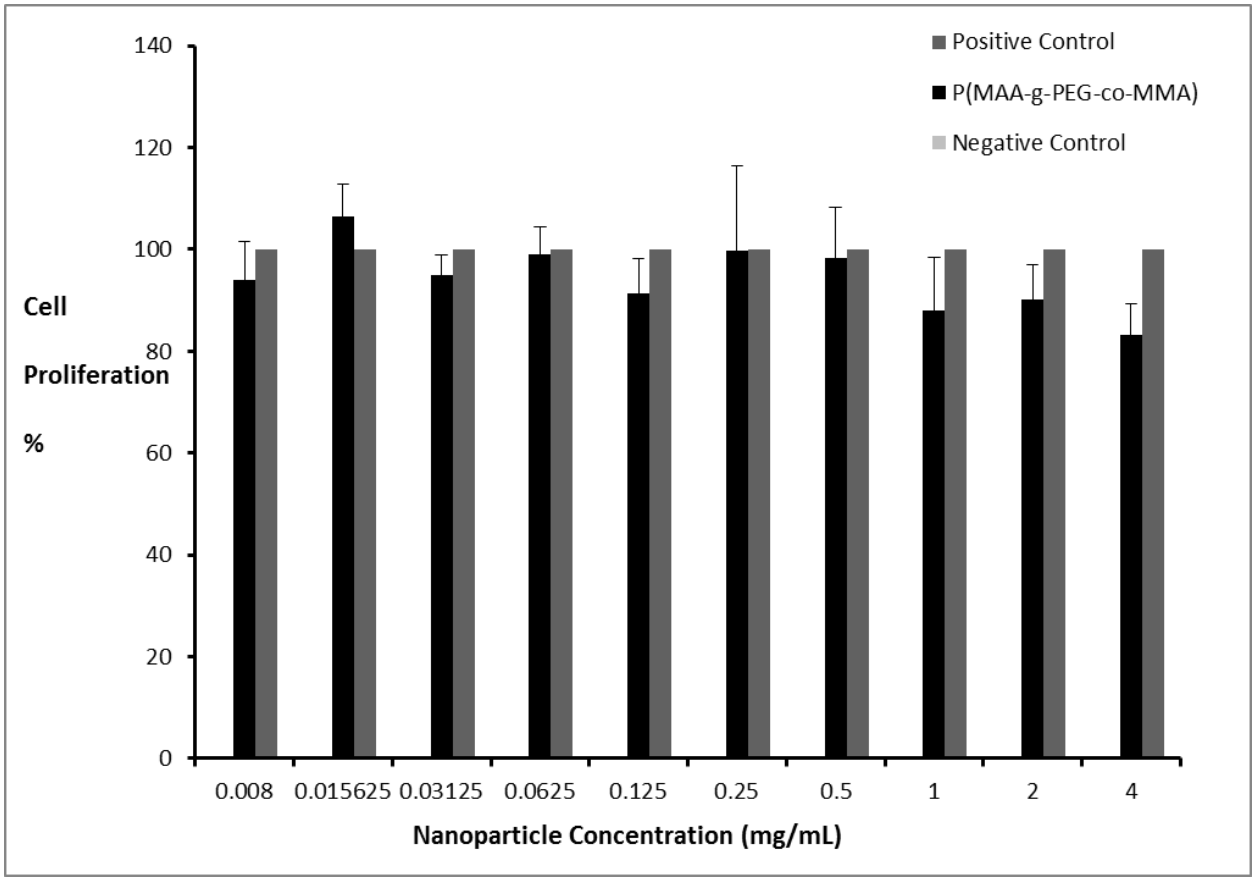

Figure 6.32 - *in vitro* cell proliferation % of evaluated by MTS assay for P(MAA-g-PEG-co-MMA); n=4. Data are expressed as mean of measurements ± SD.

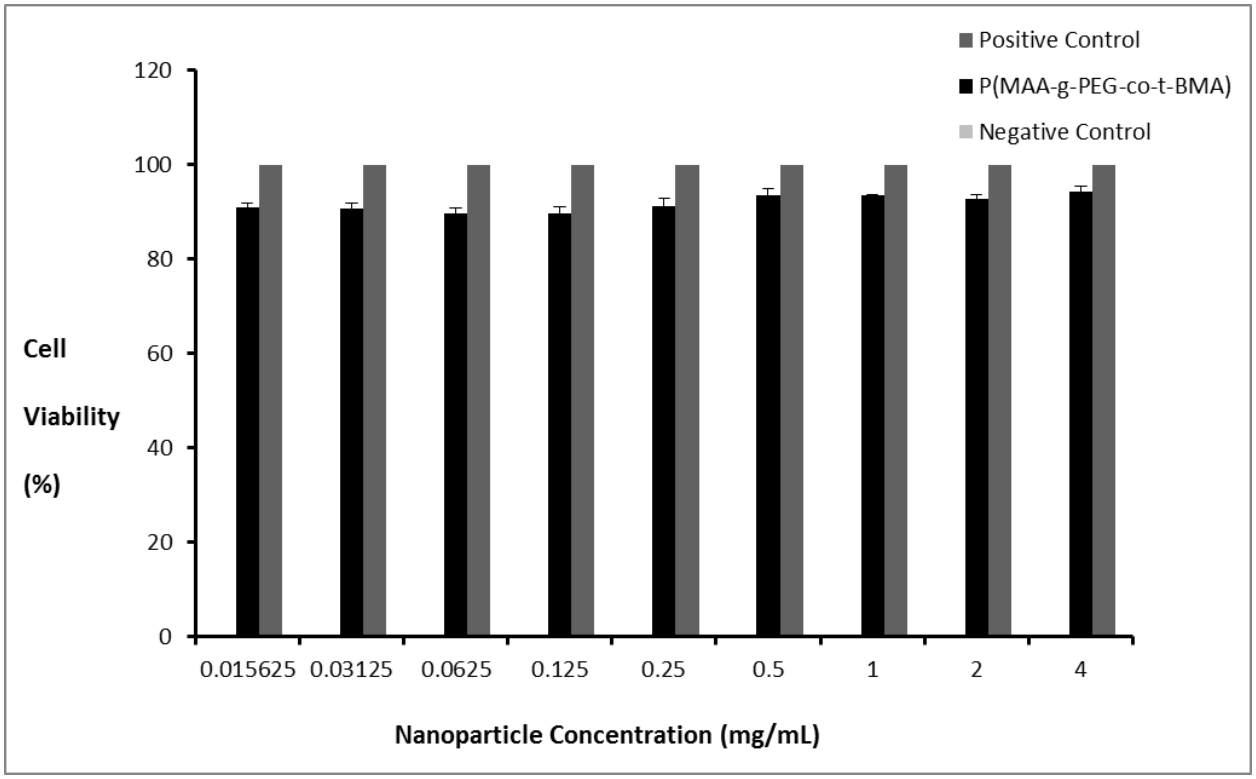

Figure 6.33 - *in vitro* cell viability % of evaluated by LDH assay for P(MAA-g-PEG-co-tBMA); n=4. Data are expressed as mean of measurements ± SD.

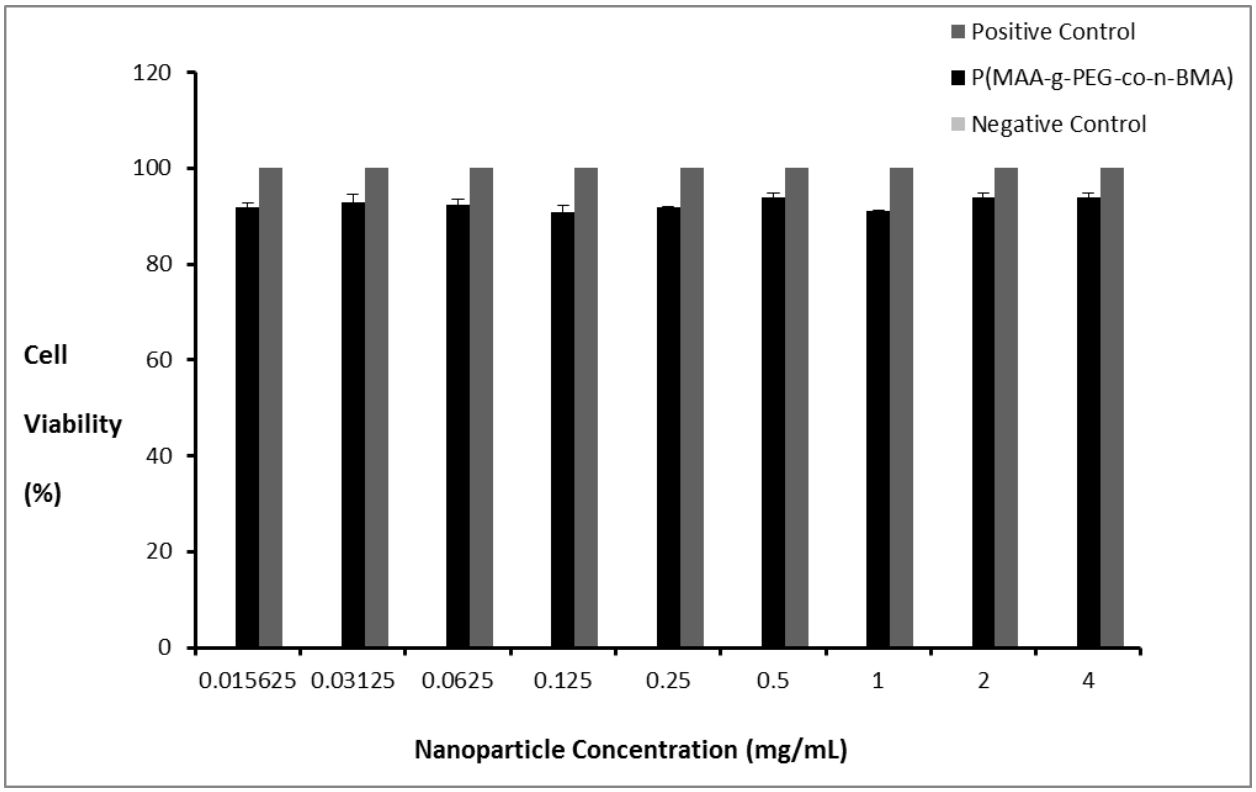

Figure 6.34 - *in vitro* cell viability % of evaluated by LDH assay for P(MAA-g-PEG-co-nBMA); n=4. Data are expressed as mean of measurements ± SD.

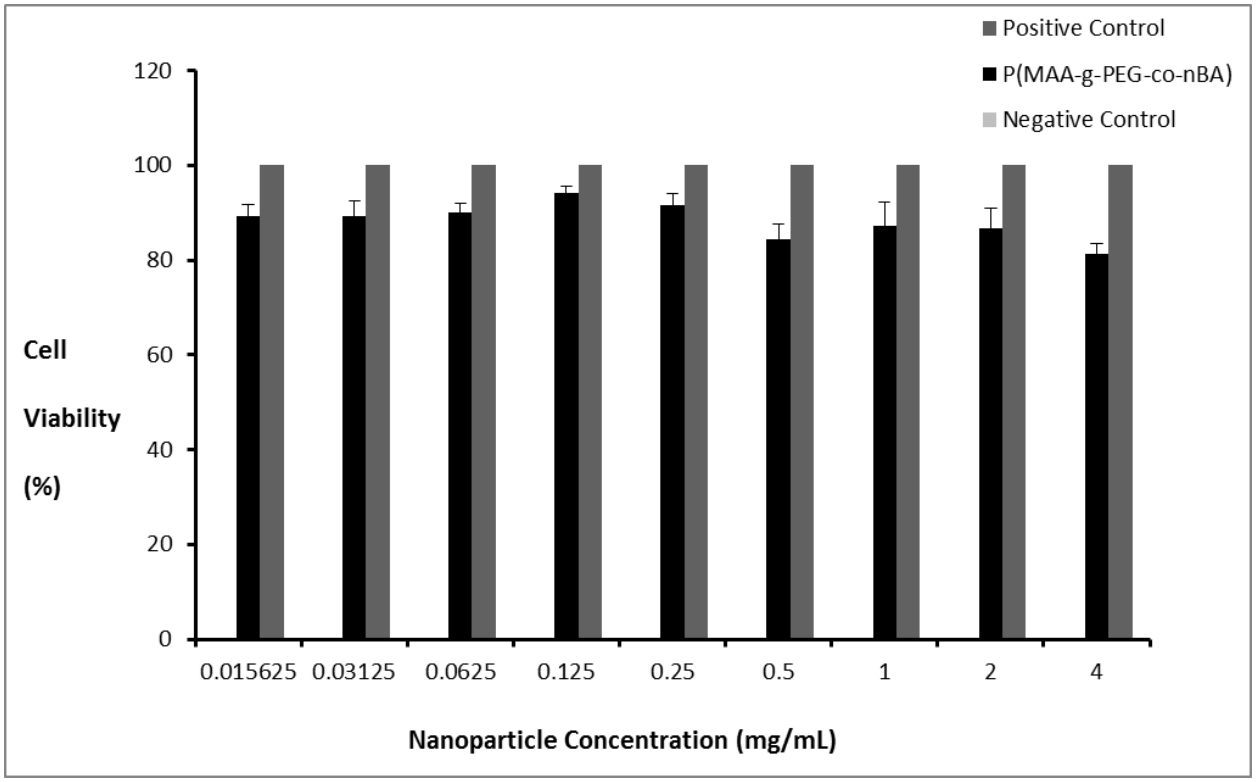

Figure 6.35 - *in vitro* cell viability % of evaluated by LDH assay for P(MAA-g-PEG-co-nBA); n=4. Data are expressed as mean of measurements ± SD.

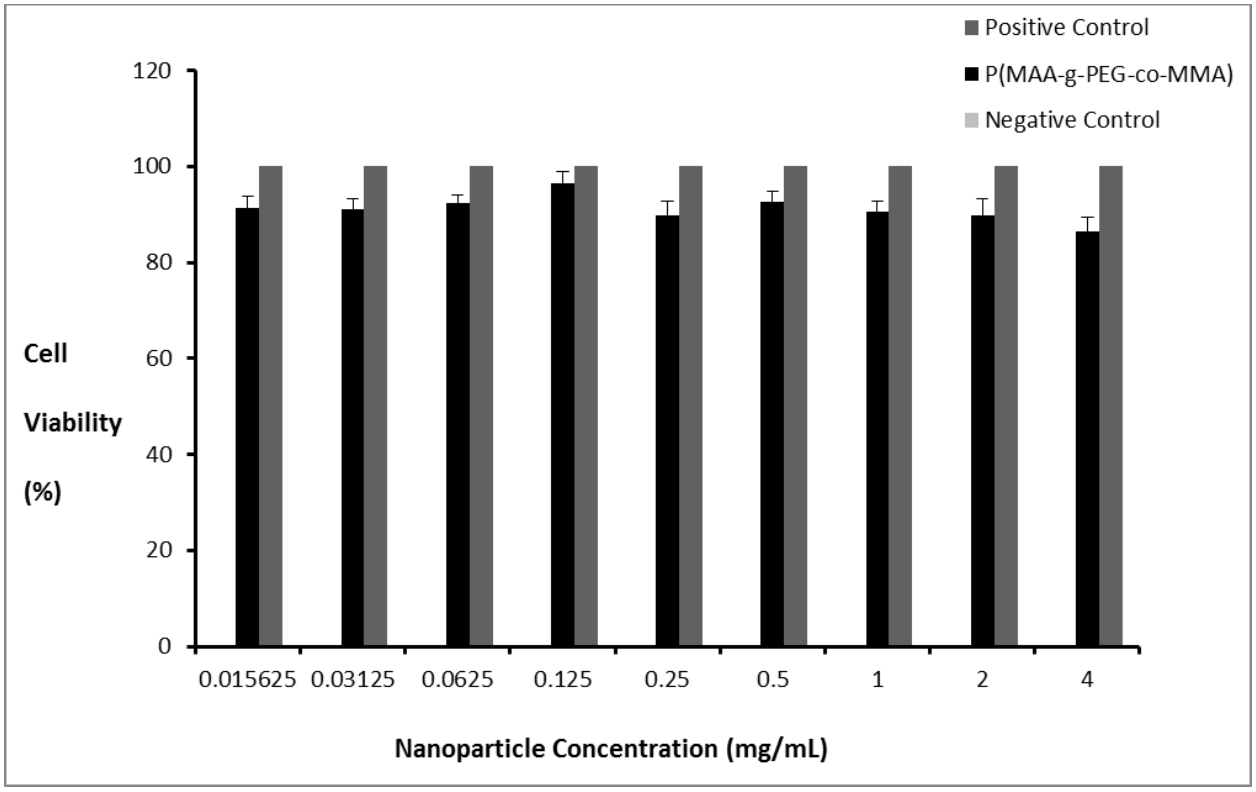

Figure 6.36 - *in vitro* cell viability % evaluated by LDH assay for P(MAA-g-PEG-co-MMA); n=4. Data are expressed as mean of measurements ± SD.

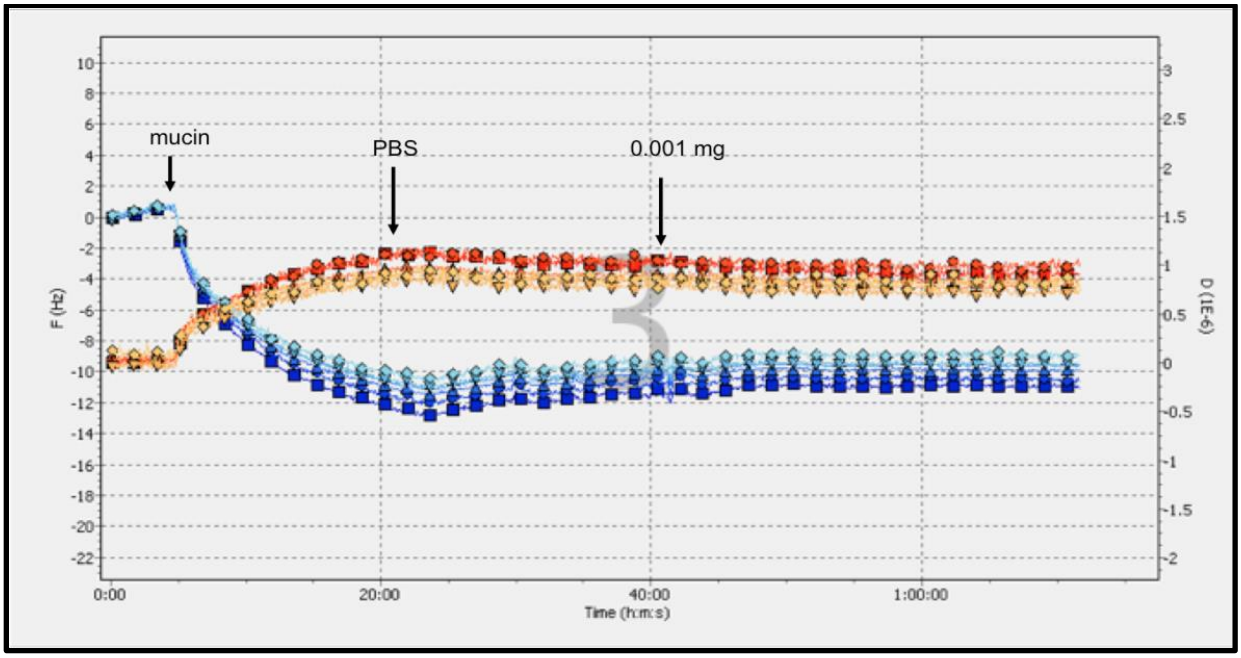
mucin
PBS
0.001 mg
F (Hz)
D (1E-6)
Time (h:m:s)
0:00
20:00
40:00
1:00:00

(a)

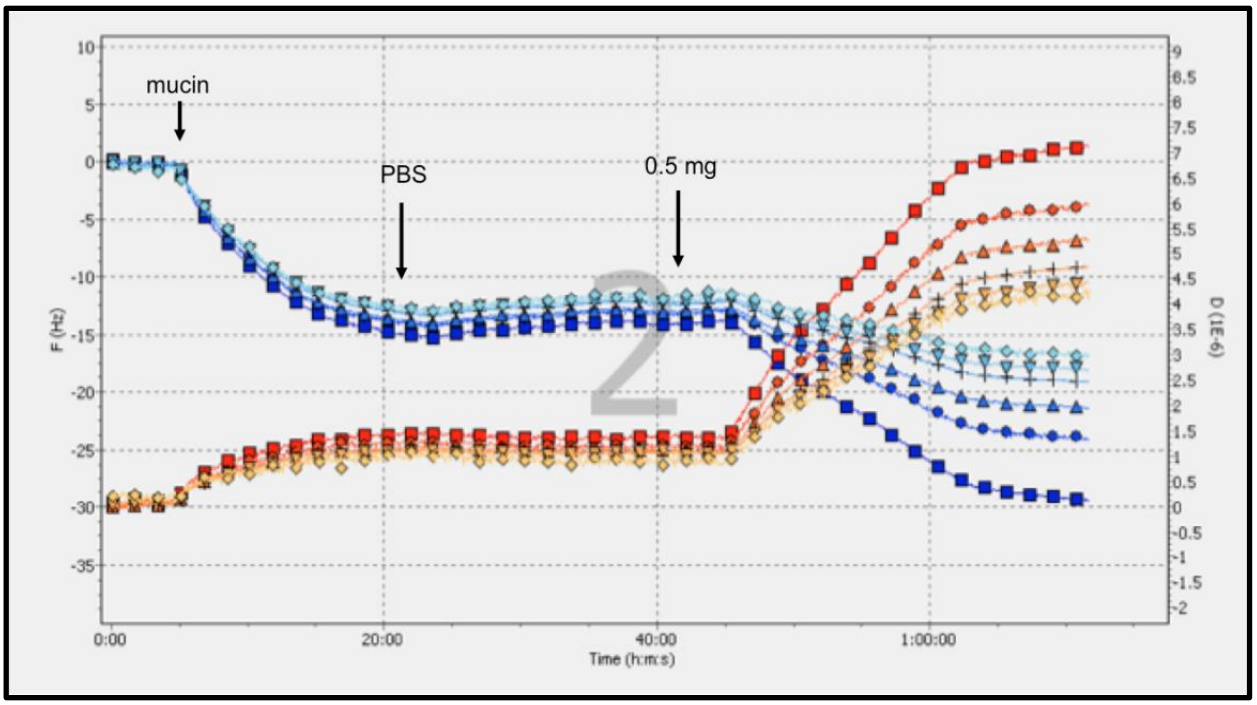
mucin
PBS
0.5 mg
F (Hz)
D (1E-6)
Time (h:m:s)
0:00
20:00
40:00
1:00:00

(b)

Figure 6.37 - Mucoadhesion studies performed with a quartz crystal microbalance with (a) 0.001 mg/ml polymeric nanoparticles, (b) 0.5 mg/ml polymeric nanoparticles.

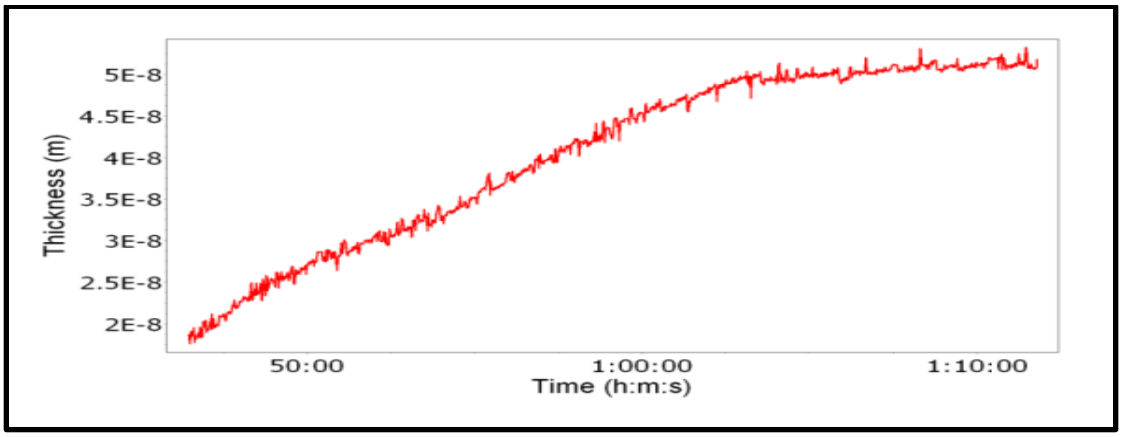

(a)

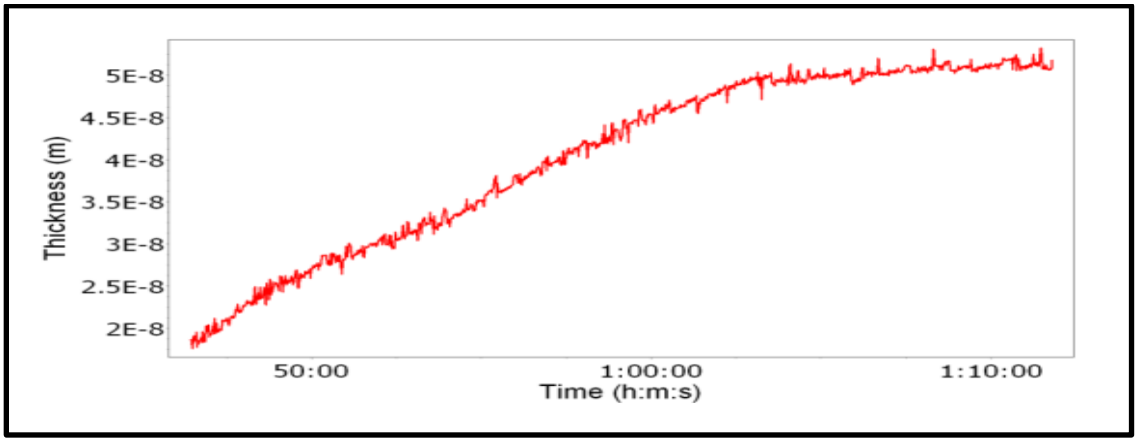

(b)

Figure 6.38 - Change in (a) mass and, (b) thickness of immobilized mucin owing adhesion of polymeric nanoparticles.

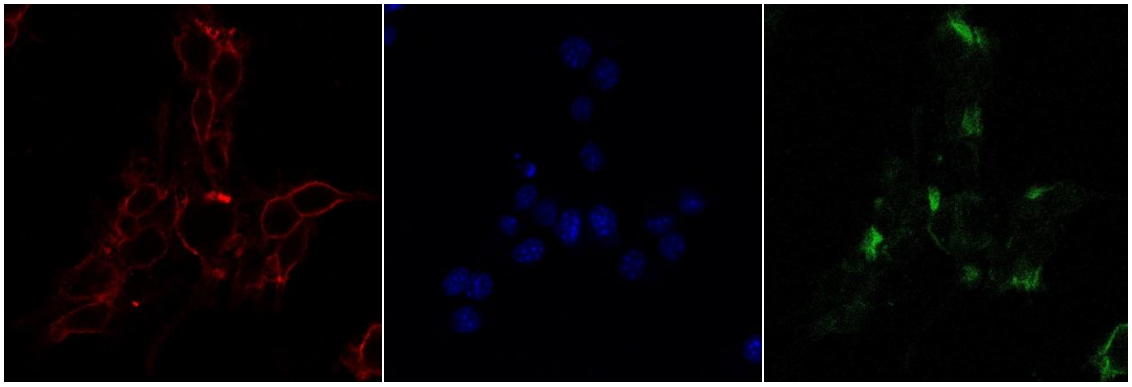

(A)

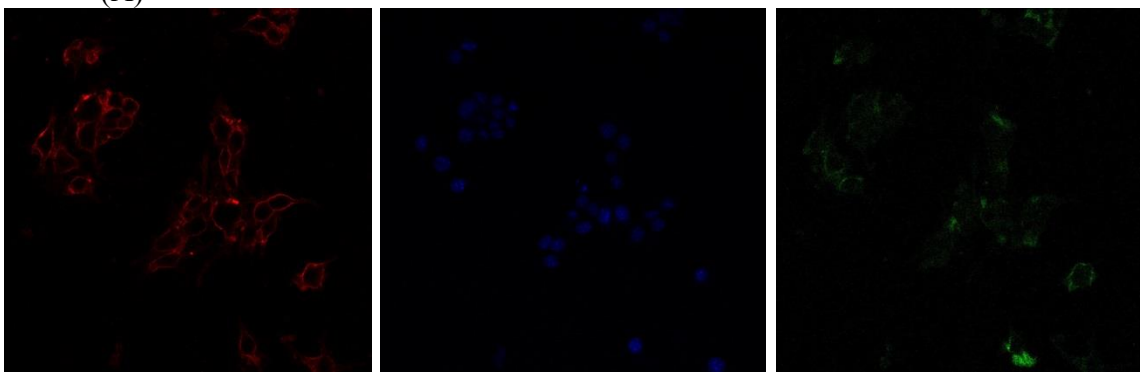

(B)

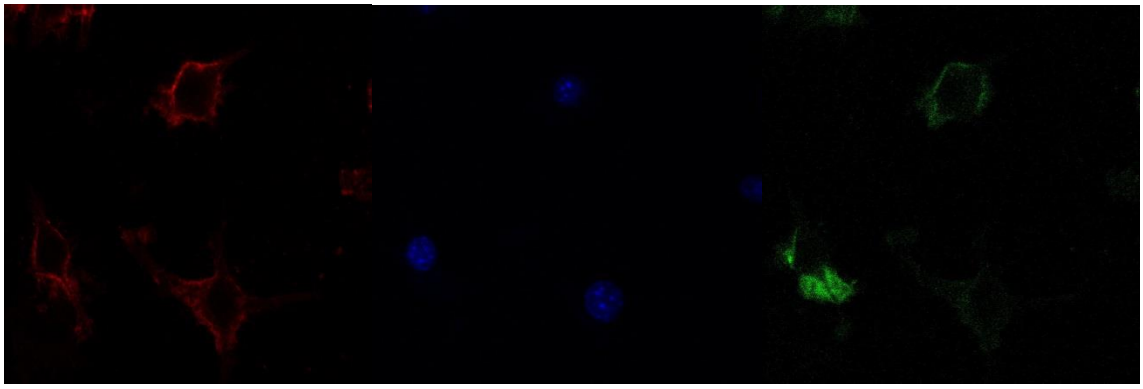

(C)

Figure 6.39 - Confocal microscopy images of fluorescently tagged polyanionic nanoparticles incubated with RAW 264.7 for 2 hr. Red: Alexa Fluor® 594 wheat-germ agglutinin (WGA); Blue: DAPI; Green: AlexaFluor® 488 tagged nanoparticles.

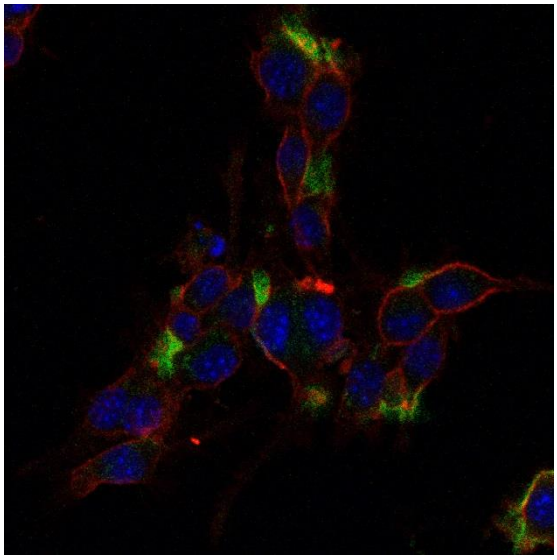

(a)

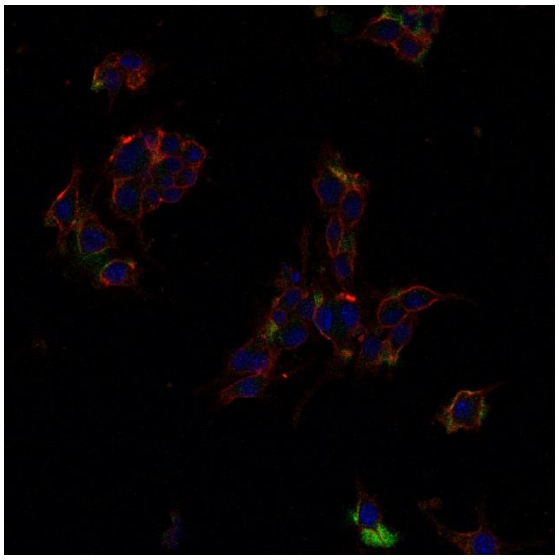

(b)

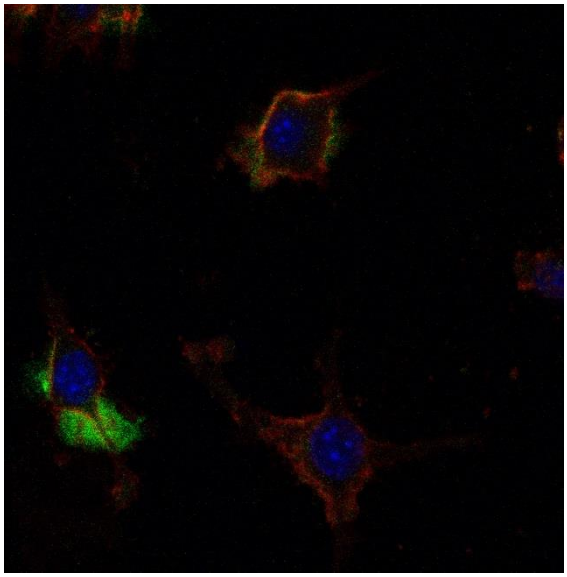

(c)

Figure 6.40 - Composite confocal microscopy images with merged color channels of fluorescently tagged polyanionic nanoparticles incubated with RAW 264.7 for 2 hr. Red: Alexa Fluor® 594 wheat-germ agglutinin (WGA); Blue: DAPI; Green: AlexaFluor® 488 tagged nanoparticles.

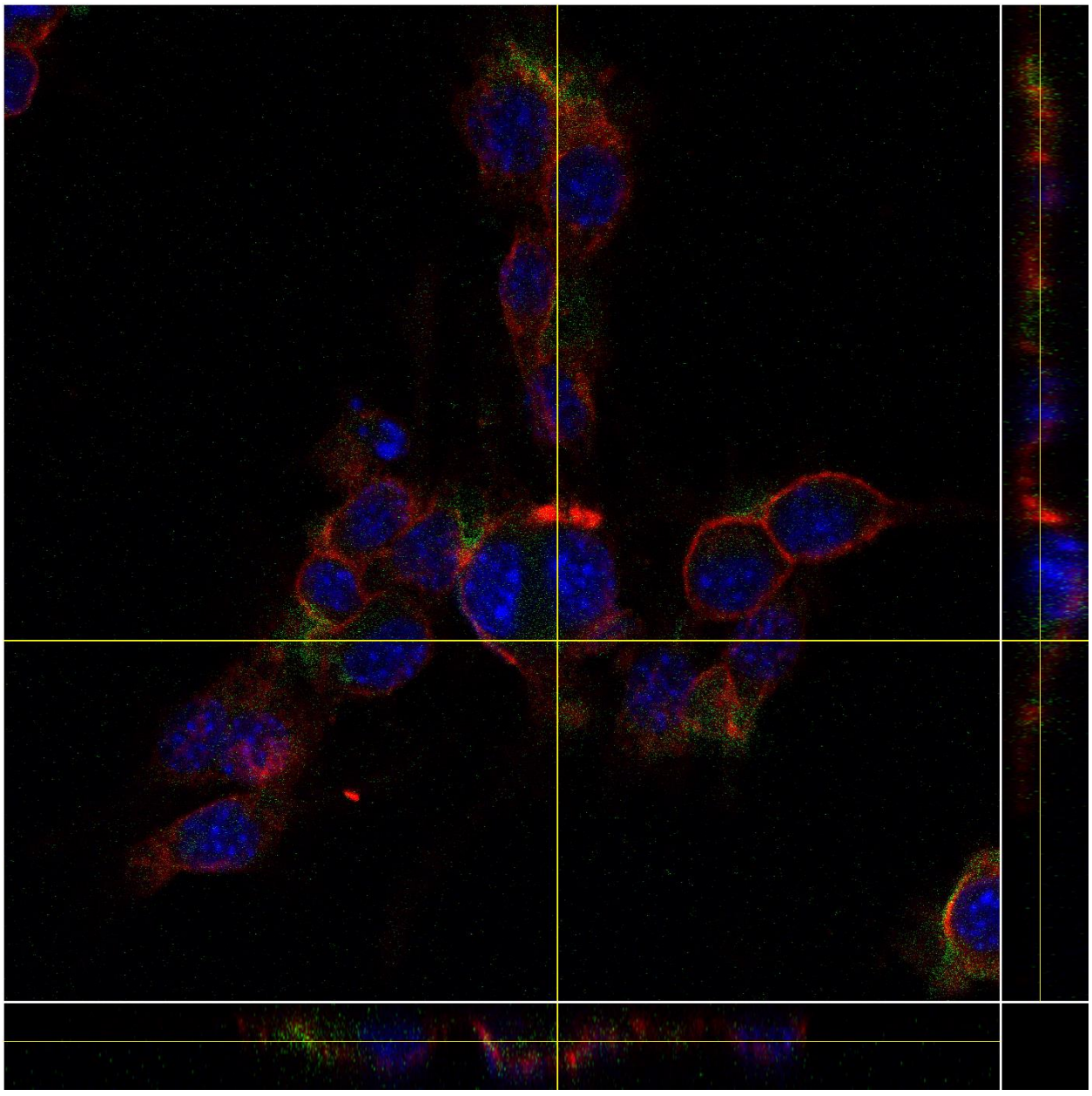

Figure 6.41 - Montage of Z-stack orthogonal view, with XZ –planes and YZ planes to visualize internalization of polyanionic nanoparticles.

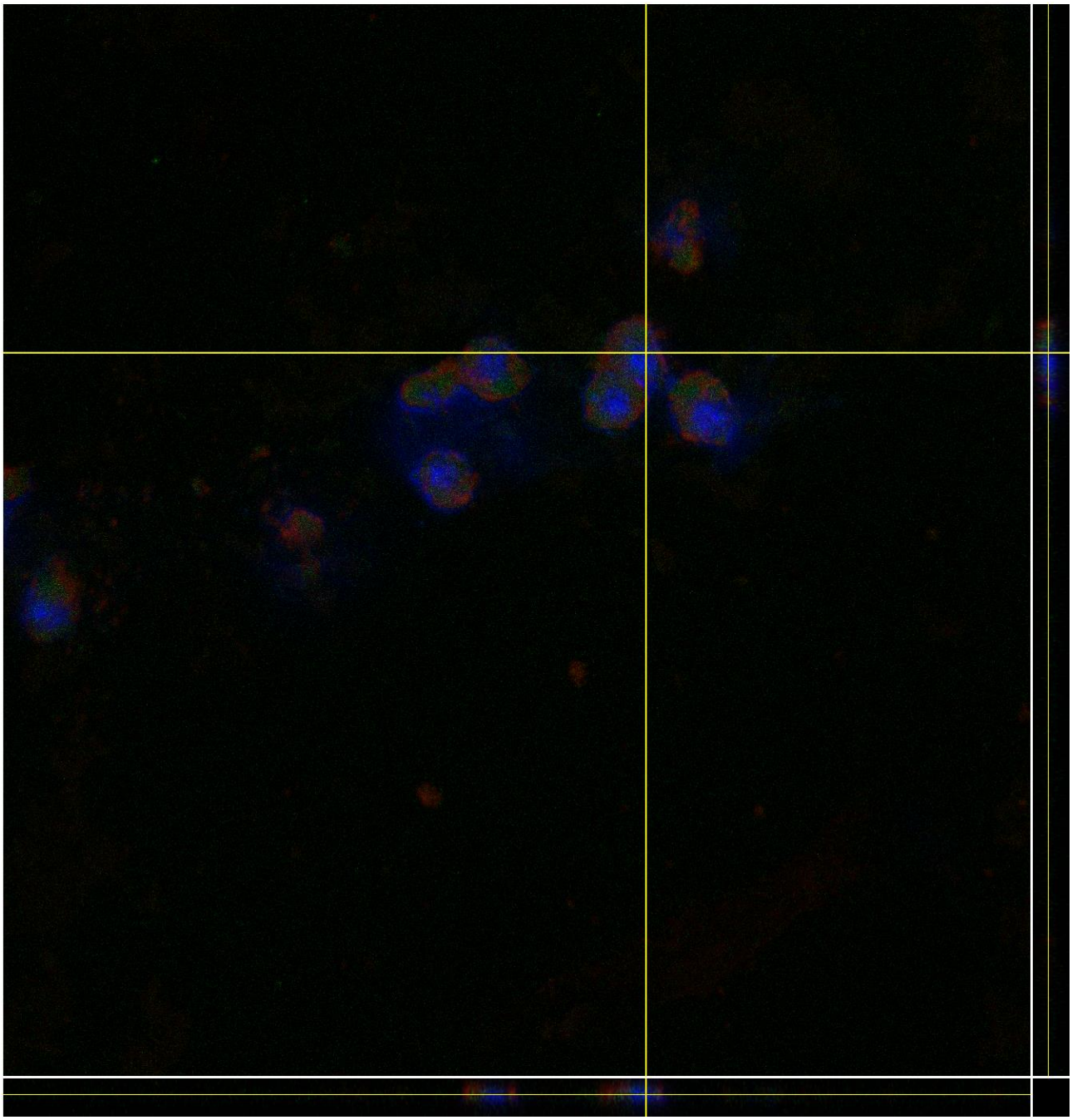

Figure 6.42 - Montage of Z-stack orthogonal view, with XZ –planes and YZ planes to visualize internalization of polycationic nanoparticles.

6.7 REFERENCES

[1] Spencer DS, Puranik AS, Peppas NA. Intelligent nanoparticles for advanced drug delivery in cancer treatment. Current Opinion in Chemical Engineering 2015; 7:84-92.

[2] Sharpe LA, Daily AM, Horava SD, Peppas NA. Therapeutic applications of hydrogels in oral drug delivery. Expert Opinion on Drug Delivery 2014; 11:901-915.

[3] Chen R, Khormaee S, Eccleston ME, Slater NKH. The role of hydrophobic amino acid grafts in the enhancement of membrane-disruptive activity of pH-responsive pseudo-peptides. Biomaterials 2009; 30:1954-1961.

[4] Du Y, Lo E, Ali S, Khademhosseini A. Directed assembly of cell-laden microgels for fabrication of 3D tissue constructs. Proceedings of the National Academy of Sciences of the United States of America 2008; 105:9522-9527.

[5] Dong L, Agarwal AK, Beebe DJ, Jiang H. Adaptive liquid microlenses activated by stimuli-responsive hydrogels. Nature 2006; 442:551-554.

[6] Tokareva I, Minko S, Fendler JH, Hutter E. Nanosensors Based on Responsive Polymer Brushes and Gold Nanoparticle Enhanced Transmission Surface Plasmon Resonance Spectroscopy. Journal of the American Chemical Society 2004; 126:15950-15951.

[7] Plapied L, Duhem N, des Rieux A, Préat V. Fate of polymeric nanocarriers for oral drug delivery. Current Opinion in Colloid & Interface Science 2011; 16:228-237.

[8] Shen Q, Lin Y, Handa T *et al.* Modulation of intestinal P-glycoprotein function by polyethylene glycols and their derivatives by in vitro transport and in situ absorption studies. International Journal of Pharmaceutics 2006; 313:49-56.

[9] Primard C, Rochereau N, Luciani E *et al.* Traffic of poly(lactic acid) nanoparticulate vaccine vehicle from intestinal mucus to sub-epithelial immune competent cells. Biomaterials 2010; 31:6060-6068.

[10] Sheetal RDM, Sudip KD, Nandita GD. Polymeric Nanoparticles for Small-Molecule Drugs: Biodegradation of Polymers and Fabrication of Nanoparticles. In: Drug Delivery Nanoparticles Formulation and Characterization. Informa Healthcare; 2009. pp. 16-34.

[11] Blanchette J, Peppas N. Oral Chemotherapeutic Delivery: Design and Cellular Response. Ann Biomed Eng 2005; 33:142-149.

[12] Liechty WB, Caldorera-Moore M, Phillips MA *et al.* Advanced molecular design of biopolymers for transmucosal and intracellular delivery of chemotherapeutic agents and biological therapeutics. Journal of Controlled Release 2011; 155:119-127.

[13] Torchilin VP. Micellar nanocarriers: pharmaceutical perspectives. Pharmaceutical research 2007; 24:1-16.

[14] Jones M, Leroux J. Polymeric micelles - a new generation of colloidal drug carriers. European journal of pharmaceutics and biopharmaceutics : official journal of Arbeitsgemeinschaft fur Pharmazeutische Verfahrenstechnik e.V 1999; 48:101-111.

[15] Gil ES, Hudson SM. Stimuli-reponsive polymers and their bioconjugates. Progress in Polymer Science 2004; 29:1173-1222.

[16] Schmaljohann D. Thermo- and pH-responsive polymers in drug delivery. Advanced Drug Delivery Reviews 2006; 58:1655-1670.

[17] Liechty WB, Scheuerle RL, Peppas NA. Tunable, responsive nanogels containing t-butyl methacrylate and 2-(t-butylamino)ethyl methacrylate. Polymer 2013; 54:3784-3795.

[18] Peppas NA. Physiologically Responsive Hydrogels. Journal of Bioactive and Compatible Polymers 1991; 6:241-246.

[19] Dudhani AR, Kosaraju SL. Bioadhesive chitosan nanoparticles: Preparation and characterization. Carbohydrate Polymers 2010; 81:243-251.

[20] des Rieux A, Fievez V, Garinot M *et al.* Nanoparticles as potential oral delivery systems of proteins and vaccines: a mechanistic approach. Journal of controlled release : official journal of the Controlled Release Society 2006; 116:1-27.

[21] Frohlich E. The role of surface charge in cellular uptake and cytotoxicity of medical nanoparticles. International journal of nanomedicine 2012; 7:5577-5591.

[22] Quinting GR, Cai R. High-Resolution NMR Analysis of the Tacticity of Poly(n-butyl methacrylate). Macromolecules 1994; 27:6301-6306.

[23] Wischke C, Neffe AT, Steuer S *et al.* AB-polymer networks with cooligoester and poly(n-butyl acrylate) segments as a multifunctional matrix for controlled drug release. Macromolecular bioscience 2010; 10:1063-1072.

[24] Chu C-C, Wang Y-W, Yeh C-F, Wang L. Synthesis of Conductive Core−Shell Nanoparticles Based on Amphiphilic Starburst Poly(n-butyl acrylate)-b-poly(styrenesulfonate). Macromolecules 2008; 41:5632-5640.

[25] Richard RE, Schwarz M, Ranade S *et al.* Evaluation of Acrylate-Based Block Copolymers Prepared by Atom Transfer Radical Polymerization as Matrices for Paclitaxel Delivery from Coronary Stents. Biomacromolecules 2005; 6:3410-3418.

[26] Fujisawa S, Atsumi T, Kadoma Y. Cytotoxicity of methyl methacrylate (MMA) and related compounds and their interaction with dipalmitoylphosphatidylcholine (DPPC) liposomes as a model for biomembranes. Oral diseases 2000; 6:215-221.

[27] Jaruga E, Sokal A, Chrul S, Bartosz G. Apoptosis-independent alterations in membrane dynamics induced by curcumin. Experimental cell research 1998; 245:303-312.

[28] Curcio A, Torella D, Cuda G *et al.* Effect of stent coating alone on in vitro vascular smooth muscle cell proliferation and apoptosis. American journal of physiology. Heart and circulatory physiology 2004; 286:H902-908.

[29] Alfrey T. Copolymerization. Interscience Publishers; 1964.

[30] Odian GG, Odian G. Principles of polymerization. Wiley-Interscience New York; 2004.

[31] Peracchia MT, Fattal E, Desmaële D *et al.* Stealth® PEGylated polycyanoacrylate nanoparticles for intravenous administration and splenic targeting. Journal of Controlled Release 1999; 60:121-128.

[32] Gref R, Domb A, Quellec P *et al.* The controlled intravenous delivery of drugs using PEG-coated sterically stabilized nanospheres. Advanced Drug Delivery Reviews 1995; 16:215-233.

[33] Peracchia MT, Vauthier C, Desmaele D *et al.* Pegylated nanoparticles from a novel methoxypolyethylene glycol cyanoacrylate-hexadecyl cyanoacrylate amphiphilic copolymer. Pharmaceutical research 1998; 15:550-556.

[34] Tress M, Mapesa EU, Kossack W *et al.* Glassy Dynamics in Condensed Isolated Polymer Chains. Science 2013; 341:1371-1374.

[35] Coates J. Interpretation of infrared spectra, a practical approach. Encyclopedia of analytical chemistry 2000.

[36] Forbes DC, Peppas NA. Differences in molecular structure in cross-linked polycationic nanoparticles synthesized using ARGET ATRP or UV-initiated polymerization. Polymer 2013; 54:4486-4492.

[37] Atkinson JR, Hay JN, Jenkins MJ. Enthalpic relaxation in semi-crystalline PEEK. Polymer 2002; 43:731-735.

[38] Ali MM, Sabnis A, Dewitt D *et al.* Therapeutic polymeric nanoparticle compositions with high glass transition temperature or high molecular weight copolymers. In: Google Patents; 2011.

[39] Catoni SEM, Trindade KN, Gomes CAT *et al.* Influence of poly(ethylene grycol) - (PEG) on the properties of influence of poly(3-hydroxybutyrate-CO-3-hydroxyvalerate) - PHBV. Polímeros 2013; 23:320-325.

[40] Ahmed SA, Gogal RM, Jr., Walsh JE. A new rapid and simple non-radioactive assay to monitor and determine the proliferation of lymphocytes: an alternative to [3H]thymidine incorporation assay. Journal of immunological methods 1994; 170:211-224.

[41] Berridge MV, Herst PM, Tan AS. Tetrazolium dyes as tools in cell biology: new insights into their cellular reduction. Biotechnology annual review 2005; 11:127-152.

[42] Scudiero DA, Shoemaker RH, Paull KD *et al.* Evaluation of a soluble tetrazolium/formazan assay for cell growth and drug sensitivity in culture using human and other tumor cell lines. Cancer research 1988; 48:4827-4833.

[43] Chan FK, Moriwaki K, De Rosa MJ. Detection of necrosis by release of lactate dehydrogenase activity. Methods in molecular biology (Clifton, N.J.) 2013; 979:65-70.

[44] Lai SK, Wang Y-Y, Hanes J. Mucus-penetrating nanoparticles for drug and gene delivery to mucosal tissues. Advanced Drug Delivery Reviews 2009; 61:158-171.

[45] Ensign LM, Cone R, Hanes J. Oral drug delivery with polymeric nanoparticles: The gastrointestinal mucus barriers. Advanced Drug Delivery Reviews 2012; 64:557-570.

[46] Yun Y, Cho Yw Fau - Park K, Park K. Nanoparticles for oral delivery: targeted nanoparticles with peptidic ligands for oral protein delivery.

Chapter 7: Modulation of Hydrophobic Solute Permeation through Anionic Crosslinked Hydrogels for Cancer Drug Delivery Applications

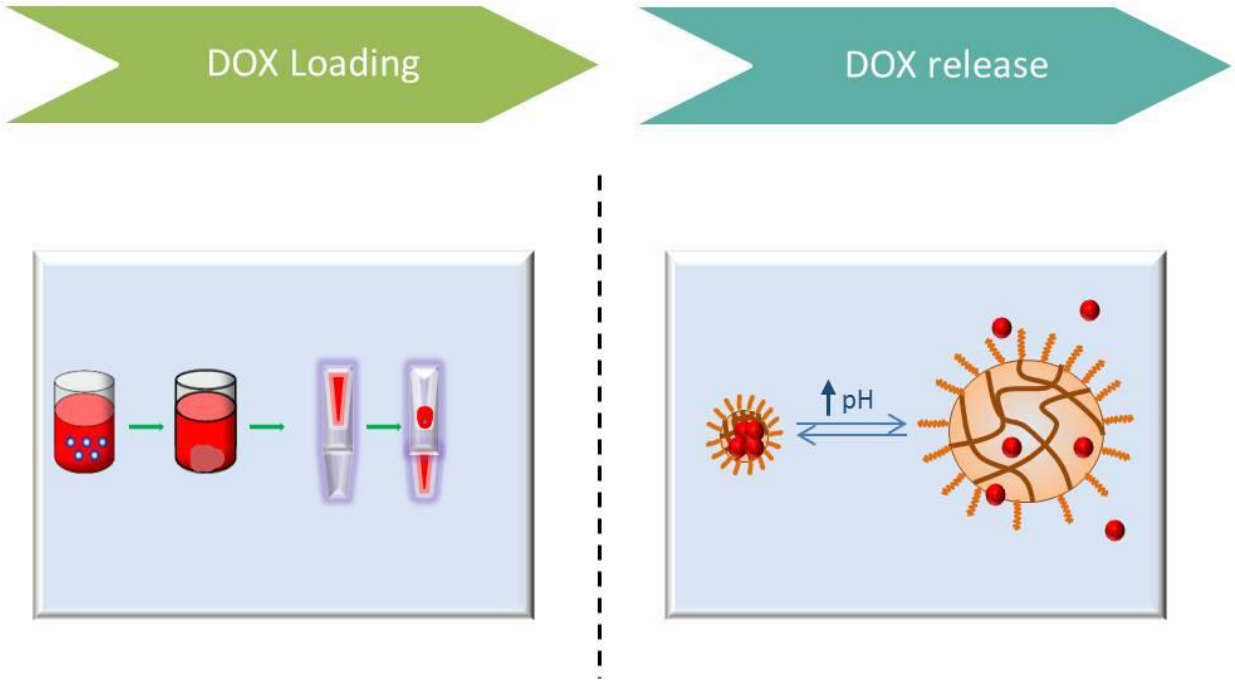

- Formulations were evaluated for their ability to load and release doxorubicin, a hydrophobic chemotherapeutic
- Studies were conducted to determine the diffusivity and permeability of doxorubicin through membranes in drug diffusion cells that were synthesized with similar feed composition
- Powder X-ray diffraction was also used to substantiate amorphous nature of doxorubicin-loaded nanoscale hydrogels

2.1 INTRODUCTION

Loading and release experiments were performed using doxorubicin as a model hydrophobic drug. Doxorubicin is an anthracycline antibiotic that acts by intercalating between DNA, or by generation of free radical species through redox cycling, eventually causing cell death by inhibition of DNA topoisomerase II [52]. The molecular structure of doxorubicin contains an anthraquinone fragment which is the planar chromophore component responsible for its bright red color. Presence of Beta-hydroxycarbonyl groups in the molecular structure allows for strong chelation between doxorubicin and the phosphate groups of cell DNA. Formation of harmful radicals is also singularly responsible for the notorious cardiotoxicity of doxorubicin, the most prominent side-effect upon intravenous administration. Doxorubicin, despite its side effects, is the most extensively used chemotherapeutic and is essential in treating breast cancer, oesophageal carcinomas, Kaposi's sarcoma, and Hodgkin and non-Hodgkin lymphomas.

Based on the BDDCS system, doxorubicin is classified as a class IV drug (low solubility, low permeability) and has an oral bioavailability of 5%. Doxorubicin is the most commonly used chemotherapeutic as it is effective against a number of cancer malignancies such as breast, lung, lymphomas, bone and colon cancers. Doxorubicin has a molecular weight of about 543 g/mol and a solubility of less than 1 mg/ml in water.

2.2 MATERIALS AND METHODS

2.2.1 Synthesis of polymer formulations

Nanoparticle polymer formulations were synthesized as described in Section 6.2.1. Briefly, Nanoscale polyanionic hydrogels were synthesized by UV-initiated free radical polymerization of a pre-polymer solution mixture. The pre-polymer mixture was comprised of monomers - methacrylic acid (MAA), tert-butyl methacrylate (t-BMA), poly(ethylene glycol) monomethyl ether methacrylate (PEGMMA) (molecular weight ~ 2080), and cross linking agent tetraethylene glycol dimethacrylate (TEGDMA) at 1% mole fraction of total monomer amount. The surfactants sodium dodecyl sulfate and Brij-30® were then added to the system followed by Irgacure 2959 at 0.5 wt% of total monomer. The hydrophobic monomer was varied in each case to yield a different core hydrophobicity for each formulation.

Membrane formulations for the drug diffusion and partitioning studies were synthesized using a film polymerization technique. In similar fashion to the nanoparticle synthesis, the pre-polymer mixture was comprised of monomers - methacrylic acid (MAA), tert-butyl methacrylate (t-BMA) or other hydrophobic monomer, poly(ethylene glycol) monomethyl ether methacrylate (PEGMMA) (molecular weight ~ 2080), and cross linking agent tetraethylene glycol dimethacrylate (TEGDMA) at 1% mole fraction of total monomer amount. No surfactants were added and the solvent was ethanol instead of water. The mixture was placed in a sonic bath and sonicated for 10 mins, before being transferred the gap between two plates, and placed under a UV flood source for 30 mins. The resultant film was washed in water for 7 days and then punched into appropriates sized disks for the membrane drug diffusion and partitioning studies.

2.2.2 Doxorubicin loading studies

Doxorubicin was loaded into the P(MAA-co-tBMA-g-PEG) nanoscale hydrogels by imbibition or equilibrium partitioning. In this method, a 0.15mg/ml stock solution of doxorubicin was prepared in 1X PBS solution, using 2 vol% Dimethyl sulfoxide (DMSO) to solubilize the hydrophobic drug. Adriamycin (doxorubicin hydrochloride, purchased from Biotang Inc., MA) was first solubilized in DMSO, followed by addition of 1X PBS (pH 7.4). The stock solution was kept stirring for 24 hours to ensure mixing. Nanoscale hydrogel particles were then added to the stock solution at a concentration of 1.2 mg/ml and were allowed to stir for a period of 6 hours. During the 24 hour period, 200 ul samples were taken in triplicate at distinct time intervals to analyze the doxorubicin concentration of the stock solution with time. Samples were taken at regular time intervals and nanoparticles were filtered off using Amicon® Ultracel®-0.5 centrifugal filter devices (MWCO: 30,000) (Millipore, MA) centrifuged at 14,000g for 20 min, and filtrate doxorubicin analyzed using HPLC. Doxorubicin in the samples was detected using Waters HPLC, and 45:55 Acetonitrile:Water solvent ratio was run for 10 mins, and displayed an elution peak for doxorubicin (maximum absorbance wavelength = 485 nm) at ~ 3.7 mins. The doxorubicin concentration in the membrane and its partition coefficient was calculated by performing a mass balance for doxorubicin.

After 24 hours, 1 N HCl was added to collapse the polyanionic hydrogel nanoparticles and entrap the drug molecules that may have diffused into the nanoparticles over the 6 hour period. The drug-loaded nanoparticles were then isolated from the doxorubicin stock solution using Amicon® Ultra®-15 centrifugal filter devices (Millipore,

MA) with molecular weight cut-off 30,000. The drug loaded nanoparticles thus obtained as retentate as a result of the centrifugal filtration process, were rinsed with water to remove any surface adsorbed doxorubicin.

$$\text{Doxorubicin Loading Efficiency} = \frac{C_o - C_f}{C_0} * 100 \quad (7.1)$$

Where, C_o is the initial doxorubicin concentration and C_f is the final doxorubicin concentration remaining in the solution.

2.2.3 Doxorubicin release studies

Release experiments were performed in beakers with constant stirring and at 37 °C. To perform the release studies, 5 mg of doxorubicin-loaded nanoparticles were added to a beaker containing 1X PBS. To simulate the gastric pH conditions, first the drug-loaded nanoparticles were released at a pH 2.0 for a period of 2 hours (representative of the gastric emptying time). The pH was then raised to 7.4 for the remaining duration of the experiment to mimic the neutral conditions of the small intestine. Samples were taken at regular time intervals and nanoparticles were filtered off using centrifugal filter devices (Amicon® Ultracel®-0.5 centrifugal filter devices, MWCO: 30,000, Millipore, MA), and filtrate doxorubicin analyzed using HPLC. Doxorubicin in the samples was detected using Waters HPLC, and 45:55 Acetonitrile:Water solvent ratio was run for 10 mins, and displayed an elution peak for doxorubicin (maximum absorbance wavelength = 485 nm) at ~ 3.7 mins. The doxorubicin concentration in the membrane and its partition coefficient was calculated by performing a mass balance for doxorubicin.

2.2.4 Powder X-ray diffraction studies

We tested the amorphous nature of our DOX-loaded nanoparticle drug formulations using powder X-ray diffraction (P-XRD). P-XRD experiments were conducted using drug-loaded powder samples of the formulations and pure DOX powder as obtained from the manufacturer. The P-XRD patterns were obtained using a R-AXIS SPIDER (Rigaku Corporation, Tokyo, Japan) instrument using a 3 kW sealed Cu (1.54Å) filament radiation. Measurements were conducted at a voltage of 40kV and a current of 40mA.

2.2.5 Solute diffusion studies

To better understand solute-polymer interactions, we studied diffusion of doxorubicin through a microscale membrane containing the same monomer components as their nanoscale counterparts. To perform doxorubicin diffusion studies, we used a Valia-Chen diffusion cell (Crown Glass Co., Inc., Somerville, NJ), which consists of side-by-side donor and receptor reservoirs. These diffusion cells have been used extensively in the past to study solute diffusion and permeation through ionic hydrogels. Previously, however, studies were conducted with hydrophilic solutes, and this is the first instance of the evaluation of drug diffusion studies performed in Valia-Chen diffusion with hydrophobic solutes diffusing through hydrogels with a hydrophobic component.

To simulate physiological conditions of drug diffusion, the temperature was maintained at 37^0C, and a physiologically relevant buffer (1X PBS) was used. The apparatus comprised of two half-cells- a donor cell and a receptor cell. Each half cell has

a volume of 3 mL and a side opening with a diameter of 9mm to place the hydrogel membrane. Before securing the membrane in the side opening, the membrane was pre-swollen and equilibrated under the same pH conditions and buffer as the actual diffusion experiment. The membrane was then secured firmly between the half-cells to avoid any loss of solvent by evaporation. It is crucial that the membrane remain swollen during the course of the diffusion experiment to ensure proper diffusion of the solute through the hydrogel. The hydrogel membranes used in the experiment were membrane versions of the four formulations synthesized using the film polymerization method mentioned above, namely, P(MAA-g-PEG-co-tBMA), P(MAA-g-PEG-co-nBA), P(MAA-g-PEG-co-nBMA), and P(MAA-g-PEG-co-MMA). Doxorubicin was the model solute used to evaluate and compare the ability of these hydrogels to permeate hydrophobic solutes.

The donor cell was filled with a 0.15 mg/ml solution of doxorubicin, consistent with the solute concentration we have used throughout our drug loading experiments. The doxorubicin solution was prepared by dissolving doxorubicin (Adriamycin, Selleck Chemicals) in 1X PBS solution containing 2% v/v DMSO. The receptor cell contained 1X PBS to emulate physiological conditions of drug release. Samples (50 ul) were taken from the donor and receptor cells every day and replaced with appropriate solutions to compensate for mass lost when taking samples. The doxorubicin concentrations in donor and receptor cells were thus analyzed as a function of time. Doxorubicin in the samples was detected using HPLC. The HPLC equipment comprised of a Waters 2695 Separation Module (Waters Corporation, Milford, MA) attached to a Waters 2487 Dual λ Absorbance Detector (Waters Corporation, Milford, MA). Analysis was performed using

a reverse-phase analytical HPLC method that used water with 0.1% volume trifluoroacetic acid (TFA) as solvent A, and acetonitrile with 0.1% volume trifluoroacetic acid (TFA) as solvent B. During the process, the mobile phase consisted of 45% Acetonitrile (solvent B) and 55% Water (solvent B) ratio; it was run for 10 mins and displayed an elution peak for doxorubicin (maximum absorbance wavelength = 485 nm) at ~ 3.7 mins.

2.2.6 Membrane partitioning

Next, we determined the solute partition coefficients in the four P(MAA-g-PEG-co-hydrophobic monomer) membranes. Before conducting the partitioning experiments, the membranes were pre-swollen and equilibrated in the same pH conditions and buffer as the actual permeation experiment (pH 7.4, 1X PBS). The membranes were then placed in 30 mL of doxorubicin stock solution (Adriamycin in 2%v/v 1X PBS) with a concentration of 0.15 mg/mL. Samples were taken every day and analyzed using the HPLC method previously described. Doxorubicin in the samples was detected using Waters HPLC, and 45:55 Acetonitrile:Water solvent ratio was run for 10 mins, and displayed an elution peak for doxorubicin (maximum absorbance wavelength = 485 nm) at ~ 3.7 mins. The doxorubicin concentration in the membrane and its partition coefficient was calculated by performing a mass balance for doxorubicin.

2.3 RESULTS AND DISCUSSION

2.3.1 Synthesis of polymer formulations

To assess the capacity of our proposed nanoscale hydrogel system to load a hydrophobic therapeutic, and arrive at an optimal formulation, we quantify the loading of the hydrophobic drug doxorubicin into the panel of formulations we have synthesized. These formulations are summarized in Figure 7.1.

Basically, we synthesized nanoscale and microscale versions of each formulation obtained by changing the hydrophobic monomer component. We then studied the differences in doxorubicin loading, permeability, and partitioning observed upon varying the hydrophobic monomer. Given the marked difference in the scale of the formulations and the kinetics of the polymerization synthesis process, it is plausible that any trends anticipated may be skewed despite the use of a UV initiated free radical polymerization owing to adaptations that had to be made to synthesize the entire panel of nanoparticles using the same emulsion process, and all microparticles using the same film polymerization technique.

Upon synthesis, numerous differences between the nanoscale and membrane version of formulations became apparent. For instance, P(MAA-g-PEG-co-tBMA) films were relatively more hydrophilic and prone to breaking, as opposed to the P(MAA-g-PEG-co-tBMA) nanoparticles that are relatively more hydrophobic. On the other hand, P(MAA-g-PEG-co-nBMA) and P(MAA-g-PEG-co-nBA) were extremely tough and opaque to visible light suggesting a higher degree of hydrophobicity. Given the marked difference in the scale of the formulations and the kinetics of an emulsion polymerization synthesis process and film polymerization technique, it is plausible that any trends

anticipated between nanoparticles and their membrane counterparts, may be skewed despite the use of similar monomers and feed compositions because different proportions of the monomer actually got incorporated within the polymer network in the reaction time.

2.3.2 Doxorubicin loading studies

To systematically study and obtain a nanoparticle formulation that can efficiently load doxorubicin, loading of doxorubicin into the P(MAA-g-PEG-co-hydrophobic monomer) nanoscale hydrogels were performed by incubating each formulation with a doxorubicin stock solution of 0.15 mg/ml. Samples were taken at intervals of 2, 4, 6, and 24 h and amount of free doxorubicin in the solution was evaluated. Equation 7.1 was used to calculate loading efficiency. Partitioning or the partition coefficient was calculated using equation 7.2.

$$K_d = \frac{C_{np}}{C_o} = \frac{C_o - C_e}{C_o} \quad (7.2)$$

Where, Kd = partition coefficient, C_{np} = Concentration of doxorubicin in nanoparticles, C_o= initial solution concentration of DOX, and C_e= equilibrium solution concentration of DOX (measured at 24 hr time point). The results for loading efficiencies and partition coefficients are shown in Table 7.2.

Loading of hydrophobic therapeutics into nanoscale hydrogels containing a hydrophobic core per se, is expected to be influenced by the hydrophobic interactions between the drug and the hydrogel, and the ability of the hydrogel to swell and permit

diffusion of the drug. The loading efficiencies are shown in Figure 7.2. P(MAA-g-PEG-co-MMA) showed the highest loading efficiency and partitioning. The high degree of swelling and size and volume phase transition undergone by the P(MAA-g-PEG-co-MMA) nanoscale hydrogels at the loading pH 7, it is possible that these hydrogels are able to afford an increased mesh size that can permit ready diffusion of doxorubicin into the polymer network despite being relatively hydrophilic as compared to other polymer networks we synthesized, in addition to having an optimal distribution of hydrophobic groups that can retain the doxorubicin once it has diffused into the network. On the contrary, the more hydrophobic P(MAA-g-PEG-co-tBMA) nanoscale hydrogels load most of their equilibrium amount of doxorubicin in the first 4-6 hrs of loading itself, indicating a faster but loading that may not be overall as efficient. P(MAA-g-PEG-co-nBA) nanoscale hydrogels which showed appreciable swelling and size transition, demonstrated the lowest loading efficiencies which could be attributed to a poorer distribution of hydrophobic groups that allow for more swelling but less doxorubicin entrapment and retention.

2.3.3 Doxorubicin release studies

To investigate the ability of our nanoscale hydrogels to release doxorubicin specifically at the site of the small intestine, and examine retention at a pH that mimics the stomach, release studies were conducted with doxorubicin-loaded nanoparticles, and are shown in Table 7.3. In the first stage of the release study, the pH of the 1X PBS solutions was maintained at pH 2 to emulate the pH of the stomach, and the release of

DOX was evaluated. In the low pH phase of the study, we assess if the nanoscale hydrogels are capable of retaining the drug at pH conditions similar to that of the stomach. In this study, the P(MAA-g-PEG-co-tBMA) nanoparticles showed the most release, with 14.47% of drug released at the 2h mark. The P(MAA-g-PEG-co-nBMA) hydrogels released the released the least amount around 6%. After 2 hours, the pH was raised to a pH 7 to simulate the pH of the small intestine and the release of DOX was evaluated. The release at the 24 hour time point was denoted as M_∞ and the release percent results are presented as M_t/ M_∞ where M_t is the mass of the DOX that was released at time t. P(MAA-g-PEG-co-nBMA) nanoscale hydrogels showed the lowest efficiency of release suggesting that a more prominent hydrophobic presence can actually impede substantial release of the drug, promoting and inducing association and partitioning of the drug within the polymer network instead of release. P(MAA-g-PEG-co-tBMA) released most of the loaded drug, about 95.55% of the loaded drug after about 6h at pH 7 (total 8h). P(MAA-g-PEG-co-MMA) released about 74.71% of the drug in 6h at pH 7. The almost linear release response of P(MAA-g-PEG-co-tBMA) may suggest surface or close to surface loading of doxorubicin in these nanoscale hydrogels despite considerable surface washing. It could also mean that small size of these hydrogels imply minimal diffusion path length for doxorubicin to diffuse out assuming similar tortuosity in all nanoscale hydrogel formulation pores.

2.3.4 Powder X-ray diffraction studies

A general theory for inducing an improvement in apparent drug solubility prescribes that an increase in solubility comes with a concomitant decrease in permeability, as a part of the defining decree of the thermodynamic solubility-permeability trade-off [1]. This is a prominent feature in reformulations of lipophilic drugs using cyclodextrin-complexation and micellization, where affinity of the lipophilic drug with the solubilizing moiety reduces free fraction of the drug available for intestinal membrane permeability. Reduced free drug concentration in the unstirred water layer in contact with the intestinal membrane, leads to smaller concentration gradients and consequently, lower thermodynamic driving force for intestinal permeation/partitioning [2]. Controlled release formulations such as the ones used by us are an improvement because they rely on sustained release of the drug over time to maintain sufficient concentration gradients across the intestinal wall.

To further amplify the advantages of using controlled release formulations, one widely employed method for improving solubility of hydrophobic therapeutics is the encapsulation of lipophilic drugs in amorphous solid dispersions, followed by using techniques such as spray drying [3]. This spray-drying technique requires the use of an amorphous solid dispersion of a lipophilic drug in a polymer formulation, and produces a considerable advancement in apparent drug solubility via supersaturation.

Arguments in favor of amorphous formulations over crystalline ones are grounded in thermodynamic predictions as well as experimental testing [4]. Hancock and Parks found that the theoretical solubility advantage of amorphous formulations is anywhere

between 10 to 1600 fold, based on predictive calculations assuming the amorphous form to be equilibrium supercooled liquid or pseudo-equilibrium glass [5]. While *in vitro* and *in vivo* dissolution of amorphous formulations is difficult to measure in non-equilibrium conditions, the solubility advantage is significantly higher than their crystalline counterparts.

Powder X-ray diffraction is a powerful, non-destructive solid-state technique routinely exploited by the pharmaceutical industry for determining the amorphous or crystalline nature of powder pharmaceutical formulations, identifying and monitoring batch differences and uniformities, excipient compatibility, and detection of impurities [6]. X-ray diffraction has also been applied to resolve if drug-loaded particles are amorphous which can be correlated to formation of a homogeneous, single phase with a higher apparent solubility than crystalline/partially crystalline drug alone [7].

We tested the amorphous nature of our drug formulations using powder X-ray diffraction (P-XRD). Presence of crystalline lattices in drug loaded particles display relatively sharper peaks in congruence with one-dimensional crystal diffraction patterns, as opposed to purely amorphous formulations that reveal a broad scattering profile with no sharp peaks [8]. Angle of diffraction (θ), or in this case measured angle of diffraction (2θ) for the various drug-loaded formulations in reported in Table 7.1, along with crystal lattice d-spacing values as calculated through use of Bragg's law. Further polymorphic determination was enabled by executing elemental scans that compared sample peak positioning to crystal patterns of similar molecules from single-crystal X-ray diffraction studies. For comparison, the P-XRD pattern for free doxorubicin powder is provided in

Figure 7.4. Our analysis revealed that all DOX-loaded polymer nanoparticle formulations (except P(MAA-g-PEG-co-nBMA)) display broad featureless diffraction patterns and are purely amorphous within resolution of our powder X-ray diffraction detection (Figures 7.5 to 7.8).

We compared the P-XRD patterns of DOX-loaded nanoparticles to that of DOX alone. Visually the DOX-loaded nanoparticles appear slightly red owing to the red color imparted by DOX, but for P-XRD patterns, we ran an elemental scan which displayed good comparison with peaks for compounds similar to DOX and containing Nitrogen (present in DOX, but absent in our polymer nanoparticles), substantiating the presence of DOX in the amorphous formulations via P-XRD. All analysis for simultaneous elemental information scanning and complementary peak comparison were performed using DIFFRAC.EVA (Bruker Corp., Billerica, MA) XRD data analysis software (Bruker Corp., Billerica, MA). Figures 7.9 to 7.14 compare, match and visually indicate P-XRD pattern for DOX-loaded polymer nanoparticles with crystal structure peaks of known compounds.

2.3.5 Solute diffusion studies

Hydrogel permeability of various small molecules and large molecules has previously been studied to gain a nuanced understanding of the size of solutes which can diffuse through the polymer [9-13], using an experimental set-up comprising of diffusion cells or Valia-Chen cells. Diffusion cells were used for experimental elucidation of solute diffusion and permeability, owing to a lack of experimental methods for evaluation of

solute diffusion and permeability through polymeric nanoparticles, although methods involving simulation of diffusion have been explored [14]. Solute diffusion and permeation through the membrane hydrogel networks were investigated for doxorubicin for all four formulations of the P(MAA-g-PEG-co-hydrophobic monomer) using diffusion cells/Valia-Chen cells. A schematic showing the Valia-Chen cell is shown in Figure 7.15. Plots of recipient cell concentration (mg/ml) which can be correlated with mass permeated with time can be seen in Figure 7.16. P(MAA-g-PEG-co-MMA) gels witnessed an almost linear rate of permeation indicating steady state permeation. P(MAA-g-PEG-co-tBMA) which we observed to soft and gel-like underwent a collapse and rupture, possibly due to swelling stress over a two day period, at the end of 2 days, and hence permeation rate and subsequent calculations are based on their behavior for the two days. P(MAA-g-PEG-co-nBMA) and P(MAA-g-PEG-co-nBA) were extremely hard, opaque, seemingly hydrophobic and allowed minimal permeation at the end of 3 days, possibly due to small mesh sizes and hydrophobic interactions that permitted size exclusion of doxorubicin. Permeability coefficients were calculated using the slopes of linear regression fits based on and presented in Table 7.3.

2.3.6 Membrane partitioning

Partitioning of the solute in the membranes increased over time. Permeation is believed to proceed with a lag phase that can be attributed to size exclusion phenomena as is previously suggested. As the membranes equilibrate in the doxorubicin solution for a longer period of time and become fully ionized, more free space is available for

doxorubicin to diffuse into the gel and undergo partitioning. This partitioning is likely to be driven by hydrophobic interactions between doxorubicin and the hydrophobicity of the membrane. The mesh size of membranes prepared in this manner typically ranges 100 Angstrom to 320 Angstrom, while doxorubicin has a diameter of about 10 Angstrom. Hence, it can be anticipated that partitioning of doxorubicin increases linearly if the experiment is performed over a long enough time period. The difference in permeation across the membranes that differ only in hydrophobic monomer as such indicate, that diffusion and partitioning of doxorubicin within the membranes indicate that any changes in swelling phenomena and mesh size changes may dominate the results in diffusion that occur as a result of increasing hydrophobicity of the membranes, and is tabulated in Table 7.4, and shown in Figure 7.17.

A careful calculation of the mesh size can help us understand how the drug diffusion changes with changes in mesh size resulting from changing the hydrophobic monomer. However, there appears to be little or no correlation between the nanoscale hydrogels and membrane hydrogels that are synthesized with the same feed composition. This is essentially the effect of a compositional drift that occurs differently in the synthesis of nanoscale hydrogels via emulsion polymerization, as compared to the compositional drift that occurs in the synthesis of the membrane hydrogels. While there may be some thermodynamic correlation between partitioning within membrane versions of the hydrogel and nanoscale version with same final composition, it is understood that there will be a fundamental difference in kinetics of diffusion on the nanoscale and microscale per se. Given the lack of correlation between the two forms of the hydrogel

system and the minimal diffusion observed in the case of membrane hydrogels, we did not pursue any further evaluation of the membrane hydrogels, as we no longer consider it to be within the scope of assessing the merit of nanoscale hydrogels for oral delivery of doxorubicin.

2.4 NANO FORMULATION DOSAGE FEASIBILITY

In this section, we estimate the dosage feasibility of our nanoscale hydrogel formulation by calculating the amount of orally deliverable formulation required to administer the equivalent of a typical intravenous dosage of doxorubicin. Now, typical intravenous dosage of doxorubicin given to patients is about 50 mg/m^2 per week (typically given over a period of 48 hrs via IV infusion per week). Usually this regimen is divided into three 48-hour treatments over the course of three weeks, with subsequent treatment depending on off-target side-effects/toxicity and response to treatment. Boyd's formula is used to calculate body surface area in determining the total mass of doxorubicin to be administered.

For this estimate, we use the following Boyd's formula to calculate the body surface substituting H and W of a patient with average height and weight of 180 cm and 80 kg,

$= 0.0003207 \times (W)^{(0.7285-0.0188\log(W)} \times (H)^{0.3} = 2.0107\ m^2$

Thus, total DOX dosage required = 100.53473 mg. We used a drug concentration of 0.15 mg/ml, in combination with a 1 mg/ml concentration of nanoparticles. Assuming a conservative estimate of 60% loading efficiency, we find the amount of nanoparticles loaded into 1 mg of nanoparticle formulation to be 0.09 mg. Bioavailability of free

doxorubicin drug has been estimated to be 5% in some intestinal absorption models [15]. If we assume a lower conservative estimate of 10% bioavailability (intestinal absorption) and a release of 90% of loaded drug, we obtain the mass of doxorubicin absorbed into the blood stream per mg of nanoparticles used. This value is equal to: 0.09 mg x 0.1 x 0.9 = 0.0081 mg DOX/mg nanoparticle delivered. Hence, to ensure delivery of 100 mg of doxorubicin that is equivalent to a weekly total, we will need 12.345 g of nanoparticles per week. This is the amount to be given orally over a week, and can be accomplished via two tablets Capsule size 000 (each approximately with a mass ~ 6g) or four tables per week of capsule size 12 (each approximately with a mass ~ 3g), or a tablet of capsule size 11 taken once daily over the entire week of treatment (each approximately with a mass ~ 1.6g). Thus, based on this estimate the use of aforementioned nanoscale formulations is feasible from a practical, pharmacological standpoint.

2.5 CONCLUSIONS

We examined and compared the capacity of the nanoparticle formulations to load and release the hydrophobic therapeutic, doxorubicin. Loading studies were performed at pH 7.4 when the hydrogel networks are fully swollen. The capacity of loading hydrophobic therapeutics into the nanoscale hydrogel formulation is expected to be influenced by the hydrophobic interactions between the drug and the hydrogel, and the ability of the hydrogel to swell and permit diffusion of the drug during the loading procedure. By changing the hydrophobic comonomer in the nanoparticle formulations, we were able to successfully load doxorubicin, with loading efficiencies ranging from 40-

70%, with the P(MAA-g-PEG-co-MMA) formulation showing the highest loading efficiency. Further, we investigated the ability of these formulations to perform favorably under pH conditions similar to those encountered during transit through the GI tract. Specifically, we examined their ability to retain doxorubicin at an acidic pH expected to be found at the site of the stomach, and release the drug in response to alkaline conditions of the small intestine. P(MAA-g-PEG-co-tBMA) released most of the loaded drug, about 95.55% of the loaded drug after about 6 hours at pH 7 (total 8h). P(MAA-g-PEG-co-MMA) released about 74.71% of the drug in 6 hours at pH 7. The almost linear release response of P(MAA-g-PEG-co-tBMA) may suggest surface or close to surface loading of doxorubicin in these nanoscale hydrogels despite considerable surface washing. It could also mean that small size of these hydrogels imply minimal diffusion path length for doxorubicin to diffuse out assuming similar tortuosity in all nanoscale hydrogel formulation pores. Powder X-ray diffraction analysis revealed the amorphous nature of the drug formulations suggesting an increase in the solubility of doxorubicin under conditions mimicking the site of drug release. Solute diffusion and permeation were explored indirectly through the use of membrane hydrogel networks with the same monomer feed composition as the nanoscale hydrogel formulations, although little or no correlation exists between the behavior of the nanoscale and macroscale networks. It is, however, worthwhile to note that partitioning of the solute in the membranes increased over time, while permeation is believed to proceed with a lag phase that can be attributed to size exclusion phenomena. Nanoscale hydrogel formulations exhibited the capacity to load and release the hydrophobic therapeutic doxorubicin, and varying the hydrophobic

comonomer keeping the same nominal feed composition can play a role in modulating drug loading/release efficiencies.

2.6 REFERENCES

[1] Dahan A, Miller JM. The solubility-permeability interplay and its implications in formulation design and development for poorly soluble drugs. The AAPS journal 2012; 14:244-251.

[2] Beig A, Agbaria R, Dahan A. Oral delivery of lipophilic drugs: the tradeoff between solubility increase and permeability decrease when using cyclodextrin-based formulations. PloS one 2013; 8:e68237.

[3] Miller JM, Beig A, Carr RA, Spence JK, Dahan A. A win-win solution in oral delivery of lipophilic drugs: supersaturation via amorphous solid dispersions increases apparent solubility without sacrifice of intestinal membrane permeability. Molecular pharmaceutics 2012; 9:2009-2016.

[4] Hancock BC, Parks M. What is the true solubility advantage for amorphous pharmaceuticals? Pharmaceutical research 2000; 17:397-404.

[5] Panda RN, Hsieh MF, Chung RJ, Chin TS. FTIR, XRD, SEM and solid state NMR investigations of carbonate-containing hydroxyapatite nano-particles synthesized by hydroxide-gel technique. Journal of Physics and Chemistry of Solids 2003; 64:193-199.

[6] Randall CS, Rocco WL, Rico P. XRD: XRD in Pharmaceutical Analysis: A Versatile Tool for Problem-Solving. American Pharmaceutical Review 2010; 13:52.

[7] Lobmann K, Grohganz H, Laitinen R, Strachan C, Rades T. Amino acids as co-amorphous stabilizers for poorly water soluble drugs--Part 1: preparation, stability and dissolution enhancement. European journal of pharmaceutics and biopharmaceutics : official journal of Arbeitsgemeinschaft fur Pharmazeutische Verfahrenstechnik e.V 2013; 85:873-881.

[8] Ting JM, Navale TS, Bates FS, Reineke TM. Precise Compositional Control and Systematic Preparation of Multimonomeric Statistical Copolymers. ACS Macro Letters 2013; 2:770-774.

[9] Bell CL, Peppas NA. Modulation of drug permeation through interpolymer complexed hydrogels for drug delivery applications. Journal of controlled release 1996; 39:201-207.

[10] Gudeman LF, Peppas NA. pH-sensitive membranes from poly (vinyl alcohol)/poly (acrylic acid) interpenetrating networks. Journal of membrane science 1995; 107:239-248.

[11] Bell CL, Peppas NA. Water, solute and protein diffusion in physiologically responsive hydrogels of poly (methacrylic acid-g-ethylene glycol). Biomaterials 1996; 17:1203-1218.

[12] Peppas NA, Wright SL. Drug diffusion and binding in ionizable interpenetrating networks from poly (vinyl alcohol) and poly (acrylic acid). European journal of Pharmaceutics and Biopharmaceutics 1998; 46:15-29.

[13] Peppas NA, Wright SL. Solute diffusion in poly (vinyl alcohol)/poly (acrylic acid) interpenetrating networks. Macromolecules 1996; 29:8798-8804.

[14] Buxton GA, Clarke N. Drug diffusion from polymer core–shell nanoparticles. Soft Matter 2007; 3:1513-1517.

[15] Artursson P, Karlsson J. Correlation between oral drug absorption in humans and apparent drug permeability coefficients in human intestinal epithelial (Caco-2) cells. Biochemical and biophysical research communications 1991; 175:880-885.

Table 7.1: Powder X-ray diffraction peak values for doxorubicin-loaded formulations

DOX-loaded nanoparticle formulation		
	2θ value	d-spacing
P(MAA-g-PEG-co-MMA)	17.189	5.154
P(MAA-g-PEG-co-nBMA)	17.135 31.599 45.322 56.36 27.246 56.934	5.17 2.829 1.999 1.631 3.27 1.616
P(MAA-g-PEG-co-nBA)	17.728	4.999
P(MAA-g-PEG-co-tBMA)	17.587	5.039

Table 7.2: Doxorubicin loading efficiencies and partition coefficients with nanoscale hydrogel formulations at the end of the study. Calculated as % efficiency = C_o-C_t/C_o ; n= 3, Reported as mean +/- SD. $K_d = c_m/c_e = (c_0 - c_e)/c_e$;

Nanoscale Hydrogel Formulation	Equilibrium Loading Efficiency (%)	Partitioning Coefficient K_d
P(MAA-g-PEG-co-tBMA)	56.63 ± 0.1	1.306
P(MAA-g-PEG-co-nBMA)	58.88 ± 0.4	1.432
P(MAA-g-PEG-co-nBA)	40.59 ± 2.2	0.6832
P(MAA-g-PEG-co-MMA)	70.13 ± 2.9	2.348

Table 7.3: Permeability coefficients/slopes for the diffusion of doxorubicin through the membrane formulations.

Membrane Formulation	Slope/Permeability Coefficient (cm^2/s) (in 10^{-6} cm^2/s)
P(MAA-g-PEG-co-tBMA)	1.444
P(MAA-g-PEG-co-nBMA)	0.9722
P(MAA-g-PEG-co-nBA)	0.9722
P(MAA-g-PEG-co-MMA)	4.75

Table 7.4: Membrane formulation and their permeability coefficients, partitioning coefficients, and diffusion coefficients

Membrane Formulation	Slope/Permeability Coefficient (cm^2/s) (in 10^{-6} cm^2/s)	Partitioning Coefficient $K_d = c_m/c_e = (c_0 - c_{e)}/c_e$	Diffusion Coefficient $= P/K_d$ (cm^2/s)
P(MAA-g-PEG-co-tBMA)	1.444	1.465	9.8570×10^{-7}
P(MAA-g-PEG-co-nBMA)	0.9722	0.3360	2.8931×10^{-6}
P(MAA-g-PEG-co-nBA)	0.9722	0.1726	5.633×10^{-6}
P(MAA-g-PEG-co-MMA)	4.75	0.8485	5.5979×10^{-6}

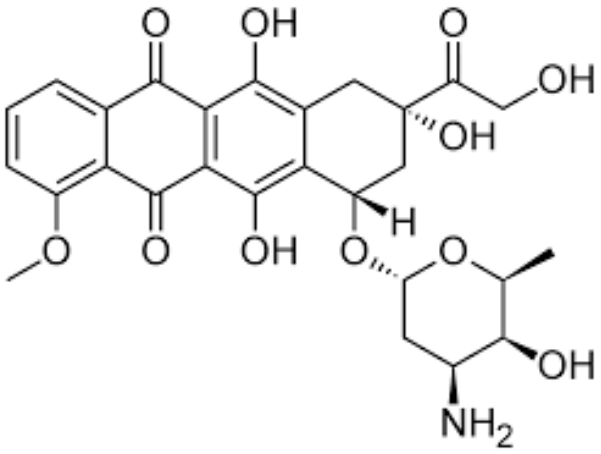

Figure 7.1: Molecular structure of doxorubicin.

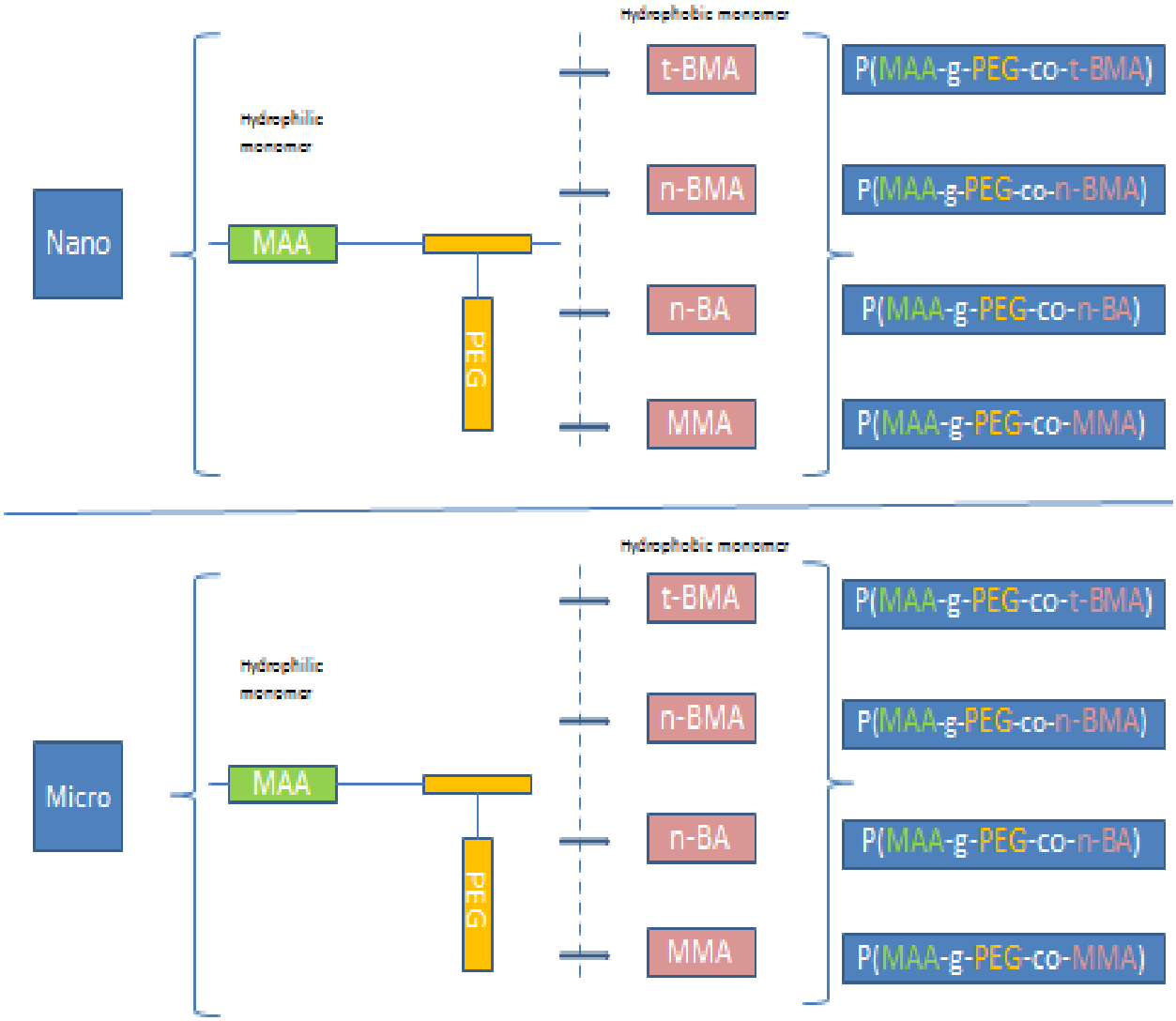

Figure 7.2: Formulation map showing nanoscale formulations for drug loading and relase studies, and powder X-ray diffraction. Micro or membrane formulations of the same component monomers had to be synthesized for compatibility with drug diffusion studies/cells and membrane partitioning.

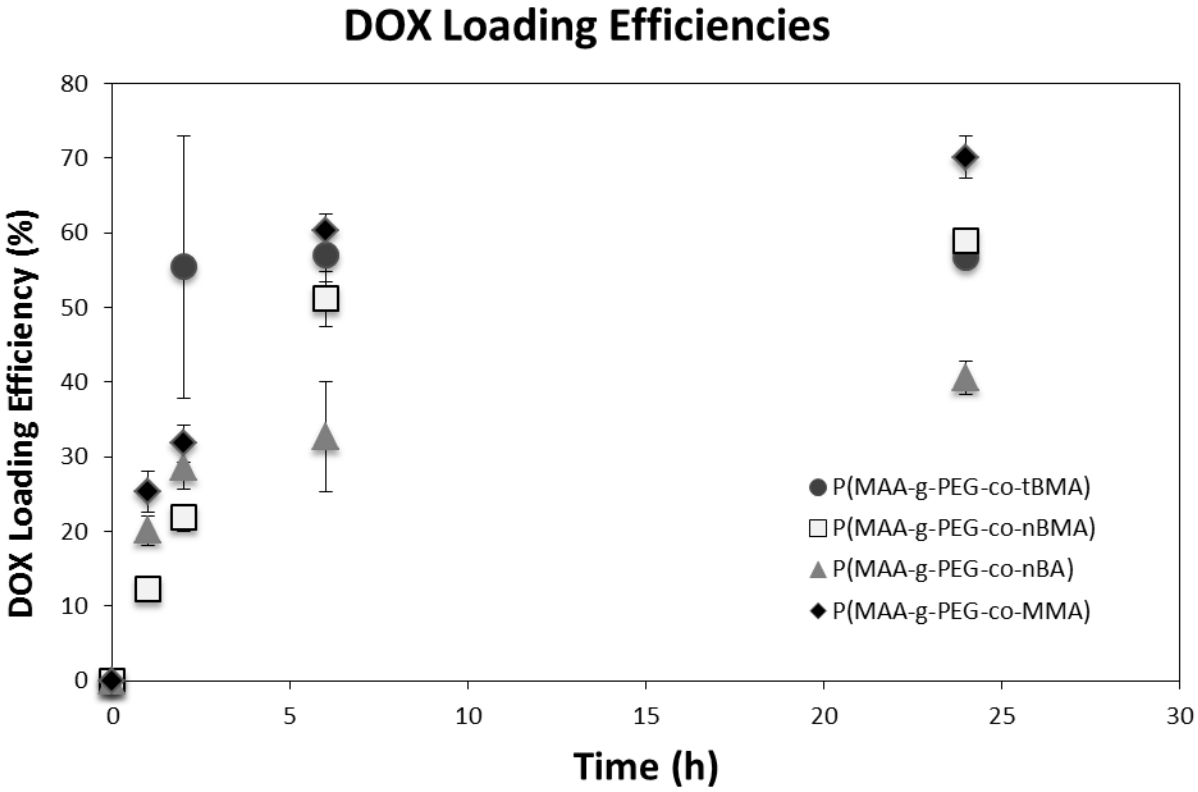

Figure 7.3: Doxorubicin loading efficiencies with nanoscale hydrogel formulations. Calculated as % efficiency = C_o-C_t/C_o ; n= 3, data points shown are mean of measurements +/- SD. Loading efficiency among treatment groups is statistically significant with $p<0.05$.

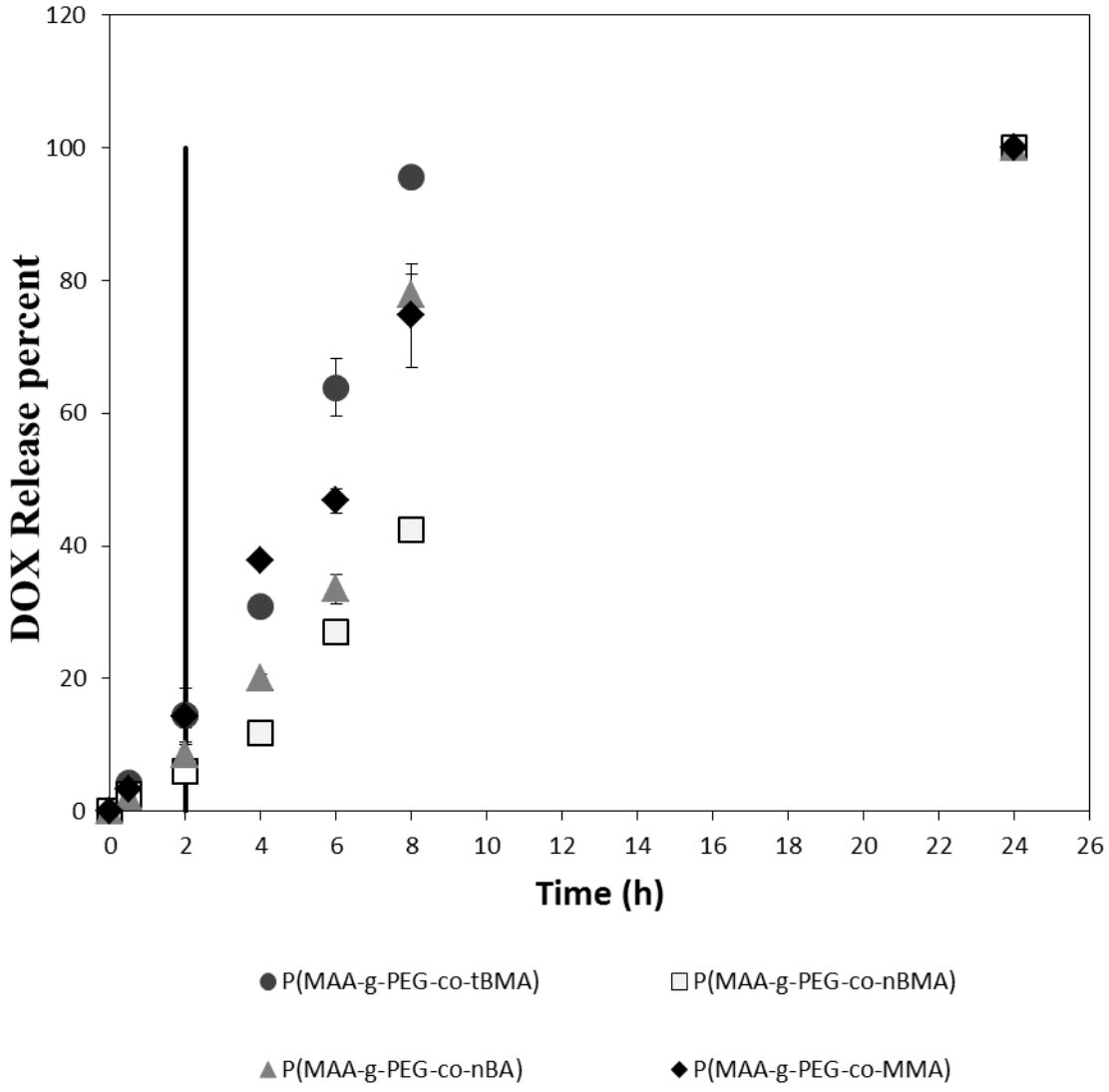

Figure 7.4: Doxorubicin release efficiencies with nanoscale hydrogel formulations. Calculated as % efficiency = C_o-C_t/C_o ; n= 3, data points shown are mean of measurements +/- SD. Loading efficiency among treatment groups is statistically significant with $p<0.05$.

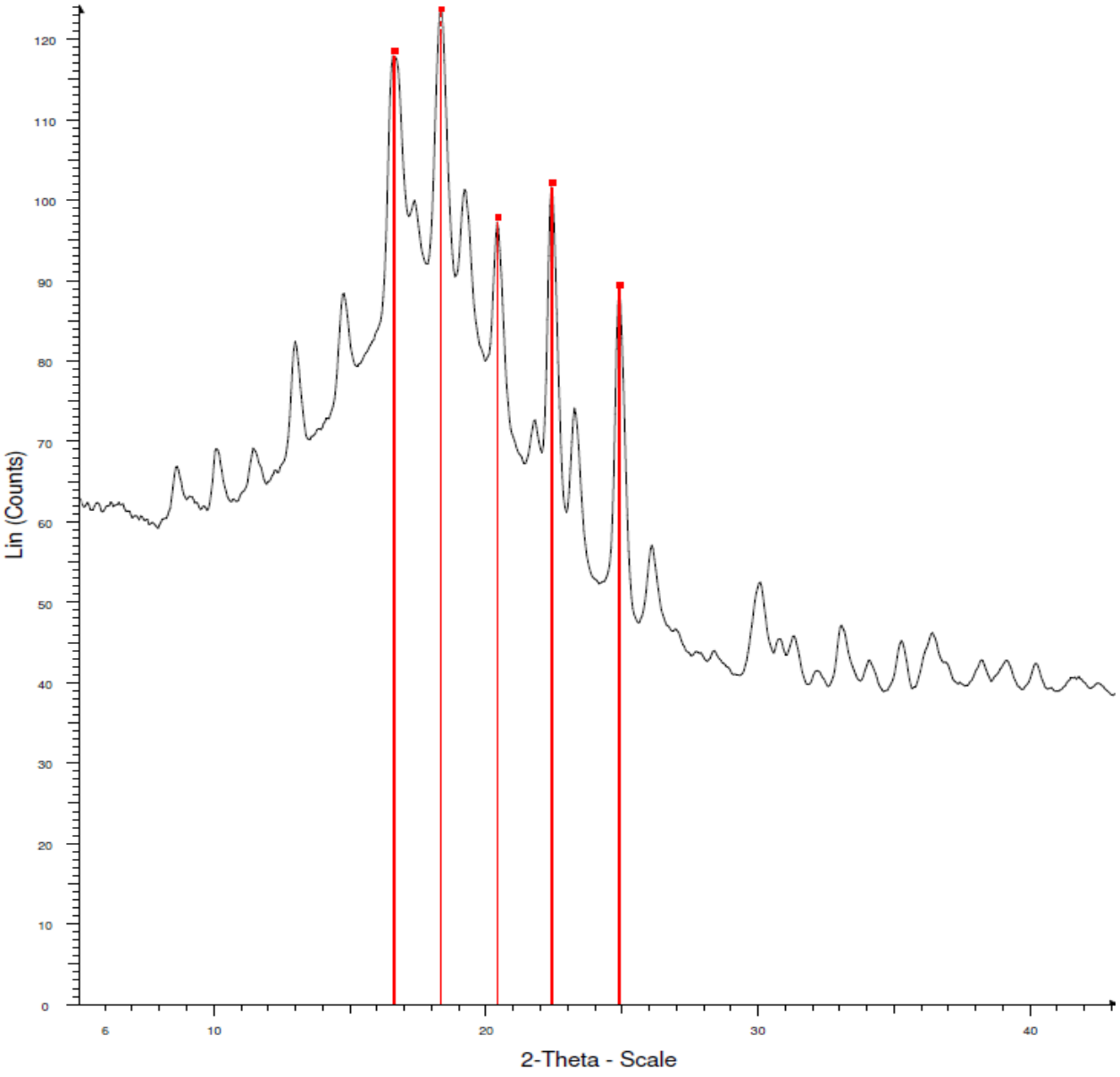

Figure 7.5: Powder X-ray diffraction pattern for free doxorubicin powder as obtained from manufacturer. Sharp peaks (indicated by red lines) imply a partially crystalline powder.

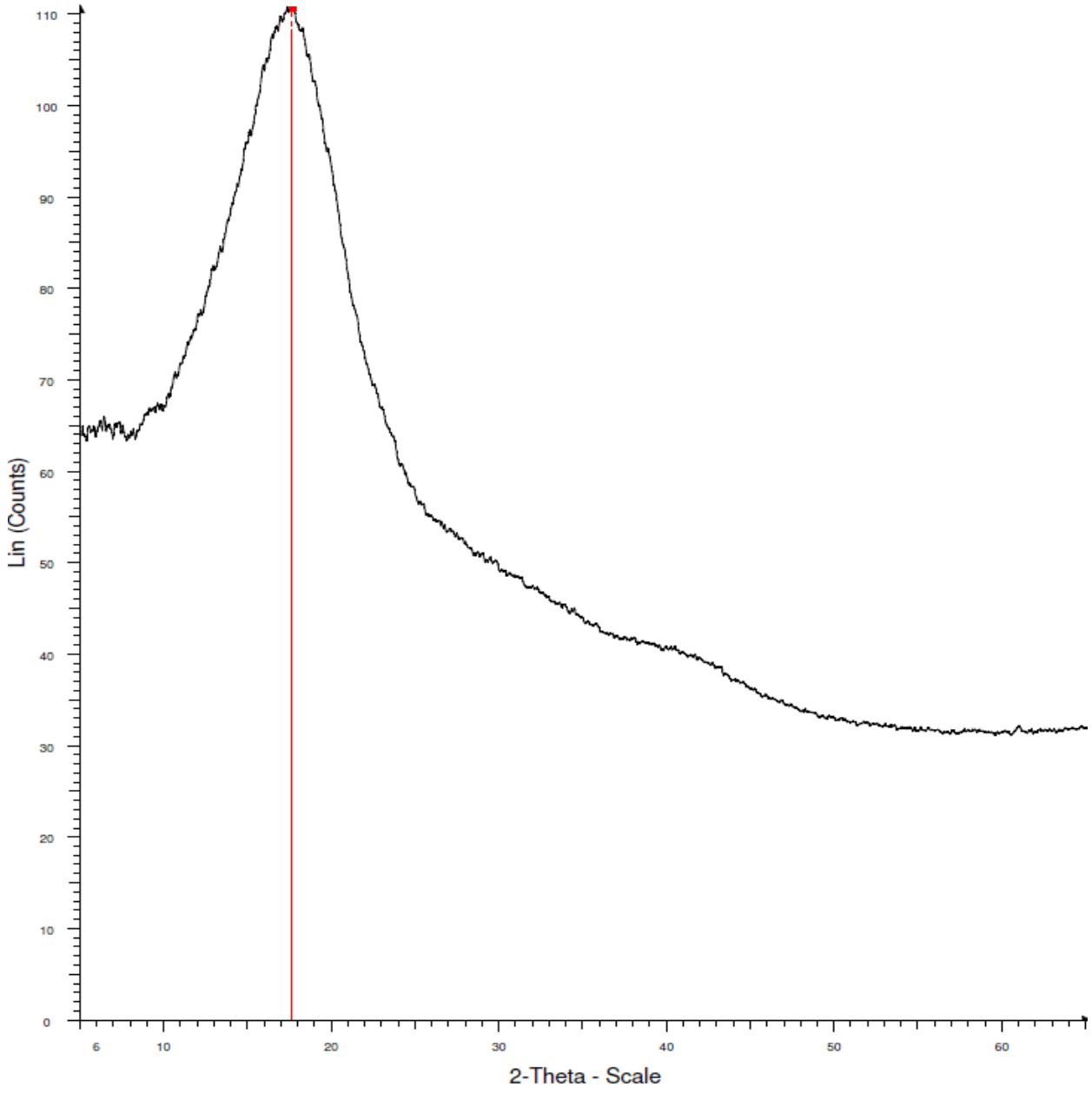

Figure 7.6: Powder X-ray diffraction pattern for doxorubicin loaded P(MAA-g-PEG-co-tBMA). Absence of any peaks implies an amorphous powder.

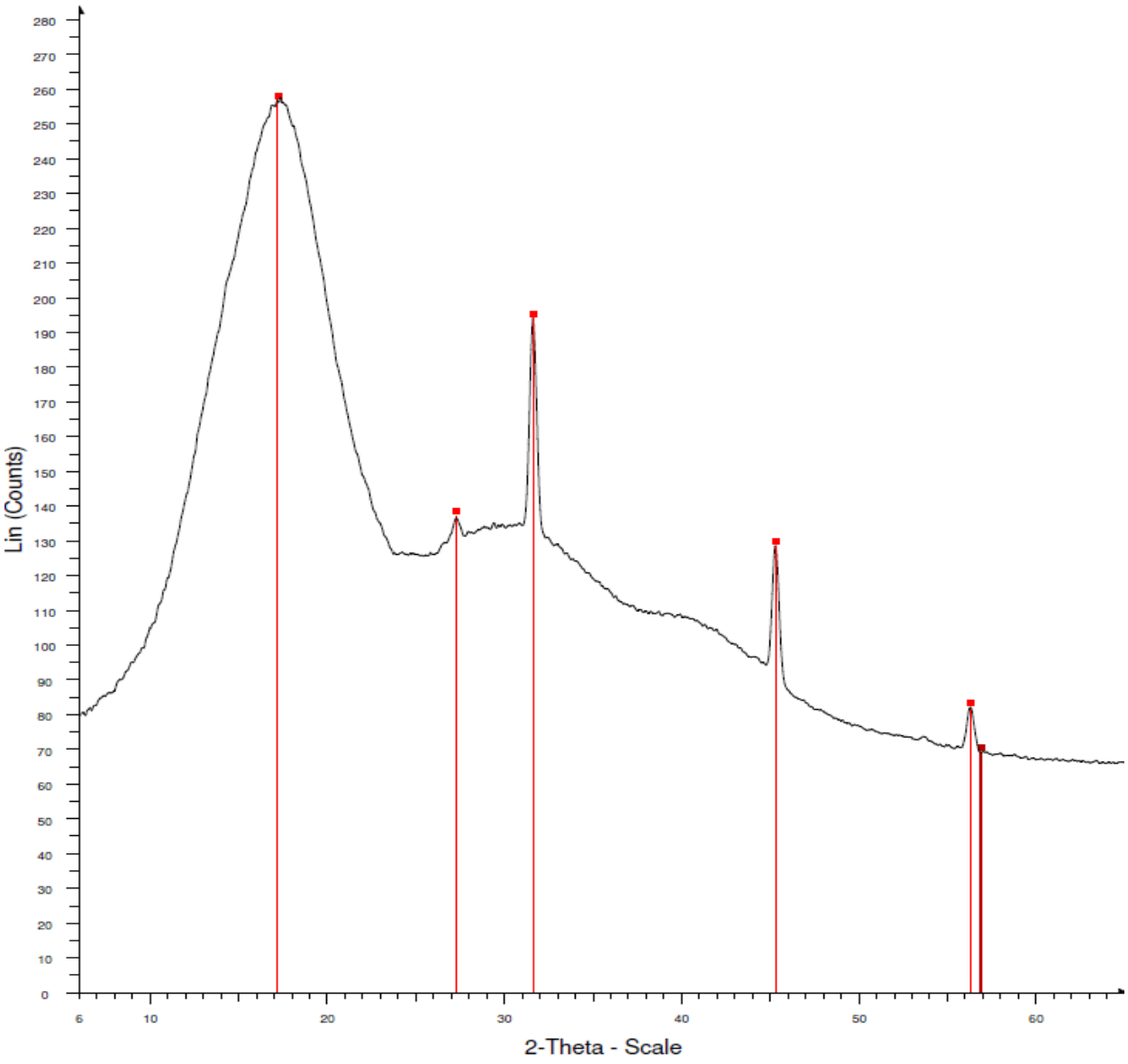

Figure 7.7: Powder X-ray diffraction pattern for doxorubicin loaded P(MAA-g-PEG-co-nBMA). Presence of peaks at 2θ=31.599, 45.322, 56.36 suggests powder is not fully amorphous and has a crystalline character to it.

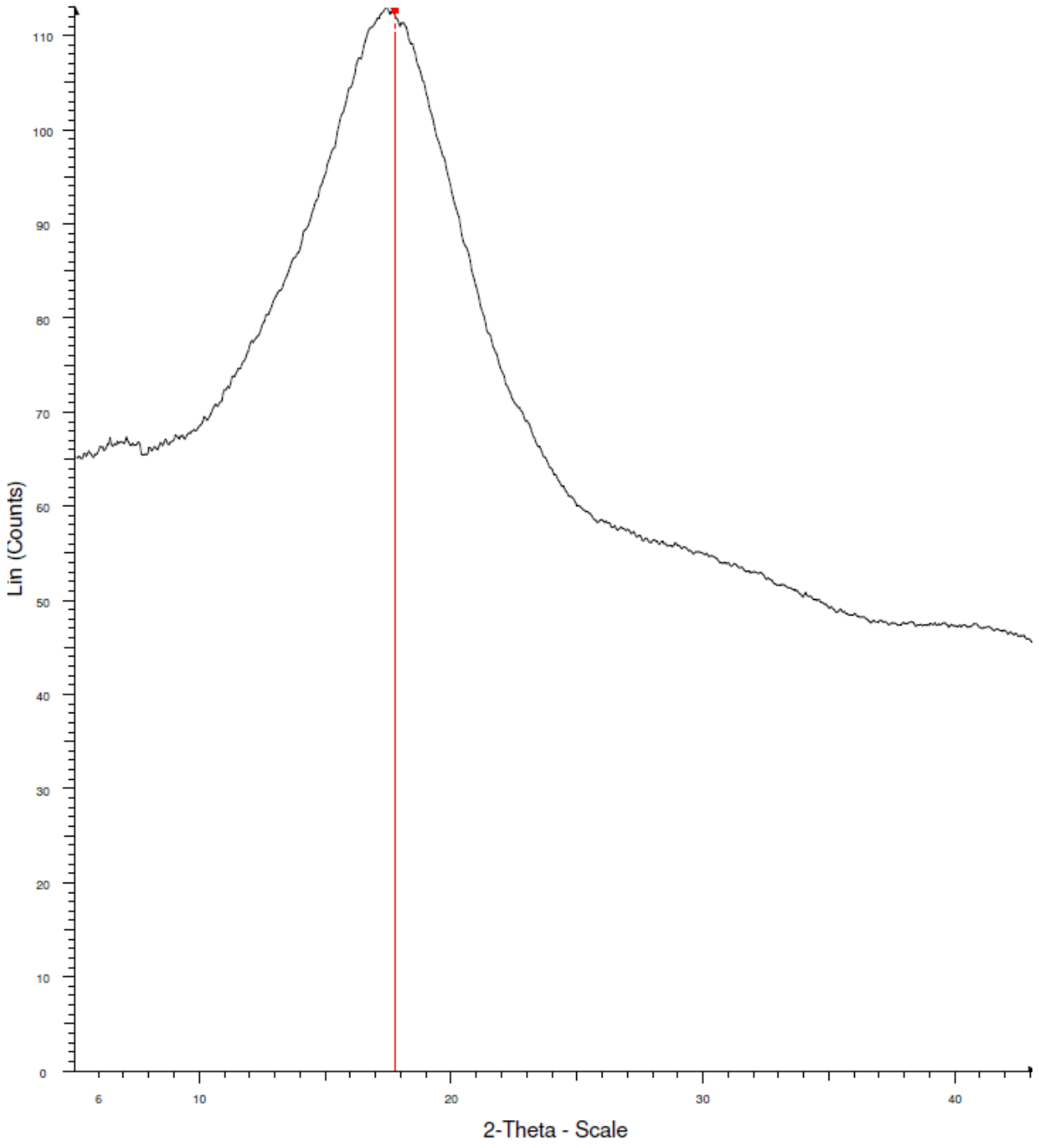

Figure 7.8: Powder X-ray diffraction pattern for doxorubicin loaded P(MAA-g-PEG-co-nBA). Absence of any peaks implies an amorphous powder.

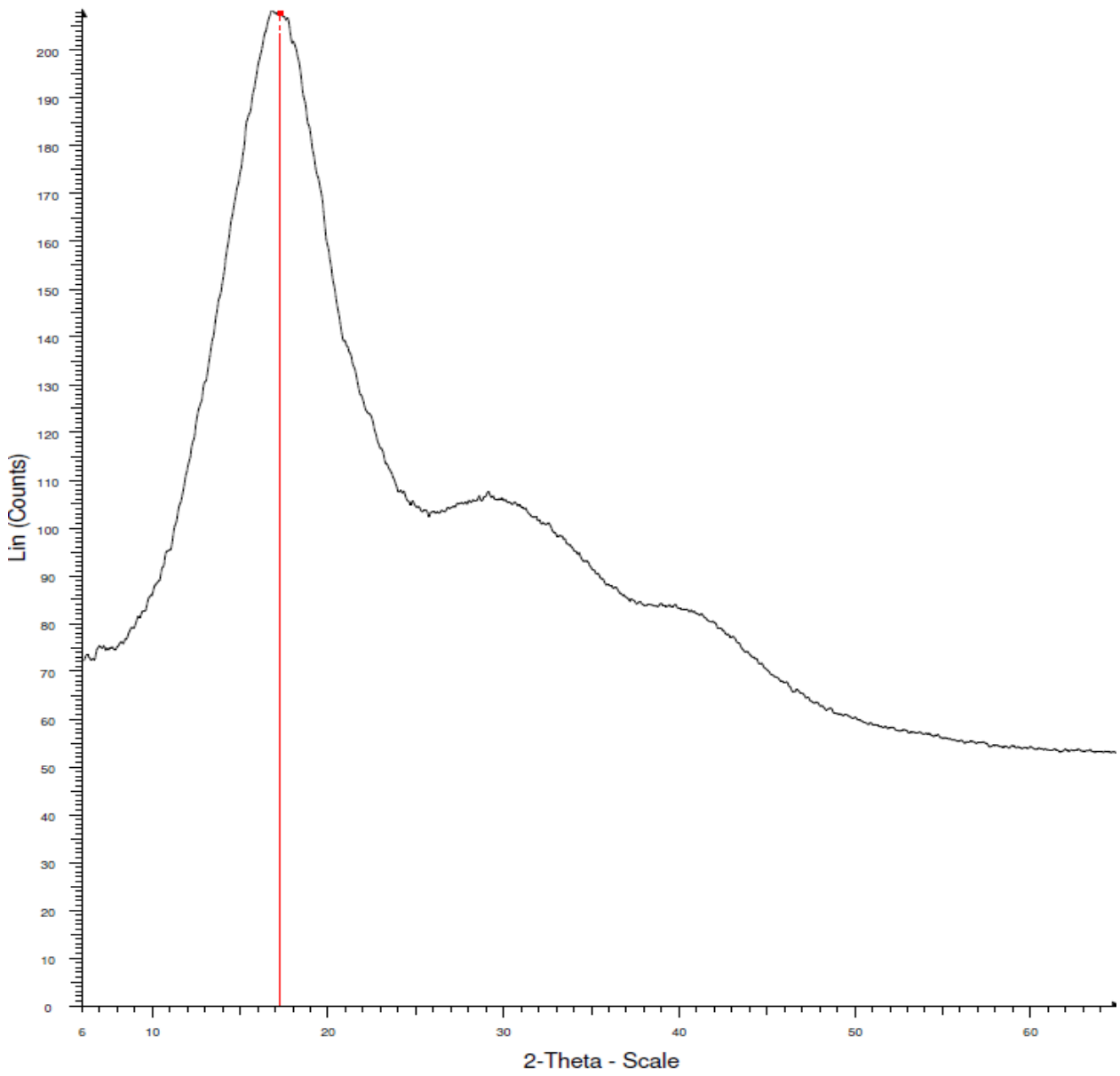

Figure 7.9: Powder X-ray diffraction pattern for doxorubicin loaded P(MAA-g-PEG-co-MMA). Absence of any peaks implies an amorphous powder

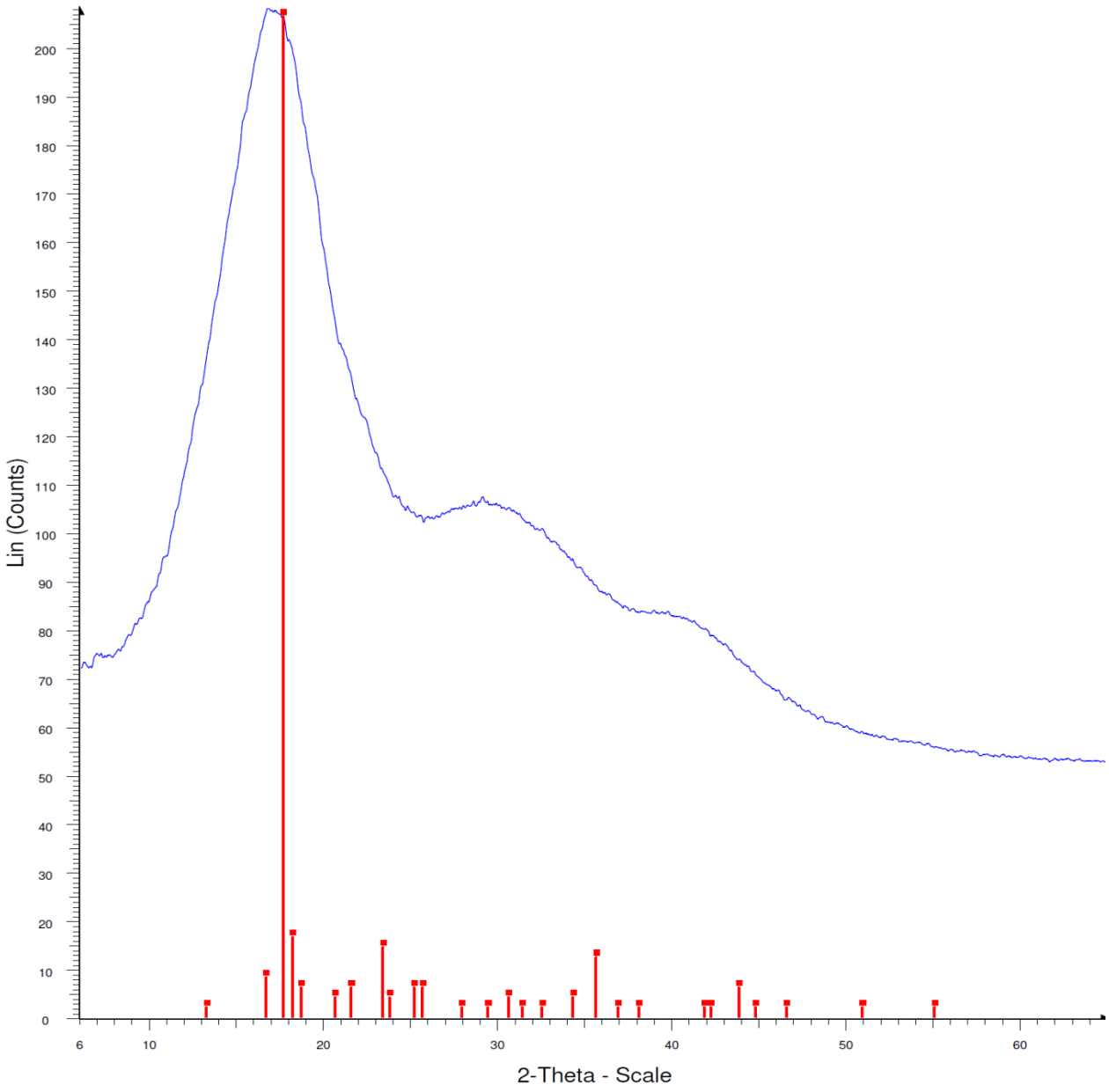

Figure 7.10: Elemental data scanning and Peak comparison. Powder X-ray diffraction pattern of Doxorubicin-loaded P(MAA-g-PEG-co-MMA) nanoscale hydrogels (blue) and compared with peaks of 5-beta-dihydrotestosterone standard, which has a structure similar to doxorubicin, implying presence of doxorubicin in amorphous powder.

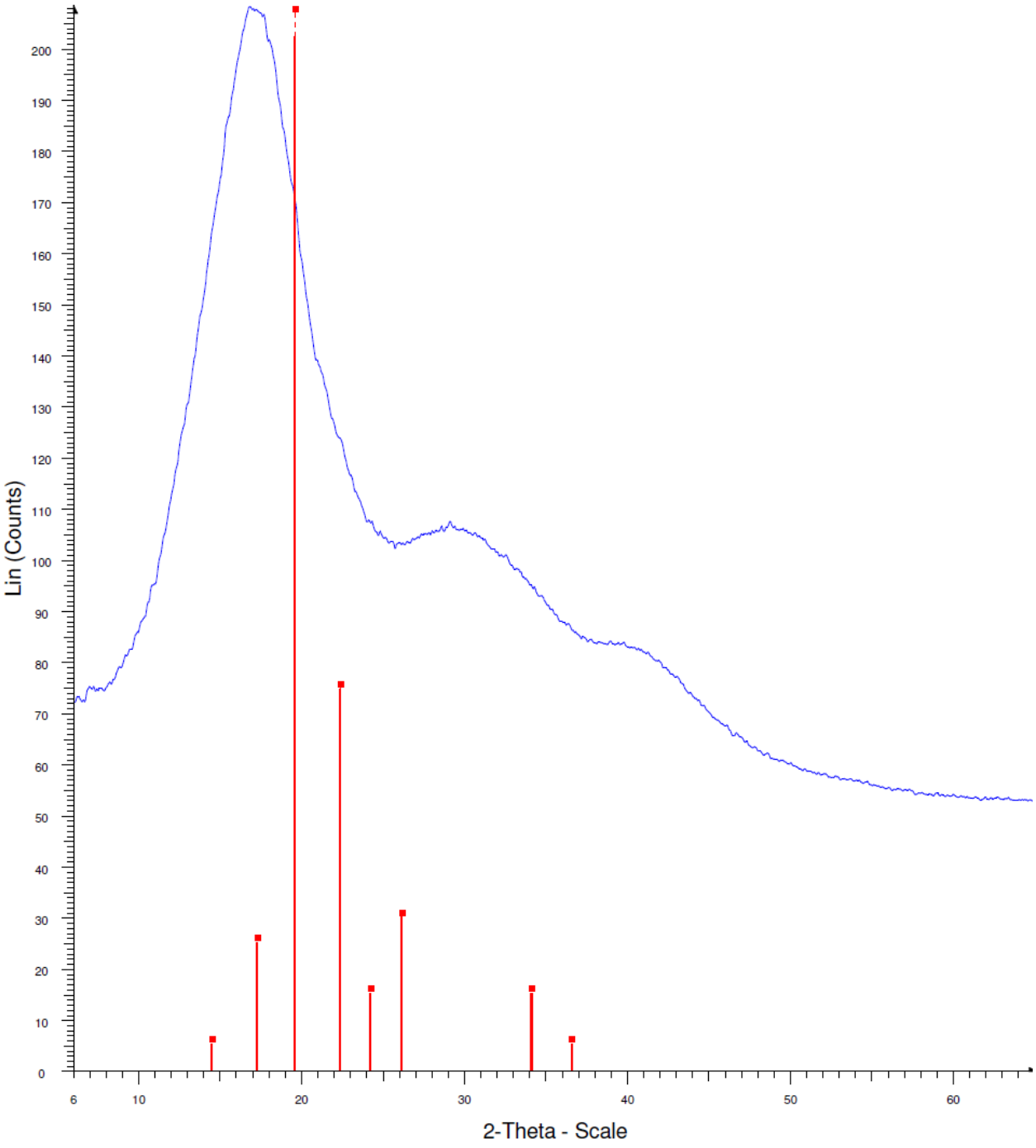

Figure 7.11: Elemental data scanning and Peak comparison. Powder X-ray diffraction pattern of Doxorubicin-loaded P(MAA-g-PEG-co-MMA) nanoscale hydrogels (blue) and compared with peaks of L-lactide-poly(ethyleneglycol)

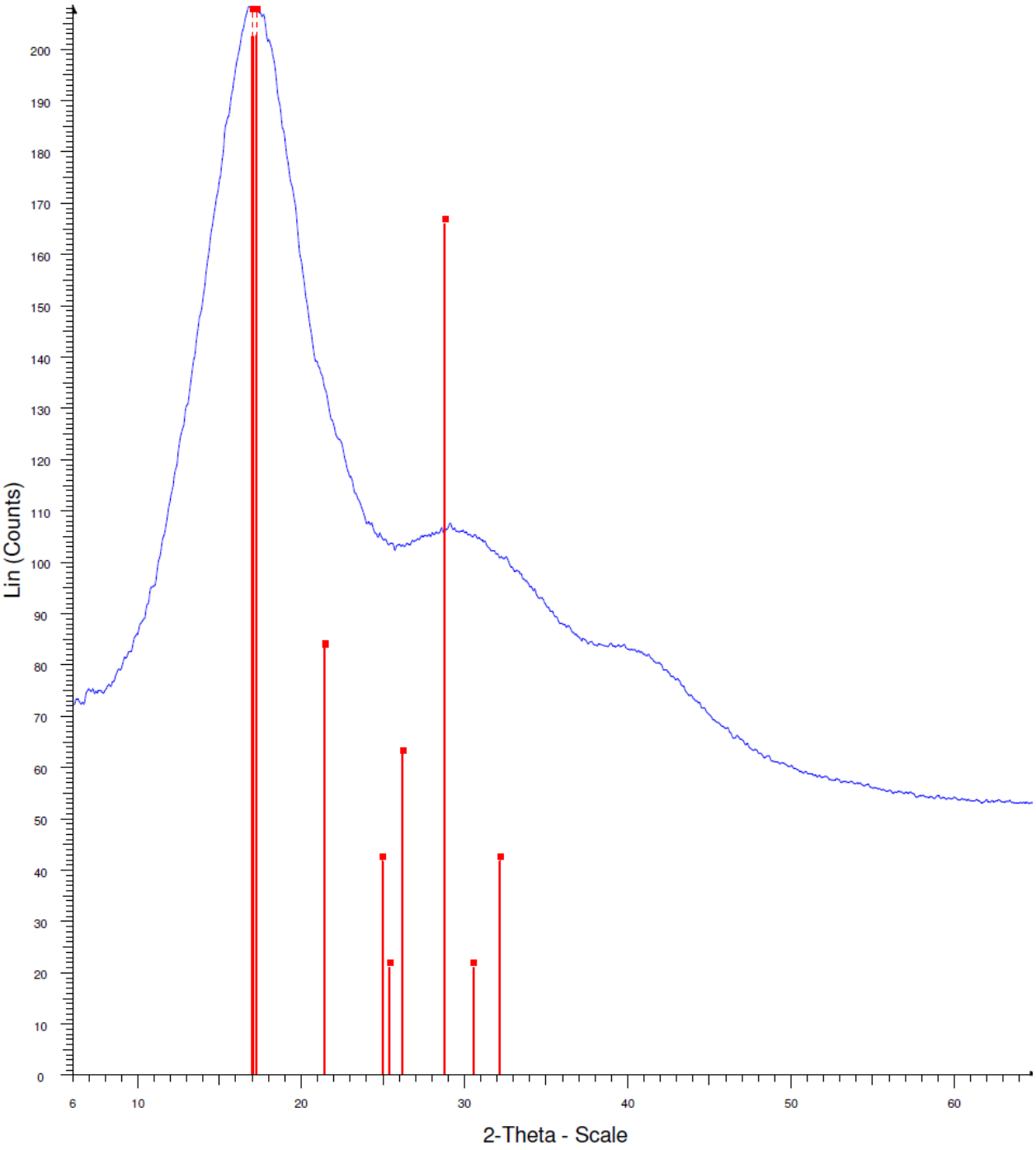

Figure 7.12: Elemental data scanning and Peak comparison. Powder X-ray diffraction pattern of Doxorubicin-loaded P(MAA-g-PEG-co-MMA) nanoscale hydrogels (blue) and compared with peaks of Succinic acid-2-urea

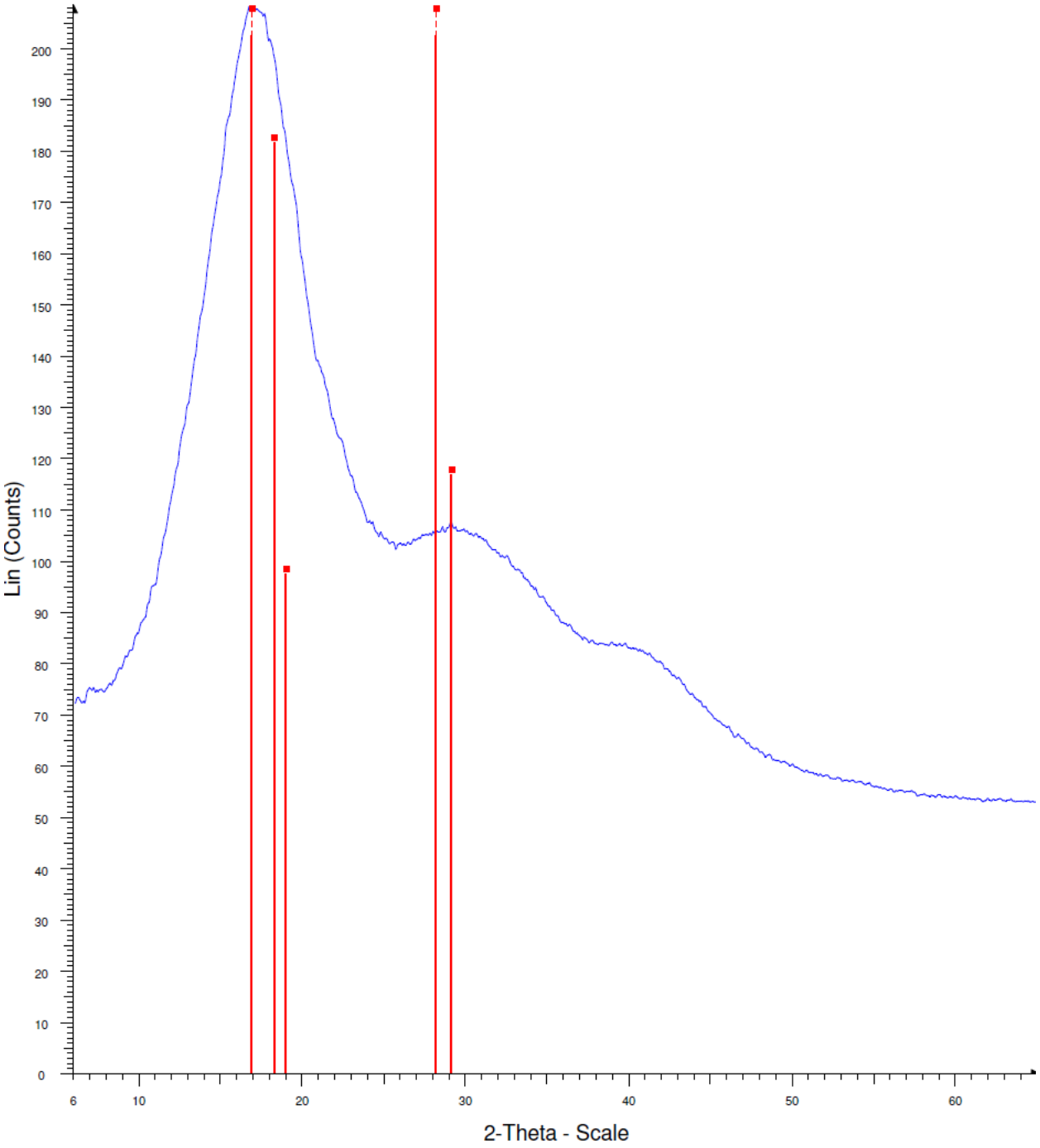

Figure 7.13: Elemental data scanning and Peak comparison. Powder X-ray diffraction pattern of Doxorubicin-loaded P(MAA-g-PEG-co-MMA) nanoscale hydrogels (blue) and compared with peaks of 3-(3-Methyltoluyl)-1,2,2-trimethylcyclopentanecarboxylic acid.

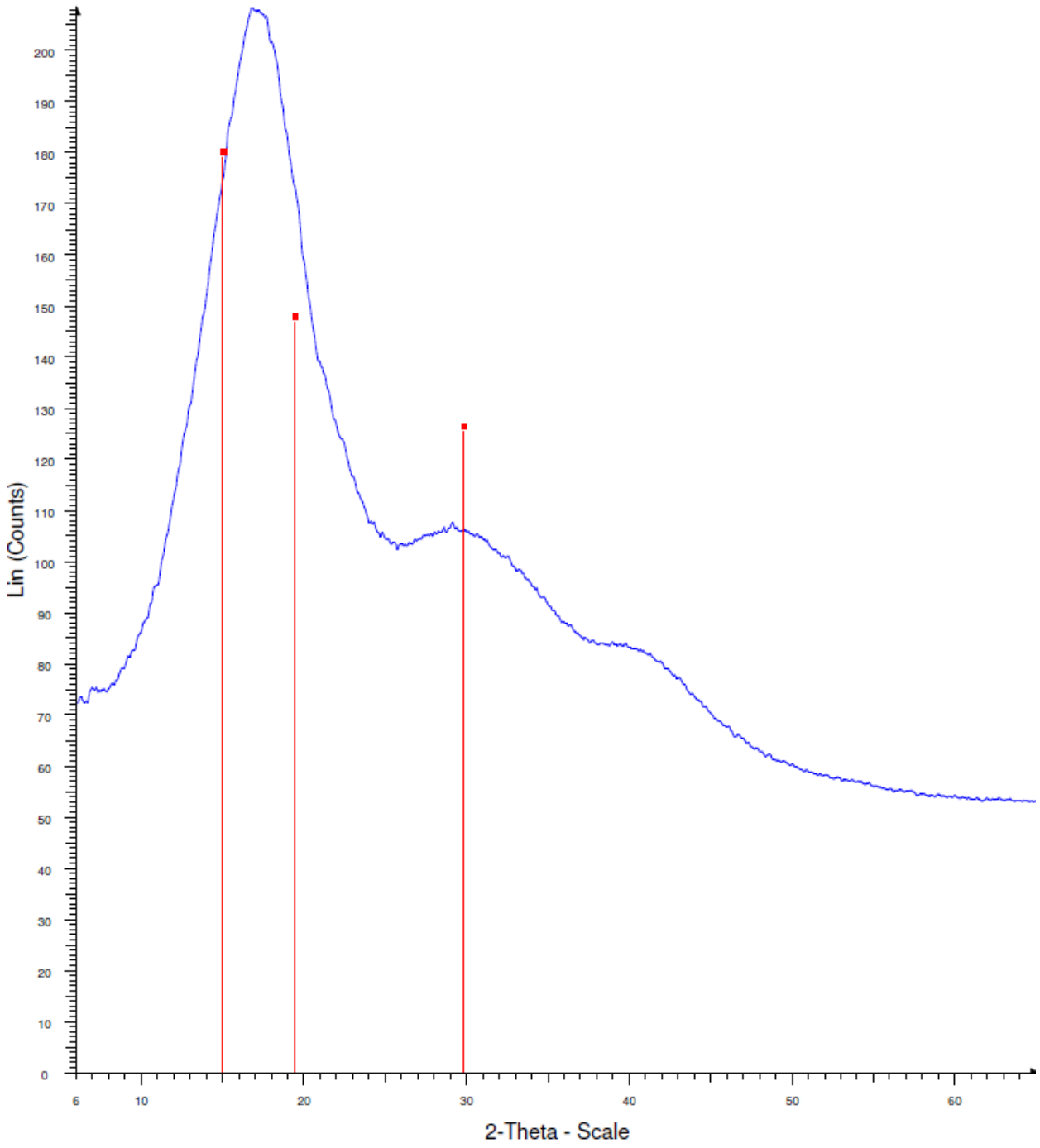

Figure 7.14: Elemental data scanning and Peak comparison. Powder X-ray diffraction pattern of Doxorubicin-loaded P(MAA-g-PEG-co-MMA) nanoscale hydrogels (blue) and compared with peaks of Indole-2-carboxylic acid 2,4-dinitrobenzoic acid.

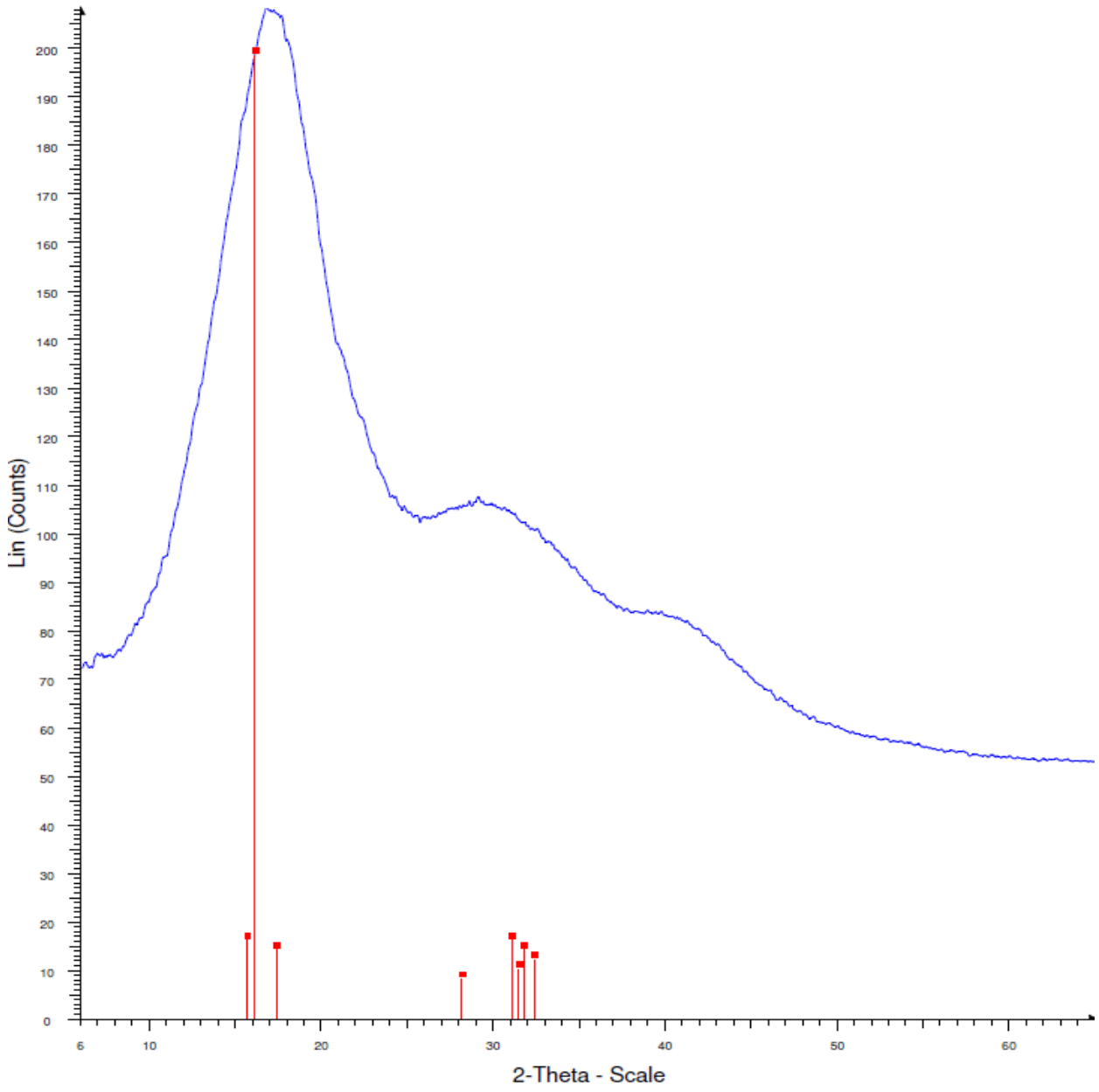

Figure 7.15: Elemental data scanning and Peak comparison. Powder X-ray diffraction pattern of Doxorubicin-loaded P(MAA-g-PEG-co-MMA) nanoscale hydrogels (blue) and compared with peaks of 3-Aminobenzoic acid 5-nitroquinoline.

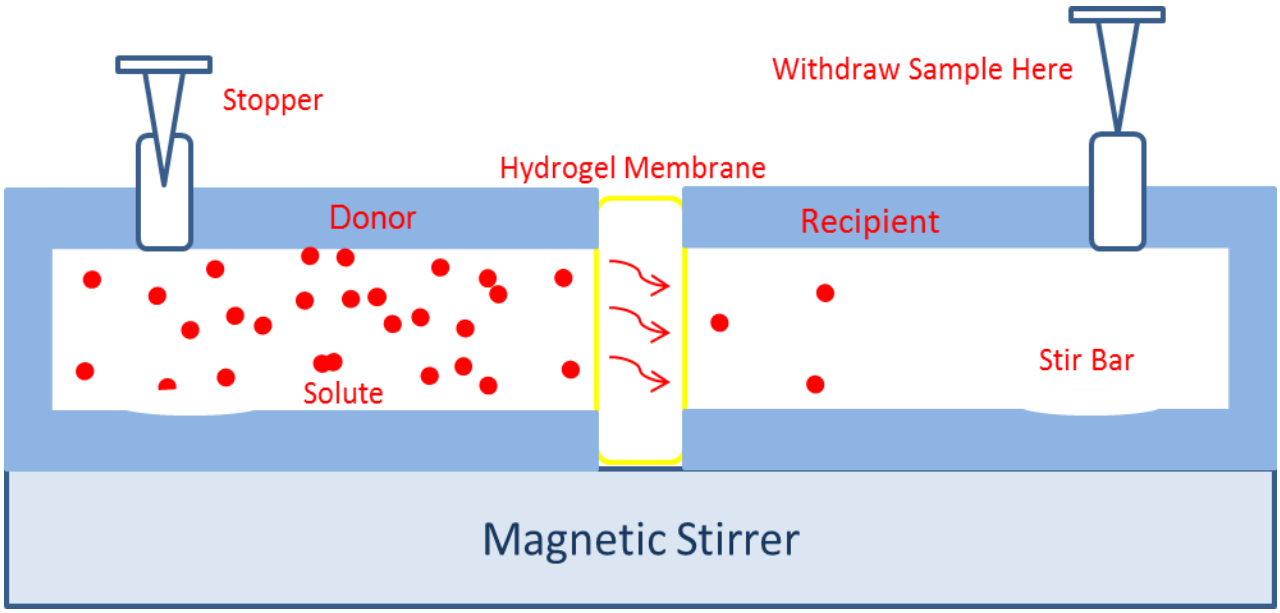

Figure 7.16: Schematic of solute diffusion cells or Valia-chen cells for drug diffusion studies.

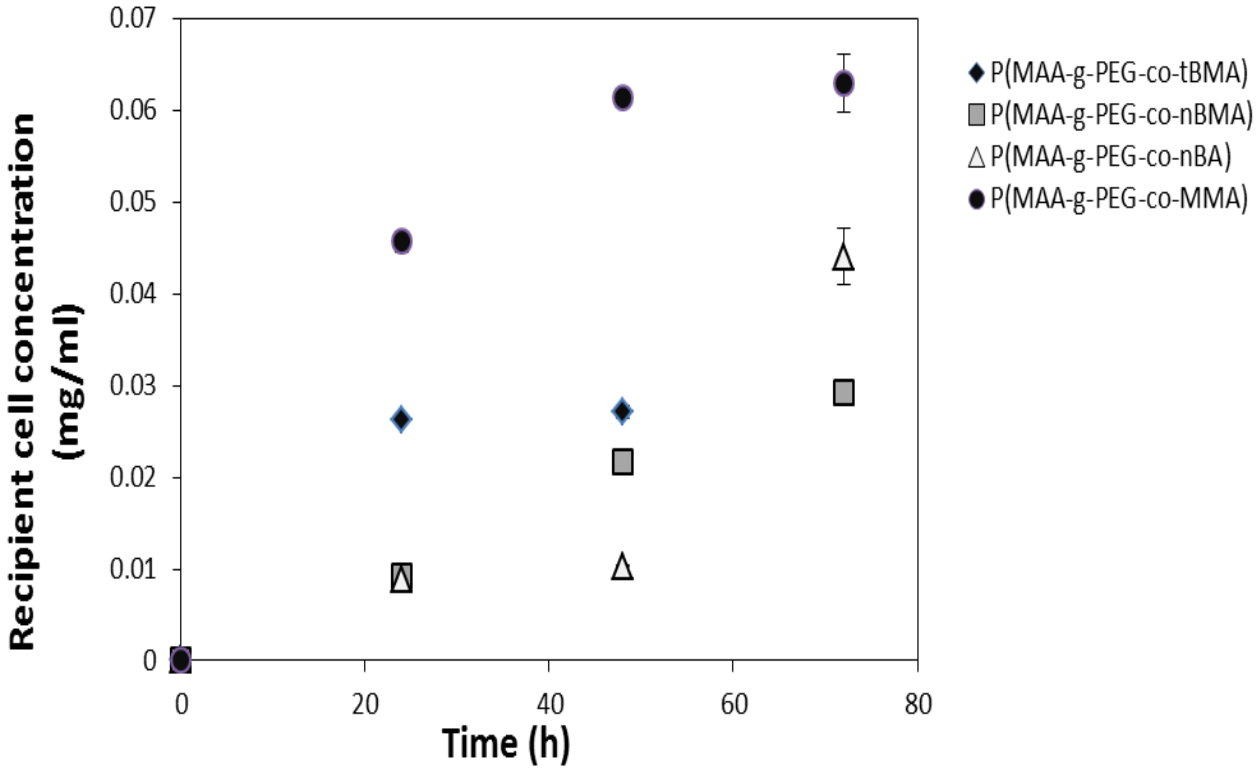

Figure 7.17: Recipient cell concentration of doxorubicin in solute diffusion studies performed using diffusion cells and membrane formulations. Data points shown are expressed as mean +/- SD.

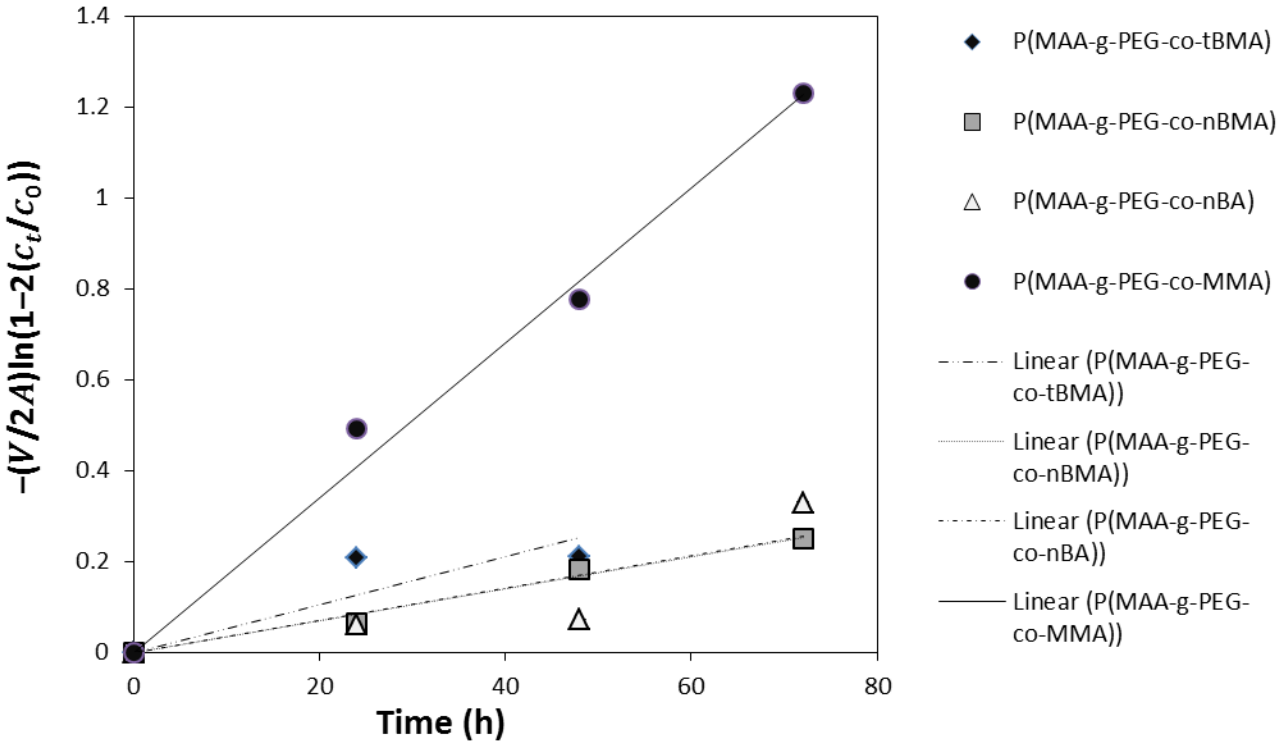

Figure 7.18: Calculation of slope for doxorubicin solute permeability studies conducted in Valia-Chen diffusion cells.

Chapter 8: Evaluation of the Effect of Nanoscale Hydrogels on the Permeability of Hydrophobic Therapeutics across *in vitro* Cell Models

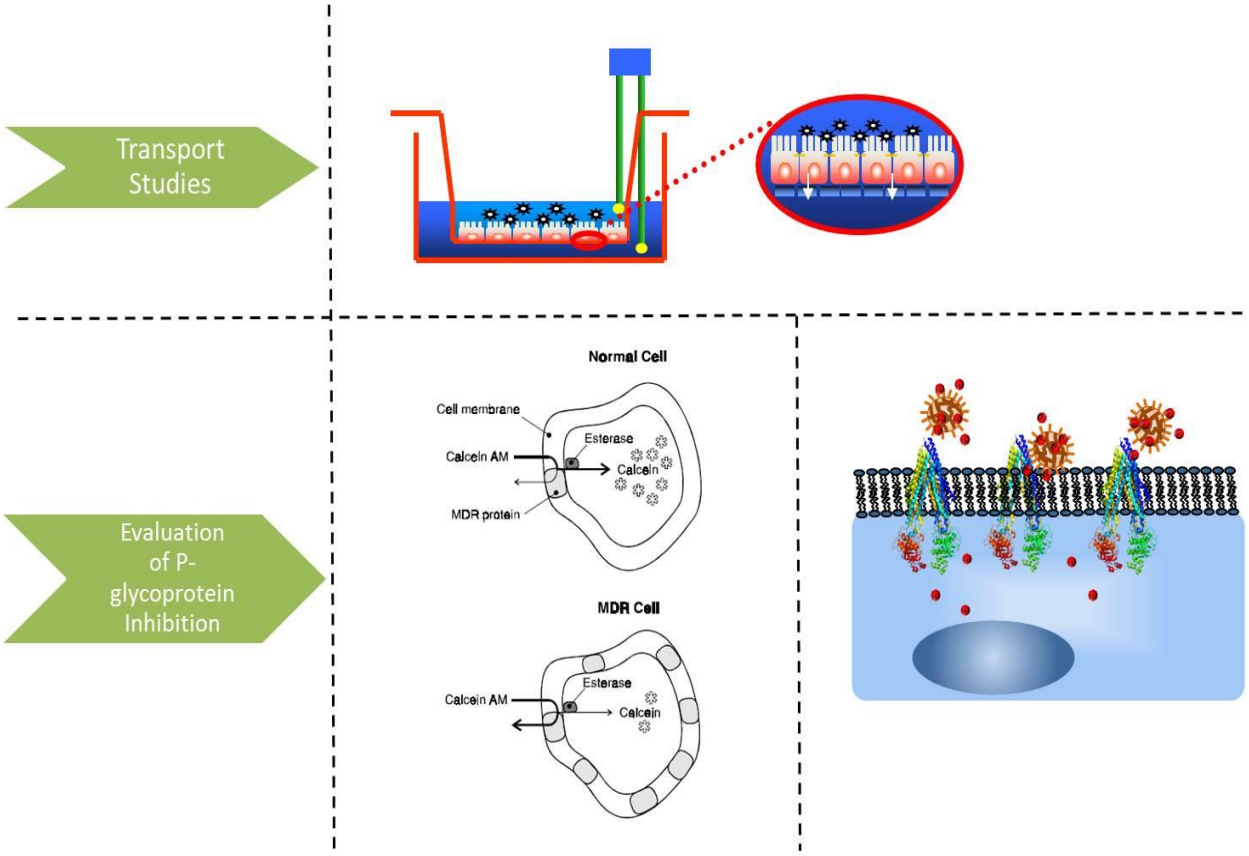

- Increased permeability of hydrophobic therapeutics across the GI tract is an important aim for oral drug delivery systems
- Permeability of doxorubicin is greatly reduced due to the drug efflux transporter P-glycoprotein
- To evaluate transport of doxorubicin across intestinal epithelial monolayer, transport studies were conducted *in vitro* for all formulations
- Elucidation of the impact of nanoscale hydrogels on P-glycoprotein was achieved using a P-gp overexpressing multidrug resistant cell line and compared with non-overexpressing cell lines
- Two assays were used to evaluate this interaction – Calcein AM retention in the presence of hydrogels, and cellular proliferation of multidrug resistant cancer cells in the presence of doxorubicin-loaded nanoparticles

8.1 INTRODUCTION

This chapter is part of the integrative approach towards understanding the in vivo and clinical behavior of the orally deliverable platform we have developed. Recently, owing to high costs associated with in vivo and clinical development of drug formulations, there is a growing emphasis on development of *in vitro* screening techniques that can better predict and evaluate the efficacy of formulations at the early product development stage itself. Here, we present the *in vitro* investigation of the potential influence of our nanoscale hydrogel platform on the permeability of hydrophobic therapeutic doxorubicin subsequent to oral administration.

In this Chapter, we first evaluate and compare the transport of doxorubicin across an in vitro intestinal epithelium model. To investigate the potential of the nanoscale hydrogels to inhibit P-glycoprotein related drug efflux, we assess the ability of our nanoscale formulations to inhibit the overly expressed drug efflux proteins that impede transport across intestinal epithelium and also confer drug resistance to cancer cells. By surface functionalizing pH responsive polymer nanoparticles with polyoxyethylene chains, we hypothesize that the nanoscale delivery vehicle can potentially sensitize drug resistant cancer cells and empower an improved treatment modality against multidrug resistant cancer. By implementing a tailorable polymer nanotechnology-based oral delivery platform, we can provide chemotherapeutics unprecedented access to otherwise “inaccessible” cytoplamsic regions of multidrug resistant tumor cells without eliciting any adverse effects. Such a multifunctional system that responds to changes in the pH and intelligently inhibits only cancerous cells

precludes the usage of other pharmacological agents and complex, cost prohibitive treatment strategies that are currently implemented to combat multidrug resistant cancer.

In this proposed work, we describe a promising new strategy that involves nanoscale system that can help evade barriers instituted by metastatic tumors to elude traditional cancer drugs and are designed to be orally delivered with the intention of improving patient quality of life. This work, thus, looks to develop a broadly applicable platform that can deliver a robust and actively targeted therapeutic package, by intelligently sensing and reacting to the gastrointestinal tract milieu and ensuring its delivery to the site of action by deactivating any drug efflux associated barriers that a drug may otherwise encounter. To address outstanding questions regarding the spread of tumor metastases through blood vessels, my work explores the potential of using a nanoscale platform that can deliver a wide range of therapeutics, in addition to releasing traditional chemotherapeutics in a controlled manner to destroy any other circulating tumor cells. It can help establish the structural framework for a nanotechnological toolbox that enables cancer drugs to infiltrate cancer's evasive mechanisms and may be a promising new approach to non-invasively treat metastatic cancer, a disease condition which has now attained the "chronic" status.

As previously mentioned, a promising approach to overcoming this drug resistance on the cellular scale would be to inhibit the drug efflux pump receptors and increase accumulation of chemotherapeutics within the cytoplasm, thereby empowering the cytotoxic drug to exert its therapeutic effect by localizing at the nucleus. Several pharmacological efforts have explored delivering a variety of appropriate ligands to

interdict the drug efflux pumps, but they have not been without unfavorable consequences due to local cytotoxicity to normal cells. In this work, we discuss the possibility of incorporating such an inhibitory functionality within the delivery system itself, thereby avoiding co-delivery of other pharmacological agents and thus, any additional unwanted side effects. By implementing a tailorable polymer nanotechnology-based oral delivery platform, we can provide chemotherapeutics unprecedented access to the now "inaccessible" cytoplamsic regions of multidrug resistant tumor cells without eliciting any adverse effects.

During the past few decades, significant efforts have been directed towards understanding and interdicting the basic cellular mechanisms by which tumor cells acquire resistance to traditional chemotherapeutics such as doxorubicin, tamoxifen, cisplatin, methotrexate etc. Owing to multidrug resistance exhibited by such cancerous cells, normal cells are more affected by the drug than cancerous cells, since the drug diffuses through tissues and cells indiscriminately but leads to death of normal cells while cancerous cells continue progression and evasion of apoptosis. Increasing evidence points to one major mechanism of multidrug resistance- an over-abundance of efflux pump proteins on tumor cell membranes. Proteins such as P-glycoprotein, MRP1, MRP2, and BCR, have been observed to be over-expressed in multiple cancer cell lines and are responsible for removing cancer drugs (which are substrates for such receptors) to the extracellular matrix and away from their site of therapeutic action [1]. This leads to a precipitous decrease in the intracellular concentration of the drug and drastically reduces the efficacy/ability of the drug to act against cancer cells. Interestingly, P-gp is also

amply expressed in many cancers (small and large intestine, liver, pancreas, kidney, ovary, and testicle) along with other metabolizing organs such as small and large intestine, and the liver [1]. Small intestine and the liver often metabolize orally administered anticancer drugs to reduce their bioavailability by coupling p-gp reception with CYP450 metabolizing enzyme action. A further application, any solution to overcome multidrug resistance could also help shed insight into ways that can broadly improve oral bioavailability of such cancer drugs as well.

One strategy to resolve this issue would be to inhibit these cell membrane proteins responsible for the reduced efficacy of cancer drugs. While there may be small molecule inhibitors capable of thwarting the action of such efflux pumps, their advantage is not without deleterious pharmacological consequence. Several reports have identified excipients that can inhibit of P-gp proteins and can interdict the functioning of a wide variety of ABC transporter proteins. Much focus has been given to developing nanoparticles that can co-deliver small molecule inhibitors of P-gp such as verapamil along with chemotherapeutics. However, the results of using such co-delivery led to increase in vivo toxicity and were limited to reversing drug resistance only in a few cancers. One excipient that has shown striking promise has been polyethylene glycol. Presence of PEG (MW~300) in the vicinity of cancer drugs was found to inhibit rat jejunal membrane and over-expressing Colon adenocarcinoma cells [2]. In this project, we propose to examine the efficacy of PEG by grafting PEG to our nanoparticles. PEG grafted nanoparticles can interact with P-gp receptors expressed on cancer cells to reduce their function, while simultaneously releasing chemotherapeutics. Such a delivery system

that not only delivers but also guarantees one-way transport of drugs is crucial in the treatment of metastatic cancer.

For this study, we plan on using Caco-2 cells which are known to over-express p-gp proteins on their cell membrane as a model to study release of chemotherapeutics from the nanoscale, PEGylated hydrogel particles. We look to evaluate/demonstrate the ability of the nanoparticles to increase transport of drug across the cell line using a transport study. In addition, we intend to understand the mechanism of P-gp binding/inhibition, the mechanism that is used by these nanoparticles to evade p-gp barriers in metastatic cancer cells. A detailed understanding of how PEGylated nanoparticles can inhibit p-gp and can help further the vast/substantial body of research that can help create a structural framework of nanoscale particles that can help overcome multidrug resistance.

The inhibitory effect of PEG is typically believed to be the consequence of either or both of the two mechanisms: (1) direct inhibition/modulation of ATP binding sites of drug efflux transport proteins, (2) alteration of cell membrane fluidity leading to conformational changes in transport proteins. Previous work suggests that PEG, being osmotically active causes local osmotically-driven water transfer across cell membranes, thereby altering membrane fluidity. Membrane fluidity changes lead to a modification in the structure of drug efflux transport proteins commonly over-expressed in tumor cells, indirectly reducing the binding ability of the proteins. Similarly, it is likely that the oxyethylene groups in PEG may cause nonspecific steric hindrance of drug binding sites or may embed themselves in cell membranes, impeding drug-protein interaction in the

binding sites. Both these mechanisms lead to an overall decrease of ATPase activity of the efflux proteins in multidrug resistance cells.

Common methods of overcoming multidrug resistance usually rely on passive diffusion of nanoparticles into resistant cells, leading to higher apparent, intracellular drug concentrations. However, intravenous administration of nanoparticles is associated with challenges of their own such as immunogenicity, renal clearance, and endosomal sequestration leading prior to drug release. In addition to inhibition of drug efflux pumps, PEG also fulfills a number of other functions such as improved mucoadhesion in the small intestine and enhanced biocompatibility. Hence, it is not surprising that other approaches use polyethylene glycol alone as an excipient or a solubilizing agent that may or may not encapsulate the drug.

8.2 MATERIALS AND METHODS

8.2.1 Transport Studies with Nanoparticle Formulations

8.2.1.1 ***Cell Culture:***

To provide a model for the intestinal epithelial layer, across which we expect doxorubicin to be transported, we used a Caco-2 cell culture, a widely implemented and most popular *in vitro* intestinal cell model [3-5], that was plated on 12-well Corning® Costar® Transwell® plates (Corning Inc., New York). The 12 well plates were equipped with 24mm Corning® Costar ® Transwell® cell culture inserts (Corning Inc., New York) with a 0.4 um polyester membrane for cell growth.

Caco-2 cells were cultured in T-75 flasks until about 80% confluent. Cells were then subcultured, counted and plated onto Transwell® inserts placed in 12 well plates at a

seeding density of $1x10^5$ cells/cm^2. Subsequent to plating, the cells were cultured for 21-24 days with media replaced every other day.

8.2.1.2 ***Transepithelial Electrical Resistance (TEER) Studies:***

In the 21-24 days leading up to the study, Caco-2 cells were monitored for the formation of tight junctions by performing TEER measurements. Measurement of TEER values was performed using a chopstick electrode and an EVOM epithelial volt-ohm meter (World Precision Instruments, Sarasota, FL). TEER measurements were performed every other day prior to media change to indirectly gauge development of tight junctions that are characteristic of Caco-2 cell monolayers.

Tight junction formation was assessed by calculating resistance of cell layer, denoted by R_{cell} , and computed using the equation:

$$R_{cell} = R_t - R_0$$

Where,

R_t= Resistance at any given time t,

R_0= Resistance related to membrane and media without any Caco-2 cells

After 21-24 days of culturing Caco-2 cells in the Transwell® plates and ensuring attainment of constant TEER values in all wells, the cells were considered to be ready for the actual transport study. The transport of doxorubicin in the presence of the library of nanoscale hydrogels synthesized as described in Chapter 6 was evaluated and compared, to judge the impact of each hydrophobic monomer incorporated on the transport of doxorubicin. Prior to conducting the transport study, cell media was removed from the apical and basolateral side, and washed thrice with pre-warmed Hank's Balanced Salt Solutions (HBSS) on both sides. The washing was followed with replacing both apical and basolateral sides of the insert with the HBSS solution. HBSS was used as a buffering system to ensure maintenance of physiological pH and osmotic balance of the solutions

across the insert during the course of the transport study. The cells were then allowed to equilibrate in their new culture environment for a 2 hour time period, after which their TEER values were measured to ensure absence of any disruptions in tight junction formation.

The transport study was started by replacing the HBSS solution on the apical side, with pre-dissolved, sterile solutions of nanoparticles in HBSS. Nanoparticle solutions of the four formulations were used at a concentration of 1 mg/ml as particle controls to assess the impact of pre-swollen polyanionic nanoparticles alone on the tight junctions. Another control used included free doxorubicin (0.15 mg/ml) in the presence of cells. Control cells were incubated with HBSS alone without any media or doxorubicin. For studying doxorubicin transport in the presence of nanoparticles, doxorubicin (250 µL of 0.15 mg/ml) and nanoparticle formulations (250 µL of 1 mg/ml) were added separately in a 1:1 ratio to bring the total apical solution volume to 500 µL. TEER values were measured every 15 min for 3 hr. Samples from both apical and basolateral side of the inserts were taken every 30 min and analyzed for doxorubicin using UV-Vis spectroscopy.

8.2.2 Transport Studies with PEGylated and non-PEGylated Formulations

8.2.2.1 ***Cell Culture***

To provide a model for the intestinal epithelial layer, across which we expect doxorubicin to be transported, we used a Caco-2 cell culture that was plated on 12-well Corning® Costar® Transwell® plates (Corning Inc., New York). The 12 well plates were equipped with 24mm Corning® Costar ® Transwell® cell culture inserts (Corning Inc., New York) with a 0.4 um polyester membrane for cell growth.

Caco-2 cells were cultured in T-75 flasks until about 80% confluent. Cells were then subcultured, counted and plated onto Transwell® inserts placed in 12 well plates at a seeding density of $1x10^5$ cells/cm^2. Subsequent to plating, the cells were cultured for 21-24 days with media replaced every other day.

8.2.2.2 ***Transepithelial Electrical Resistance (TEER) Studies:***

In the 21-24 days leading up to the study, Caco-2 cells were monitored for the formation of tight junctions by performing TEER measurements. Measurement of TEER values was performed using a chopstick electrode and an EVOM epithelial volt-ohm meter (World Precision Instruments, Sarasota, FL). TEER measurements were performed every other day prior to media change to indirectly gauge development of tight junctions that are characteristic of Caco-2 cell monolayers.

Tight junction formation was assessed by calculating resistance of cell layer, denoted by R_{cell} , and computed using the equation:

$$R_{cell} = R_t - R_0$$

Where,

R_t= Resistance at any given time t,

R_0= Resistance related to membrane and media without any Caco-2 cells

After 21-24 days of culturing Caco-2 cells in the Transwell® plates and ensuring attainment of constant TEER values in all wells, the cells were considered to be ready for the actual transport study. The transport of doxorubicin in the presence PEGylated and non-PEGylated microscale hydrogels were studied to study the impact of poly(ethylene glycol) on the transport of doxorubicin in an intestinal epithelial cell model. We used a microscale hydrogel system to test this particular hypothesis because non-PEGylated nanoparticles of the system used in other studies were unstable, and aggregated and collapsed out of solution. PEG provides additional colloidal stability to the emulsion and

facilitates formation of nanoparticles. Absence of PEG prevented the formation of PEG. For this transport study, we used P(MAA-co-NVP-g-PEG) microparticles as a substitute for our system. We use the non-PEGylated version, namely, P(MAA-co-NVP) to investigate any differential gain in the increase of doxorubicin transport that may be arising from PEGylation.

Similar to the previous transport study, prior to conducting the transport study, cell media was removed from the apical and basolateral side, and washed thrice with pre-warmed Hank's Balanced Salt Solutions (HBSS) on both sides. The washing was followed with replacing both apical and basolateral sides of the insert with the HBSS solution. HBSS was used as a buffering system to ensure maintenance of physiological pH and osmotic balance of the solutions across the insert during the course of the transport study. The cells were then allowed to equilibrate in their new culture environment for a 2 hour time period, after which their TEER values were measured to ensure absence of any disruptions in tight junction formation.

The transport study was started by replacing the HBSS solution on the apical side, with pre-dissolved, sterile solutions of the particles in HBSS. Particle solutions of the four formulations were used at a concentration of 1 mg/ml as particle controls to assess the impact of pre-swollen polyanionic nanoparticles alone on the tight junctions. Another control used included free doxorubicin (0.15 mg/ml) in the presence of cells. Control cells were incubated with HBSS alone without any media or doxorubicin. For studying doxorubicin transport in the presence of nanoparticles, doxorubicin (250 µL of 0.15 mg/ml) and particle formulations (250 µL of 1 mg/ml) were added separately in a 1:1 ratio to bring the total apical solution volume to 500 µL. TEER values were measured every 15 min for 3 hr. Samples from both apical and basolateral side of the inserts were taken every 30 min and analyzed for doxorubicin.

8.2.3 Doxorubicin Uptake Studies using Image Flow Cytometry

To prepare for the doxorubicin uptake study, colon adenocarcinoma cells (Caco-2 cells) were seeded at 1 x 10^5 cells/well in 6- well plates and grown to 80% confluence, and washed with PBS prior to incubation with DOX-loaded nanoparticles. Subsequent to attaining confluence, Caco-2 cells were incubated with 200 µL of doxorubicin loaded nanoparticles at a concentration of 1 mg/ml. Cells were exposed to nanoparticles for a period of 3 hours, after which the solution was aspirated and cells washed 3x with PBS. Following the rinses, cells were incubated in 2 mL DMEM and the Hoechst 33342 nuclear stain was added to each well at a final concentration of 2.5 µg/ml. Cells were allowed to incubate with the stain for a period of 45 mins. To generate cell suspensions from the adherent Caco-2 cells, trypsin-EDTA was added and incubated at 37^{o}C for 8 min. To avoid deleterious effects to Caco-2 cells, DMEM was added to neutralize the trypsin and the collected cell suspension centrifuged for 4 min at 50xg. Post-centrifugation supernatant was discarded and the cell pellet resuspended to obtain Caco-2 cells tagged with a nuclear stain and ready to be imaged for doxorubicin uptake. Propidium iodide was added to the cell suspensions just prior to flow uptake and analysis with ImageStream.

Cellular uptake of doxorubicin released from doxorubicin-loaded nanoparticles was observed in Caco-2 cells using image stream cytometry. The Amnis ImageStream^x (Seattle, WA) imaging flow cytometer has lasers at 405 nm, 488 nm, 658 nm, and 785 nm. For studies conducted for doxorubicin uptake, we used the following channels to

collect fluorescent emission data - Channel 1 (430 – 505 nm) for Hoescht (nuclear stain); Channel 2 (505 - 595 nm) for doxorubicin; Channel 4 (595 – 660 nm) for propidium iodide which offers distinguishability between live and dead cells, Channel 5 (brightfield images), and Channel 6 (745 – 800 nm) for side scatter. A 60x objective was used to image the cells. Flow velocity of the fluid was fixed at 40 mm/sec.

8.2.4 Evaluation of P-glycoprotein Inhibition

8.2.4.1 Evaluation of P-glycoprotein Inhibition using Multidrug Resistance Assay

All previous studies and attempts at understanding transport and permeability with doxorubicin were conducted with Caco-2 cells, which while known to express P-glycoprotein, their P-glycoprotein expression varies dramatically based on passage number and gene expression levels *in vitro*. To obtain a more robust understanding of the influence of the nanoparticle formulations and their influence on P-glycoprotein, we used a different set of cell lines with varied levels of P-gp expression.

Three cell lines were used to conduct the Vybrant® Multidrug Resistance Assay (Life Technologies) with the nanoparticles. P-gp overexpressing and doxorubicin resistant, lung carcinoma cell line - NCI H69/LX4 (Sigma Aldrich/European Collection of Cell Cultures) was obtained. This cell line (originated at MRC Clinical Oncology, Cambridge, UK) has been certified to overexpress P-gp and is resistant to doxorubicin by the P-gp efflux mechanism. The cell line was obtained at passage number 5, and cultured in RPMI 1640 media with 2mM L-glutamine & 10% FBS along with and 0.4 µg/mL doxorubicin (to maintain resistance) as recommended. As a control of normal Pgp expression, NCI H69 (Sigma Aldrich/European Collection of Cell Cultures) which is

verified to show normal expression of P-gp was also used. Raji B (B lymphpoma) cells were used as another control of P-gp underexpression. All cells were cultured until sufficient cells were available for assay.

All nanoparticles formulations were studied with the assay, First, nanoparticle solutions ranging from 4 mg/ml to 8 µg/ml were prepared in PBS. As reference, cyclosporin A and verapamil hydrochloride, known inhibitors of Pgp were used as controls, in addition to blank PBS. Cells were added to 96-well microplates at a concentration of 5 x 10^5 cells in RPMI 1640 media. 50 uL of nanoparticles, reference inhibitors were added to the cells and incubated for 15 mins at 37^{o}C. After incubation for 15 mins, microplates were washed 3x by centrifuing for 5 mins at 200g, and supernatant removed and resuspended in 200 ul cold RPMI 1640 media. Calcein retention was measured by fluorescence at 494 nm(ex)/525(em).

8.2.4.1 Evaluation of P-glycoprotein Inhibition using Cellular Proliferation Assay

Lastly, as a final *in vitro* measure of the nanoparticle formulations to exert a P-gp inhibitory/modulatory effect, we evaluated the ability of doxorubicin to induce an anti-proliferative effect on P-gp overexpressing/doxorubicin-resistant cell line – H69/LX4. As controls – H69 and Raji cells were also used.

For evaluating cellular proliferation, an MTS assay was used with all three cell lines. P-gp overexpressing and doxorubicin resistant, lung carcinoma cell line - NCI H69/LX4 (Sigma Aldrich/European Collection of Cell Cultures) was cultured in RPMI 1640 media with 2mM L-glutamine & 10% FBS along with and 0.4 µg/mL doxorubicin (to maintain resistance) as recommended. As a control of normal Pgp expression, NCI

H69 (Sigma Aldrich/European Collection of Cell Cultures) which is verified to show normal expression of P-gp was also used. Raji B (B lymphpoma) cells were used as another control of P-gp underexpression. All cells were cultured until sufficient cells were available for assay.

All nanoparticles formulations were studied in the presence of doxorubicin with the assay. Cells were added to 96-well microplates at a concentration of 50,000 cells/well in RPMI 1640 media. First, nanoparticle solutions ranging from 4 mg/ml to 8 µg/ml were prepared in RPMI 1640 medium, and added to cells. As reference, the anti-proliferative ability of doxorubicin alone was evaluated. The microplates were incubated at 37^{o}C for 4 hours. Subsequent to which the solutions were removed, and cells washed thrice with RPMI 1640 media by centrifugation 300g for 5 mins. 20 ul of MTS reagent was then added to each well and incubated for 2 hr. Microplates were then read for absorbance of formazan indicative of cellular proliferation.

8.3 RESULTS AND DISCUSSION

8.3.1 Transport Studies with Nanoparticle Formulations

To assess permeation of doxorubicin in the presence and absence of nanoscale hydrogel formulation, we conducted transport studies using an *in vitro* intestinal cell model. Caco-2 cells were cultured on Transwell® plates for a period of 21-24 days to allow for development of tight junctions. Tight junction development was monitored for the 21-24 day period by TEER measurements performed using a chopstick electrode and an EVOM epithelial volt-ohm meter. The TEER values typically increase from 100 ohm-

cm^2 (resembling blank HBSS control and undeveloped tight junctions) to 400-500 ohm-cm^2 at the end of the 21-24 day culture period. In contrast to human small intestinal epithelial cell monolayers that exhibit TEER values of 50-100 ohm-cm^2, the *in vitro* intestinal cell model displayed TEER values of about 400-500 ohm-cm^2 at the end of the 21-24 day culture period. These tighter junctions obtained in an *in vitro* experimental setting are representative of colonic tight junctions and it is understood that the permeability values will be attenuated/underestimated as compared to actual *in vivo* permeability values.

Permeation studies were performed under same conditions for all four nanoparticle formulations serving as vehicle controls for evaluating impact of each nanoparticle formulations on tight junction integrity, as well as free doxorubicin serving as the free drug control. To investigate the impact of each formulation on the in vitro intestinal transport of doxorubicin in the presence of the nanoparticles, the formulation was incubated with doxorubicin on the apical side of the Transwell® for a 3 hr period, with doxorubicin concentration analyzed regularly on the basolateral side. TEER measurements were also taken to monitor tight junction integrity throughout the experiment. All formulations were used at a concentration of 1 mg/ml to allow for proper comparison between formulations.

The particle control, or wells containing nanoparticle formulation alone contributed to about 20% decrease in TEER measurements which likely to be caused due to chelation of Ca^{2+} by the nanoparticle formulation on the apical side driving an influx of Ca^{2+} from the basolateral side to the apical side to maintain homeostasis. Chelation of

Ca^{2+} by P(MAA-g-EG) hydrogels and resulting flux has previously been reported by Ichikawa and Peppas [6]. Since all four nanoparticle formulations comprise of MAA and PEG, it is a strong possibility that they impact tight junctions in a similar manner, and may providing a pathway of explanation to the decrease in TEER values. Of notable mention is the inference that a nanoparticle concentration of 1 mg/ml is sufficient to saturate and reach the cell membrane layer and cause Ca^{2+} chelation, in contrast to microparticle formulations that typically result in attenuated TEER values at concentrations of about 20 mg/ml.

Doxorubicin transport studies were performed with and without nanoscale hydrogels to evaluate the impact of the formulation on in vitro intestinal permeability of doxorubicin, and play a role in the determination of an optimal formulation for the end goal of improving intestinal permeability. As previously mentioned, nanoparticle formulations were pre-swollen in HBSS under sterile conditions at a concentration of 1 mg/ml and doxorubicin at a concentration of 0.15 mg/ml (polymer:drug=1:0.15), an optimal ratio arrived at based on cytotoxicity studies, loading and release studies, and pharmacological feasibility calculations.

The in vitro intestinal model of Caco-2 cells was seeded on Transwell® plates, and their health and tight junction development monitored as mentioned in the TEER studies section. For the actual transport study, the nanoparticle solution and drug solution were added directly onto the cells on the apical side. Samples from the basolateral side were collected over a 3 hr time period and doxorubicin was analyzed using a UV-Vis plate reader.

Apparent permeability was determined using the following equation:

$$P_{app} = \frac{dQ(t)}{dt} \times \frac{1}{A \times C_{A0}}$$

In this equation, A is the known area of the cell monolayer and C_{A0} is the initial apical concentration of doxorubicin added. dQ/dt is the slope of the linear regression model fit of the transport profile of doxorubicin concentration over the 3 hr period based on the basolateral concentrations. This equation is derived from the Fick's first law of diffusion applied to a chemically homogeneous monolayer of known thickness. Q(t) is the cumulative amount of doxorubicin transported from the apical side to the basolateral side at time t. Lastly, apparent permeability P_{app} is defined as (K x D)/h, where K is the partition of distribution coefficient of doxorubicin within the cell monolayer, D is the diffusion coefficient of the doxorubicin within the cell monolayer (cm^2/s), and h is the height or thickness of the cell monolayer.

The apparent permeability values of doxorubicin in the presence of each of the four formulations are shown in Table. By far, the P(MAA-g-PEG-co-MMA) formulation is the best performing of them all with an apparent permeability of . The higher permeability in the presence of MMA could be attributed to the relatively optimal distribution of methacrylic acid moieties available for Ca^{+2} chelation and increased transport via tight junction opening, and methyl methacrylate hydrophobic groups that may allow the nanoparticles to come closer to the cell monolayer leading to increased

doxorubicin transport by passive diffusion. The apparent permeability of free doxorubicin without any nanoparticles was higher than with nanoparticles alone. This can be possibly ascribed to the solubility-permeability interplay we previously referred to in Chapter 7. Presence of nanoparticles with lipophilic moieties in the vicinity can cause some absorption of doxorubicin within the particle core. This reduces the free doxorubicin concentration available for transport on the apical side at the cell membrane interface, leading to a smaller concentration gradient than that when doxorubicin is present without any nanoparticles. Lower concentration gradient implies lower transport, and thus lowers apparent permeability. This is touted to be an inherent limitation of solubility improving nanoformulations, but we can be overcome by combining our amorphous solid dispersions with next-stage pharmaceutical processing techniques like spray drying that rely on supersaturation to mitigate the solubility-permeability interplay. Indeed, we note that the tight junction values for in vitro intestinal models indicate tighter junctions being formed *in vitro* than *in vivo*, and we anticipate the apparent permeability values for all formulations to be higher *in vivo* than the *in vitro* values obtained. Lastly, all apparent permeability values are in the range of 10^{-6} cm/s, and are consistent with values found in the literature involving transport studies with in vitro cell models.

8.3.2 Transport Studies with PEGylated and Non-PEGylated Formulations

To evaluate if there is any improvement in the permeation of doxorubicin in the presence and absence of PEGylation hydrogel formulation, we conducted transport studies using an *in vitro* intestinal cell model. In this study, we focus on the impact of PEG on doxorubicin. PEG has been shown to interact with tight junction proteins in

addition to interacting with P-glycoprotein as we have previously mentioned. Doxorubicin transport studies were performed with microparticles containing PEG and compared to transport with formulations without PEG.

Caco-2 cells were cultured on Transwell® plates for a period of 21-24 days to allow for development of tight junctions. Tight junction development was monitored for the 21-24 day period by TEER measurements performed using a chopstick electrode and an EVOM epithelial volt-ohm meter. The TEER values typically increase from 100 ohm-cm^2 (resembling blank HBSS control and undeveloped tight junctions) to 400-500 ohm-cm^2 at the end of the 21-24 day culture period. In contrast to human small intestinal epithelial cell monolayers that exhibit TEER values of 50-100 ohm-cm^2, the *in vitro* intestinal cell model displayed TEER values of about 400-500 ohm-cm^2 at the end of the 21-24 day culture period. These tighter junctions obtained in an *in vitro* experimental setting are representative of colonic tight junctions and it is understood that the permeability values will be attenuated/underestimated as compared to actual *in vivo* permeability values.

Permeation studies were performed under same conditions for the two formulations namely, P(MAA-co-NVP-g-PEG) and P(MAA-co-NVP). To investigate the impact of each formulation on the in vitro intestinal transport of doxorubicin in the presence of the nanoparticles, the formulation was incubated with doxorubicin on the apical side of the Transwell® for a 3 hr period, with doxorubicin concentration analyzed regularly on the basolateral side. TEER measurements were also taken to monitor tight

junction integrity throughout the experiment. All formulations were used at a concentration of 1 mg/ml to allow for proper comparison between formulations.

The in vitro intestinal model of Caco-2 cells was seeded on Transwell® plates, and their health and tight junction development monitored as mentioned in the TEER studies section. For the actual transport study, the nanoparticle solution and drug solution were added directly onto the cells on the apical side. Samples from the basolateral side were collected over a 3 hr time period and doxorubicin was analyzed using a UV-Vis plate reader. The apparent permeability values of doxorubicin in the presence of each of the four formulations are shown in Table. By linear-fitting the mass of doxorubicin transported from apical-to-basolateral side versus time, we obtained a slope or apparent permeability for doxorubicin to be 6.805 x 10^{-6} cm/s for the PEGylated formulation, while the slope obtained for the non-PEGylated formulation was 4.472 x 10^{-6} cm/s. Our measurements demonstrate and increased transport of doxorubicin from the apical-to-basolateral side with PEGylated formulations. However, this study does not clearly reveal if the increased transport is due to interaction of PEG with P-gp receptors or the interaction of PEG with tight junction proteins that may lead to increased paracellular transport of doxorubicin, or a combination of the two [6, 7]. To more clearly elucidate the interactions of PEGylated nanoparticles with P-gp receptors we measured calcein AM retention with P-gp overexpressing cells as described further in section 8.3.4.1.

8.3.3 Image Flow Cytometry

Amnis IDEAS® software was used to create the fluorescent compensation matrices, and to obtain images of in-focus cells using the Gradient RMS feature that

reviews image sharpness. Propidium iodide positive cells were ignored as they represent dead cells since propidium iodide can permeate only dead cells, and all attention was diverted to live cells (about 1000-2000 live cells were imaged). Any debris present was also gated according to side scatter that is capable of discriminating cell complexity/granularity from brightfield area. Single cells were honed in by surveying the brightfield aspect ratio in comparison to the brightfield area based on the fact that single cells have high aspect ratios. However, in case of Caco-2s single cells were hard to obtain since many of them adhered to each other forming clumps precluding an ideal number of cells for any in-depth analysis. Pictured in Figure is a panel of representative fluorescent micrographs of Caco-2 cells. Channel 1 shows cell nuclei in blue, Channel 2 was used to collect fluorescent data from the natural fluorescence of doxorubicin, and while Channel 5 was used to obtain brightfield images are displayed to show cellular granularity. Composite images of Channel 1 and Channel 2 show colocalization of doxorubicin and the nucleus visually verifying internalization and uptake of Caco-2 by doxorubicin. Composite of all three channels 1, 2, and 5, offers further evidence to the internalization of doxorubicin and Caco-2.

8.3.4 Evaluation of P-glycoprotein inhibition

8.3.4.1. Evaluation of P-glycoprotein Inhibition: Multidrug Resistance Assay

An investigation of the influence of nanoparticles on P-gp mediated efflux was conducted using a Vybrant® Multidrug Resistance Assay (Life Technologies). This *in vitro* assay compares the capacities of the nanoparticle formulations to interfere with the P-gp mediated efflux of a known fluorescent substrate, namely, Calcein AM

(acetoxymethyl calcein), and has been used extensively in the literature for screening drug compounds and inhibitors for their P-gp inhibitory effect [8-11]. To detect inhibition of calcein AM efflux in the presence of the nanoparticle formulations, we used a pair of cell lines- one multidrug resistant cancer cell line which overexpresses P-gp (H69/LX4) and the parental cell line (H69) which does not overexpress P-gp. As previously mentioned, the multidrug resistant cell line is derived from the parental cell line by exposure to increasing concentration of doxorubicin over a period 6-9 months and numerous replication cycles. Beyond the results described above, a kinetic understanding of the inhibition by these formulations is not facilitated by this assay, however given the possible non-specific nature of the interactions of PEG with P-gp, these formulations can be assumed to be interacting in the capacity of P-gp modulators, rather than competitive inhibition. Results of the assay were analyzed by normalizing fluorescence of treatment groups to that untreated parental cells as prescribed in the assay protocol. Relative fluorescence has also been used to analyze Calcein AM studies in other investigations. Formulations were ranked on the basis of effectiveness in inhibition of calcein AM efflux by comparing the amount of polymer concentration required to obtain a certain extent of P-gp inhibition and thus, calcein retention and increased fluorescence. A dose-response curve was plotted to evaluate the ability of the formulations to increase calcein retention in MDR cells. Specifically, we evaluated the polymer concentration of each formulation to attain 50% of calcein AM specific fluorescence in parental cells to compare effectiveness across all formulations, and the curves are shown in Figures 8.4 to 8.7. P(MAA-co-tBMA-g-PEG) formulation performed better than the other formulations in

this study, with concentration of 0.125 mg/ml being able to restore atleast 50% of calcein-specific fluorescence compared to similarly treated parental cells as shown in Figure 8.4. This result can be attributed to the smaller size of these nanoscale hydrogels, since higher surface area-to-volume ratio can allow for better presentation of the PEG grafts (which are believed to modulate Pgp-mediated behavior) to the Pgp proteins expressed on the cell membrane surface. It is also possible that the relatively hydrophobic nature of this formulation was able to enhance proximity to the cell membrane surface, allowing for interaction with P-gp receptors. P(MAA-co-nBA-g-PEG) nanoscale hydrogels also exhibited favorable behavior at increasing calcein retention in MDR cells as compared to parental cells. P(MAA-co-MMA-g-PEG) nanoscale hydrogels were only able to restore 20-30% of the calcein-specific fluorescence and performed inadequately as compared to all other formulations. P(MAA-co-nBMA-g-PEG) nanoscale hydrogels showed some increase in retention, although the increase was not sufficient to appreciably restore greater than 50% of the relative fluorescence.

8.3.4.2 Evaluation of P-glycoprotein Inhibition: Cellular Proliferation

In order to further elucidate the effects of the nanoscale hydrogels on Pgp-mediated efflux, we measured the cytotoxic or anti-proliferative effect of doxorubicin on the multidrug resistant H69/LX4 cells and the parental H69 cells, in the presence of the formulations. As previously mentioned, the H69/LX4 cells used in this study are resistant to doxorubicin, and exclude doxorubicin from the cytoplasm through a Pgp-mediated efflux. We hypothesized that the presence of the nanoscale formulations would sensitize the doxorubicin resistant cells by interacting with P-gp receptors. As another way to

compare the effectiveness of these formulations, the anti-proliferative effects of doxorubicin were measured for all formulations with H69/LX4 cells and H69 cells. While such sensitization studies have been conducted for parenteral formulations [8-13], this is the first study of its kind where drug sensitization studies are being conducted with orally deliverable nanoparticle formulations to understand their interactions with P-gp receptors. Formulations were compared for their capacities to facilitate the anti-proliferative effect of doxorubicin on the multidrug resistant cell lines. Cell proliferation was measured using an MTS assay and is shown in Figures 8.8-8.11. At the end of four hours, there were no significant differences among treatment groups for the cellular proliferations obtained for the formulations. Similarly, we did not observe a dramatic sensitization of the cells to doxorubicin at the end of the four hours when we measured the relative proliferation of the MDR cells. It is possible that a four hour time point may be insufficient to highlight the differences among the formulations to mediate P-gp efflux, and improve the anti-proliferative potential exerted by doxorubicin upon multidrug resistant H69/LX4 cells. The four hour period was chosen keeping consistent with the time these formulations will potentially spend in the small intestine, but further studies may be conducted on a 3-4 day time period to reflect the doubling time of these cells as has been seen elsewhere in the literature.

8.4 CONCLUSIONS

Nanoscale hydrogel formulations were investigated for their capacity to modulate transport and permeability of hydrophobic therapeutic, doxorubicin *in vitro*. Transport of

doxorubicin in the presence of nanoparticles was studied to assess the impact of the formulation on doxorubicin permeability across an intestinal cell model. The P(MAA-g-PEG-co-MMA) formulation was observed to showed highest permeability improvement of doxorubicin across the intestinal epithelial cell model as indicated by transport studies. Similarly, the role of PEG in influencing doxorubicin permeability in vitro was investigated. PEGylated particles showed an increase in transport as opposed to non-PEGylated formulations. This may be attributed to an interaction of PEG with tight junctions that results in opening of the junctions or/and possibly interaction of PEG with P-gp efflux pumps. Further studies to understand the interaction of these nanoscale hydrogel formulations with P-glycoprotein were conducted using a calcein AM assay and cellular proliferation assay. In the calcein AM study, multidrug resistant H69/LX4 cells exhibited greater calcein AM retention when incubated with P(MAA-co-tBMA-g-PEG) nanoscale hydrogels, demonstrating atleast 50% restoration of calcein-specific fluorescence. In addition, the cellular proliferation assay was used to evaluate the ability of the hydrogel formulations to sensitize doxorubicin-resistant H69/LX4 cells to the anti-proliferative ability of doxorubicin. However, none of the formulations showed a large decrease in cellular proliferation of H69/LX4 cells at the end of the four-hour study. Results from the calcein AM study, in combination with the transport studies support the hypothesis that the panel of nanoscale hydrogel formulations synthesized can influence *in vitro* permeability of doxorubicin, and can potentially exhibit favorable behavior anticipated from nanoscale hydrogels to be used for oral delivery of hydrophobic therapeutics. Lastly, the set of in vitro studies described in this chapter serve as a novel

paradigm or set of tests that can be used together, as part of an integrative physicochemical and biological approach for *in vitro* testing or screening of nanoscale oral formulations.

Table 8.1 Doxorubicin transport with nanoscale hydrogel formulations

Formulation	**Apparent Permeability (Papp) (x 10^6 cm/s)**
P(MAA-g-PEG-co-tBMA)	5.56
P(MAA-g-PEG-co-nBMA)	2.77
P(MAA-g-PEG-co-nBA)	3.53
P(MAA-g-PEG-co-MMA)	6.94

Table 8.2 Doxorubicin transport with hydrogel formulations containing PEG and hydrogel formulations without PEG

Formulation	**Apparent Permeability (Papp) (x 10^6 cm/s)**
[P(MAA-co-NVP) **w/ PEG**] Microparticles + DOX	6.805
[P(MAA-co-NVP) **w/o PEG**] Microparticles	4.472

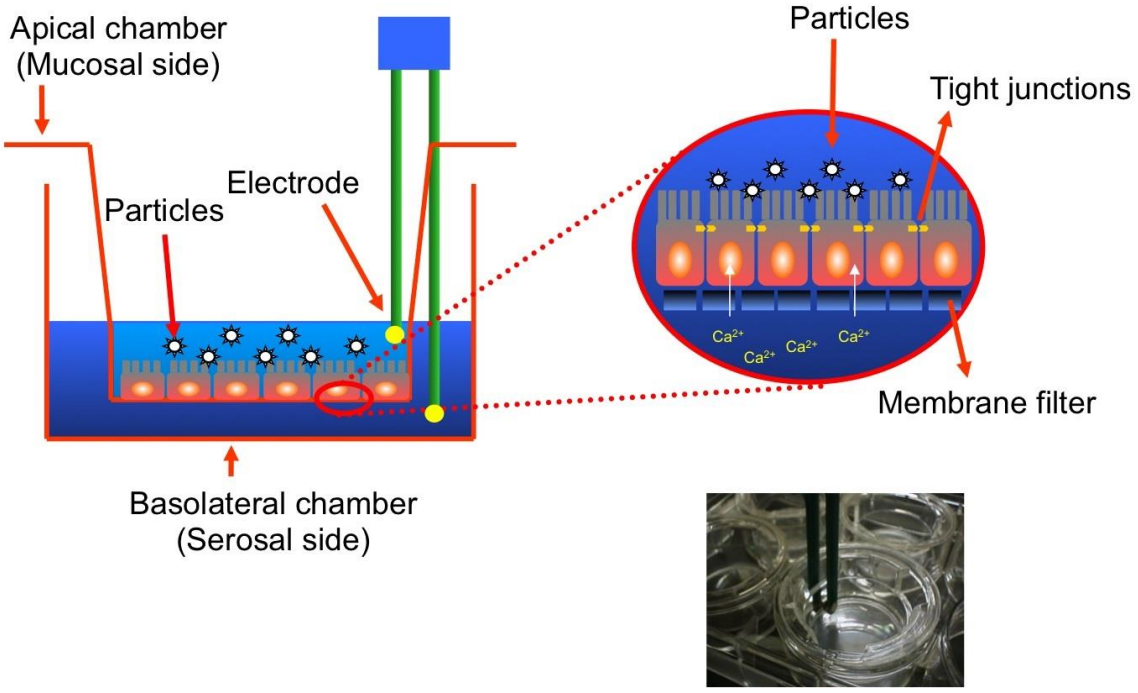

Figure 8.1: A schematic of the set-up for the transport studies conducted using Transwell® plates.

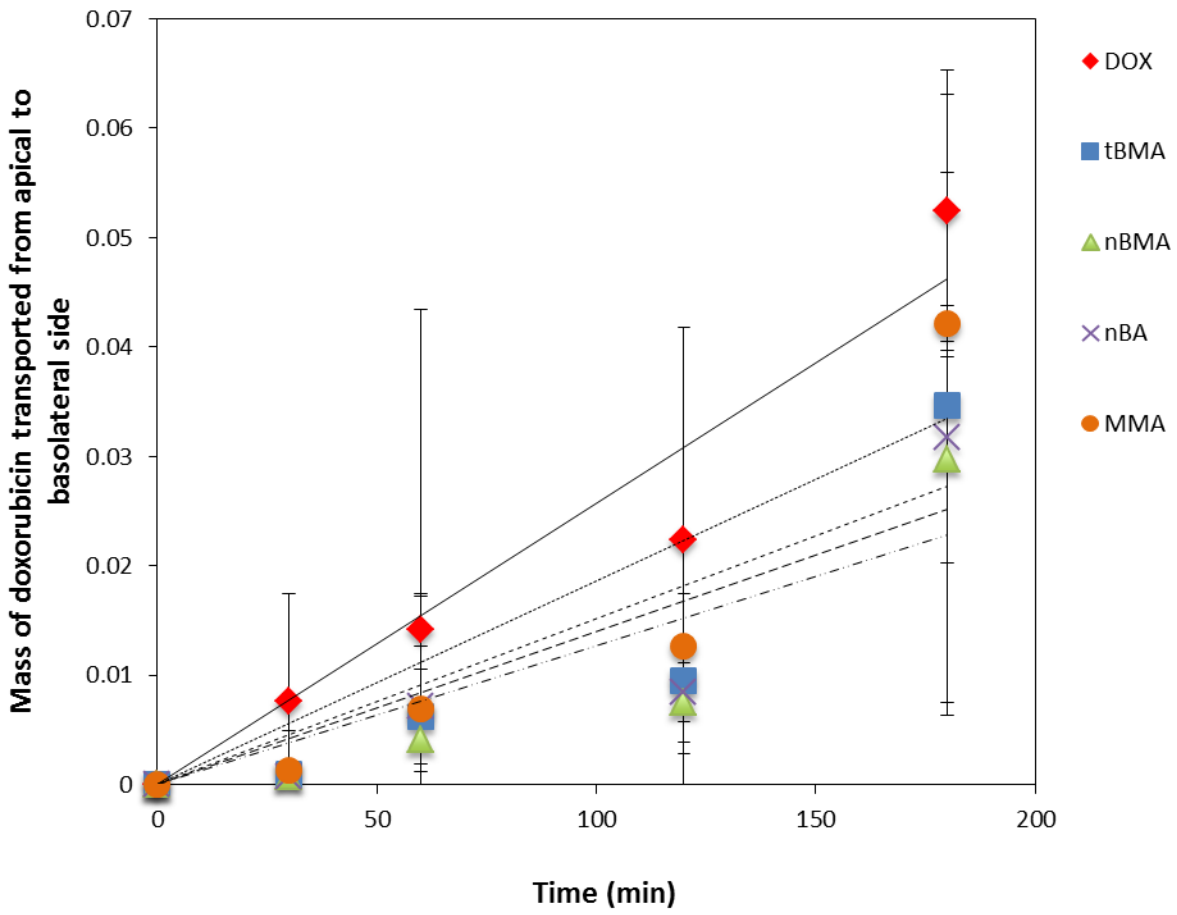

Figure 8.2: Doxorubicin transport with nanoscale hydrogel formulations. Studies were conducted with 1 mg/ml nanoscale hydrogel formulations incubated with Caco-2 cells and 0.15 mg/ml doxorubicin. n=4, Data points represent mean +/- SD.

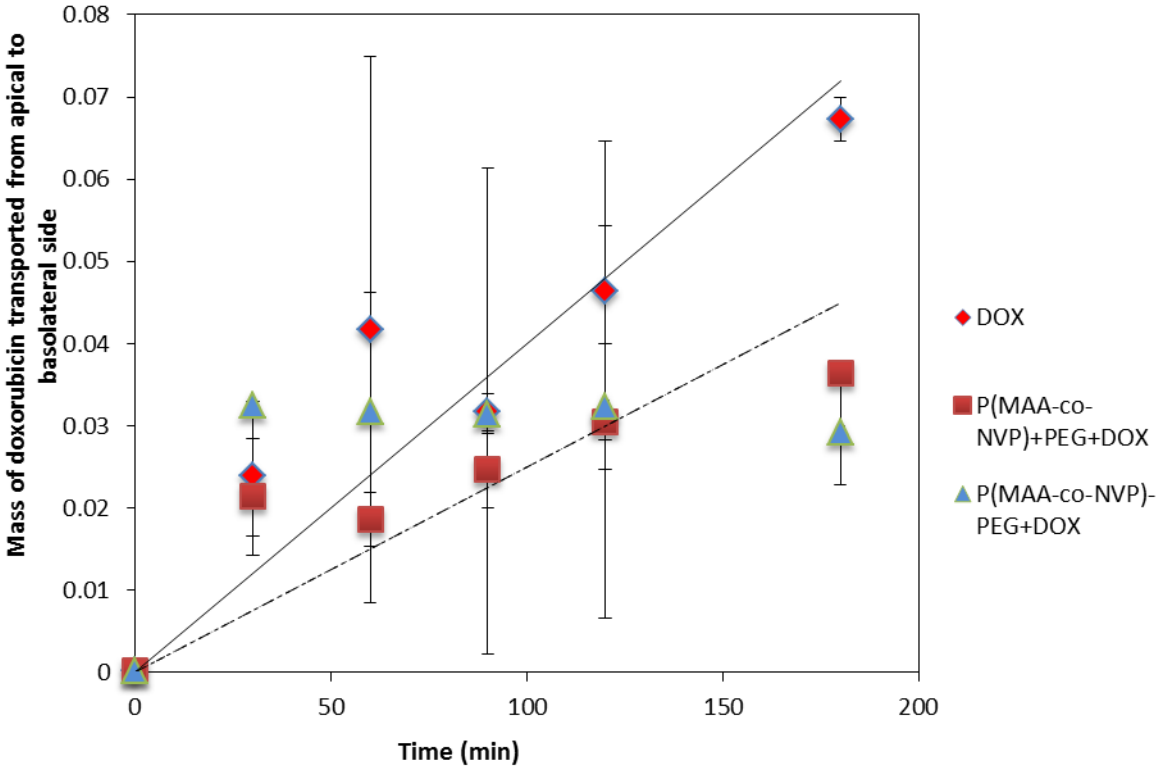

Figure 8.3: Transport of doxorubicin in the presence of PEGylated formulation vs non-PEGylated formulations. Studies were conducted with 1 mg/ml hydrogel formulations incubated with Caco-2 cells and 0.15 mg/ml doxorubicin. n=4, Data points represent mean +/- SD.

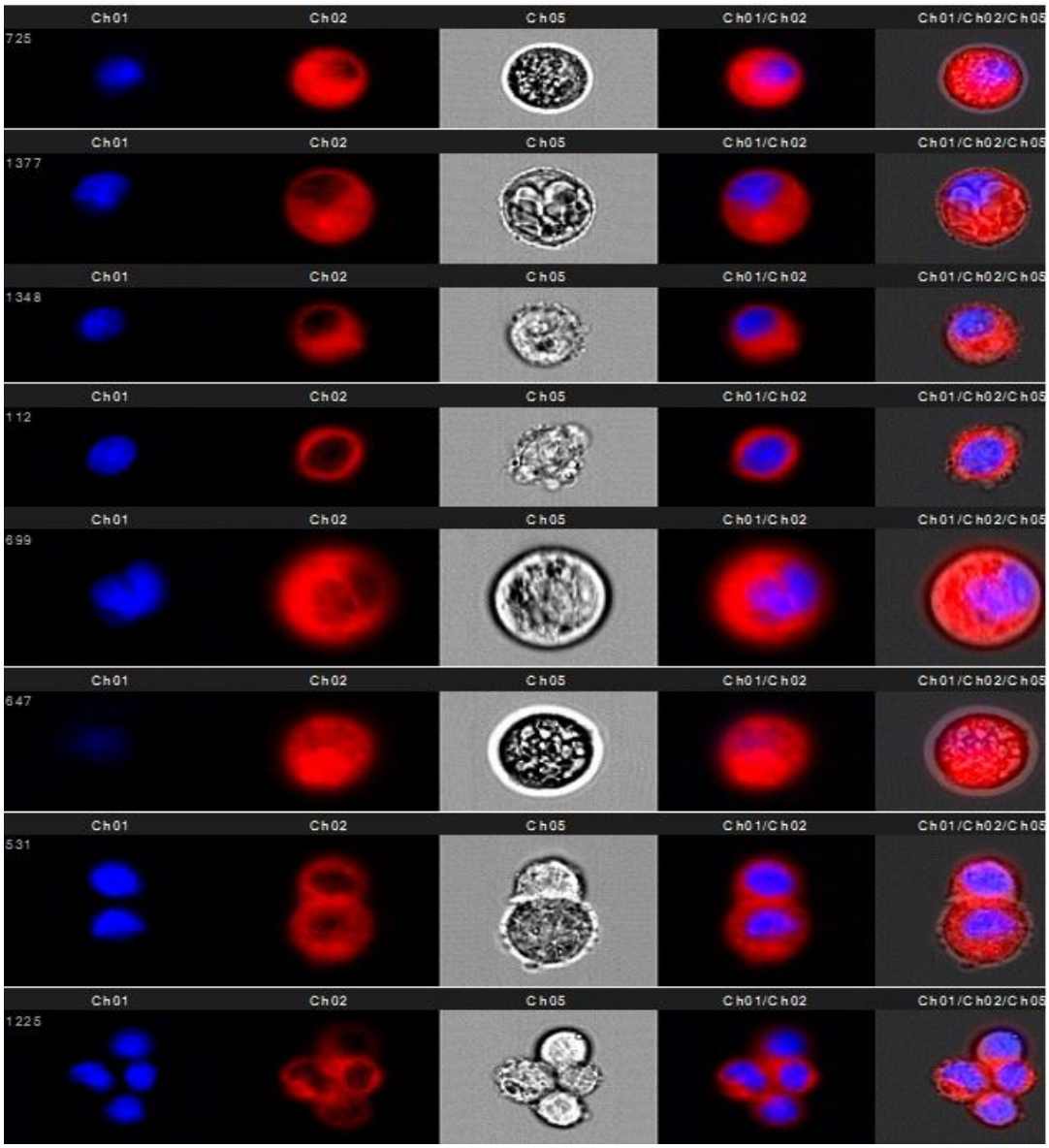

Figure 8.4: Representative fluorescent micrographs of doxorubicin uptake by Caco-2 cells. Channel 1: cell nuclei in blue, Channel 2: doxorubicin, Channel 5: brightfield images.

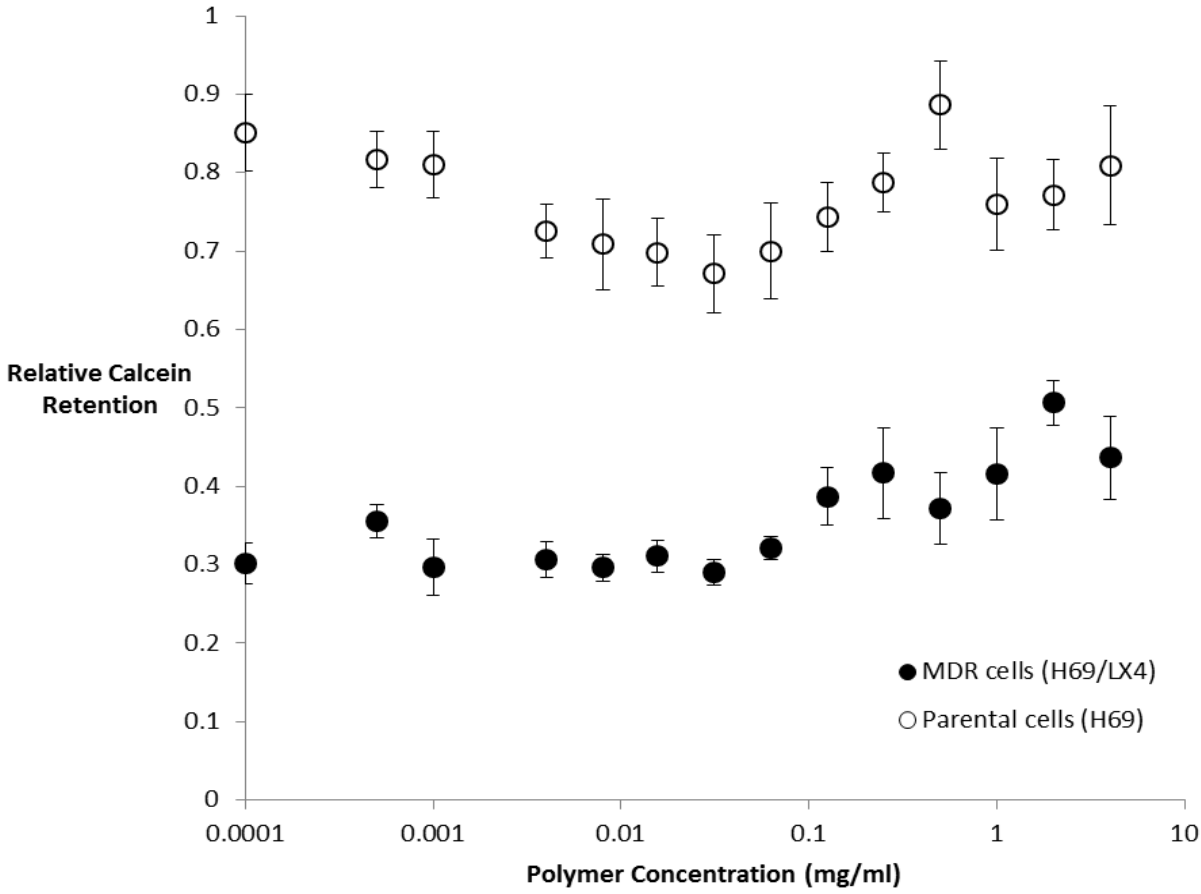

Figure 8.5: Relative calcein retention in P-gp overexpressing multidrug resistant cells (H69/LX4) and parental cells (H69) upon incubation with calcein AM (a P-gp substrate) and P(MAA-co-tBMA-g-PEG) nanoscale hydrogel formulation. Increase in calcein retention can be observed beyond a concentration of 0.125 mg/ml. Relative calcein retention calculated by normalizing calcein fluorescence for sample to untreated parental cells. n=3, data points represent mean +/-SD.

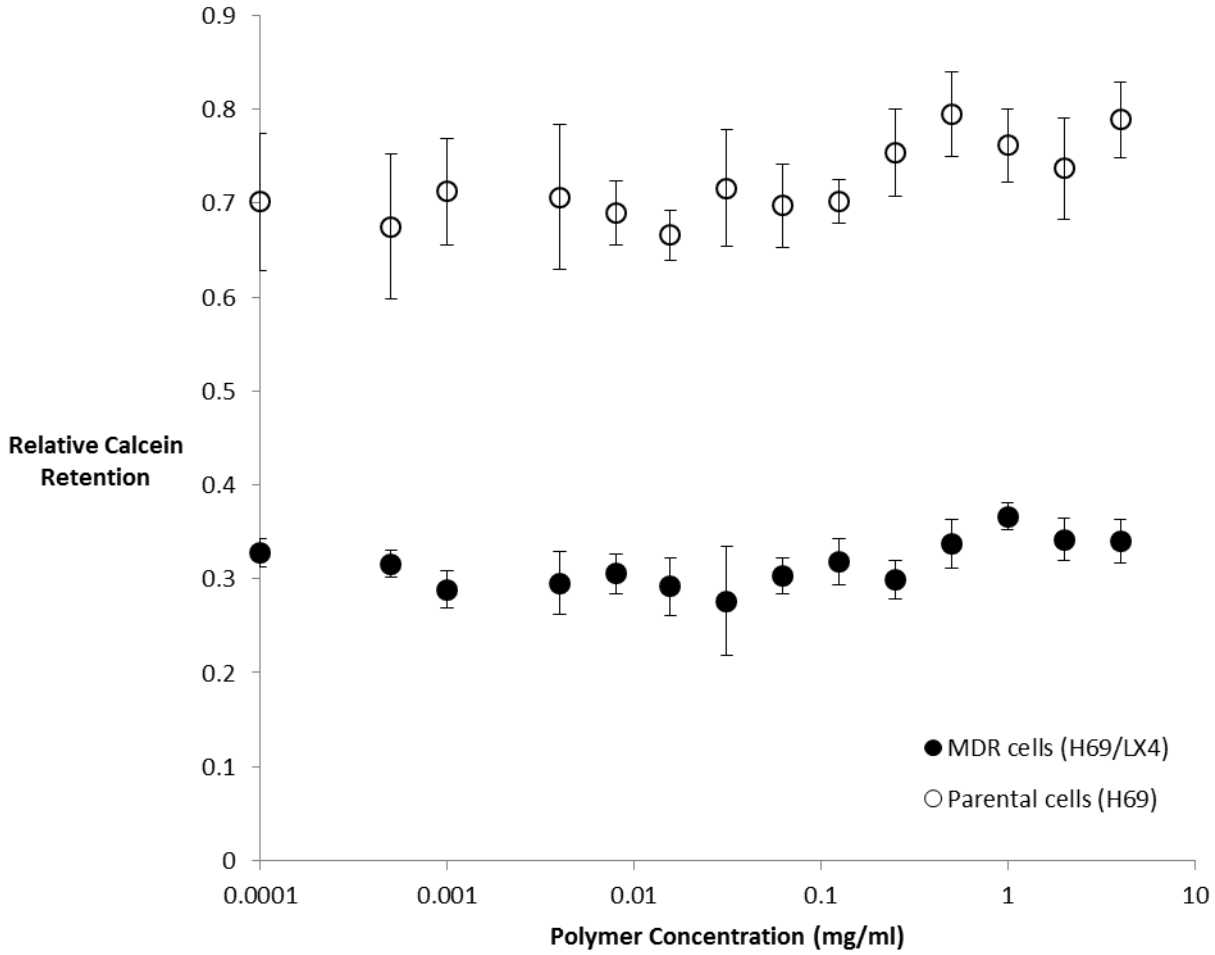

Figure 8.6: Relative calcein retention in P-gp overexpressing multidrug resistant cells (H69/LX4) and parental cells (H69) upon incubation with calcein AM (a P-gp substrate) and P(MAA-co-nBMA-g-PEG) nanoscale hydrogel formulation. Relative calcein retention calculated by normalizing calcein fluorescence for sample to untreated parental cells. n=3, data points represent mean +/-SD.

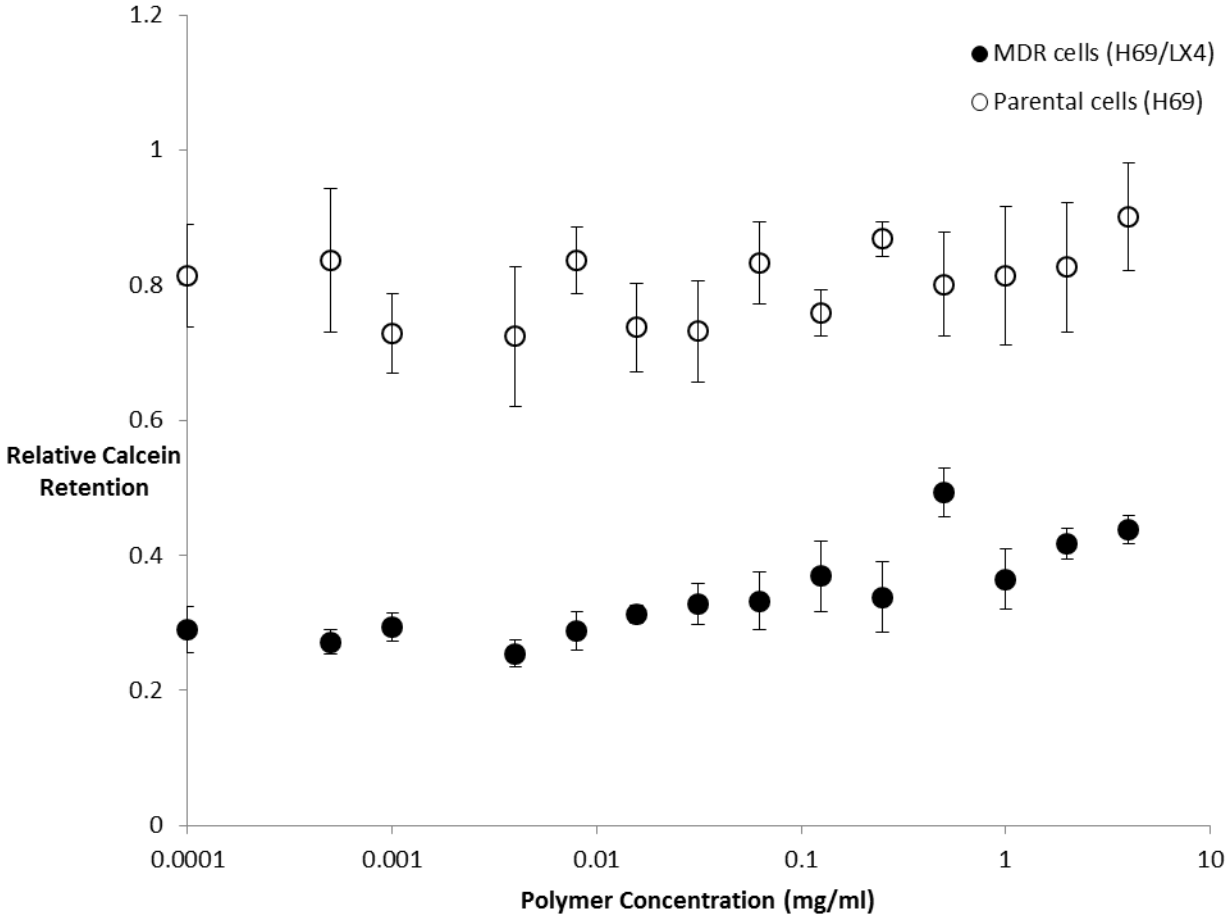

Figure 8.7: Relative calcein retention in P-gp overexpressing multidrug resistant cells (H69/LX4) and parental cells (H69) upon incubation with calcein AM (a P-gp substrate) and P(MAA-co-nBA-g-PEG) nanoscale hydrogel formulation. Increased calcein retention was observed beyond a concentration of 0.5 mg/ml. Relative calcein retention calculated by normalizing calcein fluorescence for sample to untreated parental cells. n=3, data points represent mean +/-SD.

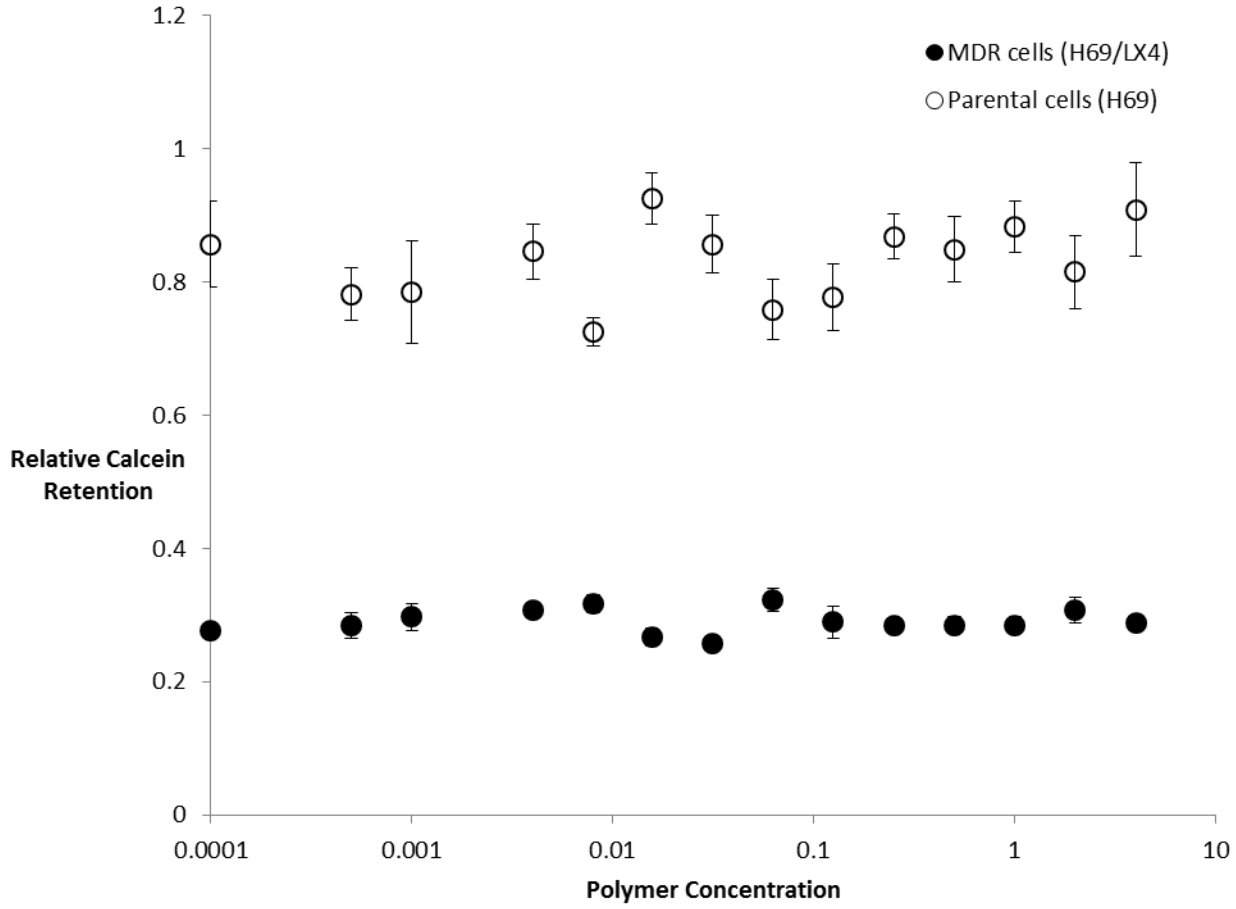

Figure 8.8: Relative calcein retention in P-gp overexpressing multidrug resistant cells (H69/LX4) and parental cells (H69) upon incubation with calcein AM (a P-gp substrate) and P(MAA-co-MMA-g-PEG) nanoscale hydrogel formulation. No significant increase in calcein retention was observed. Relative calcein retention calculated by normalizing calcein fluorescence for sample to untreated parental cells. n=3, data points represent mean +/-SD.

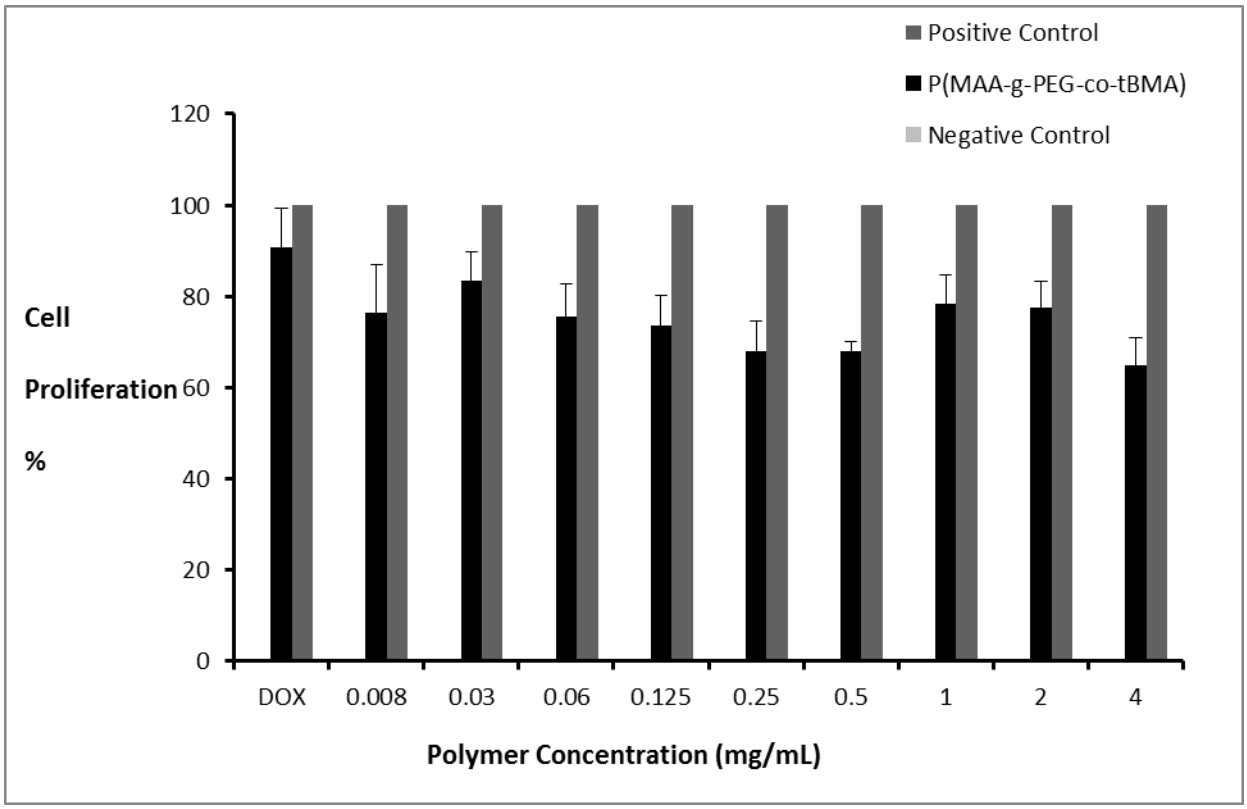

Figure 8.9: Cellular proliferation MTS assay with P(MAA-g-PEG-co-tBMA) and doxorubicin against doxorubicin-resistant H69/LX4 cells. n=4, data expressed as mean +/- SD.

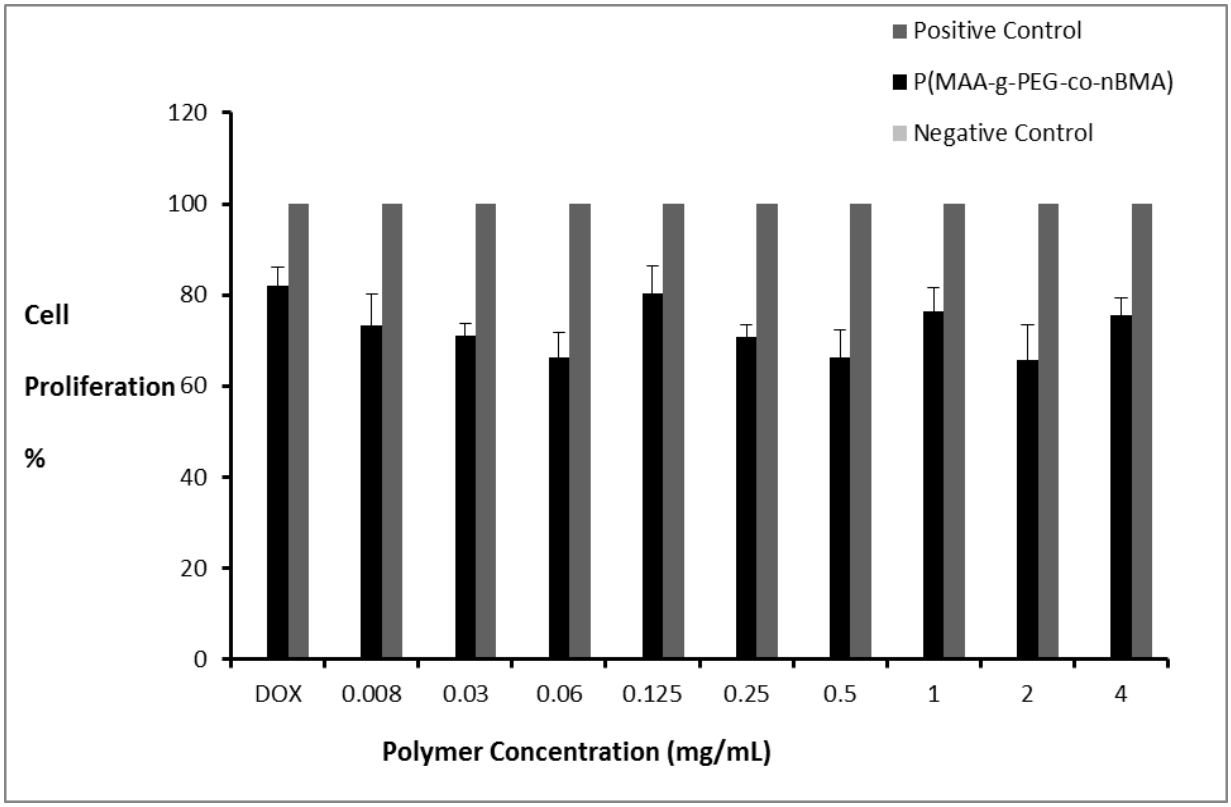

Figure 8.10: Cellular proliferation MTS assay with P(MAA-g-PEG-co-nBMA) and doxorubicin against doxorubicin-resistant H69/LX4 cells. n=4, data expressed as mean +/- SD.

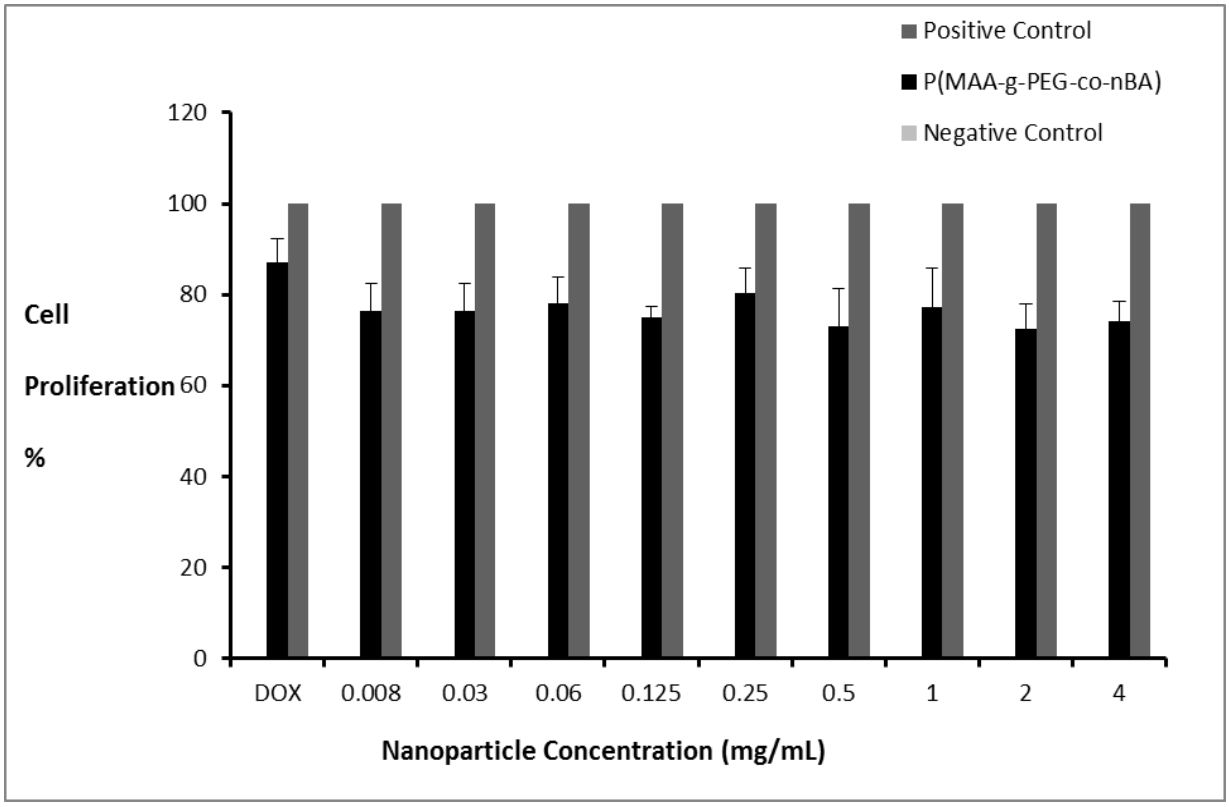

Figure 8.11: Cellular proliferation MTS assay with P(MAA-g-PEG-co-nBA) and doxorubicin against doxorubicin-resistant H69/LX4 cells. n=4, data expressed as mean +/- SD.

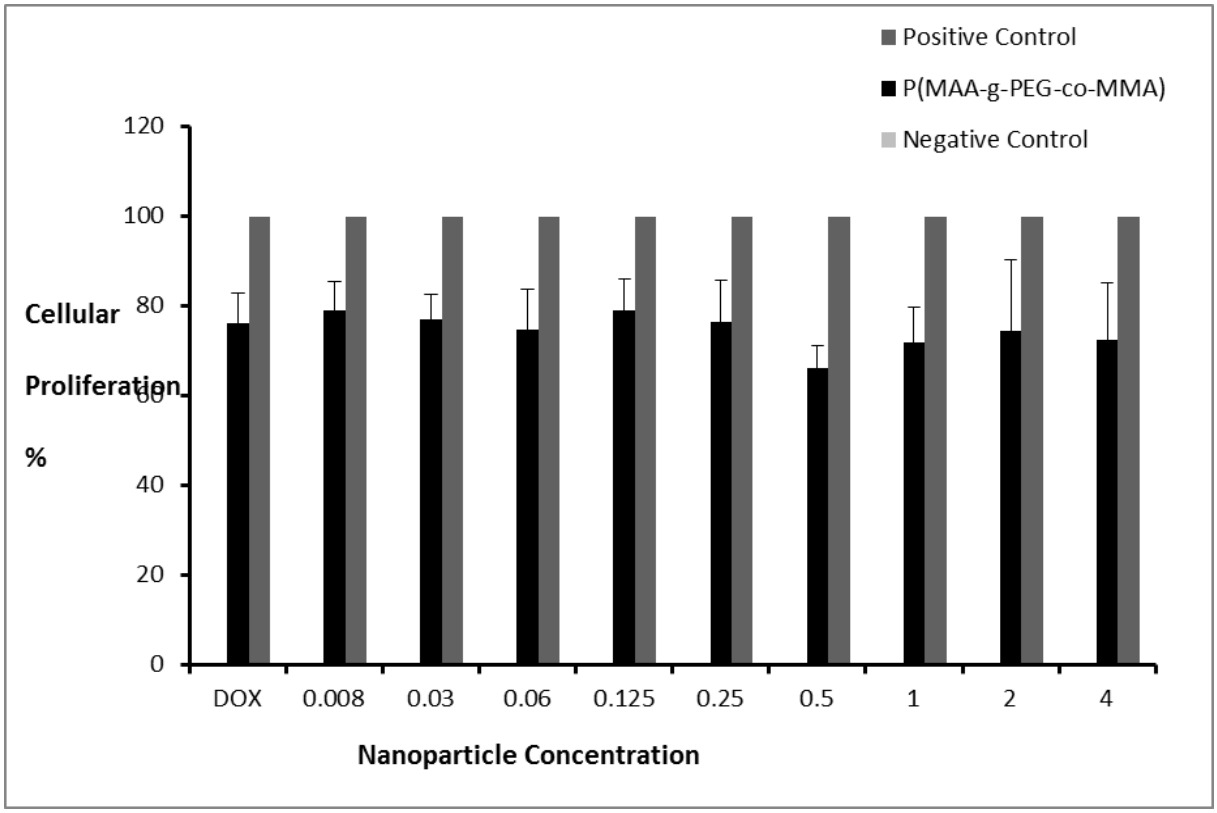

Figure 8.12: Cellular proliferation MTS assay with P(MAA-g-PEG-co-MMA) and doxorubicin against doxorubicin-resistant H69/LX4 cells. n=4, data expressed as mean +/- SD.

8.5 REFERENCES

[1] Szakacs G, Paterson JK, Ludwig JA, Booth-Genthe C, Gottesman MM. Targeting multidrug resistance in cancer. Nature reviews. Drug discovery 2006; 5:219-234.

[2] Shen Q, Lin Y, Handa T, Doi M, Sugie M, Wakayama K, Okada N, Fujita T, Yamamoto A. Modulation of intestinal P-glycoprotein function by polyethylene glycols and their derivatives by in vitro transport and in situ absorption studies. Int J Pharm 2006; 313:49-56.

[3] Koetting MC, Peppas NA. pH-Responsive poly(itaconic acid-co-N-vinylpyrrolidone) hydrogels with reduced ionic strength loading solutions offer improved oral delivery potential for high isoelectric point-exhibiting therapeutic proteins. International Journal of Pharmaceutics 2014; 471:83-91.

[4] Denker BM, Nigam SK. Molecular structure and assembly of the tight junction. The American journal of physiology 1998; 274:F1-9.

[5] Gumbiner B. Structure, biochemistry, and assembly of epithelial tight junctions. The American journal of physiology 1987; 253:C749-758.

[6] Ichikawa H, Peppas NA. Novel complexation hydrogels for oral peptide delivery: in vitro evaluation of their cytocompatibility and insulin-transport enhancing effects using Caco-2 cell monolayers. Journal of biomedical materials research. Part A 2003; 67:609-617.

[7] Foss AC, Peppas NA. Investigation of the cytotoxicity and insulin transport of acrylic-based copolymer protein delivery systems in contact with caco-2 cultures. European Journal of Pharmaceutics and Biopharmaceutics 2004; 57:447-455.

[8] Mistry P, Stewart AJ, Dangerfield W, Okiji S, Liddle C, Bootle D, Plumb JA, Templeton D, Charlton P. In vitro and in vivo reversal of P-glycoprotein-mediated multidrug resistance by a novel potent modulator, XR9576. Cancer research 2001; 61:749-758.

[9] Robson C, Wright KA, Twentyman PR, Lambert PA, Griffin RJ. Chemical synthesis and biological properties of novel fluorescent antifolates in Pgp- and MRP-overexpressing tumour cell lines. Biochemical pharmacology 1998; 56:807-816.

[10] Rautio J, Humphreys JE, Webster LO, Balakrishnan A, Keogh JP, Kunta JR, Serabjit-Singh CJ, Polli JW. In vitro p-glycoprotein inhibition assays for assessment of clinical drug interaction potential of new drug candidates: a recommendation for probe substrates. Drug metabolism and disposition: the biological fate of chemicals 2006; 34:786-792.

[11] Na K, Lee ES, Bae YH. Self-organized nanogels responding to tumor extracellular pH: pH-dependent drug release and in vitro cytotoxicity against MCF-7 cells. Bioconjugate chemistry 2007; 18:1568-1574.

[12] Kamiyama E, Nakai D, Mikkaichi T, Okudaira N, Okazaki O. Interaction of angiotensin II type 1 receptor blockers with P-gp substrates in Caco-2 cells and hMDR1-expressing membranes. Life sciences 2010; 86:52-58.

[13] Li PY, Lai PS, Hung WC, Syu WJ. Poly(L-lactide)-vitamin E TPGS nanoparticles enhanced the cytotoxicity of doxorubicin in drug-resistant MCF-7 breast cancer cells. Biomacromolecules 2010; 11:2576-2582.

Chapter 9: Conclusions and Future Recommendations

In this thesis, novel pH-responsive, nanoscale hydrogels capable of delivering hydrophobic therapeutics orally were developed. The nanoscale hydrogels described here were evaluated for design criteria desirable from an effective oral delivery system that can potentially improve the solubility and GI tract permeability of hydrophobic therapeutics, and makes an original and significant contribution to the existing literature on using nanotechnology for oral delivery of hydrophobic therapeutics. Lastly, the set of *in vitro* studies described in this chapter serve as a novel paradigm and a comprehensive set of tests that can be used together, as part of an integrative physicochemical and biological approach for *in vitro* testing or screening of nanoscale oral formulations.

Four nanoscale hydrogel formulations with unique hydrophobic monomers at the same nominal feed composition were synthesized using a robust, reproducible photoemulsion polymerization method. These novel nanoscale hydrogels were then fully characterized for their physicochemical and biological characteristics. Composition of the copolymer was varied by incorporating four different hydrophobic monomers, namely, tert-butyl methacrylate, n-butyl methacrylate, n-butyl acrylate, and methyl methacrylate. A combination of ^{1}H-NMR and FTIR verified the unique composition of each formulation. All four nanoparticle formulations underwent a transition in size in response to an increase in pH from 4 to 7.5 in physiologically relevant buffer with a critical swelling of around 4.9, as measured by dynamic light scattering measurements. Depending upon the hydrophobic monomer incorporated within the polymer network, dynamic light scattering revealed a compositional trend as the size of the formulations

ranged from about 100-500 nm at the relevant pH. Incorporation of methyl methacrylate in the copolymer resulted in the formation of nanoparticles with the largest size transition as demonstrated by dynamic light scattering measurements. Higher nanoparticle size can be attributed to the emulsion characteristics, while the swelling behavior is likely the result of interplay between reactivity ratios of component monomers as well as emulsion properties. Negative zeta potential as determined by electrophoretic light scattering measurements is attributable to the presence of deprotonated carboxylic acid groups on the polymer backbone, and is in good agreement with literature and the design rationale.

We analyzed cytocompatibility of the nanoparticles with an *in vitro* intestinal cell model. Despite considerable changes in swelling properties with a change in the hydrophobic monomer, all formulations displayed appreciable cytocompatibility in the presence of an *in vitro* intestinal cell model. The viability data from the LDH assay was supported by an MTS assay that confirmed healthy cellular proliferation in the presence of the nanoparticles. By displaying amenable physicochemical properties and agreeable cytocompatibility, the pH-responsive nanocarriers thus, exhibited the key characteristics expected from a potential oral drug delivery system. Both the size and swelling response of the nanoscale hydrogels could be controlled by varying the hydrophobic monomer component of the formulation. Incorporation of a different hydrophobic monomer did not appear to affect the . However, incorporation of did result in a fold increase in the swelling response. Relate molecular and nanoscale structure to function

We examined and compared the capacity of the nanoparticle formulations to load and release the hydrophobic therapeutic, doxorubicin. The physicochemical and

structural properties of the nanoparticles were ideal for the encapsulation of hydrophobic therapeutics. Doxorubicin, a broad spectrum hydrophobic chemotherapeutic was chosen as the model delivery payload to test the loading capacity of nanoscale hydrogels. Loading studies were performed at pH 7.4 when the hydrogel networks are fully swollen. The capacity of loading hydrophobic therapeutics into the nanoscale hydrogel formulation is expected to be influenced by the hydrophobic interactions between the drug and the hydrogel, and the ability of the hydrogel to swell and permit diffusion of the drug during the loading procedure. By changing the hydrophobic comonomer in the nanoparticle formulations, we were able to successfully load doxorubicin, with loading efficiencies ranging from 40-70%, with the P(MAA-g-PEG-co-MMA) formulation showing the highest loading efficiency. Further, we investigated the ability of these formulations to perform favorably under pH conditions similar to those encountered during transit through the GI tract. Specifically, we examined their ability to retain doxorubicin at an acidic pH expected to be found at the site of the stomach, and release the drug in response to alkaline conditions of the small intestine. P(MAA-g-PEG-co-tBMA) released most of the loaded drug, about 95.55% of the loaded drug after about 6 hours at pH 7 (total 8h). P(MAA-g-PEG-co-MMA) released about 74.71% of the drug in 6 hours at pH 7. The almost linear release response of P(MAA-g-PEG-co-tBMA) may suggest surface or close to surface loading of doxorubicin in these nanoscale hydrogels despite considerable surface washing. It could also mean that small size of these hydrogels imply minimal diffusion path length for doxorubicin to diffuse out assuming similar tortuosity in all nanoscale hydrogel formulation pores. Powder X-ray diffraction

analysis revealed the amorphous nature of the drug formulations suggesting an increase in the solubility of doxorubicin under conditions mimicking the site of drug release. Solute diffusion and permeation were explored indirectly through the use of membrane hydrogel networks with the same monomer feed composition as the nanoscale hydrogel formulations, although little or no correlation exists between the behavior of the nanoscale and macroscale networks. It is, however, worthwhile to note that partitioning of the solute in the membranes increased over time, while permeation is believed to proceed with a lag phase that can be attributed to size exclusion phenomena. Nanoscale hydrogel formulations exhibited the capacity to load and release the hydrophobic therapeutic doxorubicin, and varying the hydrophobic comonomer keeping the same nominal feed composition can play a role in modulating drug loading/release efficiencies.

Nanoscale hydrogel formulations were investigated for their capacity to modulate transport and permeability of hydrophobic therapeutic, doxorubicin *in vitro*. The P(MAA-g-PEG-co-MMA) formulation was observed to showed highest permeability improvement of doxorubicin across the intestinal epithelial cell model as indicated by transport studies. Similarly, the role of PEG in influencing doxorubicin permeability in vitro was investigated. PEGylated particles showed an increase in transport as opposed to non-PEGylated formulations. This may be attributed to an interaction of PEG with tight junctions that results in opening of the junctions or/and possibly interaction of PEG with P-gp efflux pumps. Further studies to understand the interaction of these nanoscale hydrogel formulations with P-glycoprotein were conducted using a calcein AM assay and cellular proliferation assay. In the calcein AM study, multidrug resistant H69/LX4 cells

exhibited greater calcein AM retention when incubated with P(MAA-co-tBMA-g-PEG) nanoscale hydrogels, demonstrating atleast 50% restoration of calcein-specific fluorescence. In addition, the cellular proliferation assay was used to evaluate the ability of the hydrogel formulations to sensitize doxorubicin-resistant H69/LX4 cells to the anti-proliferative ability of doxorubicin. However, none of the formulations showed a large decrease in cellular proliferation of H69/LX4 cells at the end of the four-hour study. Results from the calcein AM study, in combination with the transport studies support the hypothesis that the panel of nanoscale hydrogel formulations synthesized can influence *in vitro* permeability of doxorubicin, and can potentially exhibit favorable behavior anticipated from nanoscale hydrogels to be used for oral delivery of hydrophobic therapeutics. Lastly, the set of in vitro studies described in this chapter serve as a novel paradigm or set of tests that can be used together, as part of an integrative physicochemical and biological approach for *in vitro* testing or screening of nanoscale oral formulations. The observed interactions can be subsequently explored for more information regarding the interactions between PEGylated nanoparticles and P-glycoprotein receptors.

The work described in this thesis specifically focused on improving solubility and permeability of a small molecule hydrophobic therapeutic for the treatment of liver cancer. For oral administration based treatment of a cancer such as liver cancer, it is essential that the drug be released at the site of the small intestine, and that it is transported across the GI tract into the blood stream. To facilitate the oral delivery of the hydrophobic therapeutics, we looked at design parameters and material properties of

polymeric hydrogels that can be modulated. Despite the success in formulating a delivery system for a poorly water-soluble drug, some concerns remain - mainly, local cytotoxicity of doxorubicin to the intestinal lining, and lack of a mechanism to guide the small molecule chemotherapeutic to the site/organ of action. These two concerns are separate projects that need a dedicated undertaking of their own, and the synthetic chemistry involved in accommodating these modifications depend largely on the type of therapeutic being delivered, and the afflicted organ being targeted. In addition, owing to the small size of the nanoparticles, they can also be passively uptaken by intestinal cells such as M cells. Finally, we speculate on some of the modifications that could help bridge the mismatch between perceived shortcomings and desirable performance for reaping potential clinical benefits.

To mitigate these concerns, several areas of this work can be pursued as future work. For instance, conjugation of doxorubicin or any other model hydrophobic drug, to permeation enhancers such as bile acids, surfactants can further reinforce the transport of the drug across the intestinal cell wall. Depending on the cancer being treated using these nanoscale oral delivery formulations, the drug can be conjugated with a suitable targeting ligand to guide delivery to tumoral / sub-cellular site of action. Moreover, to further enhance the loading capacity of these hydrogels, several other hydrophobic monomers may be investigated to observe variations in size and swelling behavior. The use of microparticles can also increase loading ability and be a good safeguard against marginal passive uptake of carriers by intestinal M cells.

Additionally, other diverse approaches for cancer therapy can also be pursued. The field of nanomedicine for cancer therapy, especially, has seen a drastic increase in research focus and publications in the past 5 years or so. The following approaches are representative of some of the more recent work in the field for the treatment of primary, metastatic and multidrug resistant cancers. Peptide/aptamer ligand conjugation for improved targeting ability of nanoparticles can be used to overcome physiological barriers to oral drug delivery. In addition, switching the charge on the hydrogels by varying the hydrophilic monomer, these nanoscale hydrogels can be used for the intravenous delivery for treatment of metastatic cancer/ anti-angiogenic therapy using nanotechnology. Concomitant gene therapy or delivery of multiple drugs can be used to normalize the tumor microenvironment and improve treatment outcomes. Finally, subsequent evaluation of these nanoscale hydrogels for the oral delivery of hydrophobic therapeutics should involve *in vivo* studies in an appropriate animal disease model to obtain a truer assessment of hydrophobic drug bioavailability.

Appendices

APPENDIX A: RECENT ADVANCES IN DRUG ELUTING STENTS

International Journal of Pharmaceutics 441 (2013) 665–679

Contents lists available at SciVerse ScienceDirect

International Journal of Pharmaceutics

journal homepage: www.elsevier.com/locate/ijpharm

Review

Recent advances in drug eluting stents

Amey S. Puranik[a], Eileen R. Dawson[b], Nicholas A. Peppas[a,b,c,*]

[a] Department of Chemical Engineering, The University of Texas at Austin, Austin, TX 78712, USA
[b] Department of Biomedical Engineering, The University of Texas at Austin, Austin, TX 78712, USA
[c] College of Pharmacy, The University of Texas at Austin, Austin, TX 78712, USA

ARTICLE INFO

Article history:
Received 4 July 2012
Received in revised form 17 October 2012
Accepted 18 October 2012
Available online 29 October 2012

Keywords:
Drug eluting stent
Stent
Controlled release
Restenosis
Sirolimus

ABSTRACT

One of the most common medical interventions to reopen an occluded vessel is the implantation of a coronary stent. While this method of treatment is effective initially, restenosis, or the re-narrowing of the artery frequently occurs largely due to neointimal hyperplasia of smooth muscle cells. Drug eluting stents were developed in order to provide local, site-specific, controlled release of drugs that can inhibit neointima formation. By implementing a controlled release delivery system it may be possible to control the time release of the pharmacological factors and thus be able to bypass some of the critical events associated with stent hyperplasia and prevent the need for subsequent intervention. However, since the advent of first-generation drug eluting stents, long-term adverse effects have raised concerns regarding their safety. These limitations in safety and efficacy have triggered considerable research in developing biodegradable stents and more potent drug delivery systems. In this review, we shed light on the current state-of-the-art in drug eluting stents, problems related to them and highlight some of the ongoing research in this area.

Contents

1. Introduction 666
2. Bare metal stents 666
   2.1. Initial stent design 666
   2.2. Stent improvement 667
3. Biological mechanisms 667
   3.1. Atherosclerosis 667
   3.2. Restenosis 668
   3.3. In-stent restenosis 669
4. First-generation drug eluting stents 669
   4.1. Sirolimus eluting stents 669
      4.1.1. Cypher sirolimus eluting stent 670
      4.1.2. Limitations 671
   4.2. Paclitaxel eluting stents 671
      4.2.1. Taxus® paclitaxel eluting stents 671
      4.2.2. Limitations 671
5. Second-generation drug eluting stents 672
   5.1. Zotarolimus eluting stents 672
   5.2. Everolimus eluting stents 672
6. Future research 672
   6.1. Biocompatible stents 672
   6.2. Biodegradable stents 673
   6.3. Non-polymer stents 674
      6.3.1. Microfabricated reservoirs in drug eluting stents 674
      6.3.2. Nanofabricated reservoirs in drug eluting stents 675

* Corresponding author at: Department of Chemical Engineering, The University of Texas at Austin, Austin, TX 78712, USA. Tel.: +1 512 471 6644; fax: +1 512 471 8227.
E-mail address: peppas@che.utexas.edu (N.A. Peppas).

0378-5173/$ – see front matter © 2012 Elsevier B.V. All rights reserved.
http://dx.doi.org/10.1016/j.ijpharm.2012.10.029

6.4. Drug carrier eluting stents 675
6.5. Gene eluting stents 676
7. Conclusions 677
Acknowledgements 677
References 677

1. Introduction

Atherosclerosis, the hardening of arteries due to build-up of lipoproteins, is one of the leading causes of death in the United States (Massaro et al., 1979). One of the most common treatments for vessel occlusion due to atherosclerotic lesion formation is stent implantation. Stents are hollow cylinders that are implanted in a collapsed state and then guided into place and opened using the assistance of an angioplasty balloon (Burt and Hunter, 2006). While stenting has become a widely used procedure, it is not without complications.

Principally, many patients experience restenosis, or the re-narrowing of the arteries. This is due to the body's own wound healing response to the mechanical injury associated with stent implantation. This wound healing response can be broken down into two separate processes: neointimal hyperplasia and vessel remodeling. The placement of the stent initializes a variety of reactions including de-endothelialization, crushing of the plaque, and stretching of the artery (Costa and Simon, 2005). In addition to these initial reactions to the mechanical damage initiated by stent implantation, a series of cellular events are triggered, beginning with platelet and fibrin deposition at the injury site which leads to a cascade of events leading ultimately to leukocyte recruitment and increased cellular proliferation, specifically increased proliferation of vascular smooth muscle cells as well as monocytes and macrophages (Costa and Simon, 2005; Welt and Rogers, 2002).

Ultimately, it is this increase in cellular proliferation that leads to restenosis. It is for this reason that those looking to eliminate restenosis focus on doing so by attempting to halt increased cellular division. In stent restenosis rates are typically reported to occur in 15–20% of patients receiving a bare metal stent for the treatment of simply coronary lesions, but may occur in up to 30–60% of patients with complex lesions. Thus, despite widespread stent use restenosis continues to pose significant problems, and is still the greatest drawback associated with stent implantation over long periods of time.

Drug eluting stents are biomaterials capable of delivering drugs locally and in a controlled manner, to eradicate the increased cellular proliferation ensuing metallic stent implantation. Clinical and long-term outcomes of implanting drug eluting stents have justified their role in curbing undesirable neointimal hyperplasia and even identified thrombosis related risks (Luescher et al., 2007; Joner et al., 2006; Van der Hoeven et al., 2005; Kukreja et al., 2008; Nakazawa, 2011). This review lays emphasis on the current developments in drug eluting stents while providing mechanistic insight into the problems associated with them, and recognizing benchmarks for future research. A profound understanding of the underlying biological phenomena leading to in-stent restenosis and stent thrombosis is critical towards appreciating the key principles driving innovation in this field.

2. Bare metal stents

2.1. Initial stent design

Work began on therapies for occluded arteries in 1965, using a procedure called transluminal recanalization (Dotter and Judkins, 1964). This process involved gradually reopening the occluded artery by the addition of a series of wider sets of catheters, with each additional catheter forcing the region of occlusion open slightly more. Once the occlusion had been remedied they suggested that perhaps repeated dilation or the use of a splint of some sort could be used to hold the lumen open. The splint, they hypothesized, would act as a false lumen, forcing open the previously occluded region while the body was allowed to heal itself, suggesting that the re-intimalization would be just as likely to occur on their splint as it would on the patient's own tissue.

Balloon angioplasty, a procedure later pioneered by Andreas Gruntzing, is currently one of the most popular treatments for heart attacks and has been recommended as the standard of care in the Journal of the American Medical Association. Balloon angioplasty uses, with the help of a guide wire, a balloon-tipped catheter to force through stenotic lesions. Once in the desired location, the balloon is inflated, forcing open the occluded region.

Coronary angioplasty does not necessarily provide a permanent fix to an occluded artery. When first being used, coronary angioplasty was often accompanied with a number of risks, most notably abrupt coronary closure. Although effective initially, restenosis occurs in anywhere from 32 to 50% of patients (King, 1997; Serruys et al., 1994).

Four years after Dotter's landmark publication, he began experimenting with the usage of the prosthetic devices described previously to hold open the lumen of a canine artery. It was not until the 1980s, however, that extensive experimentation with stent designs really began.

By using catheters, and more specifically balloon tipped catheters, scientists were able to develop new procedures to non-surgically implant a stent device to effectively hold open arteries. Investigations began on using a wire comprised of a heat-sensitive memory alloy, nitinol. This material could be made into the desired shape and then, after cooling, the wire could be straightened in order to be introduced into the body via a catheter. Once inside the body, the temperature of the body will cause the nitinol to warm, causing the material to return to its original shape. Using a guide wire, it was possible successfully implant nitinol wire coils into the aortas of canines (Cragg et al., 1983). They found that the nitinol coils they used appeared to have a low tendency of thrombosis, which they directly attributed to the devices ability to refrain from altering vessel wall and lumen interactions. More promising then the nitinol's possible anti-thrombolytic response was the usage of a catheter and guide wire to implant a device that would effectively open within the artery, thus providing the possible application to be used as stent to maintain vessel patency.

A combinatorial method of a stent implantation along with angioplasty was soon developed. A stainless steel graft was designed that would have a high resistance to radial collapse as well as the ability to retain a desired diameter after balloon inflation. In this fashion, an expandable graft was implanted by mounting the device onto an angioplasty catheter. When the catheter is expanded within the occluded artery, the stent is opened and able to remain within the vessel after the balloon is deflated and removed. Initial studies completed with a canine provided somewhat mixed results. For shorter time periods, little to no stenosis was seen. At longer time points, however, there appeared to be a slight reduction in the diameter of the lumen and partial thrombosis was observed in two of the animals. Grafts removed and examined revealed the body's

surface modification of the implanted stent. The stent, over time, became coated with fibrin suggesting evidence of early stages of organization with what they seem to hope is re-endothelialization of the region. The stent used in this particular system had a large number of drawbacks. The material itself was fairly stiff, and thus, could only really be implemented in a linear region of the artery. Even in their limited studies they found this to be an issue, having the stent cause a kink within the artery leading to thrombosis. They also suggested that at the point of transition between the artery and the stent an increase in sheer stress could exist which may ultimately lead to neointimal proliferation (Palmaz et al., 1985). Similarly, a delivery system comprising a guide wire and an invaginated balloonlike structure that houses the stent has also been developed. Low hydraulic pressure effects stent release from the device and enables its placement within the artery. These stents were composed of a stainless steel alloy that allowed the device to be both radially self-expanding as well as longitudinally flexible (as compared to the Palmaz stent) (Rousseau et al., 1987).

Long-term studies on restenosis after placement of stents could not truly be completed until a significant amount of time had passed from the first ground-breaking procedures. Long-term results of patients who had received the Palmaz-Schatz stents provided some surprising results. Briefly this stent is comprised of a meshwork of steel and deployed by a coaxial balloon system. The incidence of restenosis in patients who received a single-stent implantation was found to be 30.2% while studies indicate that the incidence of restenosis after receiving angioplasty alone ranges from 28 to 41% (Ellis et al., 1992). Although stents were able to effectively prevent the immediate re-closing of the artery often seen after balloon angioplasty, they do not appear to be very effective in ultimately reducing restenosis development. Up until this point, most work primarily focused on designing a stent based on the mechanical properties it could afford, which although important, does not appear to help restenosis in long-term applications. It was therefore necessary to change focus on restenosis as a process, on the cellular level in order to prevent further occlusion of the arteries.

2.2. Stent improvement

Neointimal proliferation, as described briefly previously, is considered to be a component of normal vascular healing in response to injury. Because balloon angioplasty and stent implantation causes an actual physical injury in the artery, the body's inflammatory response is the natural result of any stent implantation. With a greater understanding of the cellular processes involved in restenosis, it is possible to alter stent therapy to account for this problem. Several approaches have been suggested to improve the procedure and reduce tissue proliferation, these include: improving implantation techniques, stent design, coating the stent with a pharmacological factor, and gene therapy. Because many different biological and cellular mechanisms contribute to restenosis, drugs that target only a single pathway may have limited value in ultimately relieving the problem. By coating the stent with a drug, it may be possible to deliver the drug directly to a site-specific area without having to be concerned about possible interactions of the drug in other areas of the body. With the addition of a time release mechanism, it may also be possible to deliver this pharmacological factor over a given, perhaps prolonged, time period. In this situation, it is also possible to release a number of pharmacological factors a single time, allowing for more comprehensive targeting of restenosis. The drug or drugs can be incorporated into the stent in a number of ways; it can be linked to the stent surface, embedded and released from within polymer materials, or surrounded by and released through a carrier (Fattori and Piva, 2003).

Before beginning any type of design of a drug delivery system, the efficacy of delivering a drug to the artery after stent implantation must be determined. If, for example, delivery is altered in any way, this can be factored into the design of the drug delivery system, i.e. perhaps a higher dosage of drug is necessary to achieve the same arterial delivery as seen prior to stent implantation. Because the artery may be damaged by implantation of stents, altered delivery of the drug may be of concern. Therefore, the effect of stent implantation on drug deposition within the artery was examined (Baumbach et al., 1999). Their results indicated that stent implantation prior to drug delivery did not cause any alterations in drug deposition of paclitaxel, a commonly used drug for the reduction of neointimal growth. Also of note, the amount of drug delivered to the system actively (via a high pressured injection) or passively (via lower pressured infusion) did result in different drug deposition within the artery. These two facts will be of the utmost importance when choosing design parameters for drug delivery via stents.

3. Biological mechanisms

While atherosclerosis involves a fibroproliferative response to excessive amounts of lipids within blood vessels, restenosis due to angioplasty or implantation of metallic stents is mainly due to the arterial vessel wall's response-to-injury mechanism. This section reviews the biological mechanisms that lead up to the undesirable luminal narrowing that necessitates the use of drug eluting stents and helps better understand the logic behind the use of commonly used anti-restenotic drugs.

3.1. Atherosclerosis

One of the most common causes of injury to the arterial epithelium is the formation of the oxidized low density lipoproteins (oxLDL). oxLDL dysfunctionalizes the endothelium by inducing genetic changes within the endothelial cell that result in increased permeability and augmented adhesiveness. Increased adhesion of the endothelial cells to monocytes in the blood flow facilitates monocyte-endothelial cell association and transport of the monocyte into the endothelium (Stary et al., 1994; Feig et al., 1982). Further, endotheilial cells produce several monocyte activators in response to oxLDL. Monocytes along with T-cells from the blood flow elicit an inflammatory response by encouraging adherence of monocytes and T-cells to the site of injury. Such a dysfunctional endothelium is also known to attract blood platelets. Monocytes localizing the "injured" endothelium from the blood flow eventually result in the formation of macrophages (Fig. 1A).

Macrophages formed subendothelially consume oxLDL, which itself acts as a chemoattractant to monocytes and release cytokines and growth signals to further their cause and call upon other inflammatory species. Macrophages ingest the oxLDL, becoming lipid-laden foam cells and become the growing atherosclerotic lesion, in addition to encumbering unfortunate oxidation of other LDL in the intima (Frostegard et al., 1990). This unfortunate oxidation amplifies the vicious cycle of regulatory and proliferative molecule production triggering further macrophage, endothelial cell and smooth muscle cell replication and migration. Smooth muscle cells activated as a result of these inappropriate signals migrate from their original site of residence in the media to the intima, exacerbating the inchoate fatty lesions. Similarly, other smooth muscles that do not themselves migrate, produce chemotactic/mitogenic signals effecting/causing migration of monocytes furthering the progression of the atherosclerotic plaque (Cushing et al., 1990). Smooth muscle cells covering lipid-filled macrophages create a connective tissue matrix constituting of collagen, elastic fibers and proteoglycans.

T-lymphocytes called into action mainly due to the interleukin-2 produced by activated macrophages, can also release IFN-γ,

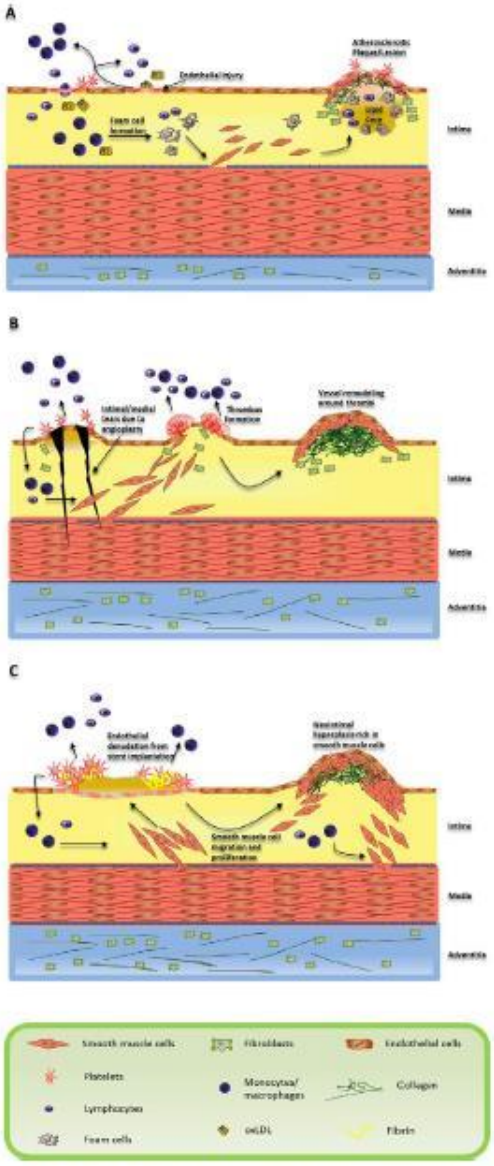

Fig. 1. Illustration of the mechanisms leading to (A) Atherosclerosis, (B) Restenosis due to angioplasty and (C) in-stent restenosis.
(A) Dysfunction of endothelial cells triggers a response-to-injury mechanism increasing monocyte and lymphocyte adherence to the endothelium. Interaction of these cells with the endothelium leads to recruitment of more monocytes/macrophages, lymphocytes, platelets, and smooth muscle cells. Lipid accumulation produces foam cells, which along with lymphocytes and smooth muscle cells drives plaque/lesion formation. (B) Angioplasty causes intimal and medial tears which attract platelets and result in thrombi formation. Smooth muscle cells and collagen then synthesized as a result of the response-to-injury mechanism lead to vessel remodeling. (C) Stent implantation causes endothelial denudation and crushing of the plaque triggering an inflammatory response. Eventually, smooth muscle cell migration and proliferation leads to formation of neointima.

GM-CSF, or TNF-α, thereby further accentuating the deleterious effects of an excess of regulatory factors in the exacerbating environment. Lipid-filled monocytes upon further encapsulation by connective tissue such as collagen, elastic fibers and proteoglycans culminate into the formation of fibrous plaque or an advanced lesion signifying the advent of atherosclerosis. Once the lesion has developed, platelets can adhere to it and can become a part of the atherosclerotic vicious circle by releasing the array of the aforementioned growth-regulatory molecules such as PDGF, TGFα, TGFβ, and IGF-I (Stary et al., 1994).

Chronologically speaking, in response to oxLDL production, the monocytes and T-lymphocytes are the first to be summoned inside the arterial intima. Interactions amongst these T-lymphocytes and the macrophages derived from the monocytes appearing at the outset of lesion formation, in addition to the interaction between these macrophages and the endothelium, may be responsible for both replication and growth signal production, as well as cytokine related gene expression. Endothelial cells activated by the macrophages through chemotactic signals, along with the macrophages themselves, call upon the smooth muscle cells from the media into the intima. Subsequent interaction between the species present in the milieu of the potentially atherosclerotic microenvironment result in advancement of lesion progression (Berliner and Heinecke, 1996).

The products released by macrophages, smooth muscle cells, platelets, and endothelial cells are responsible for recruitment of other macrophages, T-cells and smooth muscle cells from the media to the site of injury. The net mass of lipid accumulated macrophages (foam cells), T-cells and smooth muscle cells result in the formation of a rudimentary fatty streak within the endothelium of the artery. Accumulation of cellular species ensue the release of growth signals and cytokines by inflammatory cells around the fatty lesion. Foam cells devoured during the inflammatory attack may relocate to the blood stream by passing through the endothelium, thereby injuring it in transit. This new injury becomes thrombogenic by as like a seed to blood platelets. Blood platelets execute the job of releasing growth-regulatory molecules and cytokines to activate other platelets, macrophages, T-cells, smooth muscle cells and even endothelial cells. Thus, the cycle continues and fatty streaks advance to form fibrous plaques that hinder blood flow to critical organs. A protective response to a hyperlipidemic endothelium culminates into the formation of a fibrous lesion covering the interior lipid core and cellular debris (Ross, 1995).

3.2. Restenosis

The presence of atherosclerotic plaque compromises the integrity of the lumen of coronary arteries, thereby hindering blood flow to the heart and lungs. Balloon angioplasty, the technique most commonly used to combat atherosclerosis involves inflating a balloon attached to the distal end of a catheter tube at the site of the plaque. Implications of mechanically dilating arteries included the possibility of over-distension of vessels lined with plaque in intimate contact with the endothelium. Consequently, the compressive force exerted by the balloon catheter led to reduction of plaque, axial dispersion and extrusion of the fibrous plaque, and more importantly vessel expansion.

Angioplasty procedures may undergo early failure primarily due to the elastic recoil of the arteries in response to forced dilation by the balloon catheter (Haude et al., 1993). On the other hand, late failure post-angioplasty is mainly because of thrombosis derived vessel remodeling by vascular smooth muscle cell migration and proliferation in the thrombi. Mechanical stress encountered by arterial walls during the angioplasty procedure can tear the intima and media and injure the endothelium (Fig. 1B). Over a period of

time, the endothelial injury becomes thrombogenic and attracts blood platelets to it (Castanedazuniga et al., 1980).

Moreover, the process of trying to expand the vessel wall, typically results in denudation of endothelial cells underlying the plaque being subjected to compressive and extrusive forces. Dislodgment of endothelial cells leads to extrication of subintimal species that effect platelet adherence and aggregation initiating the response-to-injury mechanism commonly held accountable for atherosclerotic vessel thickening. Prominently, tissue factor exposure following injury has been implicated for enticing platelets and activating them to commence a response-to-injury mechanism. Platelet aggregation is promoted by the IIb/IIIa membrane glycoprotein receptors present on platelets activated by endothelial denudation. A conformational change in the receptor makes it susceptible for fibrinogen binding, eventually resulting in the crosslinking of platelets, which in turn aids in the aggregation of platelets (Ross, 1993).

Not only does platelet aggregation release thrombogenic factors that cooperate and complement platelet adhesion and aggregation, but also releases mitogenic and chemotactic factors for vascular smooth muscle cell migration and activation such as PDGF, FGF, TGF-β, as is described for the response-to-injury mechanism atherosclerosis. These fibrin/erythrocyte rich thrombi accommodate migration of VSMCs from the media so that they can neovascularize around the injury and lead to stenosis of the lumen. In comparison with atherosclerotic plaque lesions, restenotic injuries, angioplasty or stent-related, contain more of collagen and extracellular matrix components produced by proliferating cells than cellular material itself. The proportion of fibrous/extracellular matrix material grows as the restenosis advances. As a result, anti-restenotic therapies aiming to contain cellular proliferation alone have not really been successful (Faxon et al., 1987).

The inflammatory response to restenotic injury is also predicated upon leukocyte recruitment to the wounded site and their migration through the accumulated platelet thrombus into the intima. Leukocytes attach to the platelets already adhering to the wound. P-selectin presented by activated platelets plays an important role in facilitating the initial attachment and subsequent strong association (Marx et al., 2011). After securing the leukocytes to P-selectin, transplatelet migration is then achieved by integrin class of adhesion molecules. Employment of neutrophils and monocytes by the inflammatory machinery intensifies the leukocyte recruitment through upregulation of cell adhesion molecule expression, integrin activation and synthesis of chemokines.

In addition to platelets attracting leukocytes and other inflammatory cells, other cellular entities present in the restenotic lesion such as smooth muscle cells, endothelial cells and macrophages release molecules that further partake in generating a more prolific inflammatory response. Monocyte chemoattracnt cytokines such as MCP-1 released by these cells ensure recruitment of monocytes, basophils and T cells. Similarly, interleukin-8 (IL-8), another chemokine secreted by somatic cells amplifies neutrophil recruitment (Cushing et al., 1990).

3.3. In-stent restenosis

The re-narrowing of arteries after placing stents is called in-stent restenosis and is dominated by neointimal growth, from smooth muscle cell proliferation, covering the stent surface. Metallic stents are effective in opposing the acute elastic recoil of the blood vessel and the subsequent negative remodeling in response to the stretching caused by the stents. Long-term institution of stents in contact with the arterial walls can incite a prolonged, severe inflammatory response, in addition to neointimal hyperplasia (Lowe et al., 2002).

Placement of conventional, bare metals stents immediately results in deendothelialization of the surface subjected to stent-based trauma, crushing of the plaque lining the vessel wall causing deep, local and prolonged injuries to the media and adventitia, along with stretching the arteries to serve the primary purpose of increasing luminal blood flow (Fig. 1C). Growth factors released because of arterial injuries in the media and/or adventitia drive vascular smooth muscle cells into the media. Vascular smooth muscle cells are stirred into the G1/S cell cycle phase, enhancing their replication and migration into the intima. Deendothelialization also triggers an inflammatory response that is bolstered by the cytokines released from active vascular smooth muscle cells and leukocytes drawn towards the injury in a manner similar to that observed as a consequence of atherosclerotic and angioplasty-based injuries.

A collaborated paracrinal response from leukocytes, platelets, and VSMCs further augments the proliferation of active VSMCs and migration of more VSMCs from the media, culminating in a sizeable amount of new intimal cell growth (neointimal hyperplasia) over a period of weeks (Ramcharitar et al., 2007). With the passage of time, as the stent surface becomes endothelialized, the cellular and inflammatory response wanes. However, there is still a significant quantity of extracellular matrix components such as collagen, proteoglycans been synthesized by VSMCs in the intima. These components primarily constitute the neointimal hyperplasia engulfing the stent surfaces and blocking blood flow (Marx et al., 2011).

Surface de-endothelialization attracts platelets and activates them to produce adhesion molecules such as P-selectin. P-selectin binds to the inflammatory system agents such as leukocytes that are patrolling the circulation system, via P-selectin glycoprotein receptors present on their cell surface. P-selectin bound leukocytes can roll along the injured surface and firmly latch on to it through integrins (e.g. Mac-1 attaches to endothelial counterligands such as intercellular adhesion molecule-1) or platelet/firbrinogen receptors such as GP I and GPIIb/IIIa.

Chemokines released from activated VSMCs are purported to enable absorption of the leukocytes into the arterial tissue. Growth factors are simultaneously released by already activated platelets, leukocytes, and VSMCs, encouraging further activation, migration from the media into the intima and replication of VSMCs. Once activated, the VSMCs proliferate to generate a neointima replete with extracellular components such as collagen and proteoglycans. Formation of collagen and other ECM entities presumably leads to vessel shrinkage and negative remodeling in restenotic injuries, while also assisting smooth muscle cell migration. However, the permanent fixture of robust, metallic stents against a shrinking vessel has been largely successful at thwarting such negative remodeling of the vessel (Marx et al., 2011).

Advances in understanding the biological mechanisms underlying in-stent restenosis have helped us arrive at suitable drugs that can inhibit restenosis. A summary of some commonly used drugs for preventing in-stent restenosis and their mechanism of action are presented in Table 1.

4. First-generation drug eluting stents

4.1. Sirolimus eluting stents

Sirolimus (Rapamycin), an immunosuppressive agent/drug with anti-migratory and anti-proliferative effects on vascular smooth muscle cells has been used to prevent rejection in organ transplantation and was the first drug to be used in the first-ever US FDA approved drug eluting Cypher stent in April 2003. Prior to being approved by the FDA, sirolimus-eluting stents went through a number of clinical trials that endorsed the anti-proliferative and

Table 1
Summary of mechanism of action and resulting outcome for anti-restenotic pharmaceutics currently used in drug eluting stents.

Sr. no.	Anti-restenotic drug	Binding target	Mode of action	Final result
1	Sirolimus	FK-506 Binding Protein 12	-Binds to cytosolic FKBP12	Smooth muscle cell cycle arrest in G1-S phase
2	Biolimus A9		-Prevents activation of mammalian target of rapamycin (mTOR)	
3	Zotarolimus			
4	Everolimus			Smooth muscle cell and T-lymphocyte cell cycle arrest in G1-S phase
5	Novolimus			
6	Tacrolimus		-Binds to cytosolic FKBP12	T-lymphocyte cell cycle arrest in G1-S phase
			-Prevents activation of calcineurin -Inhibition of T-lymphocyte signal transduction -Prevention of IL-2 transcription	
7	Pimecrolimus	Macrophilin-12	-Binds to macrophilin-12 -Prevents inhibition of calcineurin	
8	Paclitaxel	Microtubules	-Binds and stabilizes microtubules	-Smooth muscle cell replication arrested in G0–G1 phase and G2-M phase
			-Disassembly of microtubules for cell replication prevented	
9	Dexamethasone	Specific steroid-binding protein receptor	-Binds with cytoplasmic receptor to form steroid-receptor complex -Complex associates with DNA and directs production of apoptotic proteins -Prevention of IL-1 and IL-2 transcription	-Reduction in inflammatory response
10	Curcumin	Microtubules	-Binds to microtubules	-Smooth muscle cell replication arrested in G0–G1 phase -Inhibits platelet aggregation
			-intercalates between DNA and RNA prohibiting replication	

anti-restenotic ability of sirolimus. Before becoming popular as the commonly used agent in drug eluting stents, this antibiotic isolated from the bacterium *streptomyces hygroscopicus* was used primarily as an immunosuppressant in prophylaxis of organ transplant rejection (Vasquez, 2000). It has also been investigated as an anti-cancer agent owing to its anti-proliferative abilities (Muthukkumar et al., 1995).

4.1.1. Cypher sirolimus eluting stent

The CYPHER™ stents have been implanted in more than 3 million patients globally since their approval in 2003. The Cypher stents comprises of two layers of polymer coated on a balloon expanding BX Velocity™ stent which is made up of stainless steel 316L, that has been laser cut and electropolished. The conventional bare metal stent is then coated with Parylene C, known for its increased dielectric constant, used conventionally for improving moisture resistance and biocompatibility of biomedical devices. The Cypher stent utilizes poly(ethylene-co-vinyl acetate) (PEVA) and poly(n-butyl methacrylate) (PBMA) as the non-erodible polymer coating that carries the sirolimus. A coating of a blend of PEVA and PBMA copolymer, mixed with the sirolimus (in a ratio of 67% polymer to 33% drug) is created by first dissolving the copolymer in THF, followed by the addition of lipophilic sirolimus to the copolymer/THF mixture. The first layer of the drug-polymer mix is then spray-coated with PBMA in THF to form an enclosing topcoat which acts as a rate controlling membrane (Acharya and Park, 2006) (Fig. 2). This rate controlling membrane is necessary to prevent the initial drug burst which can be associated with a constant release membrane reservoir type system and also further elongate the release of the sirolimus. Clinical trials implementing the Cypher indicate that sirolimus is released slowly over four to six weeks with 80% released by the fourth week, and 100% released by the sixth week. Complete elimination of restenosis with these stents was a result of the reduction in hyperplasia, and thus, no additional treatment for these patients was needed (Fattori and Piva, 2003).

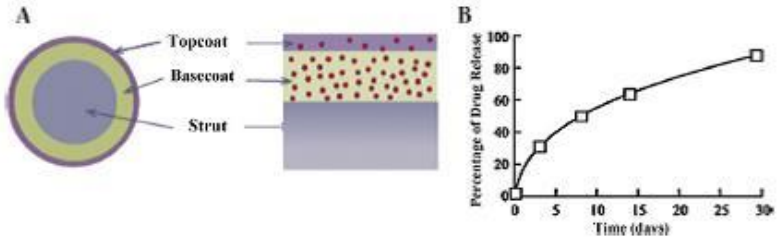

Fig. 2. Schematic of sirolimus eluting Cypher stent: (A) cross-sectional and side views (B) in vitro sirolimus release profile. Adapted from Acharya and Park (2006) by permission.

4.1.2. Limitations

Inspite of the remarkable decrease in restenosis rates offered by sirolimus eluting stents, their long-term success has been marked by the incidence of late stent thrombosis due to hypersensitivity and inflammatory reactions. Stent thrombosis usually occurs very late (>12 months) or late (>30 days) after the implantation of the drug eluting stent. However, there have been reports confirming the occurrence of acute/subacute stent thrombosis within 24 h or 30 days as well (McFadden et al., 2004; Joner et al., 2006). Stent-related coronary death has been attributed to the delayed arterial healing response patented by deficient re-endotheliazation and strut coverage of the stents that eventually leads to thrombosis and severe inflammatory reactions especially after discontinuance of dual antiplatelet therapy (Virmani et al., 2004). Pathological studies related to clinical trials and autopsies have shed light into the late-thrombosis associated with these stents. Local hypersensitivity to the sirolimus eluting stents characterized by eosinophils, lymphocytes, and giant cells throughout the stented segment was found to greatly contribute to the late-stent thrombosis. Stent malposition caused by positive arterial remodeling has also been observed in stents that evoke considerable inflammatory response.

Recent work has suggested that, while malapposition alone does not cause thrombogenicty, overall size of clots increased and appears to be related to blood recirculation patterns associated with the malappositioned stent (Kolandaivelu et al., 2011). When compared to bare metal stents malapposed to the same degree, drug eluting stents continued to reduce thrombogenicity.

These undesirable hypersensitivity responses associated with stent devices implanted for more than a year are believed to be caused by a combination of effects related to the non-erodible polymer coating, sirolimus, drug load and drug pharmacokinetics.

PEVA-PBMA, the polymeric carrier used in these stents, is guaranteed to elicit a chronic, local inflammatory reaction of CD45-positive lymphocytes and eosinophils, after a period of 4 months, resulting in the release of various growth factors that activate the smooth muscle cell proliferation cycle, thereby explaining the presence of late neointimal growth in most late-stent thrombosis related deaths (Finn et al., 2005; Wilson et al., 2009). The role of a non-biocompatible permanent polymeric coating in late thrombosis has given impetus to research in the area of biocompatible and biodegradable coatings that endow stents with the ability to control drug release in addition to reducing late stent thrombosis.

Apart from the stent and the polymeric coating, other innate factors escalating the risk of thrombosis include poor left ventricular function, diabetes mellitus, increasing age, acute coronary syndrome at presentation, renal failure, and presence of bifurcational lesions (Iakovou et al., 2005a; Park et al., 2006).

While the polymeric coating may be culpable in late stent thrombosis, sirolimus itself may be deemed responsible for acute/subacute stent thrombosis. The very phosphatidylinositol-3 kinase pathway that plays an important role in smooth muscle cell proliferation, is also known to downregulate tissue factor expression in endothelial cells and monocytes (Steffel et al., 2006). Inhibition of mTOR by the sirolimus-FKBP12 complex in endothelial cells, thus, leads to thrombin and tumor necrosis factor-α prompted increased tissue factor expression and activity (Guha and Mackman, 2002). Penetration of sirolimus in the endothelial cells of the arterial intima could possibly be the source of thrombosis within 30 days of stent placement, wherein almost 80% of sirolimus is eluted.

4.2. Paclitaxel eluting stents

The National Cancer Institute's plant extract screening program for antitumor activity led to the discovery of paclitaxel, which was approved by the FDA for its antineoplastic use for ovarian cancer treatment in 1992. It is currently used for the intravenous treatment of lung (FDA approved-1998), breast (FDA approved-1994) and ovarian cancer. This Pacific Yew tree bark extract has been substantiated to wield its anti-proliferative abilities in order to minimize in-stent restenosis (Wani et al., 1971; Schiff et al., 1979). A flurry of clinical trials soon after the FDA approval of sirolimus-eluting stents in 2003 fronted the way for the FDA approval of paclitaxel-eluting TAXUS stents in 2004.

4.2.1. Taxus® paclitaxel eluting stents

The Taxus® stent developed by Boston Scientific comprises of a triblock copolymer that includes a hydrophobic moiety in the form of isobutylene, which can better associate with the hydrophobic drug paclitaxel and enhance loading and release kinetics of the same. This polymer matrix, called the Translute™ polymer, uses a poly(styrene-b-isobutylene-b-styrene) terpolymer for superior paclitaxel delivery. The styrene layer on the top acts as a rate controlling layer allowing controlled release of paclitaxel over a prolonged period of time (Fig. 3) (Acharya and Park, 2006).

4.2.2. Limitations

Despite the promising antineoplastic talents of paclitaxel, incidence of in-stent thrombosis with long term usage of the Taxus stents has been a major cause of concern from the standpoint of their utility as anti-restenotic devices. Clinical trials, long term assessment of performance and pathological investigation of autopsies have contributed towards gaining further insight into the mechanisms of late stent thrombosis in paclitaxel eluting stents. The antiproliferative qualities of paclitaxel also end up hampering the chances of re-endothelialization of stents. Moreover, the hypersensitivity reactions from the non-erodible nature of the Taxus polymer coating of poly(styrene-isobutylene-styrene) caused inflammation contributed by eosinophils, lymphocytes, and giant cells (Nakazawa et al., 2011). In contrast to sirolimus eluting stents, however, the Taxus stents were found to be positively remodeled mainly as a consequence of stent malapposition

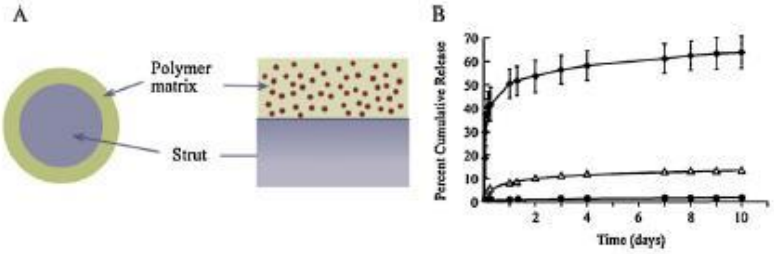

Fig. 3. Schematic of paclitaxel eluting Taxus stent: (A) cross-sectional and side views (B) in vitro paclitaxel release profile. Adapted from Acharya and Park (2006) by permission.

originating from the excessive accumulation of fibrin on the stent abluminal surface.

It is believed that the fibrin resulting from the use of paclitaxel, undergoes degradation to form fibrin fragment E, which is known to activate smooth muscle cell proliferation and migration. Along with the detrimental pro-apoptotic action, the release kinetics of paclitaxel has been found to be inferior to sirolimus. While both the drugs are found to infiltrate the arterial wall owing to their lipophilic nature, paclitaxel tends to accumulate preferentially in the adventitia rather than distributing itself among the arterial layers (Ishida and Tanaka, 1982; Naito et al., 2000). Since, smooth muscle cells are predominant in the arterial media; the prevailing presence of paclitaxel in the adventitia instead of the media/intima is not as effective at checking neointimal hyperplasia as sirolimus. The transmural diffusivity of paclitaxel is also not as high as that of sirolimus and is further diminished by the presence of red blood cell count/thrombus adhering to the site of stent-related vascular injury.

In sum, the combinatorial effects of paclitaxel loading, pharmacokinetics and polymer coating are considered responsible for the late-stent thrombosis and long term prevention of neointima formation in the case of Taxus stents. Use of vascular diagnostic techniques such as late lumen loss measurement via intravascular ultrasound along with quantitative angiography have illustrated the better efficacy of sirolimus eluting stents as compared to paclitaxel eluting stents. Iakovou and colleagues showed the presence of a diffuse restenosis pattern in 50% of Taxus stents in addition to 21% of severe restenotic lesions resulting in total vessel occlusion Iakovou et al., 2005b).

5. Second-generation drug eluting stents

5.1. Zotarolimus eluting stents

Better awareness and understanding of the inadequacies of sirolimus-eluting and paclitaxel-eluting stents set off the search for more efficacious and selective anti-proliferative agents that have lower systemic toxicity and do not delay endothelial healing. Endeavor® (Medtronic, Inc., Minneapolis, MN) was approved by the FDA in February 2008. The Endeavor® stent uses Abbott Vascular's zotarolimus drug and a cobalt alloy stent coated with a biocompatible phosphorylcholine coating on Medtronic Vascular's cobalt-chromium based Driver™ metallic stent platform (Sketch et al., 2005).

Zotarolimus is the first ever drug synthesized exclusively for treatment of in-stent restenosis. Zotarolimus is produced by the tetrazole ring substitution of the hydroxyl group at the C_{42} position. The presence of a tetrazole ring instead of a hydroxyl group makes zotarolimus extremely lipophilic. This hydrophobicity restricts the solubilization of zotarolimus in the luminal blood flow; leading to an immense decline in the systemic exposure risk and the negligible concentrations of the anti-proliferative agent also tends to be conducive to stent re-endothelialization. As expected, the lipophilic nature of zotarolimus helps the greatly required slow, dissolution-limited kinetics of release along with increased transport across cell membranes. Preliminary indications are that Zotarolimus is even more potent than its sirolimus counterpart, with only very slight concentrations necessary to achieve comparable results in terms of reducing the incidence of adverse vascular events associated with restenosis (Buellesfeld and Grube, 2004; Rogers, 2005).

Zotarolimus is a sirolimus-analog and an immunosuppressant that acts by binding itself to the protein FKBP-12 (Buellesfeld and Grube, 2004; Rogers, 2005) like sirolimus. The FKBP-12-bound zotarolimus blocks mTOR's phosphorylation ability thereby halting the progress of cell proliferation in the G1 phase. The phosphorylcholine coating on the stent mimics the cell membrane of red blood cells in the plasma, thereby avoiding hypersensitivity and inflammatory reactions. They are actually purported to utilize a blend of three polymers comprising a ten carbon hydrophobic polymer that controls drug release, a polyvinyl pyrrolidone for fast release and the biocompatible phosphorylcholine coating; to form the BioLinx polymer.

While the use of the sirolimus eluting Cypher stent was recently discontinued, the sirolimus-analog bearing Endeavor® stents are still preferred in cases where there is a substantial thrombosis risk or with complex lesions and for the overall purpose of better anti-restenotic action.

5.2. Everolimus eluting stents

Unlike the extremely lipophilic zotarolimus, everolimus is a relatively polar immunosuppressant macrolide with a 2-hydroxyethyl chain at the C_{40} position of sirolimus. The everolimus eluting stent Xience V™ (Abbott Laboratories) is another second generation drug eluting stent which got approved by the FDA in July 2008. In addition to a change in inhibitor and different polymeric platform, these stents also have some changes in their stent design that may add to their therapeutic utility and minimize late/very late endothelial response generator.

Everolimus like sirolimus and zotarolimus, also binds to FKBP-12 protein upon cellular uptake. The mTOR protein kinase inhibited by the FKBP-12-everolimus blocks expression of p70 S6 kinase pathway and halts ribosomal protein production and subsequently the smooth muscle cell proliferation cycle at the G1/S phase. Everolimus also suppresses T-cell mediated immune response, thus reducing the inflammatory/hypersensitivity response to the polymer used. Combination therapies of everolimus with tacrolimus hold great promise for the future of stent technology (Terada et al., 1992; Kuo et al., 1992). The more polar nature of everolimus helps lower the tissue concentration of anti-proliferative drugs.

The Xience V® stent (Abbott Laboratories) has a L-605 Co-Cr balloon expandable stent with better stent design characteristics such as high flexibility and deliverability, acceptable recoil and better compliance (Hagemeister et al., 2005; Tanimoto et al., 2007). The low strut thickness and the resulting lower surface area in contact with luminal blood flow allows the smaller exposed stent surface to be covered with endothelial cells more rapidly. Also, the lower surface area minimizes the risk of hypersensitivity reaction due to the polymer coating. The Xience V uses a hydrophilic poly(vinylidene fluoride-co-hexafluoropropylene) (PVDF-HFP) coating for better biocompatibility of the adluminal surface, while the poly(butyl methacrylate) (PBMA) allows for slow, sustained drug release (Carter et al., 2006).

The major limitations of sirolimus-eluting stents were mainly due to platelet aggregation resulting from a lack of endothelial surface coverage of the stent, mainly due to adequate blood plasma concentration of sirolimus which resulted in a thrombogenic response to the stents. The possibility of such an adverse eventuality is significantly minimized with everolimus eluting stents. Similarly, the biocompatible, hydrophilic fluoropolymer coating instead of the PEVA/PBMA or SIBS coating in the first generation drug eluting stents, drastically reduce the hypersensitivity reactions to the polymer. Further, everolimus eluted from these has also demonstrated macrophage clearance by autophagy in rabbit arteries (Verheye et al., 2007).

6. Future research

6.1. Biocompatible stents

The second-generation of drug eluting stents focused on increasing the efficacy of the anti-restenotic effect expected from

drug release by means of formulating more potent sirolimus analogues. Future research approaches in this field lay more emphasis on tending to the safety concerns posed by the polymeric stent coatings.

Instead of completely disqualifying the use of polymeric coatings on stents, another way to increase the overall hemocompatibility of the stent is by way of enriching the stent surface coating with inert or bioactive components. Non-thrombogenic coatings that may aid re-endothelialization are an encouraging alternative to conventional drug-eluting stents. Meanwhile, it is important to note that stent thrombus formation is triggered by adsorption of plasma proteins such as fibrinogen, fibronectin, tissue and complement factors, which in turn, is determined by stent surface hydrophobicity, morphology, roughness, and electrical charge (Sydow-Plum and Tabrizian, 2008).

Initial attempts towards the generation of biocompatible materials were relegated to the use of inert materials that avoided any sort of response from the body. However, further evaluation of the performance of such "inert" biomaterials shed light into changes that take place when a material is implanted into the arteries. This information, along with an enhanced understanding of blood-biomaterials interactions led us to a point where we could identify and synthesize materials that could proactively encourage endothelializaiton of the implant within the arteries.

Phosphorylcholine, a naturally occurring lipid group that constitutes the cell membrane has been celebrated for its biocompatibility in blood (Babapulle and Eisenberg, 2002). However, phosphorylcholine coated stents have not shown promising results despite the favorable characteristics of phosphorylcholine such as biocompatibility, non-allergenicity as well as lower inflammatory response. In fact, except stents coated with anti-proliferative drugs, there has been no significant clinical success in the area of favorable stent coatings. As previously mentioned, Phosphorylcholine is already a part of the coating used for the zotarolimus eluting Endeavor® stents.

Heparin, a negatively charged glycosaminoglycan and commonly used anticoagulant has been known to confer biomaterials with non-thrombogenic faculties. It therefore, seemed rational to coat stents with heparin to contend the thrombus formation commenced as a result of the injury incurred by stent implantation. Heparin can be attached to biomaterials by ionic bonding with cationic polymers, physically attached to surface by dip coating, chemically connected by covalent bonds or even eluted from polymer-heparin dispersions. Heparin hampers thrombin formation by forming a ternary complex with the cofactor antithrombin III which inhibits thrombin and thus, arrests progression of the coagulation cascade preventing thrombosis (Serruys et al., 1998). Despite the attractive utility of heparin in the long-term safety and efficacy of stents, there has been no major, perceptible benefit with heparin coated stents.

Heparin was first applied to Palmaz-Schatz stents coated with a three layered polymeric coating (comprising of a dextran sulfate layer between two polyamine layers) with heparin covalently linked to the polyamine backbone of the polymer. However, these stents were ineffective at preventing thrombus formation (Hardhammar et al., 1996). A stainless steel stent heparin consisting of hydrophobic binding agent was coated with with Duraflo II that allowed effective heparin binding to stent surface without altering the anti-coagulant activity of heparin (DeScheerder et al., 1997). The lack of inhibition of neoinitimal hyperplasia in vivo, despite presence of heparin coating was believed to be attributable to the antiplatelet therapy with ticlopidine. The long term human trials of heparin-coated stents performed by Serruys et al. in the BENESTENT II trial indicated the reduction in stent thrombosis; however, it was unclear if it was in fact the dual antiplatelet therapy with aspirin and ticlopidine that resulted in the non-thrombogenicity. In addition, coating with heparin alone did not demonstrate any antiproliferative effects.

Similarly, heparin coated Wiktor stent had heparin covalently bonded to a tantalum stent surface, in the international randomized multicenter trial MENTOR. Again, despite the presence of low thrombosis rates initially, the heparin was unable to inhibit smooth muscle cell proliferation and thus, restenosis (Vrolix et al., 2000). These clinical studies in fact, identified the importance of neointimal hyperplasia in restenosis and shifted the focus towards the more potent inhibitors of smooth muscle cell proliferation that presently dominate the drug eluting stent market.

Apart from heparin and phosphorylcholine, other strategies undertaken to improve the biocompatibility of drug eluting stents include coating the surface with endothelial cells/endothelial progenitor cells (Garg et al., 2010; Luo et al., 2011), cluster of differentiation 34 antibodies (CD-34) known to attract endothelial cells (Ako et al., 2007), poly(bis(trifluoroethoxy)phosphazene) (Satzl et al., 2007), and even corticosteroids (Babapulle and Eisenberg, 2002). Similarly, the Jostent coronary stent graft coated with a poly(tetrafluoroethylene) (PTFE) layer has shown promising results in clinical trials owing to the inherent ability of PTFE to prevent neointimal in-growth by shielding the potentially thrombogenic surface of the stent from blood components (Gercken et al., 2002).

6.2. Biodegradable stents

Polymers remaining behind after complete elution of drug pose a significant thrombogenic risk and are accountable for the subsequent hypersensitivity and inflammatory reactions (Luescher et al., 2007). Fortunately, developments in the synthesis of natural and synthetic materials that can be degraded biologically have brought the idea of degradable stents to fruition.

Biodegradable stents represent an area of marked interest, since they can accomplish diverse objectives such as being able to dilate arteries for a stipulated period of time, release anti-restenotic drugs and can be tailored to undergo biological degradation with kinetics that can be appropriately tuned by modifying the materials used. Biodegradable drug-eluting stents are defined to be stents that either have a completely biodegradable platform or are coated with a biodegradable polymer on a conventional bare metal stent. In either case, the goal is to avoid an inflammatory response to the polymer coating that culminates into thrombosis for a conventional drug eluting stent.

Synthetic biodegradable polymers that have been investigated for stent coating purposes include but are not limited to poly(L-lactic acid) (PLLA), poly(D,L-lactide) (PDLLA) and poly(lactic-co-glycolic acid) (PLGA). These polymers typically undergo ester bond degradation to form products such as lactic acid and glycolic acid, which can then be cleared from the system without triggering an undesirable inflammatory response.

The utility of blending biodegradable polymers to achieve the requisite mechanical strength and degradation rate has been investigated previously (Ye et al., 1998). The microporous PLLA/PCL blended stents afforded a distinctive advantage by offering to act as a biodegradable scaffold and providing the βGal reporter gene directly to rabbit carotid arteries. Although, concerns regarding complement-based inflammatory responses to PLLA as well as extremely short gene elution times persisted. One way to eliminate an inflammatory response to PLLA involved using PLLA just as the stent platform, while coating it with a PLGA layer that can further act as a sirolimus reservoir (Wang et al., 2006). In such a study, issues related to the rates of drug elution can be overcome by varying the composition of the layers, the drug loaded, and PLGA degradation rate. Other strategies include replacing PLLA with other natural, degradable biopolymers such as collagen, alginate, chitosan, or an appropriate combination of these so as to avoid

an inflammatory response completely (Chen et al., 2005; Peng et al., 2007; Chen et al., 2009).

Covering metallic stents with a biodegradable polymeric layer that can elute an anti-restenotic drug also serves to accomplish an analogous intention, while being able to provide the requisite radial force and be able to restrict recoil expected from a typical drug eluting stent. The polymer coating can be arranged to degrade after serving its anti-restenotic purpose, thereby precluding any adverse effects attributable to the polymers. Elution of an anti-restenotic drug addresses concerns associated with smooth muscle cell related neointimal growth that stems from the procedure itself and is believed to cease within 6 months (Bennett, 2003). Also, metallic stents implanted within the arteries subsequent to inhibition of any neointimal proliferation are accepted to have fewer inflammatory/stenosis related detrimental effects incidents (Colombo and Karvouni, 2000). Presence of a metallic stent that can offer strong radial support and permit use of several coating techniques for more diverse polymer coatings that may not be compatible with the use of a biodegradable polymer based stent platform (Raval et al., 2011).

The BioMatrix and BioMatrix II (Biosensors International, Newport Beach, California) are a couple of prominent drug eluting stents with a biodegradable poly(D,L-lactic acid) (PLA) coating releasing a macrolide, immunosuppressive sirolimus-analog Biolimus A9. The BioMatrix stents have been approved by the Conformité Européenne (CE). The PLA-biolimus A9 formulation (in 1:1 ratio) coated on the stent surfaces in contact with the vessel wall by an automatic micro-pipette coating process. Presence of drug on the abluminal surfaces of the stent in addition to the more lipophilic nature of biolimus A9 are presumed to increase arterial wall uptake of the anti-proliferative drug while reducing systemic side-effects, while the presence of a non-permanent PLA coating is used to minimize risk of stent thrombosis (Ostojic et al., 2008).

Other noteworthy biodegradable stents that have been approved by the CE include the Infinnium and Supralimus stents manufactured by the Sahajanand Medical Technologies Pvt. Ltd., India), which deliver paclitaxel and sirolimus, respectively. Both these stents comprise of PDLLA-co-PGA, PNVP, PLLA-co-PCL polymeric coatings that are degraded in vivo after having served the purpose of acting as a drug barrier to the eluting drug and have exhibited their safety and efficacy in the SIMPLE II clinical trials for the treatment of de novo coronary lesions. LUC-Chopin^{2TM} (Balton, Poland), another CE approved drug eluting stent, displayed moderate inflammatory reactions to paclitaxel release in addition to focal thrombus formation with fibrin deposits and incomplete re-endotheilaliz ation despite degradation of the PLGA coating on the stent. Some other CE approved drug eluting stents with a PLGA biodegradable coat include EucaTax, which has a permanent endothelium-compatible natural coating of glycocalyx (Camouflage^{TM}) top-coated with paclitaxel eluting biodegradable PLGA (Grabow et al., 2010).

It is during the six months after the procedure that the scaffolding effect of stents is important and it is also during this time period that restenosis therapy is crucial (Saito, 2005). As a result, after this period any polymer remaining behind can only exacerbate inflammatory responses. Most of the issues related to biodegradable stents can be attributed to adverse responses occurring during the first six months of implantation when the polymer has not been degraded completely or the oligomer type degradation products that can elicit undesirable responses the extent of which can vary from polymer to polymer (Erne et al., 2006).

6.3. Non-polymer stents

Taking cue from the fact that the polymers coated on the metallic stent stir up hypersensitivity and inflammatory reactions which promote stent thrombosis, researchers have worked on strategies to eliminate the use of polymers in stents. Polymers were primarily used as a diffusional barrier to release the anti-proliferative drug over a sufficiently long period of time. Since most anti-restenotic drugs target the smooth muscle cell proliferation at a particular stage of the cell cycle (For e.g. Sirolimus: G1/S; Paclitaxel: G2/M), it is important to ensure uninterrupted delivery of these drugs during the established SMC proliferation and migration time period of 2–3 weeks. The use of a permanent, durable polymer coating on stents allows for finer engineering and tailoring of the drug release kinetics by instituting a physical diffusional barrier that allows control by changing the thickness of polymer membrane, type of polymer used, and surface area. It is important to note that delivery can also be achieved by loading these drugs into reservoirs present in the metallic stent surface (Acharya and Park, 2006).

6.3.1. Microfabricated reservoirs in drug eluting stents

Loading anti-restenotic drugs into grooves and holes present on bare metal stent struts, which act as drug reservoirs for such non-polymer stents, can also help attain the above qualities of a good controlled release system. The Janus Carbostent^{TM} (Sorin Biomedica, Italy) is one of the first reservoir-based, non-polymer stent, which obtained a CE mark in 2004. In the Janus stent, the sirolimus-analog tacrolimus is loaded into a groove/cut, which acts a drug reservoir on the stent surface and about 50% of the loaded tacrolimus is released within 30 days of implantation. In order to avert thrombogenic reactions associated with the metallic stent itself, the stainless steel 316L stent had a passive turbostatic carbon film coating (Bartorelli et al., 2003).

The BioFreedom^{TM} (Biosensors International, Newport Beach, California) involve Biolimus A9 coating onto mechanically created microscale reservoirs on the textured abluminal stent surface of a BioFlex II 316L stainless steel S-stent. The presence of reservoirs allows drug to be eluted from the stent without concerns regarding polymer-associated adverse tissue responses, thereby reducing the duration of dual antiplatelet therapy as well. The abluminal reservoirs provide for rapid transfer of the lipophilic agent into the vessel wall tissues, where Biolimus A9 can exert its anti-proliferative therapy over the smooth muscle cell multiplication cycle. While the use of the more lipophilic Biolimus A9 itself reduces systemic exposure, the existence of micro-textures on the vessel wall side curb drug release in the luminal space. The presence of polymer in the luminal space, known to instigate hypersensitivity or use of a drug that inhibits proliferation of endothelial cells that increase the chances of stent thrombosis is avoided by use of such a stent. As a result, stent platforms with abluminal reservoirs may allow for the stent to be re-endothelialized and may even be successful in achieving timely healing of the arterial vessel (Tada et al., 2010).

Better control can also be obtained by coating the stents with micro-reservoirs with a series of polymers that degrade at rates that can be tailored according to the desired pharmacokinetics. The clinical use of Conor and CoStar stents that had a degradable PLGA membrane coat was studied for eluting paclitaxel over a sufficiently long time so as to prevent in-stent restenosis; thereby averting the need to take up high doses of paclitaxel that can be detrimental to the vascular system (Finkelstein et al., 2003).

The reservoirs in such stents are carved using laser machining techniques wherein a laser beam pulse capable of removing 0.1–0.5 μm of polymer/metal facilitates the creation of micro channels <100 μm thick in the stent material. Microelectrodischarge machining, a technique applying electrical pulses using an electrode, provides the merit of allowing high-throughput batch processing of manifold stents at the same time, while offering to craft smaller size microscale features with great accuracy and reliability (Murali and Yeo, 2004). Not only do these stents have the same radial strength as conventional bare metal stents, but they

can also be instilled with microsystems that detect the blood pressure and flow rate, thereby holding the potential to behave like biosensors (Takahata and Gianchandani, 2004).

Stents entrenched with microneedles penetrating dense, advanced atherosclerotic plaques in addition to delivering therapeutics to the internal elastic lamina of the arterial wall have also been studied (Reed et al., 1998). While there are much debate over how conventional photolithography and chemical etching techniques may be used to formulate microneedles on the cylindrical stent surfaces, there is no doubt that these pioneering stents will shepherd the field of drug eluting stents to newer directions.

6.3.2. Nanofabricated reservoirs in drug eluting stents

Extensive progress in nanofabrication techniques can allow us to further hone the surface characteristics of metallic stents in addition to utilize them for loading anti-restenotic drugs. Recent work integrating the nanoscale features on the stent surface produced by sol-gel processes has successfully demonstrated ability for enhanced cellular attachment as well as drug release via the nanoscale features. Such stents were fabricated by dipping bare metal stents or spraying upon them with hydroxyapatite and titania colloidal suspensions to fashion the surface with nanoscale textures (Liu et al., 2001, 2002).

Reservoir-based metal stents can either have a polymeric coating/membrane through which the drug diffuses or may have the drug directly loaded into the reservoirs within the metallic stent itself. A stent prominent in this class of drug eluting stents is the CoStar stent (Conor Medsystems, Inc, Menlo Park, Calif) where presence of these reservoirs allows more drug quantity to be loaded in the stent itself as compared to the amount of drug that needs to be dispersed in the polymer matrix coating of conventional drug eluting stents (Krucoff et al., 2008). Lack of the need to employ polymers that can efficiently solubilize hydrophobic antirestenotic agents such as sirolimus and paclitaxel as well as toxic adhesives and lubricants, permits more flexibility in choosing a biocompatible, biodegradable polymer that can act as an effective barrier to burst-release, while possessing the required drug permeation properties at the same time.

6.4. Drug carrier eluting stents

Evolution in methods of particle synthesis has allowed us to modulate sizes and properties of drug carriers so as to achieve effectual delivery of drugs. Nano- or micro-carriers help overcome some of the inherent limitations of stents eluting drug molecules by introducing desirable capabilities such as the ability to target diseased cells, responsiveness to external stimuli and superior tunability of drug pharmacokinetics. Furthermore, improvements in electrodeposition techniques have made possible the fabrication of stents that can be efficiently coated with nano-/micro-particles. These particles containing anti-restenotic drugs are then released from the stents over time and in turn, release drugs in a controlled manner.

Furthermore, knowledge of the inflammatory nature of permanent polymers used in "conventional" drug eluting stents, prompted researchers to explore the possibility of achieving the same therapeutic success with biodegradable polymers. Stents coated with nanoparticles/microparticles loaded with anti-restenotic can successfully combine a localized and targeted controlled release system, in addition to eliminating any deleterious effects that may arise from the use of a permanent polymeric coating on the stent. Moreover, simply releasing sirolimus from a biodegradable polymeric coating on the stent can lead to degradation of sirolimus into a less potent chemical entity (Banai et al., 2005). This necessitates the protection of sirolimus in its active, anti-proliferative form from the degradative agents in blood serum and can be achieved by using polymeric nanocarriers with a lipophilic core that preferentially associates with sirolimus.

Particles studied for their utility as nanovehicles for anti-restenotic drug delivery are mainly polymeric nanoparticles such as PLGA (Joo et al., 2009), copolymeric colloidal aggregates of phosphorylcholine and n-butyl methacrylate (Kim et al., 2009), and poly(ethylene oxide)-modified poly(epsilon caprolactone) (PEO-PCL) (Deshpande et al., 2008). PLGA nanoparticles are by far the most investigated, mainly, due to their quality of being biodegradable. PLGA nanoparticles prepared by an o/w emulsion polymerization technique have shown promising results with the release of a variety of anti-restenotic drugs such as paclitaxel (Deshpande et al., 2008) and curcumin (Nam et al., 2007). However, a comprehensive in vivo study highlighting the efficacy of such nanoparticles to load and release hydrophobic anti-restenotic drugs is yet to be seen. Other nanoparticle formulations incorporate a hydrophobic moiety such as n-butyl methacrylate that can preferentially associate with sirolimus and thus, holds great promise for this application (Kim et al., 2009). Similarly, PEO-PCL particles made by a solvent displacement technique have shown efficient paclitaxel uptake with smooth muscle cells and can be coated onto stents to further enhance their therapeutic effect (Deshpande et al., 2008).

These nanoparticles can be coated onto conventional bare metal stents through a cationic deposition method, while other novel methods of coating onto stents such as the ring-shaped surface tension method, wherein capillary forces coat suspensions of nanoparticles onto stents, have also been reported recently (Joo et al., 2009).

Random copolymers containing phosphorylcholine groups have been known to be capable of possessing the amphiphilic nature required to ferry lipophilic drugs such as sirolimus (Kim et al., 2009). It was proposed to make use of a biocompatible amphiphilic polymer poly(2-methacryloyloxyethyl phosphorylcholine (MPC)-co-n-butyl methacrylate (BMA) (PMB30W) to be able to enhance delivery of sirolimus eluted from PLCG films that can serve as biodegradable coatings on stents. Sirolimus was found to be retained in a stable, potent form in the interior of the "nanovehicle" formed by the colloidal aggregation of the self-assembling PMB30W chains leading to colloidal aggregation. The lipophilic interior of the PMB30W nanoparticles comprised of n-butyl methacrylate units augmented the solubilization of sirolimus while protecting it from the outer hydrophilic environment. The hydrophilic phosphorylcholine units of the copolymeric nanoparticles are involved in forming small sized (~20 nm) nanoparticles in an aqueous medium that can passively penetrate the vascular wall up to the internal elastic lamina. The sirolimus can then be delivered to the smooth muscle cells of the media through the fenestral openings in the internal elastic lamina. This carrier-mediated approach to deliver sirolimus from biodegradable films protects degradation of sirolimus while protecting the red blood cells from its adverse effects and preventing thrombus formation due to deposition on the arterial endothelium.

Lower concentration of cytotoxic drugs such as paclitaxel can be exercised by using drug loaded nanoparticles for targeted, localized and controlled release, thereby considerably lowering systemic toxicity. Liposomal nanoparticles based on phospholipids and cholesterol are known for their ability to effectively transport lipophilic drugs like sirolimus and rapamycin owing to the presence of both hydrophobic and hydrophilic moieties. Systemically administered 1:3 distearoyl phosphatidylglycerol, 1,2 distearoly-sn-gylcero-3-phosphcholine liposomal nanoparticles for the delivery of clodronate were developed to inhibit neointimal prolierfation in a rabbit carotid artery injured by balloon angioplasty (Danenberg et al., 2002). The circulation time/targeting ability of such liposomal nanocarriers can be enhanced by surface

modification or conjugation to antibodies/ligands. Morimoto and associates used pegylated 3,5-dipentadecyloxybenzamidine hydrochloride (TRX-20) liposomes to load the glucocorticoid prednisolone phosphate (Joner et al., 2008). The endocytosis-mediated cellular uptake of the cationic lipid nanoparticles was shown to allow for the actively targeted release of the drug in the cells.

The nanoparticle eluting stent technology developed is of great prospect and involves coating nanoparticles onto metallic stents via cationic electrodeposition coating technology. Biodegradable PLGA nanoparticles are typically used because of their ability to encapsulate water-soluble, next-generation drugs (DNAs, oligonucleotides, proteins such as antimonocyte chemoattractant protein-1), improve cell membrane penetration via endocytosis and increase intracytoplasmic release. In a recent study, these nanoparticles were prepared by an emulsion solvent diffusion method with surface modification with chitosan (Nakano et al., 2009). Furthermore, PLGA is known to not increase the thrombosis risk (in porcine coronary artery models), or work against endothelial regeneration, in addition to its biodegradability and biocompatibility, thereby indicating that PLGA nanoparticle eluting stents can be safely used in humans (Nakano et al., 2009).

Similarly, paclitaxel and C6 ceramide have been incorporated into polymeric nanoparticles of poly(ethylene oxide)-modified poly(epsilon caprolactone) and may be considered for the role of nanoparticles to be eluted from coated stents (Deshpande et al., 2008). PLGA nanoparticles loaded with the angiotensin-converting-enzyme inhibitor, lisinopril that have been used with local delivery by catheters and polylactide nanoparticles delivering the PDGF receptor inhibitor AG-1295 post balloon angioplasty injuries are potential candidates for nanoparticles that can be released from stents and implement controlled release of anti-restenotic drugs (Varshosaz and Soheili, 2008).

The use of another drug delivery system that combines localized drug delivery with controlled drug release was demonstrated by using curcumin loaded PLGA nanoparticles. Curcumin, a natural ingredient known for its anti-proliferative effects, was loaded into PLGA nanoparticles using a spontaneous emulsion method (Nam et al., 2007). The electrophoretic deposition method was found to be a highly reproducible, fast, flexible and reasonably economical coating method while the PLGA nanoparticles provided for an effective biodegradable barrier to anti-proliferative drug release.

Similarly, stainless steel 316L stent can be uniformly coated with a poly(2-hydroxy-ethyl-methacrylate) based hydrogel via an air spray technique and PLGA (50:50) microspheres incorporated with a model hydrophilic molecule such as Rhod-dex can be prepared by a double emulsion-solvent evaporation technique. These microsphere-integrated drug eluting stents can be used to achieve localized, site-specific delivery of hydrophilic antiproliferative drugs like gemcitabine and fludarabine (Indolfi et al., 2011). They allow for better control of release kinetics, unlike direct release of conventional lipophilic drugs which results in faster release kinetics and rapid uptake by the cell membranes.

6.5. Gene eluting stents

Technological advancements have given us the opportunity to understand the mechanisms leading to in-stent restenosis. This in addition to the enormous progress made in nucleic-acid based drug discovery, recombinant DNA technology and gene transfer have served to provide us strong if not superior, remedial alternatives to conventional therapeutics. These nucleic acid based therapeutics, usually a RNA/DNA molecule, if locally delivered can block a specific regulatory gene that plays a significant role in the pathophysiological restenosis mechanism (Santiago and Khachigian, 2001). Genes coding for the FK506 binding protein 12 that are upregulated in in-stent restenosis can be targeted using this mode of therapy and can thus help intrinsically mediate the cascade of reactions leading to in-stent restenosis (DeYoung and Dichek, 1998).

To test this hypothesis, a plasmid DNA-eluting gene was formulated and coated with a biodegradable PLGA polymer via micro-emulsification (Klugherz et al., 2000). The functionality of such a revolutionary stent was demonstrated by using a GFP-DNA whose uptake, transfection and subsequent expression could be observed by fluorescence microscopy. It was hypothesized that the DNA eluted from the PLGA coated stainless steel stent diffused through microscopic injuries produced by stent deployment. These superficial tears aided the encapsulated GFP-DNA to diffuse through the arterial cell walls into the smooth muscle cells of the media. The supplementary use of another gene that expresses an apoptosis-inducing cell surface protein that could combat the inflammatory response induced by PLGA was also hypothesized (Klugherz et al., 2000).

Similarly, the merits of gene-eluting stents were reinforced by locally delivering a plasmid DNA containing the coding sequence for the human vascular endothelial growth factor (phVEGF-2) (Walter et al., 2004). A 15 mm electropolished and phosphorylcholine coated version of the previously mentioned stent BiodivYsio (Abbott Vascular Devices, Galway, Ireland) was used for the local delivery of this plasmid DNA. The VEGF expressed as a result of gene transfection enhanced endothelial recovery by serving to activate endothelial cell proliferation pathways, unlike other anti-proliferative drugs that inhibit them.

The ability to deliver genes/plasmid DNA opened a window of opportunity in the realm of local nucleic acid therapeutic delivery for in-stent restenosis, which was further explored by Juan and colleagues. Delivery of siRNA in order to inhibit mRNAs from producing proteins that play a key role in the pathophysiological mechanisms of in-stent restenosis was studied. Delivery of siRNA was achieved by means of a pullulan hydrogel solution dip coated onto stainless steel stents. Apart from being a highly biodegradable polysaccharide, the pullulan can be chemically modified and cationized for increased cellular uptake in vivo. The stents were immersed in a 10 μm aqueous solution of siRNA for an hour to load the nucleic acid therapeutic (San Juan et al., 2009). The target for the siRNA delivery was the MMP-2 gene sequence that codes for the matrix metalloproteinase 2, a zymogen which hydrolyzes extracellular matrices in its active form, permitting migration of smooth muscle cells from the media into the intima (Hlawaty et al., 2007). Similarly, SS316L stents coated with hyaluronic acid have displayed effective gene transfection of plasmid DNA/polyethyleneimine (PEI) polyplexes fortifying claims related to stents being efficacious platforms for gene delivery.

In contrast to the use of a plasmid DNA for gene delivery, gene transfer therapy operates on the basis of the principle of gene transduction mediated by a viral vector such as the adenovirus. The delivery of an adenoviral vector inhibiting metalloproteinase-3 by use of PC-coated BiodivYsio stents has also been demonstrated (Abbott Vascular Devices, Galway, Ireland) (Johnson et al., 2005). Similarly, the efficacy of adenoviral and adeno-associated viral vectors for delivering a reporter lacZ gene to the smooth muscle cells was compared using the same PC-coated BiodivYsio stents (Abbott Vascular Devices, Galway, Ireland), which ensures good hemocompatibility without eliciting unfavorable tissue responses and can carry viral vectors (Sharif et al., 2006). It was noted that adenovirus mediated delivery evinced shorter transgene expression owing to protein response to adenoviral vectors while the adeno-associated viral vector showed better and durable transgene expression. While their previous research article used a lacZ reporter gene to study transgene expression, a more recent article by that group illustrates the use of non-viral vectors, specifically, liposomes instead of

adenoviruses to deliver a gene with therapeutic effects in order to tackle restenosis in stented arteries of New Zealand White rabbits (Sharif et al., 2012).

Both Co-Cr metal stents and PC-coated BiodivYsio stents (Abbott Vascular Devices, Galway, Ireland) were used to successfully accomplish "lipoplex-mediated" eNOS gene delivery to the stented vessel wall. The "lipoplex" was a complex between a plasmid DNA containing the eNOS gene and lipofectin liposomes and were coated onto the aforementioned stents using pipetting and air-drying technique. eNOS (endothelial Nitric Oxide synthase) expression increases the nitric oxide production in the arterial vasculature. Nitric oxide is purported to enhance re-endothelialization by preventing platelet aggregation and reducing neointimal hyperplasia by inhibiting vascular smooth muscle cell proliferation and migration. It was also noted that the liposomal particles themselves have a lower immunogenic response as compared to viral vectors and can carry larger payloads.

Along with gene delivery and gene transfer, recent work advocates the use of surface functionalized siRNA that can be coated onto stent surfaces and can help reduce inflammatory reactions to stent surface by effecting E-selectin receptor knockdown (Nolte et al., 2011). In this study, the negatively charged siRNA was complexed with the positively charged amino groups of PEI (polyethylenimine) to form a gelatinous coating. However, studies with animal models need to be done with these "gene silencing surfaces" to substantiate the safety of these coatings with respect to adverse reactions to PEI and efficacy of the surface for reducing neointimal hyperplasia.

7. Conclusions

Substantial clinical data from the use of drug eluting stents in patients since 2003 has given us a better understanding of the merits and demerits of first generation drug eluting stents. Instead of simply targeting smooth muscle cells to inhibit neointima formation, the need to restore the arterial endothelium at the site of injury has also gained paramount importance. It is evident that strategies which aim at re-endothelialization of the stent struts should be combined effectively with approaches preventing smooth muscle cell proliferation and migration. This can be achieved in a variety of ways considering the gamut of technological research and development that this field has witnessed. Numerous antiproliferative drugs available including novel drugs such as nucleic acid drugs which can elicit endothelial regrowth, biodegradable polymers that can avoid hypersensitivity have given us a holistic perspective of the progress in this field. Improved stent design and polymeric coatings that allow for targeted delivery of superior drugs to the arterial wall in combination with drugs that bring about re-endothelialization and can be released after all of the anti-proliferative drug has been released, can work as a potent solution to the problem of in-stent restenosis. It is therefore, necessary to synergize these research and development efforts to arrive at the optimum treatment option and develop the next-generation of drug eluting stents for treating in-stent restenosis.

Acknowledgements

This work was supported in part by a grant from the National Institutes of Health (EB 1R01-000346-18 and by a Fellowship (to ERD)) from the Cancer Prevention and Research Institute of Texas (CPRIT).

References

Acharya, G., Park, K., 2006. Mechanisms of controlled drug release from drug-eluting stents. Adv. Drug Deliv. Rev. 58, 387–401.

Ako, J., Bonneau, H.N., Honda, Y., Fitzgerald, P.J., 2007. Design criteria for the ideal drug-eluting stent. Am. J. Cardiol. 100, 3M–9M.

Babapulle, M.N., Eisenberg, M.J., 2002. Coated stents for the prevention of restenosis: Part I. Circulation 106, 2734–2740.

Banai, S., Chorny, M., Gertz, S.D., Fishbein, I., Gao, J.C., Perez, L., Lazarovichi, G., Gazit, A., Levitzki, A., Golomb, G., 2005. Locally delivered nanoencapsulated tyrphostin (AGL-2043) reduces neointima formation in balloon-injured rat carotid and stented porcine coronary arteries. Biomaterials 26, 451–461.

Bartorelli, A.L., Trabattoni, D., Fabbiocchi, F., Montorsi, P., de Martini, S., Calligaris, G., Teruzzi, G., Galli, S., Ravagnani, P., 2003. Synergy of passive coating and targeted drug delivery: the tacrolimus-eluting Janus CarboStent. J. Interv. Cardiol. 16, 499–505.

Baumbach, A., Herdeg, C., Kluge, M., Oberhoff, M., Lerch, M., Haase, K.K., Wolter, C., Schroder, S., Karsch, K.R., 1999. Local drug delivery: impact of pressure, substance characteristics, and stenting on drug transfer into the arterial wall. Catheter. Cardiovasc. Interv. 47, 102–106.

Bennett, M.R., 2003. In-stent stenosis: pathology and implications for the development of drug eluting stents. Heart 89, 218–224.

Berliner, J.A., Heinecke, J.W., 1996. The role of oxidized lipoproteins in atherogenesis. Free Radical Bio. Med. 20, 707–727.

Buellesfeld, L., Grube, E., 2004. ABT-578-eluting stents—the promising successor of sirolimus- and paclitaxel-eluting stent concepts? Herz 29, 167–170.

Burt, H.M., Hunter, W.L., 2006. Drug-eluting stents: an innovative multidisciplinary drug delivery platforms. Adv. Drug Deliv. Rev. 58, 345–346.

Carter, A.J., Brodeur, A., Collingwood, R., Ross, S., Gibson, L., Wang, C.A., Haller, S., Coleman, L., Virmani, R., 2006. Experimental efficacy of an everolimus eluting cobalt chromium stent. Catheter. Cardiovasc. Interv. 68, 97–103.

Castanedazuniga, W.R., Formanek, A., Tadavarthy, M., Vlodaver, Z., Edwards, J.E., Zollikofer, C., Amplatz, K., 1980. The mechanism of balloon angioplasty. Radiology 135, 565–571.

Chen, M.-C., Chang, Y., Liu, C.-T., Lai, W.-Y., Peng, S.-F., Hung, Y.-W., Tsai, H.-W., Sung, H.-W., 2009. The characteristics and in vivo suppression of neointimal formation with sirolimus-eluting polymeric stents. Biomaterials 30, 79–88.

Chen, M.C., Liang, H.F., Chiu, Y.L., Chang, Y., Wei, H.J., Sung, H.W., 2005. A novel drug-eluting stent spray-coated with multi-layers of collagen and sirolimus. J. Control. Release 108, 178–189.

Colombo, A., Karvouni, E., 2000. Biodegradable stents—fulfilling the mission and stepping away. Circulation 102, 371–373.

Costa, M.A., Simon, D.I., 2005. Molecular basis of restenosis and drug-eluting stents. Circulation 111, 2257–2273.

Cragg, A., Lund, G., Rysavy, J., Castaneda, F., Castanedazuniga, W., Amplatz, K., 1983. Non-surgical placement of arterial endoprosthesis–a new technique using nitinol wire. Radiology 147, 261–263.

Cushing, S.D., Berliner, J.A., Valente, A.J., Territo, M.C., Navab, M., Parhami, F., Gerrity, R., Schwartz, C.J., Fogelman, A.M., 1990. Minimally modified low-density-lipoprotein induces monocyte chemotactic protein-1 in human endothelial-cells and smooth muscle cells. Proc. Natl. Acad. Sci. USA 87, 5134–5138.

Danenberg, H.D., Fishbein, I., Gao, J.C., Monkkonen, J., Reich, R., Gati, I., Moerman, E., Golomb, G., 2002. Macrophage depletion by clodronate-containing liposomes reduces neointimal formation after balloon injury in rats and rabbits. Circulation 106, 599–605.

DeScheerder, I., Wang, K., Wilczek, K., Meuleman, D., VanAmsterdam, R., Vogel, G., Piessens, J., VandeWerf, F., 1997. Experimental study of thrombogenicity and foreign body reaction induced by heparin-coated coronary stents. Circulation 95, 1549–1553.

Deshpande, D., Devalapally, H., Amiji, M., 2008. Enhancement in anti-proliferative effects of paclitaxel in aortic smooth muscle cells upon co-administration with ceramide using biodegradable polymeric nanoparticles. Pharm. Res. 25, 1936–1947.

DeYoung, M.B., Dichek, D.A., 1998. Gene therapy for restenosis—are we ready? Circ. Res. 82, 306–313.

Dotter, C.T., Judkins, M.P., 1964. Transluminal treatment of arteriosclerotic obstruction Description of a new technic and a preliminary report of its application. Circulation 30, 654–670.

Ellis, S.G., Savage, M., Fischman, D., Baim, D.S., Leon, M., Goldberg, S., Hirshfeld, J.W., Cleman, M.W., Teirstein, P.S., Walker, C., Bailey, S., Buchbinder, M., Topol, E.J., Schatz, R.A., 1992. Restenosis after placement of Palmaz-Schatz stents in native coronary-arteries–initial results of a multicenter experience. Circulation 86, 1836–1844.

Erne, P., Schier, M., Resink, T.J., 2006. The road to bioabsorbable stents: reaching clinical reality? Cardiovasc. Interv. Radiol. 29, 11–16.

Fattori, R., Piva, T., 2003. Drug-eluting stents in vascular intervention. Lancet 361, 247–249.

Faxon, D.P., Sanborn, T.A., Haudenschild, C.C., 1987. Mechanism of angioplasty and its relation to restenosis. Am. J. Cardiol. 60, 8B–8B.

Feig, L.A., Peppas, N.A., Colton, C.K., Smith, K.A., Lees, R.S., 1982. The effect of angiotensin-II on in vivo albumin transport in normal rabbit aortic tissue. Atherosclerosis 44, 307–318.

Finkelstein, A., McClean, D., Kar, S., Takizawa, K., Varghese, K., Baek, N., Park, K., Fishbein, M.C., Makkar, R., Litvack, F., Eigler, N.L., 2003. Local drug delivery via a coronary stent with programmable release pharmacokinetics. Circulation 107, 777–784.

Finn, A.V., Kolodgie, F.D., Harnek, J., Guerrero, L.J., Acampado, E., Tefera, K., Skorija, K., Weber, D.K., Gold, H.K., Virmani, R., 2005. Differential response of

delayed healing and persistent inflammation at sites of overlapping sirolimus- or paclitaxel-eluting stents. Circulation 112, 270–278.
Frostegard, J., Nilsson, J., Haegerstrand, A., Hamsten, A., Wigzell, H., Gidlund, M., 1990. Oxidized low-density lipoprotein induces differentiation and adhesion of human monocytes and the monocytic cell-line U937. Proc. Natl. Acad. Sci. USA 87, 904–908.
Garg, S., Duckers, H.J., Serruys, P.W., 2010. Endothelial progenitor cell capture stents: will this technology find its niche in contemporary practice? Eur. Heart J. 31, 1032–1035.
Gercken, U., Lansky, A.J., Buellesfeld, L., Desai, K., Badereldin, M., Mueller, R., Selbach, G., Leon, M.B., Grube, E., 2002. Results of the Jostent coronary stent graft implantation in various clinical settings: procedural and follow-up results. Catheter. Cardiovasc. Interv. 56, 353–360.
Grabow, N., Martin, D.P., Schmitz, K.-P., Sternberg, K., 2010. Absorbable polymer stent technologies for vascular regeneration. J. Chem. Technol. Biotechnol. 85, 744–751.
Guha, M., Mackman, N., 2002. The phosphatidylinositol 3-kinase-Akt pathway limits lipopolysaccharide activation of signaling pathways and expression of inflammatory mediators in human monocytic cells. J. Biol. Chem. 277, 32124–32132.
Hagemeister, J., Baer, F.M., Schwinger, R.H.G., Hopp, H.W., 2005. Compliance of a cobalt chromium coronary stent alloy—the COVIS trial. Curr. Control. Trials Cardiovasc. Med. 6, 1–4.
Hardhammar, P.A., vanBeusekom, H.M.M., Emanuelsson, H.U., Hofma, S.H., Albertsson, P.A., Verdouw, P.D., Boersma, E., Serruys, P.W., vanderGiessen, W.J., 1996. Reduction in thrombotic events with heparin-coated Palmaz-Schatz stents in normal porcine coronary arteries. Circulation 93, 423–430.
Haude, M., Erbel, R., Issa, H., Meyer, J., 1993. Quantitative-analysis of elastic recoil after balloon angioplasty and after intracoronary implantation of balloon-expandable Palmaz-Schatz stents. J. Am. Coll. Cardiol. 21, 26–34.
Hlawaty, H., San Juan, A., Jacob, M.-P., Vranckx, R., Letourneur, D., Feldman, L.J., 2007. Inhibition of MMP-2 gene expression with small interfering RNA in rabbit vascular smooth muscle cells. Am. J. Physiol.-Heart Circ. Physiol. 293, H3593–H3601.
Iakovou, I., Schmidt, T., Bonizzoni, E., Ge, L., Sangiorgi, G.M., Stankovic, G., Airoldi, F., Chieffo, A., Montorfano, M., Carlino, M., Michev, I., Corvaja, N., Briguori, C., Gerckens, U., Grube, E., Colombo, A., 2005a. Incidence, predictors, and outcome of thrombosis after successful implantation of drug-eluting stents. JAMA 293, 2126–2130.
Iakovou, I., Schmidt, T., Ge, L., Sangiorgi, G.M., Stankovic, G., Airoldi, F., Chieffo, A., Montorfano, M., Carlino, M., Michev, I., Corvaja, N., Cosgrave, J., Gerckens, U., Grube, E., Colombo, A., 2005b. Angiographic patterns of restenosis after paclitaxel-eluting stent implantation. J. Am. Coll. Cardiol. 45, 805–796.
Indolfi, L., Causa, F., Giovino, C., Ungaro, F., Quaglia, F., Netti, P.A., 2011. Microsphere-integrated drug-eluting stents: PLGA microsphere integration in hydrogel coating for local and prolonged delivery of hydrophilic antirestenosis agents. J. Biomed. Mater. Res. Part A 97A, 201–211.
Ishida, T., Tanaka, K., 1982. Effects of fibrin and fibrinogen-degradation products on the growth of rabbit aortic smooth-muscle cells in culture. Atherosclerosis 44, 161–174.
Johnson, T.W., Wu, Y.X., Herdeg, C., Baumbach, A., Newby, A.C., Karsch, K.R., Oberhoff, M., 2005. Stent-based delivery of tissue inhibitor of metalloproteinase-3 adenovirus inhibits neointimal formation in porcine coronary arteries. Arterioscler. Thromb. Vasc. Biol. 25, 754–759.
Joner, M., Finn, A.V., Farb, A., Mont, E.K., Kolodgie, F.D., Ladich, E., Kutys, R., Skorija, K., Gold, H.K., Virmani, R., 2006. Pathology of drug-eluting stents in humans—delayed healing and late thrombotic risk. J. Am. Coll. Cardiol. 48, 193–202.
Joner, M., Morimoto, K., Kasukawa, H., Steigerwald, K., Merl, S., Nakazawa, G., John, M.C., Finn, A.V., Acampado, E., Kolodgie, F.D., Gold, H.K., Virmani, R., 2008. Site-specific targeting of nanoparticle prednisolone reduces in-stent restenosis in a rabbit model of established atheroma. Arterioscler. Thromb. Vasc. Biol. 28, 1960-U1113.
Joo, J.-R., Nam, H.Y., Nam, S.H., Baek, I., Park, J.-S., 2009. A novel deposition method of PLGA nanoparticles on coronary stents. Bull. Korean Chem. Soc. 30, 1085–1087.
Kim, H.I., Takai, M., Konno, T., Matsuno, R., Ishihara, K., 2009. Biodegradable polymer films for releasing nanovehicles containing sirolimus. Drug Deliv. 16, 183–188.
King, S.B., 1997. A US perspective on the shortcomings of PTCA. Heart 78, 6–6.
Klugherz, B.D., Jones, P.L., Cui, X.M., Chen, W.L., Meneveau, N.F., DeFelice, S., Connolly, J., Wilensky, R.L., Levy, R.J., 2000. Gene delivery from a DNA controlled-release stent in porcine coronary arteries. Nat. Biotechnol. 18, 1181–1184.
Kolandaivelu, K., Swaminathan, R., Gibson, W.J., Kolachalama, V.B., Nguyen-Ehrenreich, K., Giddings, V.L., Coleman, L., Wong, G.K., Edelman, E.R., 2011. Stent thrombogenicity early in high-risk interventional settings is driven by stent design and deployment and protected by polymer-drug coatings. Circulation 123, 1400–1409.
Krucoff, M.W., Kereiakes, D.J., Petersen, J.L., Mehran, R., Hasselblad, V., Lansky, A.J., Fitzgerald, P.J., Garg, J., Turco, M.A., Simonton III, C.A., Verheye, S., Dubois, C.L., Gammon, R., Batchelor, W.B., O'Shaughnessy, C.D., Hermiller Jr., J.B., Schofer, J., Buchbinder, M., Wijns, W., Grp, C.I.I., 2008. A novel bioresorbable polymer paclitaxel- eluting stent for the treatment of single and multivessel coronary disease. J. Am. Coll. Cardiol. 51, 1543–1552.
Kukreja, N., Onuma, Y., Daemen, J., Serruys, P.W., 2008. The future of drug-eluting stents. Pharmacol. Res. 57, 171–180.
Kuo, C.J., Chung, J.K., Fiorentino, D.F., Flanagan, W.M., Blenis, J., Crabtree, G.R., 1992. Rapamycin selectively inhibits interleukin-2 activation of p70 S6 kinase. Nature 358, 70–73.
Liu, D.M., Troczynski, T., Tseng, W.J., 2001. Water-based sol-gel synthesis of hydroxyapatite: process development. Biomaterials 22, 1721–1730.
Liu, D.M., Yang, Q.Z., Troczynski, T., 2002. Sol-gel hydroxyapatite coatings on stainless steel substrates. Biomaterials 23, 691–698.
Lowe, H.C., Oesterle, S.N., Khachigian, L.M., 2002. Coronary in-stent restenosis: current status and future strategies. J. Am. Coll. Cardiol. 39, 183–193.
Luescher, T.F., Steffel, J., Eberli, F.R., Joner, M., Nakazawa, G., Tanner, F.C., Virmani, R., 2007. Drug-eluting stent and coronary thrombosis—biological mechanisms and clinical implications. Circulation 115, 1051–1058.
Luo, C., Zheng, Y., Diao, Z., Qiu, J., Wang, G., 2011. Review: research progress and future prospects for promoting endothelialization on endovascular stents and preventing restenosis. J. Med. Biol. Eng. 31, 307–316.
Marx, S.O., Totary-Jain, H., Marks, A.R., 2011. Vascular smooth muscle cell proliferation in restenosis. Circ. Cardiovasc. Interv. 4, 104–111.
Massaro, T.A., Glatz, C.E., Peppas, N.A., Chisolm, G.M., Colton, C.K., 1979. Distribution of glycosaminoglycans in consecutive layers of the rabbit aorta. Artery 5, 1–13.
McFadden, E.P., Stabile, E., Regar, E., Cheneau, E., Ong, A.T.L., Kinnaird, T., Suddath, W.O., Weissman, N.J., Torguson, R., Kent, K.M., Pichard, A.D., Satler, L.F., Waksman, R., Serruys, P.W., 2004. Late thrombosis in drug-eluting coronary stents after discontinuation of antiplatelet therapy. Lancet 364, 1519–1521.
Murali, M., Yeo, S.H., 2004. Rapid biocompatible micro device fabrication by micro electro-discharge machining. Biomed. Microdevices 6, 41–45.
Muthukkumar, S., Ramesh, T.M., Bondada, S., 1995. Rapamycin, a potent immunosuppressive drug, causes programmed cell death in B lymphoma cells. Transplantation 60, 264–270.
Naito, M., Stirk, C.M., Smith, E.B., Thompson, W.D., 2000. Smooth muscle cell outgrowth stimulated by fibrin degradation products: the potential role of fibrin fragment E in restenosis and atherogenesis. Thromb. Res. 98, 165–174.
Nakano, K., Egashira, K., Masuda, S., Funakoshi, K., Zhao, G., Kimura, S., Matoba, T., Sueishi, K., Endo, Y., Kawashima, Y., Hara, K., Tsujimoto, H., Tominaga, R., Sunagawa, K., 2009. Formulation of nanoparticle-eluting stents by a cationic electrodeposition coating technology efficient nano-drug delivery via bioabsorbable polymeric nanoparticle-eluting stents in porcine coronary arteries. J. Am. Coll. Cardiol. Intv. 2, 277–283.
Nakazawa, G., 2011. Stent thrombosis of drug eluting stent: pathological perspective. J. Cardiol. 58, 84–91.
Nakazawa, G., Finn, A.V., Vorpahl, M., Ladich, E.R., Kolodgie, F.D., Virmani, R., 2011. Coronary responses and differential mechanisms of late stent thrombosis attributed to first-generation sirolimus- and paclitaxel-eluting stents. J. Am. Coll. Cardiol. 57, 390–398.
Nam, S.H., Nam, H.Y., Joo, J.R., Back, I.S., Park, J.-S., 2007. Curcumin-loaded PLGA nanoparticles coating onto metal stent by electrophoretic deposition techniques. Bull. Korean Chem. Soc. 28, 397–402.
Nolte, A., Walker, T., Schneider, M., Kray, O., Avci-Adali, M., Ziemer, G., Wendel, H.P., 2011. Small-interfering RNA-eluting surfaces as a novel concept for intravascular local gene silencing. Mol. Med. 17, 1213–1222.
Ostojic, M., Sagic, D., Jung, R., Zhang, Y.-L., Nedeljkovic, M., Mangovski, L., Stojkovic, S., Debeljacki, D., Colic, M., Beleslin, B., Milosavljevic, B., Orlic, D., Topic, D., Karanovic, N., Paunovic, D., Christians, U., Behalf, N.P.K.I., 2008. The pharmacokinetics of biolimus A9 after elution from the nobori stent in patients with coronary artery disease: the NOBORI PK study. Catheter. Cardiovasc. Interv. 72, 901–908.
Palmaz, J.C., Sibbitt, R.R., Reuter, S.R., Tio, F.O., Rice, W.J., 1985. Expandable intraluminal graft–a preliminary study–work in progress. Radiology 156, 73–77.
Park, D.-W., Park, S.-W., Park, K.-H., Lee, B.-K., Kim, Y.-H., Lee, C.W., Hong, M.-K., Kim, J.-J., Park, S.-J., 2006. Frequency of and risk factors for stent thrombosis after drug-eluting stent implantation during long-term follow-up. Am. J. Cardiol. 98, 352–356.
Peng, P., Voelcker, N.H., Kumar, S., Griesser, H.J., 2007. Nanoscale eluting coatings based on alginate/chitosan hydrogels. Biointerphases 2, 95–104.
Ramcharitar, S., Louise, G., Daemen, J., Serruys, P., 2007. MDrug-eluting stents, restenosis and revascularization. Herz 32, 287–295.
Raval, A., Parikh, J., Engineer, C., 2011. Mechanism and in vitro release kinetic study of sirolimus from a biodegradable polymeric matrix coated cardiovascular stent. Ind. Eng. Chem. Res. 50, 9539–9549.
Reed, M.L., Wu, C., Kneller, J., Watkins, S., Vorp, D.A., Nadeem, A., Weiss, L.E., Rebello, K., Mescher, M., Smith, A.J.C., Rosenblum, W., Feldman, M.D., 1998. Micromechanical devices for intravascular drug delivery. J. Pharm. Sci. 87, 1387–1394.
Rogers, C.D.K., 2005. Drug-eluting stents: clinical perspectives on drug and design differences. Rev. Cardiovasc. Med. 6, S3–S12.
Ross, R., 1993. The pathogenesis of atherosclerosis–a perspective for the 1990. Nature 362, 801–809.
Ross, R., 1995. Cell biology of atherosclerosis. Annu. Rev. Physiol. 57, 791–804.
Rousseau, H., Puel, J., Joffre, F., Sigwart, U., Duboucher, C., Imbert, C., Knight, C., Kropf, L., Wallsten, H., 1987. Self-expanding endovascular prosthesis—an experimental-study. Radiology 164, 709–714.
Saito, S., 2005. New horizon of bioabsorbable stent. Catheter. Cardiovasc. Interv. 66, 595–596.
San Juan, A., Bala, M., Hlawaty, H., Portes, P., Vranckx, R., Feldman, L.J., Letourneur, D., 2009. Development of a functionalized polymer for stent coating in the arterial delivery of small interfering RNA. Biomacromolecules 10, 3074–3080.
Santiago, F.S., Khachigian, L.M., 2001. Nucleic acid based strategies as potential therapeutic tools: mechanistic considerations and implications to restenosis. J. Mol. Med. (Berlin) 79, 695–706.
Satzl, S., Henn, C., Christoph, P., Kurz, P., Stampfl, U., Stampfl, S., Thomas, F., Radeleff, B., Berger, I., Grunze, M., Richter, G.M., 2007. The efficacy of nanoscale poly

bis(trifluoroethoxy)phosphazene (PTFEP) coatings in reducing thrombogenicity and late in-stent stenosis in a porcine coronary artery model. Investig. Radiol. 42, 303–311.
Schiff, P.B., Fant, J., Horwitz, S.B., 1979. Promotion of microtubule assembly in vitro by taxol. Nature 277, 665–667.
Serruys, P.W., Dejaegere, P., Kiemeneij, F., Macaya, C., Rutsch, W., Heyndrickx, G., Emanuelsson, H., Marco, J., Legrand, V., Materne, P., Belardi, J., Sigwart, U., Colombo, A., Goy, J.J., Vandenheuvel, P., Delcan, J., Morel, M.A., 1994. A comparison of balloon-expandable-stent implantation with balloon angioplasty in patients with coronary-artery disease. New Engl. J. Med. 331, 489–495.
Serruys, P.W., van Hout, B., Bonnier, H., Legrand, V., Garcia, E., Macaya, C., Sousa, E., van der Giessen, W., Colombo, A., Seabra-Gomes, R., Kiemeneij, F., Ruygrok, P., Ormiston, J., Emanuelsson, H., Fajadet, J., Haude, M., Klugmann, S., Morel, M.A., Benestent Study, G., 1998. Randomised comparison of implantation of heparin-coated stents with balloon angioplasty in selected patients with coronary artery disease (Benestent II). Lancet 352, 673–681.
Sharif, F., Hynes, S.O., McCullagh, K.J.A., Ganley, S., Greiser, U., McHugh, P., Crowley, J., Barry, F., O'Brien, T., 2012. Gene-eluting stents: non-viral, liposome-based gene delivery of eNOS to the blood vessel wall in vivo results in enhanced endothelialization but does not reduce restenosis in a hypercholesterolemic model. Gene Ther. 19, 321–328.
Sharif, F., Hynes, S.O., McMahon, J., Cooney, R., Conroy, S., Dockery, P., Duffy, G., Daly, K., Crowley, J., Bartlett, J.S., O'Brien, T., 2006. Gene-eluting stents: comparison of adenoviral and adeno-associated viral gene delivery to the blood vessel wall in vivo. Hum. Gene Ther. 17, 741–750.
Sketch, M.H., Ball, M., Rutherford, B., Popma, J.J., Russell, C., Kereiakes, D.J., Driver, I., 2005. Evaluation of the medtronic (Driver) cobalt-chromium alloy coronary stent system. Am. J. Cardiol. 95, 8–12.
Stary, H.C., Chandler, A.B., Glagov, S., Guyton, J.R., Insull, W., Rosenfeld, M.E., Schaffer, S.A., Schwartz, C.J., Wagner, W.D., Wissler, R.W., 1994. A definition of initial of fatty streak, and intermediate lesions of atherosclerosis--a report from the committee on vascular-lesions of the council on arteriosclerosis. Am.-Heart Assoc. Circ. 89, 2462–2478.
Steffel, J., Luscher, T.F., Tanner, F.C., 2006. Tissue factor in cardiovascular diseases--molecular mechanisms and clinical implications. Circulation 113, 722–731.
Sydow-Plum, G., Tabrizian, M., 2008. Review of stent coating strategies: clinical insights. Mater. Sci. Technol. 24, 1127–1143.
Tada, N., Virmani, R., Grant, G., Bartlett, L., Black, A., Clavijo, C., Christians, U., Betts, R., Savage, D., Su, S.-H., Shulze, J., Kar, S., 2010. Polymer-free biolimus A9-coated stent demonstrates more sustained intimal inhibition, improved healing, and reduced inflammation compared with a polymer-coated sirolimus-eluting cypher stent in a porcine model. Circ. Cardiovasc. Interv. 3, 174–183.
Takahata, K., Gianchandani, Y.B., 2004. A planar approach for manufacturing cardiac stents: design, fabrication, and mechanical evaluation. J. Microelectromechan. Syst. 13, 933–939.
Tanimoto, S., Serruys, P.W., Thuesen, L., Dudek, D., de Bruyne, B., Chevalier, B., Ormiston, J.A., 2007. Comparison of in vivo acute stent recoil between the bioabsorbable everolimus-eluting coronary stent and the everolimus-eluting cobalt chromium coronary stent: insights from the ABSORB and SPIRIT trials. Catheter. Cardiovasc. Interv. 70, 515–523.
Terada, N., Lucas, J.J., Szepesi, A., Franklin, R.A., Takase, K., Gelfand, E.W., 1992. Rapamycin inhibits the phosphorylation of p70 S6 kinase in IL-2 and mitogen-activated human T-cells. Biochem. Biophys. Res. Commun. 186, 1315–1321.
Van der Hoeven, B.L., Pires, N.M., Warda, H.M., Oemrawsingh, P.V., van Vlijmen, B.J., Quax, P.H., Schalij, M.J., van der Wall, E.E., Jukema, J.W., 2005. Drug-eluting stents: results, promises and problems. Int. J. Cardiol. 99, 9–17.
Varshosaz, J., Soheili, M., 2008. Production and in vitro characterization of lisinopril-loaded nanoparticles for the treatment of restenosis in stented coronary arteries. J. Microencapsul. 25, 478–486.
Vasquez, E.M., 2000. Sirolimus: a new agent for prevention of renal allograft rejection. Am. J. Health Syst. Pharm. 57, 437–448.
Verheye, S., Martinet, W., Kockx, M.M., Knaapen, M.W.M., Salu, K., Timmermans, J.-P., Ellis, J.T., Kilpatrick, D.L., De Meyer, G.R.Y., 2007. Selective clearance of macrophages in atherosclerotic plaques by autophagy. J. Am. Coll. Cardiol. 49, 706–715.
Virmani, R., Guagliumi, G., Farb, A., Musumeci, G., Grieco, N., Motta, T., Mihalcsik, L., Tespili, M., Valsecchi, O., Kolodgie, F.D., 2004. Localized hypersensitivity and late coronary thrombosis secondary to a sirolimus-eluting stent should we be cautious? Circulation 109, 701–705.
Vrolix, M.C.M., Legrand, V.M., Reiber, J.H.C., Grollier, G., Schalij, M.J., Brunel, P., Martinez-Elbal, L., Gomez-Recio, M., Bar, F., Bertrand, M.E., Colombo, A., Brachman, J., Investigators, M.T., 2000. Heparin-coated Wiktor stents in human coronary arteries (MENTOR trial). Am. J. Cardiol. 86, 385–389.
Walter, D.H., Cejna, M., Diaz-Sandoval, L., Willis, S., Kirkwood, L., Stratford, P.W., Tietz, A.B., Kirchmair, R., Silver, M., Curry, C., Wecker, A., Yoon, Y.S., Heidenreich, R., Hanley, A., Kearney, M., Tio, F.O., Kuenzler, P., Isner, J.M., Losordo, D.W., 2004. Local gene transfer of phVEGF-2 plasmid by gene-eluting stents--an alternative strategy for inhibition of restenosis. Circulation 110, 36–45.
Wang, X., Venkatraman, S.S., Boey, F.Y.C., Loo, J.S.C., Tan, L.P., 2006. Controlled release of sirolimus from a multilayered PLGA stent matrix. Biomaterials 27, 5588–5595.
Wani, M.C., Taylor, H.L., Wall, M.E., Coggon, P., McPhail, A.T., 1971. Plant antitumor agents 6. Isolation and structure of Taxol, a novel antileukemic and antitumor agent from taxus brevifolia. J. Am. Chem. Soc. 93, 2325.
Welt, F.G.P., Rogers, C., 2002. Inflammation and restenosis in the stent era. Arterioscler. Thromb. Vasc. Biol. 22, 1769–1776.
Wilson, G.J., Nakazawa, G., Schwartz, R.S., Huibregtse, B., Poff, B., Herbst, T.J., Baim, D.S., Virmani, R., 2009. Comparison of inflammatory response after implantation of sirolimus- and paclitaxel-eluting stents in porcine coronary arteries. Circulation 120, U141–U175.
Ye, Y.W., Landau, C., Willard, J.E., Rajasubramanian, G., Moskowitz, A., Aziz, S., Meidell, R.S., Eberhart, R.C., 1998. Bioresorbable microporous stents deliver recombinant adenovirus gene transfer vectors to the arterial wall. Ann. Biomed. Eng. 26, 398–408.

APPENDIX B: BACKGROUND – MULTIDRUG RESISTANT PROTEINS

Multidrug resistance proteins have always played an important in regulating the influx and efflux of drug entities through cells. Multidrug resistance proteins such as P-glycoprotein (P-gp) and multidrug resistance-associated proteins (MRP) are typically found in epithelial cells and endothelial cells of the gastrointestinal tract, liver, kidney, blood brain barrier, choroid plexus and other organs. Interestingly, these "difficult-to-deliver" organs are characterized by such multidrug resistance gate keepers, necessitating their thorough experimental investigation and formulating general strategies to overcome their impact, be profoundly studied. There is no doubt that the implications of evaluating their molecular action and methods to pre-empt their otherwise protective function, could be of tremendous prognostic import by improving bioavailability of orally administered drugs, as well as, the outcome of chemotherapy in metastatic diseases. In this review, we present an overview of recent biological findings about regarding MRPs and outline strategies to target these proteins for a therapeutic advantage for oral delivery and cancer therapy. A synergy that combines approaches to tackle these two conditions may appear to be materially taxing but can be therapeutically beneficial.

Analogies can be drawn between drug resistance in chemotherapy to antibiotic resistance in microogranisms and weed resistance in genetically-modified crops. A foray into investigating the causes of resistance to drugs on a cellular level led to an emerging consensus that implicated two chief mechanism of action. One way cells become resistant to cancer drugs is by eliciting alterations in their cell replication cycles to combat the

apoptosis-inducing nature of most cancer drugs. The second way drug resistance is achieved by chemotherapeutic-exposed cancer cells is by way of drug efflux – a tactic that greatly reduces intracellular drug concentration by recycling apoptotic drug molecules out of the cell, thereby, pre-empting cell death. Research conducted since the 1970s has convincingly demonstrated that cytotoxic cancer drugs typically used in multi regimen chemotherapy are evacuated from the cytosol using a family of energy-dependent transporters known as ATP-binding cassette (ABC) transporters. The most commonly purported culprit of this family of transporters is P-glycoprotein (Pgp, also known as ABCB1 or MDR1). While largely over-expressed in a wide range of cancer cell types, these are the same transporters naturally prevalent in epithelial and endothelial cells of various organs in the gastrointestinal tract, renal clearance system and hepatic system of the body to mediate movement of nutrients, drugs and toxic substances. The key difference between the two being that in case of resistant cancers, these are over-expressed in response to chemotherapy, whereas in epithelial and endothelial cells they are present naturally. Despite this subtle difference, pharmacological approaches have in the two distinct fields have intuitively borrowed heavily from each other to combat this unintentional resistance to accumulation/uptake of drugs by cells, and attenuated therapeutic outcomes. We begin by elucidating the multifarious components of the ABC transporter family, mentioning the current strategies to overcome resistance, and outlining future trends in this field that can be enabled by the growing body of literature in nanomedicine.

Multidrug resistance proteins, a class of proteins first discovered in the 1970s in tumor cells with a multidrug resistant phenotype (hence the name), play a pivotal role in maintaining the selectivity of the intestinal epithelial cell layer and ensuring extraction of needed nutrients, electrolytes, minerals and water. Intestinal enterocytes express this group of transporters/ plasma membrane transporters to modulate solute and fluid transport between the gut and the bloodstream, by serving as a final physiological barrier at the molecular level. Intriguingly, some members of this protein group are also found to play a pivotal role in regulating transmembrane transport of substrates across cell membranes of the epithelium in the liver, kidney, and the endothelial lining/ capillary cell surface of the blood-brain barrier. This large presence of MDR protein transporters at strategically important locations suggests their importance in body's natural detoxification mechanism, an argument subsequently underscored by strong evidence in its favor.

These "pumps" remove substrates from the cell cytosol in an energy-dependent manner, resulting in decreased intracellular concentrations of the substrate and foiling further transport of the substrate downstream. While this works when the aptly named efflux pumps facilitate removal of unwanted toxins, bacteria, and antigens, it in fact, reduces the concentration of cytotoxic drugs germane for improved chemotherapeutic efficacy. Since this family of transporters was implicated for conferring resistance to a wide range of chemotherapeutics and reduced bioavailability of a number of other therapeutics, substantial research attention has been dedicated to enhancing our understanding of how these work and can be overcome.

Concerns regarding this rather undesirable role played by MDR efflux pumps were amplified upon realization of the fact that these transmembrane receptors identify and selectively remove hydrophobic molecules, a structural characteristic of many a cancer drugs. The dawn of this realization has fomented considerable research in developing drugs, and/or combination approaches that involve evasion of efflux or inhibition of transporter function to deliver chemotherapeutics to their subcellular site of action. Broadly, these approaches have included, (a) development of entirely new chemotherapeutics/ appropriately modified renditions of existing chemotherapeutics that are not substrates to the MDR protein receptors, (b) concomitant use of drugs that inhibit the receptors, while allowing chemotherapeutics to pass through successfully, and (c) use material-based approaches to evade/inhibit drug efflux receptors.

Each of the aforementioned approaches have been accompanied by challenges owing to the broad substrate specificity of these receptors and the sheer number at the multiple physiological checkpoints a drug typically encounters. Compelling evidence supports the implication of these MDR proteins in the abysmal permeability and subsequent bioavailability of chemotherapeutics in bioequivalence studies. Orally delivered substrates undergo significant efflux, first at the site of the intestinal epithelium, which is followed by clearance from the liver and kidneys. Understanding the mechanism of action of these transporters can help further inform and elucidate strategies to overcome the unwelcome effect of MDR protein transporters. This section is of particular importance given the vast importance that is typically given to synthesis of nanocarriers to achieve greater degree of control over molecular architecture, while grossly neglecting

several other physicochemical and physiological obstacles that need to be surmounted to achieve favorable prognostic outcomes in anticancer therapy.

MOLECULAR BIOLOGY OF ABC TRANSPORTERS

ABC transporters function through a pair of two distinctive domains- two transmembrane domains (TMD) and two nucleotide binding domains (NBD), each serving a unique purpose. Structural evidence suggests that the two nucleotide-binding domains (NBD) sequester ATP to empower the efflux of the drugs by forming a common binding site, while the two transmembrane domains (TMD) trace a porous path utilizing transmembrane helices within the cell membrane to allow for efflux of drugs out of the cytosol. This structure is consistent with most members of the ABC transporter family, except the ABCG2 (or mitoxantrone-resistance protein MXR) or breast cancer resistance proteins (BCRP), which exhibit only a one half set that combines with another half set to achieve full functionality.

The evacuative phenotype of the ABC transporters and the wide range of substrates that they eliminate from the cytosol, are considered to be strong proof of their role in the general detoxification and protection of the body from foreign bodies and substances. This understanding is supported by compelling evidence uncovering the structure and function of these receptors, and their extensive presence on the surface of key pharmacological barriers that regulate substrate transport at a cellular level such as, the intestinal cells, hepatocytes, proximal tubules of the kidney, and the blood-brain barrier. Additional regulation at the cellular level by these transporters can thus further attenuate

the effective delivery of drug molecules despite optimal design in terms of physicochemical properties and chemical/metabolic transformations [5 of targeting multidrug]. This fact has ushered in a growing body of literature, not just aimed at developing high throughput screening of their tissue distribution levels, but also finding strategies that address delivery challenges associated with overcoming ABC transporters by assessing the predisposition of early stage, candidate drug molecules to act as substrates. Techniques developed by the pharmaceutical industry to screen drugs for their susceptibility to ABC transporter clearance are described in detail in subsequent sections.

The ABCB subfamily

While the manifestations of multidrug resistance have recently been shown to be driven by atleast 12 ABC transporters belonging to four subfamilies, the ABCB subfamily has been implicated with the highest and the broadest resistance to compounds. In particular, the Pgp transporter especially plays the most significant role in impeding transport in both intestinal epithelial cells, as well as multidrug resistant cells [10 from targeting multi]. While a direct correlation between Pgp expression and poor patient prognosis in response to chemotherapy in multidrug resistant cancers is still lacking, tissue culture studies and in vivo experiments have demonstrated that Pgp expression can significantly reduce favorable outcomes in chemotherapy. In fact, the first ever study showing multidrug resistance in cancer cells involved the use of Pgp inhibitors such as verapamil to stop the efflux of chemotherapeutics. Recent evidence points to certain molecules and structural families that may be more susceptible to efflux than others. Substrates for Pgp transporters are a wide range of molecules which include but are not limited to

anthracyclines, vinca alkaloids, epipodophyllotoxins and taxanes. Typically, Pgp has been found to transport unmodified neutral or positively charged hydrophobic compounds more prominently than others.

What makes tackling Pgp resistance intriguing, challenging and simultaneously slightly less daunting, is its wide substrate specificity. This promiscuity in substrate recognition, works against achievement of ideal, desirable outcomes in chemotherapy, but also open a window of opportunity to examine the use of a wide range of modulators/inhibitors of Pgp activity that can potentially reverse the detrimental efflux of chemotherapeutics by Pgp.

The ABCC subfamily

In addition to neutral or positively charged molecules, ABCC subfamily members are also denoted by the term multidrug resistance associated-proteins (MRPs) and are known to translocate organic anions and metabolic products generated by conjugation/chemical modification of toxins entering cells. Recent discoveries have indicated an active removal of compounds such as glutathione (GSH), glucuronate or sulfate conjugates of organic anions, and unconjugated bile acids. In line with the previously mentioned unfortunate effect of otherwise strategically important transporters, MRPs capacity to selectively remove therapeutic molecules that fit these molecular characteristics can lead to unwanted drug elimination. Combined with a strong enzymatic/metabolic system such as the cytochrome 450 (CYP450) that tags molecules for subsequent elimination, MRPs present another potent mechanism for drug elimination prior to their demonstration of therapeutic effect.

ABCC1, ABCC2, ABCC3, ABCC6, and ABCC10 comprise a portion of the ABCC subfamily, which display an additional group that contains an amino-terminal transmembrane domain and a cytoplasmic linker, which is also found in all other members of the ABCC subfamily like ABCC4, ABCC5, ABCC11, and ABCC12. ABCC1 or MRP1 is the most notorious subfamily member of the ABCC family with the evidenced reputation of conferring resistance to multiple hydrophobic compounds that are already substrates to Pgp, and further buttressing efflux of potent drug molecules already associated with multidrug resistance. Whether this association with substrates for Pgp transporters is a causal effect or a mere incidental result of having a similar 2 TMD and 2 NMD receptor structure, is not known with clarity at this point. While MRP1 is predominantly present in cancer cells displaying a MDR phenotype (based on observations in both clinical cancers and cancer cell lines), its homologue and close family member MRP2, is located in the apical membranes of polarized cells of the intestine and liver. This is an important observation implicating the role of MRP2 in the associated efflux of Pgp substrates that are orally administered, while MRP1 plays a synonymous role in augmenting the removal of Pgp substrates in MDR cancer cell lines. Another ABCC subfamily member of notable mention is MRP3 which is expressed in the kidney, liver and gut, and has shown propensity towards removal of several anticancer drugs and bile acid species. Additionally, gene transfection studies have revealed that MRP-6 transfected cells become resistant to anticancer agents like etoposide, teniposide, doxorubicin and daunorubicin, while MRP7 increases resistance to taxanes such as paclitaxel.

The ABCG subfamily

The ABCG subfamily is the final family member with any evidence implicating its role in the efflux of anticancer or orally ingested drug molecules either in vitro or in vivo. The most notable chemoresistance-causing member of this family is the ABCG2 transporter (also known as the mitoxantrone resistance protein (MXP) and breast cancer resistance protein (BCRP), which has shown clear demonstration of drug efflux in cancer cell lines. In cell lines engineered to overexpress these transporters, substrates were rapidly and completely removed, and included a broad range of molecules such as cytotoxic drugs, tyrosine kinase-based/anti-angiogenesis inhibitors, toxins and even carcinogens found in food.

SIGNIFICANCE OF ABC TRANSPORTERS IN ANTICANCER DRUG DELIVERY AND ORAL DRUG DELIVERY

Emergence of the role played by efflux transporters in both oral drug delivery and anticancer drug delivery has been a crucial advance, despite the fact that a stronger broadening of the database of substrates as well as implicated transporters that can contribute to undesirable drug efflux continues to grow. There are also ongoing studies looking to further develop critical experiments that can establish a correlation between reduced drug sensitivity in clinical studies and the direct impact of regulating transporter function. Thus far, evidence suggests that there are approximately 31 ABC transporters (out of 48) that could be impacting drug chemosensitivity and oral bioavalability. Other non-ABC transporters that have revealed their role in affecting oral absorption, are also being investigated for their role in inducing chemoresistivity. As previously mentioned,

only Pgp, ABCG2, and MRP1 transporters have been evaluated for their role in abating chemosensitivity in clinical trials so far. Among these, Pgp has the highest capacity and the widest substrate specificity for elimination of drugs, and as a consequence the effect of evading Pgp associated drug efflux has been most extensively studied, both in improving chemosensitivity as well as increasing drug bioavailability. Clinically speaking, trials that have co-delivered Pgp-transport inhibitors to patients alongside first- or second-line chemotherapy have demonstrated a definite benefit over simply chemotherapeutic delivery. Although it is important to note that the broad specificity of ABC transporters and lack of a comprehensive list of transporters make it difficult to conclusively confirm inhibition of Pgp-mediated efflux alone. Cross-resistance or inhibition of multiple transporters that may be structurally similar to Pgp is a possibility across the entire gamut of clinical tumor types/level of progression. Clinical evidence also points out to the fact that drug substrates triggering Pgp efflux in a set of cancer cells, end up selecting for proliferating cancer cells capable of surmounting chemosensitivity by non-Pgp-mediated transport. Given the heterogeneity of various solid tumors and the fact that resistance can be acquired by Pgp expressing cells to non-Pgp cells as well (by cross-resistance), has made establishment of a direct connection between high Pgp expression and poor clinical prognosis all the more difficult. On the contrary, the adverse impact of Pgp overexpression on patient survival has been more evident in haemotological malignancies like leukemia, due to the ease with which protein expression can be identified and quantified in a reproducible manner, as compared to solid tumors. Whether expression of other ABC transporters are just as widely relevant in

influencing patient survival post-MDR as Pgp remains to be clarified with confidence. There have been reports of ABCG2 being overexpressed in cancer stem cells that may play a role in tumor relapse subsequent to first-line chemotherapy, but once again, the degree to which ABCG2 transporters are utilized in inducing and exhibiting the final MDR phenotype second-line chemothterapy has to combat remains unclear.

OVERCOMING MULTIDRUG RESISTANCE WITH INHIBITORS

Studies associated with determining appropriate inhibitors for ABC transporters are crucial for both overcoming multidrug resistance to improve patient survival as well as, pinpointing new paradigms to link the exact effect of these transporters on clinical outcomes. Insights have been brought by using several inhibitors of Pgp, obtained by screening for molecules/structures that act as substrates to the Pgp receptor. In the past, such structure-based approaches have spawned generations of superior therapeutics for the treatment of neointimal hyperplasia in atherosclerosis, finding structural analogues to suboptimal chemotherapeutics, and finding mechanisms for receptor-mediated endocytosis of nanoparticles.

Identification of genes coding for multidrug resistance, and the synthesis of multidrug resistant cell lines is carried out by a process, which selects for surviving cells continually exposed to cytotoxic drugs (Targeting multidrug resistance in cancer). Using this approach, a number of cell lines are available for commercial testing and validation of multidrug resistance inhibition for drug formulations. The following table summarizes

some of the multidrug resistant cell lines that are available for in vitro research and the mechanism by which resistance is acquired.

In general, there are three established methods of acquiring drug resistance:

1. Decreased uptake of drugs that are substrates for uptake transporters
2. Anti-apoptotic mechanisms that alter cancer cell cycles and lead to increased repair of DNA damage
3. Increased energy-dependent efflux of hydrophobic drugs that would otherwise permeate easily through the plasma membrane

In this work, we investigate the inhibition of pathway number 3, owing to its significance in the role played for multidrug resistance towards doxorubicin and other hydrophobic drugs that we wish to encapsulate within our system. We specifically seek to explore the ability of our nanoformulation to inhibit P-glycoprotein receptors that are typically overexpressed in intestinal cells. P-gp is reported to have shown increased transport of unmodified neutral or positively charged hydrophobic compounds. Some of the common examples of chemotherapeutics transported by P-gp include but are not limited to doxorubicin, etc. We examine the inhibition of P-gp receptors using a multidrug resistant MDR1-Pgp assay kit (SOLVO Biotech), and a multidrug resistant calcein AM assay (Life Technologies). Furthermore, we observe the uptake of doxorubicin by multidrug resistant lung cancer cells using scanning confocal microscopy. We had a wide variety of cell lines to choose from as far as multidrug resistant cell lines go. Eventually, we settled on a metastatic, multidrug resistant lung cancer cell line because of the similarity between mucus covered lung epithelial cells and intestinal

epithelial cells, and because the cell line was characterized to have acquired multidrug resistance by an overexpression of P-gp receptors. Some other cell lines that can act as models for multidrug resistant cancers are presented in the tables below.

Cell Line	Disease	Cell type	Cell line type	References
ATCC® CCL-119™ [CCRF CEM]	Acute lymphoblastic leukemia	Human: T lymphoblast	Parental - Transfectionable	http://www.atcc.org/Products/All/CCL-119.aspx#generalinformation
CEM/C2 ATCC® CRL-2264™	Acute lymphoblastic leukemia	Human: T lymphoblast	Drug Resistant (atypical: toposiomerase mutation) - Transfectionable	**http://www.atcc.org/Products/All/CRL-2264.aspx**; http://www.ncbi.nlm.nih.gov/pubmed?cmd=Retrieve&list_uids=7579731&dopt=AbstractPlus
HL-60 (ATCC® CCL-240™	acute promyelocytic leukemia	Human: Promyeloblastic- myeloblastic	Parental - Transfectionable	http://www.atcc.org/Products/All/CCL-

		(morphology)		240.aspx#generali nformation
HL-60/MX2 (ATCC® CRL-2257™	acute promyelocytic leukemia	Human: lymphoblast	MDR (atypical-altered topoisomeras e catalytic activity)	http://www.atcc.or g/Products/All/CR L-2257.aspx#general information
MES-SA (ATCC® CRL-2274™)	Uterine sarcoma	Human: Epithelial – morphology fibroblast	Parental - Transfection able	
MES-SA/MX2 (ATCC® CRL-2274™)	Uterine sarcoma	Human: Fibroblast morphology (non epithelial origin)	MDR (over expression of P-gp)	**http://cancerres.a acrjournals.org/c ontent/43/10/4943 .long**; http://www.atcc.or g/Products/All/CR L- ;http://www.ncbi.n lm.nih.gov/pubme

				d?cmd=Retrieve&list_uids=4028002&dopt=AbstractPlus2274.aspx#history
EMT6/AR1	(Mouse) mammary tumor	Mouse: Epithelial-like morphology	MDR (classical-over expression of P-gp)	**http://www.sigmaaldrich.com/catalog/product/sigma/96042327?lang=en&region=US**
EMT6/P	(Mouse) Mammary tumor	Mouse: Epithelial-like morphology	Parental	
COR-L23/R	Large cell lung cancer	Human: Epithelial-like	MDR (typical but not P-gp/MDR1; instead MRP – Multi-drug	Overexpression of MRP. Also, reduced levels of glutathione and glutathione-S-transferase

			resistance-associated protein)	activity; http://www.sigmaaldrich.com/catalog/product/sigma/96042339?lang=en&region=US http://www.sigmaaldrich.com/catalog/papers/3011054
COR-L23	Large cell lung cancer	Human: Epithelial-like	Parental	http://www.sigmaaldrich.com/catalog/papers/3011054
MDR1 Knockout C2BBe1	Colon adenocarcinoma (Caco-2 subclone)	Human: Epithelial-like	MDR: MDR1 knockout/lacking in P-gp	
NCI-H69/LX4	Small cell lung cancer	Human: floating aggregates/ epithelial like	MDR (classical-over expression of P-gp)	**http://www.phe-culturecollections.org.uk/products/celllines/generalcell/detail.jsp?refId=**

				96042329&collection=ecacc_gc **http://www.sigmaaldrich.com/catalog/papers/1313690** **http://www.sigmaaldrich.com/catalog/papers/3011054** **http://www.sigmaaldrich.com/catalog/papers/20222053** http://europepmc.org/articles/PMC2001423?pdf=render
NCI-H69	Small cell lung cancer	Human: floating aggregates/ epithelial like	Parental	**http://www.phe-culturecollections.org.uk/products/celllines/generalcel**

				l/detail.jsp?refId=91091802&collection=ecacc_gc

It is well established that the multispecificity in transmembrane protein transporters drives variations in the pharmacokinetics of myriad drugs, even becoming the root cause of undesirable drug-drug interactions owing to multidrug resistance resulting from resistance that initially emerged against one drug [6,7 of in vitro methods in drug transporter interaction assessment]. Stringent guidelines for drug formulation-transporter interactions expected from drug manufacturers by regulatory authorities such as the FDA and EMA, have driven a foray into the development of in vitro tools that can help better predict and understand the structural basis for drug-transporter interactions. Moreover, the ubiquitous presence of these transporter proteins in several tissue linings that serve as pharmacological check-points for membrane transport indicates the extent of their importance in the development of effective early-stage product development screening tools. Given the changing landscape of the regulatory environment and the exorbitant costs associated with in vivo studies and clinical trials, it also makes unequivocal fiscal sense to prescreen drug formulations predictably prior to launching in vivo studies and clinical trials. Here we present some of the routinely conducted, prescribed drug-transporter studies that can aid in the forecasting of in vivo and clinical behavior arising from drug-transporter interactions. Broadly, examination of drug

formulations in the presence of entities that express properties associated with MDR function, (1) Live cell-based methods include, cancer cell lines overexpressing MDR transporters, or intestinal/hepatocytic cell monolayer models, (2) Indirect methods such as, ATPase assays (that ascertain if the drug competes with transporter proteins to utilize ATP), and membrane vesicles that overexpress transporter proteins [in vitro methods]. Each method has its merits and shortcomings, and as is the case with all in vitro methods, variability in actual clinical performance is to be presumed.

Live cell-based Methods to evaluate drug-efflux transporter interaction

These methods are best suited for hydrophobic compounds that can access the substrate binding sites of the efflux transporters located on the transmembrane domain ensconced within the lipid bilayer of the cells. As a result, free drug formulations of hydrophobic therapeutics that are able to passively come into contact with transmembrane domains of the protein can be evaluated for their interaction with transporters using this method. Hydrophilic drugs that may be unable to come into intimate contact with the substrate binding sites may be unable to elicit a robust efflux response from the transporters.

Indirect Methods to evaluate drug-efflux transporter interaction

Vesicular transport assays

Membrane vesicles that display the substrate binding site to the solvent can prove to a crucial tool in the investigation of substrate binding to the transporters. This method can definitely minimize any variations in the concentration of substrate at the binding site that may rise from poor passive diffusion of the substrate into the lipid bilayer/cytoplasmic leaflet.

APPENDIX C: BUILDING VASCULAR NETWORKS

TISSUE ENGINEERING

Building Vascular Networks

Hojae Bae,[1*] Amey S. Puranik,[2*] Robert Gauvin,[3] Faramarz Edalat,[4,5] Brenda Carrillo-Conde,[2] Nicholas A. Peppas,[2,6,7] Ali Khademhosseini[4,5,8†]

Only a few engineered tissues—skin, cartilage, bladder—have achieved clinical success, and biomaterials designed to replace more complex organs are still far from commercial availability. This gap exists in part because biomaterials lack a vascular network to transfer the oxygen and nutrients necessary for survival and integration after transplantation. Thus, generation of a functional vasculature is essential to the clinical success of engineered tissue constructs and remains a key challenge for regenerative medicine. In this Perspective, we discuss recent advances in vascularization of biomaterials through the use of biochemical modification, exogenous cells, or microengineering technology.

Tissue engineering research that combines cells and materials (biomaterials) is one of the most promising avenues to addressing the limited supply of organs for transplantation (*1*). Bioengineers are currently on the lookout for biomaterials that induce the formation of a vascular network. Vascularization strategies are crucial for the in vitro synthesis of complex tissues and organs for transplantation, because—unlike engineered skin, cartilage, or bladder tissue—cell viability and optimal function of the construct cannot be sustained through diffusion alone.

The formation and long-term survival of blood vessels within a material requires the integration of biochemical and biophysical cues. Moreover, proper maturation of an in vitro–generated vasculature is crucial for the in vivo success of engineered tissues (*2*). Vascular growth and remodeling are coupled with developmental and wound-healing processes and have been implicated in the progression of various pathological states, such as inflammation, cardiovascular diseases, and cancer. Most of these processes involve endothelial cells, which line the interior of blood vessels and form a thin layer of cells called the endothelium. This vasculature maintains tissue homeostasis by delivering the required oxygen and nutrients and removing waste products.

Incorporation of a microcirculation into engineered tissues presents multiple challenges, including the formation of microscale vascular conduits for blood flow, a functional endothelium that regulates vascular activity, and specialized cell types that perform the physiological function of the tissue of interest. Several approaches have been developed to address these challenges, including (i) the incorporation of biomolecular cues (*3*, *4*) within the material, (ii) the seeding of vascular or vascular-inducing cells in the scaffold (*5*), or (iii) the use of microfabrication technologies to engineer branched microfluidic channels within biocompatible materials (*6*). Successful application of these approaches, either individually or in combination, is expected to enhance therapeutic opportunities by building functional tissue and organ systems for regenerative medicine.

VASCULOGENESIS AND ANGIOGENESIS

To engineer vascular constructs de novo or induce vascularization from preexisting blood vessels and capillaries, one must understand the molecular mechanisms of blood vessel formation in vivo. During embryogenesis, angioblasts migrate to various regions of the developing embryo and differentiate into endothelial cells in response to local cues [for example, growth factors and extracellular matrix (ECM) components]; the endothelial cells then form a vascular plexus—a network built by connections (anastomoses) between blood vessels (*7*) (Fig. 1). But this process—called vasculogenesis—is not limited to the embryonic period and can occur in adults through the recruitment and participation of bone marrow–derived endothelial progenitor cells (*8*, *9*).

Another mechanism of blood vessel formation is through the sprouting of existing blood vessels, a process known as angiogenesis (*10*) (Fig. 1). Angiogenesis is a sequential, multistep process that begins with activation of a quiescent endothelium by angiogenic factors—vascular endothelial growth factor (VEGF), fibroblast growth factor (FGF), and angiopoietin-2 (ANG-2)—released from hypoxic or tumorigenic tissues. This step spurs degradation of the basement membrane—a thin layer of ECM between the epithelial cell layer and the endothelial cell lining of blood vessels—through up-regulation of matrix metalloproteinases (MMPs) followed by migration of an endothelial "tip cell" from the leading edge of a vascular sprout; this leading edge defines the direction of the newly growing sprout. Migration is mediated by signaling through proteins on the endothelial cell surface such as integrins, NOTCH [delta-like ligand 4 (DLL4) and JAGGED1], VEGF receptors, and neuropilins. Then, stimulated by VEGF, vascular endothelial (VE)–cadherin, and Hedgehog proteins, the endothelial cells adjacent to the tip cells begin to proliferate and elongate to form capillary sprouts, which then assemble to form a vessel lumen.

After the activation and proliferation stages, a nascent blood vessel must mature to become functional. Maturation occurs through signals such as transforming growth factor–β (TGF-β), platelet-derived growth factor B (PDGF-B), ephrin-B2, and NOTCH, which together cause vascular smooth muscle cells (pericytes) to cover and stabilize the endothelial cell channels in a process known as arteriogenesis (*7*). Tissue-engineering strategies may benefit from generating materials that can guide these biological events in the formation of vascular networks.

BIOMATERIALS FOR VASCULARIZATION

Biochemical modification of scaffolds. The considerable amount of research on angiogenesis has been pivotal in developing solutions for vascularization challenges associated with most tissue constructs and has made growth factor incorporation one of the primary material vascularization strategies investigated for three-dimensional (3D) engineered tissues (*11*–*13*). A large body of work attempting to elicit angiogenesis with the use of growth factors has shown that synthetic and natural scaffolds functionalized

[1]Department of Maxillofacial Biomedical Engineering and Institute of Oral Biology, School of Dentistry, Kyung Hee University, Seoul 130-701, Republic of Korea. [2]Department of Chemical Engineering, University of Texas at Austin, Austin, TX 78712, USA. [3]Quebec Center for Functional Materials (CQMF), Université Laval, Québec, QC GV1 0A6, Canada. [4]Center for Biomedical Engineering, Department of Medicine, Brigham and Women's Hospital, Harvard Medical School, Cambridge, MA 02139, USA. [5]Harvard–Massachussetts Institute of Technology (MIT) Division of Health Sciences and Technology, MIT, Cambridge, MA 02139, USA. [6]Department of Biomedical Engineering, University of Texas at Austin, Austin, TX 78712, USA. [7]College of Pharmacy, University of Texas at Austin, Austin, TX 78712, USA. [8]Wyss Institute for Biologically Inspired Engineering, Harvard University, Boston, MA 02115, USA.
*These authors contributed equally to this work.
†Corresponding author. E-mail: alik@rics.bwh.harvard.edu

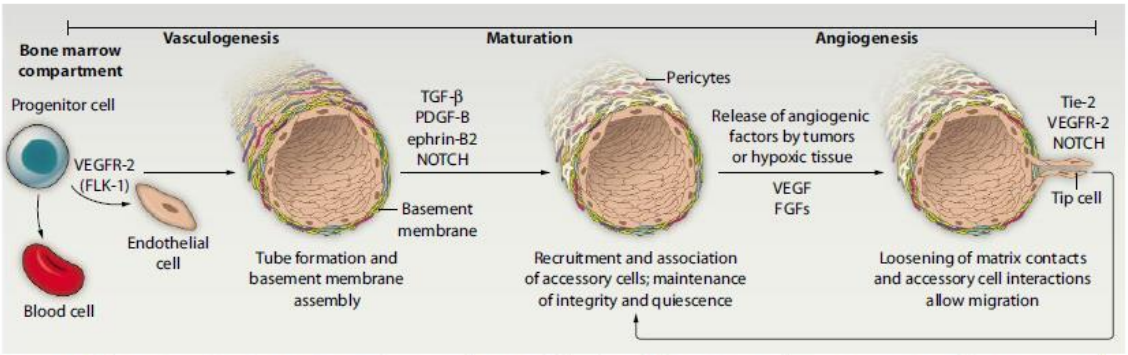

Fig. 1. Vasculogenesis and angiogenesis. Two distinct mechanisms of blood vessel formation. Vasculogenesis gives rise to the primitive vascular plexus during embryogenesis. Stimulated by tumors and hypoxic conditions, angiogenesis remodels and expands the vascular network.

with growth factors such as VEGF, basic FGF (bFGF), and PDGF could trigger the formation of vascular structures when implanted in vivo (*14*, *15*). Although these proangiogenic molecules lead to sprouting of capillary beds within the constructs, they lack the ability to direct growth of blood vessels or enable interconnectivity between the capillary networks prior to implantation.

The need for materials that could be chemically and mechanically tailored to transport and release bioactive molecules—while meeting regulatory biocompatibility and biodegradability standards—has spawned further research into the use of hydrogels (hydrated materials made from a cross-linked network of hydrophilic polymers) as scaffolds for engineered tissue constructs (*16*). The clinical success of these hydrogels depends on the integration of factors that induce rapid endothelial cell ingrowth and that stabilize the vascular network as it forms.

In addition to the classic angiogenic growth factors and peptides, recent research has evinced the multifaceted roles in angiogenesis played by other molecules, which may serve as tools for biomaterials innovation. For instance, an in vivo study by Phelps *et al.* made use of a poly(ethylene glycol) diacrylate (PEGDA)–based degradable scaffold that housed a panel of responsive elements, such as cross-links that were cleavable by proteases, RGD cell adhesive domains, and conjugated VEGF (*17*). In vitro studies in which NIH3T3 fibroblasts were seeded in these hydrogel scaffolds demonstrated that both adhesive ligands and MMP-degradable sites were necessary for cells to spread. Furthermore, upon implantation into a mouse model of hind-limb ischemia, VEGF-conjugated scaffolds resulted in rapid vascularization of the biomaterial that remained stable for at least 4 weeks.

The formation of stable vascular networks can be attributed to the widespread and prolonged availability of VEGF, likely a result of the controlled release feature of MMP-degradable implants. Diffusing VEGF was able to meet the proliferative demands of the host endothelial cells that infiltrated the scaffold aided by scaffold-associated RGD-based adhesive molecules. Consequently, endothelial-cell invasion and proliferation within the scaffold was shown to enhance the perfusion of newly formed vessels.

New data that demonstrate the importance of ephrin receptors in the mediation of cell adhesion, repulsion, and migration have inspired its use in scaffolds designed to promote vascularization (Fig. 2A). For example, Saik *et al.* developed MMP-sensitive PEGDA hydrogels immobilized with ephrin A1 ligands, which stimulate a wide range of receptors that induce vascularization (*18*). The efficacy of ephrin A1 ligand conjugation was demonstrated 14 days after implantation, by comparing vascular network parameters—vessel density, branch points, and lacunarity—of MMP-sensitive, PDGF-BB–containing PEGDA hydrogels with or without immobilized ligand. The biodegradable, bioactive hydrogels immobilized with ephrin A1 ligand produced a denser vasculature in the mouse cornea pocket relative to the non–ligand-containing scaffold.

Another approach to creating a conducive microenvironment for vascularization is the use of natural-derived materials. For example, a fibrin matrix that has been enzymatically conjugated with two multifunctional recombinant fibronectin (FN) fragments capable of binding growth factors such as VEGF, PDGF and bone morphogenetic protein-2 (BMP-2) and integrins such as $\alpha_5\beta_1$ and $\alpha_v\beta_3$ has been shown to be a potent proangiogenic material (*19*). FN III9-10/12-14–functionalized fibrin matrices enhance wound healing responses in diabetic rats via localization of growth factors and integrins, which in turn boost angiogenesis through endothelial cell recruitment and maintenance of neovessel integrity by smooth muscle cells and mesenchymal stem cells (MSCs) in the tissue.

The improved interaction between growth factors and integrins resulting from the customized FN are mainly responsible for neovascularization in cutaneous wounds and superior granulation tissue morphogenesis in bone tissue repair. Combining scaffolds with recombinant proteins that can locally implicate native biomolecules paves the way for in vivo neovascularization of host tissue. For both safety and efficacy purposes, this controlled and localized delivery of growth factors may be preferable to loading scaffolds with randomly encapsulated or chemically immobilized growth factors.

Because blood vessel formation is a highly organized process in vivo, the spatial and temporal presence of specific signaling molecules is an important aspect of the biochemical modulation of biomaterials. Thus, it is crucial to engineer materials with properties that mimic the in vivo complexities of the blood vessel formation process. For instance, the sequential expression of specific angiogenic molecules, as well as the patterned localization of these molecules within 3D spaces can be important for enhancing biochemical modulation approaches. Fortunately, these goals are within reach as a result of advances in controlled-release technology (*20*, *21*), novel chemistries, and micro- and

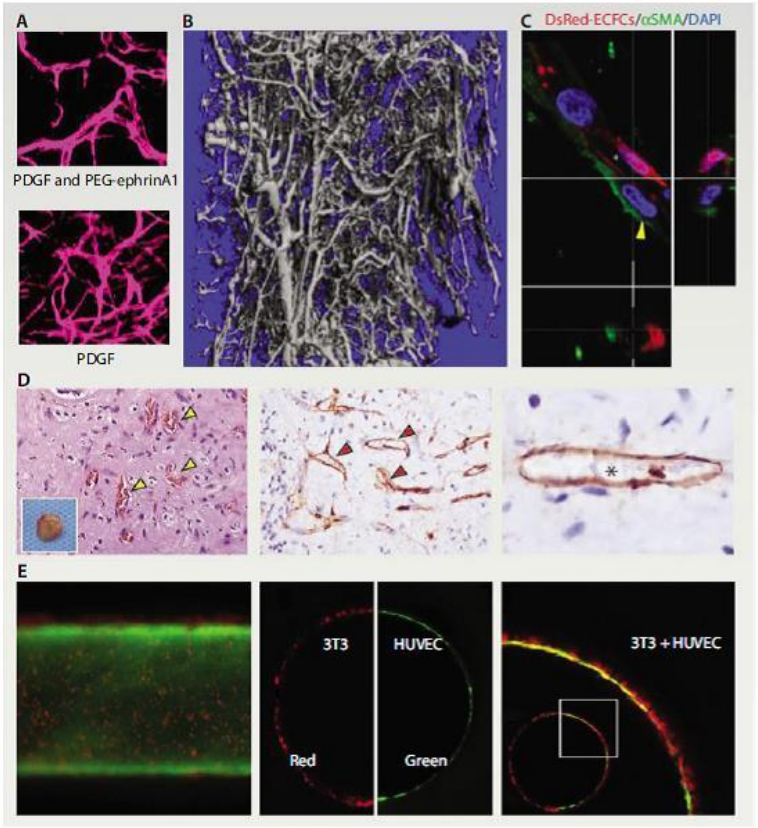

Fig. 2. Cue gardens. Biochemical cues can be integrated in hydrogels to induce vascularization. (**A**) Biomimetic hydrogels with platelet-derived growth factor (PDGF), immobilized RGDs, and poly(ethylene glycol) (PEG)-ephrinA1 (top panel) showed more robust response than hydrogels with PDGF only (lower panel) when implanted into the mouse cornea micropocket. [Reprinted from (*18*) with permission from the American Chemical Society] (**B**) Microcomputed tomography (micro-CT) image of a porous poly(L/DL-Lactide) (PLDL) copolymer filled with growth factor–treated, RGD-alginate hydrogel several weeks after implantation in a rat 8-mm segmental defect model; formation of vascular network is shown (*32*). [Reprinted from (*32*) with permission from Elsevier] (**C**) Formation of endothelial colony–forming cell (ECFC)—lined lumens within a gelatin methacrylate (GelMA) hydrogel that contains both ECFCs (DsRed) and mesenchymal stem cells (MSCs) (7 days after seeding the hydrogel with cells). ECFC-lined lumens were surrounded by MSC-derived pericyte cells that expressed α-smooth muscle actin (α-SMA) (yellow arrow). [Reprinted from (*31*) with permission from Wiley-VCH Verlag] (**D**) ECFC- and MSC-containing GelMA hydrogel implants were retrieved from the subcutaneous tissue of the dorsum of 6-week old nude mice 7 days after implantation; functional vascular network formation in vivo is shown. Top panel, image of hematoxylin and eosin (H&E)–stained GelMA explants. Numerous blood vessels containing murine red blood cells are shown (yellow arrowheads). The dark purple spots indicate nuclei of cells, and shades of light purple in the background indicate GelMA hydrogel. The inset shows the macroscopic view of the GelMA explant; middle panel, immunohistochemistry shows human cluster of differentiation 31 (CD31)–positive engineered microvessels; bottom panel, single human CD31–positive microvessel at higher magnification carrying murine erythrocytes (star). [Reproduced from (*31*) with permission from Wiley-VCH Verlag] (**E**) A microfluidic hydrogel containing microvascular-like structures fabricated using self-assembled monolayer (SAM)–based cell transfer. Left panel, double-layer construct generated using 3T3 cells (red) encircling a human umbilical–vein endothelial cell (HUVEC) (green) monolayer; middle panel, confocal cross-sectional image of the vascular construct; right panel, merged confocal image of the construct. Inset shows the entire channel section. [Reproduced from (*34*) with permission from Elsevier]

nanoengineering tools such as micromachining, photolithography, and molding (*6*, *22*).

Cell-based approaches. Because of the emergence of new cell sources, such as stem and progenitor cells, there is an increased focus on strategies that involve encapsulation of endothelial cells and other supporting cell types within biomaterials. Such an approach can take advantage of cell signaling, differentiation, and migration as well as the dynamic interactions between cells that provide the biochemical environment required for the ensuing tissue remodeling.

Initial work on the prospective merits of such a cell-based approach for vascularizing skin tissue made use of a coculture of human umbilical–vein endothelial cells (HUVECs) and human-derived fibroblasts and keratinocytes (skin cells) housed within a collagen-based scaffold (*5*). Biochemical coordination between the ECM generated by the fibroblasts and growth factors such as VEGF and TGF-β secreted by neighboring cells in the presence of HUVECs promoted the development of a vascular network both in vitro in the experimental model and in vivo after implantation in a mouse model (*23*, *24*). Furthermore, recent studies highlight the benefits gained from the addition of epithelial cells—those that line the body cavities such the gut and lungs—to stabilize and regulate the size and formation of capillaries within the vascularized model. Thus, various cell types can play a complementary role in tailoring vascularization in vitro (*25*).

Successes with the use of cocultures of HUVECs and other cell types for vascularizing skin tissue has paved the way for application to other tissue types that require denser vascular networks. For instance, Alajati *et al.* validated the concept of implanting a coculture of endothelial cells with ECM-forming fibroblasts or bone-forming osteoblasts in vivo (*26*). HUVECs and osteoblasts were encapsulated within a scaffolding material composed of VEGF and FGF-2 within Matrigel (a murine tumor–derived material that comprises ECM proteins and glycosaminoglycans), fibrin, and thrombin, and the biomaterial was implanted subcutaneously in a severe combined immunodeficiency (SCID) mouse model for up to 20 days. Subsequent analysis showed this approach was capable of forming a durable perfused vascular networks in vivo. Moreover, incorporation of FGF-2 in the matrix before implantation provided molecular assistance to cell-secreted VEGF in conferring stability upon the developing vasculature after biomaterial implantation. Stability of the

vascular network in the implant was shown to be a consequence of the interaction of host mural cells with the perfused vasculature, which remained functional for up to 60 days.

The development of stable vascular networks was also observed in mice when HUVECs and fibroblasts were combined with mouse myoblasts for vascularization of skeletal muscle tissue (*27*) and with cardiomyocytes for vascularization of cardiac tissue (*28*). In still another study, HUVECs were used to promote the differentiation of human MSCs into an endothelial lineage, promoting the formation of 3D vascular structures for up to 2 weeks in a Matrigel-based ECM (*29*). Similarly, the combination of HUVECs and human MSCs seeded in a polymeric scaffold were shown to form mature vascular networks in vivo 4 to 7 days after implantation, thus accelerating the functional remodeling of the implant when used as a bone graft (*30*).

For cell-based therapies, the scaffold is a crucial component that regulates the dynamic vascularization process. Research in this area has made use of either natural biodegradable materials, such as collagen and Matrigel, or synthetic biodegradable scaffolds, such as poly-L-lactic acid (PLLA) or poly-D,L-lactic-co-glycolic acid (PLGA). However, long-term evaluations of these materials have reflected shortcomings in their mechanical strength, durability, and even immunogenicity, thereby creating an opportunity for the creation of more suitable scaffolds for endothelial cell–based vascularization. It is possible that the inherent limitations of previously investigated natural scaffolds can be overcome by incorporating biochemical functionality, within natural hydrogels, that controls mechanical strength and rate of biodegradation, thereby combining the advantages of natural scaffolds with robust synthetic materials.

For instance, mechanically robust gelatin-based photocrosslinkable hydrogels can encapsulate and allow synergistic interaction between endothelial colony–forming cells (ECFCs) and α-smooth muscle actin (α-SMA)–expressing MSCs to form a microvasculature in vitro and in vivo that is composed of endothelial cell–lined functional blood vessels (Fig. 2C) (*31*). Furthermore, this microvasculature abets perfusion of red blood cells in the tissue construct in vivo after biodegradation of the hydrogel scaffold, the rate of which was controllable by the degree of methacrylation of the polymer and the extent of cross-linking in the material (Fig. 2D).

Microengineering strategies. With the emergence of microengineering technologies, it is becoming increasingly possible to recreate vascularized materials through microfabrication-based approaches. The advantages include the ability to control the initial architecture of the microvascular network and enable immediate perfusion through the scaffolds. Microfabricated devices with integrated microvasculature can be optimized to provide a uniform distribution of fluid flow and mass transfer across the scaffolding material; thus, cells are provided with an adequate supply of nutrients in capillary channels ranging from a few millimeters down to micrometers. Such fabrication techniques benefit greatly from the advances in noninvasive imaging technology that can be used to aid the design and function of microengineered vascular networks (Fig. 2B) (*32*).

To engineer a functional vasculature network, endothelial cells could be seeded in microengineered scaffolds containing conduits to form a confluent endothelium on the walls of the vascular channels (*33*). In one study, a 3D tissue construct composed of endothelialized hollow vascular structures was produced using a self-assembled monolayer (SAM)–based cell deposition technique and a hydrogel photocrosslinking method to provide a robust hydrogel-based scaffold for endothelial cell attachment (Fig. 2E) (*34*). Moreover, Chrobak *et al.* validated the hypothesis that the existent flow and shear conditions within such microscale channels are favorable for endothelium sustainability (*35*). These studies have demonstrated that microfabricated tissues composed of a fluidic network designed to mimic the human vasculature may one day be inosculated in vivo.

Microengineering techniques such as photolithography (a process that uses light illumination through a mask to generate structures from light-sensitive materials) and molding (a process that uses a hollowed-out pattern to which a deposited material conforms) are inherently planar; therefore, 3D structures mostly result from stacked 2D structures that comprise channels with rectangular cross sections instead of channels with the circular cross sections ubiquitous in nature (*36*). Microengineering techniques such as direct ink writing and omnidirectional printing within a gel reservoir have recently been developed to create 3D vascular structures in vitro (*37*, *38*). Despite their enormous potential, these approaches still await further improvements in the integration of other specialized cell types required to enable functionality of the tissue structures that surround the vascular network. In a recent study, a printing approach was used to generate a micropatterned sugar-based sacrificial layer around which cell-laden hydrogels could be built; the sugar-based layer is then dissolved, creating a 3D microarchitecture consisting of microvascular networks (*39*). However, despite these advances, new technologies are required to more accurately recreate the complexity of native tissues.

Another way to recreate the human tissue vasculature is with modular approaches in which smaller building blocks are assembled in a controlled manner (*40*). This approach can be used to modulate the cell microenvironment and macroscale properties of relatively large and complex engineered tissues (*41*), especially when the tissue requires perfusion and needs to perform a specialized physiological function. Recent work has shown the potential of modular assembly to produce vascularized tissues in vitro (*42*). Arrays of microgels with precisely defined structures and channels are produced by microfabrication and subsequently assembled to yield 3D structures with interconnected lumens, resembling native vasculature (*43*).

This biofabrication process was validated by placing endothelial and smooth muscle cells inside microgels in a precise and concentric fashion that mimicked the organization of blood vessels, strengthening the assembly with a secondary cross-linking step, and showing that these assemblies could be perfused with fluids. The precise design of microscale components combined with the capability of linking them together into higher-order structures represents a promising way to build vascularized 3D biomaterials in vitro.

CHALLENGES: FORM AND FUNCTION

Most recently developed vascularizing approaches for biomaterials attempt to mimic cellular communication that occurs in tissues and organs through the use of multiple cell types and biochemically modified scaffolds. These attempts to match natural biological and mechanical cues through the use of ECM components have inspired the creation of scaffolds that incorporate growth factors, integrin-binding peptides, vasculature-forming cells, and physical features that promote diffusion and transport. Studies have revealed that scaffold degradability and a combination of MMP-degradable moieties and adhesive components collectively promote ingress of endothelial cells into the biomaterial. Furthermore, in vitro release studies, such as those that compare proteolytically released VEGF with fibrin-localized

VEGF or that correlate VEGF release with vessel density, should expand our ability to precisely tune preformed tissue constructs.

However, the ability to quickly achieve a stable vascular network that can offer functionality to an ischemic organ or tissue implant remains a major challenge. Thus, for successful clinical translation of biomaterials, it is essential that researchers identify parameters that can be controlled to promote and regulate angiogenesis. The long-term in vivo function of various engineered vascular networks must also be assessed. Thus, further research into mechanisms for regulating the spatial aspects of vascularization is essential for further success in tissue engineering. Although microfabrication technologies need more in vivo studies to validate their claims of structural and functional integrity, scaffolds that recruit endogenous growth factors and stimulate the host to form a vascular network appear safe, efficient, and cost-effective. A combination of these approaches may be most suitable for creating constructs that can yield functional vasculature within the host.

REFERENCES AND NOTES

1. A. Khademhosseini, J. P. Vacanti, R. Langer, Progress in tissue engineering. *Sci. Am.* **300**, 64–71 (2009).
2. J. M. Stenman, J. Rajagopal, T. J. Carroll, M. Ishibashi, J. McMahon, A. P. McMahon, Canonical Wnt signaling regulates organ-specific assembly and differentiation of CNS vasculature. *Science* **322**, 1247–1250 (2008).
3. M. Ehrbar, V. G. Djonov, C. Schnell, S. A. Tschanz, G. Martiny-Baron, U. Schenk, J. Wood, P. H. Burri, J. A. Hubbell, A. H. Zisch, Cell-demanded liberation of VEGF121 from fibrin implants induces local and controlled blood vessel growth. *Circ. Res.* **94**, 1124–1132 (2004).
4. M. C. Peters, P. J. Polverini, D. J. Mooney, Engineering vascular networks in porous polymer matrices. *J. Biomed. Mater. Res.* **60**, 668–678 (2002).
5. A. F. Black, F. Berthod, N. L'heureux, L. Germain, F. A. Auger, In vitro reconstruction of a human capillary-like network in a tissue-engineered skin equivalent. *FASEB J.* **12**, 1331–1340 (1998).
6. J. T. Borenstein, H. Terai, K. R. King, E. J. Weinberg, M. R. Kaazempur-Mofrad, J. P. Vacanti, Microfabrication technology for vascularization tissue engineering. *Biomed. Microdevices* **4**, 167–175 (2002).
7. P. Carmeliet, R. K. Jain, Molecular mechanisms and clinical applications of angiogenesis. *Nature* **473**, 298–307 (2011).
8. O. M. Tepper, J. M. Capla, R. D. Galiano, D. J. Ceradini, M. J. Callaghan, M. E. Kleinman, G. C. Gurtner, Adult vasculogenesis occurs through in situ recruitment, proliferation, and tubulization of circulating bone marrow-derived cells. *Blood* **105**, 1068–1077 (2005).
9. M. W. Laschke, M. D. Menger, Vascularization in tissue engineering: Angiogenesis versus inosculation. *Eur. Surg. Res.* **48**, 85–92 (2012).
10. J. Folkman, Angiogenesis: An organizing principle for drug discovery? *Nat. Rev. Drug Discov.* **6**, 273–286 (2007).
11. H. F. Dvorak, V. S. Harvey, P. Estrella, L. F. Brown, J. McDonagh, A. M. Dvorak, Fibrin containing gels induce angiogenesis. Implications for tumor stroma generation and wound healing. *Lab. Invest.* **57**, 673–686 (1987).
12. Y. Kubota, H. K. Kleinman, G. R. Martin, T. J. Lawley, Role of laminin and basement membrane in the morphological differentiation of human endothelial cells into capillary-like structures. *J. Cell Biol.* **107**, 1589–1598 (1988).
13. D. E. Ingber, J. Folkman, Mechanochemical switching between growth and differentiation during fibroblast growth factor-stimulated angiogenesis in vitro: Role of extracellular matrix. *J. Cell Biol.* **109**, 317–330 (1989).
14. A. H. Zisch, M. P. Lutolf, J. A. Hubbell, Biopolymeric delivery matrices for angiogenic growth factors. *Cardiovasc. Pathol.* **12**, 295–310 (2003).
15. J. E. Leslie-Barbick, J. J. Moon, J. L. West, Covalently-immobilized vascular endothelial growth factor promotes endothelial cell tubulogenesis in poly(ethylene glycol) diacrylate hydrogels. *J. Biomater. Sci. Polym. Ed.* **20**, 1763–1779 (2009).
16. B. V. Slaughter, S. S. Khurshid, O. Z. Fisher, A. Khademhosseini, N. A. Peppas, Hydrogels in regenerative medicine. *Adv. Mater. (Deerfield Beach Fla.)* **21**, 3307–3329 (2009).
17. E. A. Phelps, N. Landázuri, P. M. Thulé, W. R. Taylor, A. J. García, Bioartificial matrices for therapeutic vascularization. *Proc. Natl. Acad. Sci. U.S.A.* **107**, 3323–3328 (2010).
18. J. E. Saik, D. J. Gould, A. H. Keswani, M. E. Dickinson, J. L. West, Biomimetic hydrogels with immobilized ephrinA1 for therapeutic angiogenesis. *Biomacromolecules* **12**, 2715–2722 (2011).
19. M. M. Martino, F. Tortelli, M. Mochizuki, S. Traub, D. Ben-David, G. A. Kuhn, R. Müller, E. Livne, S. A. Eming, J. A. Hubbell, Engineering the growth factor microenvironment with fibronectin domains to promote wound and bone tissue healing. *Sci. Transl. Med.* **3**, 100ra89 (2011).
20. H. Hosseinkhani, M. Hosseinkhani, A. Khademhosseini, H. Kobayashi, Y. Tabata, Enhanced angiogenesis through controlled release of basic fibroblast growth factor from peptide amphiphile for tissue regeneration. *Biomaterials* **27**, 5836–5844 (2006).
21. M. J. Wissink, R. Beernink, A. A. Poot, G. H. Engbers, T. Beugeling, W. G. van Aken, J. Feijen, Improved endothelialization of vascular grafts by local release of growth factor from heparinized collagen matrices. *J. Control. Release* **64**, 103–114 (2000).
22. S. E. A. Gratton, S. S. Williams, M. E. Napier, P. D. Pohlhaus, Z. Zhou, K. B. Wiles, B. W. Maynor, C. Shen, T. Olafsen, E. T. Samulski, J. M. Desimone, The pursuit of a scalable nanofabrication platform for use in material and life science applications. *Acc. Chem. Res.* **41**, 1685–1695 (2008).
23. P.-L. Tremblay, V. Hudon, F. Berthod, L. Germain, F. A. Auger, Inosculation of tissue-engineered capillaries with the host's vasculature in a reconstructed skin transplanted on mice. *Am. J. Transplant.* **5**, 1002–1010 (2005).
24. V. Hudon, F. Berthod, A. F. Black, O. Damour, L. Germain, F. A. Auger, A tissue-engineered endothelialized dermis to study the modulation of angiogenic and angiostatic molecules on capillary-like tube formation in vitro. *Br. J. Dermatol.* **148**, 1094–1104 (2003).
25. M. H. Rochon, J. Fradette, V. Fortin, F. Tomasetig, C. J. Roberge, K. Baker, F. Berthod, F. A. Auger, L. Germain, Normal human epithelial cells regulate the size and morphology of tissue-engineered capillaries. *Tissue Eng. Part A* **16**, 1457–1468 (2010).
26. A. Alajati, A. M. Laib, H. Weber, A. M. Boos, A. Bartol, K. Ikenberg, T. Korff, H. Zentgraf, C. Obodozie, R. Graeser, S. Christian, G. Finkenzeller, G. B. Stark, M. Héroult, H. G. Augustin, Spheroid-based engineering of a human vasculature in mice. *Nat. Methods* **5**, 439–445 (2008).
27. S. Levenberg, J. Rouwkema, M. Macdonald, E. S. Garfein, D. S. Kohane, D. C. Darland, R. Marini, C. A. van Blitterswijk, R. C. Mulligan, P. A. D'Amore, R. Langer, Engineering vascularized skeletal muscle tissue. *Nat. Biotechnol.* **23**, 879–884 (2005).
28. A. Lesman, M. Habib, O. Caspi, A. Gepstein, G. Arbel, S. Levenberg, L. Gepstein, Transplantation of a tissue-engineered human vascularized cardiac muscle. *Tissue Eng. Part A* **16**, 115–125 (2010).
29. J. M. Sorrell, M. A. Baber, A. I. Caplan, Influence of adult mesenchymal stem cells on in vitro vascular formation. *Tissue Eng. Part A* **15**, 1751–1761 (2009).
30. O. Tsigkou, I. Pomerantseva, J. A. Spencer, P. A. Redondo, A. R. Hart, E. O'Doherty, Y. Lin, C. C. Friedrich, L. Daheron, C. P. Lin, C. A. Sundback, J. P. Vacanti, C. Neville, Engineered vascularized bone grafts. *Proc. Natl. Acad. Sci. U.S.A.* **107**, 3311–3316 (2010).
31. Y.-C. Chen, R.-Z. Lin, H. Qi, Y. Yang, H. Bae, J. M. Melero-Martin, A. Khademhosseini, Functional human vascular network generated in photocrosslinkable gelatin methacrylate hydrogels. *Adv. Funct. Mater.* **22**, 2027–2039 (2012).
32. R. E. Guldberg, C. L. Duvall, A. Peister, M. E. Oest, A. S. Lin, A. W. Palmer, M. E. Levenston, 3D imaging of tissue integration with porous biomaterials. *Biomaterials* **29**, 3757–3761 (2008).
33. Y. Zheng, J. Chen, M. Craven, N. W. Choi, S. Totorica, A. Diaz-Santana, P. Kermani, B. Hempstead, C. Fischbach-Teschl, J. A. López, A. D. Stroock, In vitro microvessels for the study of angiogenesis and thrombosis. *Proc. Natl. Acad. Sci. U.S.A.* **109**, 9342–9347 (2012).
34. N. Sadr, M. Zhu, T. Osaki, T. Kakegawa, Y. Yang, M. Moretti, J. Fukuda, A. Khademhosseini, SAM-based cell transfer to photopatterned hydrogels for microengineering vascular-like structures. *Biomaterials* **32**, 7479–7490 (2011).
35. K. M. Chrobak, D. R. Potter, J. Tien, Formation of perfused, functional microvascular tubes in vitro. *Microvasc. Res.* **71**, 185–196 (2006).
36. J. T. Borenstein, M. M. Tupper, P. J. Mack, E. J. Weinberg, A. S. Khalil, J. Hsiao, G. García-Cardeña, Functional endothelialized microvascular networks with circular cross-sections in a tissue culture substrate. *Biomed. Microdevices* **12**, 71–79 (2010).
37. B. Y. Ahn, D. Shoji, C. J. Hansen, E. Hong, D. C. Dunand, J. A. Lewis, Printed origami structures. *Adv. Mater. (Deerfield Beach Fla.)* **22**, 2251–2254 (2010).
38. W. Wu, A. DeConinck, J. A. Lewis, Omnidirectional printing of 3D microvascular networks. *Adv. Mater. (Deerfield Beach Fla.)* **23**, H178–H183 (2011).
39. J. S. Miller, K. R. Stevens, M. T. Yang, B. M. Baker, D. H. Nguyen, D. M. Cohen, E. Toro, A. A. Chen, P. A. Galie, X. Yu, R. Chaturvedi, S. N. Bhatia, C. S. Chen, Rapid casting of patterned vascular networks for perfusable engineered three-dimensional tissues. *Nat. Mater.* **11**, 768–774 (2012).
40. A. Khademhosseini, R. Langer, Microengineered hydrogels for tissue engineering. *Biomaterials* **28**, 5087–5092 (2007).
41. J. G. Fernandez, A. Khademhosseini, Micro-masonry: Construction of 3D structures by microscale self-assembly. *Adv. Mater. (Deerfield Beach Fla.)* **22**, 2538–2541 (2010).
42. A. P. McGuigan, M. V. Sefton, Vascularized organoid engineered by modular assembly enables blood perfusion. *Proc. Natl. Acad. Sci. U.S.A.* **103**, 11461–11466 (2006).
43. Y. Du, M. Ghodousi, E. Lo, M. K. Vidula, O. Emiroglu, A. Khademhosseini, Surface-directed assembly of cell-laden microgels. *Biotechnol. Bioeng.* **105**, 655–662 (2010).

Acknowledgments: We thank Y.-s. Hwang for discussions and assistance with figures. **Funding:** Supported by the U.S. National Institutes of Health (NIH) (grants HL092836, DE021468, EB012597, and HL099073 to A.K. and EB024618 and EB012726 to N.A.P.), the National Science Foundation (DMR0847287), NIH/NCI Center for Oncophysics (Grant CTO PSOC U54-CA-143837), DTRA, and the Office of Naval Research Young Investigator award. H.B. was supported by a grant from the Kyung Hee University (KHU-20120477). **Competing interests:** The authors declare that they have no competing interests.

10.1126/scitranslmed.3003688

Citation: H. Bae, A. S. Puranik, R. Gauvin, F. Edalat, B. Carrillo-Conde, N. A. Peppas, A. Khademhosseini, Building vascular networks. *Sci. Transl. Med.* **4**, 160ps23 (2012).

Bibliography

Ahmed, S. A., R. M. Gogal, Jr., and J. E. Walsh. 1994. "A new rapid and simple non-radioactive assay to monitor and determine the proliferation of lymphocytes: an alternative to [3H]thymidine incorporation assay." *J Immunol Methods* 170 (2):211-24.

Alfrey, Turner. 1964. *Copolymerization*. Vol. 18: Interscience Publishers.

Ali, M.M., A. Sabnis, D. Dewitt, G. Troiano, J. Wright, M. Figueiredo, M. Figa, G.H.T. Van, Y.H. Song, and J. Auer. 2011. Therapeutic polymeric nanoparticle compositions with high glass transition temperature or high molecular weight copolymers. Google Patents.

Artursson, P., and J. Karlsson. 1991. "Correlation between oral drug absorption in humans and apparent drug permeability coefficients in human intestinal epithelial (Caco-2) cells." *Biochem Biophys Res Commun* 175 (3):880-5.

Atkinson, J. R., J. N. Hay, and M. J. Jenkins. 2002. "Enthalpic relaxation in semi-crystalline PEEK." *Polymer* 43 (3):731-735. doi: http://dx.doi.org/10.1016/S0032-3861(01)00668-1.

Beig, A., R. Agbaria, and A. Dahan. 2013. "Oral delivery of lipophilic drugs: the tradeoff between solubility increase and permeability decrease when using cyclodextrin-based formulations." *PLoS One* 8 (7):e68237. doi: 10.1371/journal.pone.0068237.

Bell, Cristi L, and Nikolaos A Peppas. 1996a. "Modulation of drug permeation through interpolymer complexed hydrogels for drug delivery applications." *Journal of controlled release* 39 (2):201-207.

Bell, Cristi L, and Nikolaos A Peppas. 1996b. "Water, solute and protein diffusion in physiologically responsive hydrogels of poly (methacrylic acid-g-ethylene glycol)." *Biomaterials* 17 (12):1203-1218.

Berger, Andreas P., Kurt Kofler, Jasmin Bektic, Hermann Rogatsch, Hannes Steiner, Georg Bartsch, and Helmut Klocker. 2003. "Increased growth factor production in a human prostatic stromal cell culture model caused by hypoxia." *The Prostate* 57 (1):57-65. doi: 10.1002/pros.10279.

Bergers, Gabriele, and Lisa M. Coussens. 2000. "Extrinsic regulators of epithelial tumor progression: metalloproteinases." *Current Opinion in Genetics & Development* 10 (1):120-127. doi: http://dx.doi.org/10.1016/S0959-437X(99)00043-X.

Bergers, Gabriele, Steven Song, Nicole Meyer-Morse, Emily Bergsland, and Douglas Hanahan. 2003. "Benefits of targeting both pericytes and endothelial cells in the tumor vasculature with kinase inhibitors." *The Journal of Clinical Investigation* 111 (9):1287-1295. doi: 10.1172/JCI17929.

Berridge, M. V., P. M. Herst, and A. S. Tan. 2005. "Tetrazolium dyes as tools in cell biology: new insights into their cellular reduction." *Biotechnol Annu Rev* 11:127-52. doi: 10.1016/s1387-2656(05)11004-7.

Blanchette, James, and NicholasA Peppas. 2005. "Oral Chemotherapeutic Delivery: Design and Cellular Response." *Annals of Biomedical Engineering* 33 (2):142-149. doi: 10.1007/s10439-005-8973-8.

Boder, E. T., and W. Jiang. 2011. "Engineering antibodies for cancer therapy." *Annu Rev Chem Biomol Eng* 2:53-75. doi: 10.1146/annurev-chembioeng-061010-114142.

Bogdan, Sven, and Christian Klämbt. 2001. "Epidermal growth factor receptor signaling." *Current Biology* 11 (8):R292-R295. doi: http://dx.doi.org/10.1016/S0960-9822(01)00167-1.

Buerkle, M. A., S. A. Pahernik, A. Sutter, A. Jonczyk, K. Messmer, and M. Dellian. 2002. "Inhibition of the alpha-[nu] integrins with a cyclic RGD peptide impairs angiogenesis, growth and metastasis of solid tumours in vivo." *Br J Cancer* 86 (5):788-795.

Burnett, John C, and John J Rossi. 2012. "RNA-Based Therapeutics: Current Progress and Future Prospects." *Chemistry & Biology* 19 (1):60-71. doi: http://dx.doi.org/10.1016/j.chembiol.2011.12.008.

Buxton, Gavin A, and Nigel Clarke. 2007. "Drug diffusion from polymer core–shell nanoparticles." *Soft Matter* 3 (12):1513-1517.

Buysschaert, I., T. Schmidt, C. Roncal, P. Carmeliet, and D. Lambrechts. 2008a. "Genetics, epigenetics and pharmaco-(epi)genomics in angiogenesis." *J Cell Mol Med* 12 (6B):2533-51. doi: 10.1111/j.1582-4934.2008.00515.x.

Buysschaert, Ian, Thomas Schmidt, Carmen Roncal, Peter Carmeliet, and Diether Lambrechts. 2008b. "Genetics, epigenetics and pharmaco-(epi)genomics in angiogenesis." *Journal of Cellular and Molecular Medicine* 12 (6b):2533-2551. doi: 10.1111/j.1582-4934.2008.00515.x.

Carmeliet, P., and R. K. Jain. 2011. "Molecular mechanisms and clinical applications of angiogenesis." *Nature* 473 (7347):298-307. doi: 10.1038/nature10144.

Carmeliet, Peter, Lieve Moons, Aernout Luttun, Valeria Vincenti, Veerle Compernolle, Maria De Mol, Yan Wu, Francoise Bono, Laetitia Devy, Heike Beck, Dimitri Scholz, Till Acker, Tina DiPalma, Mieke Dewerchin, Agnes Noel, Ingeborg Stalmans, Adriano Barra, Sylvia Blacher, Thierry Vandendriessche, Annica Ponten, Ulf Eriksson, Karl H. Plate, Jean-Michel Foidart, Wolfgang Schaper, D. Stephen Charnock-Jones, Daniel J. Hicklin, Jean-Marc Herbert, Desire Collen, and M. Graziella Persico. 2001. "Synergism between vascular endothelial growth factor and placental growth factor contributes to angiogenesis and plasma extravasation in pathological conditions." *Nat Med* 7 (5):575-583.

Catoni, Sara E. M., Ketlyn N. Trindade, Caio A. T. Gomes, Andréa L. S. Schneider, Ana P.T. Pezzin, and Valdir Soldi. 2013. "Influence of poly(ethylene grycol) - (PEG) on the properties of influence of poly(3-hydroxybutyrate-CO-3-hydroxyvalerate) - PHBV." *Polímeros* 23:320-325.

Chan, F. K., K. Moriwaki, and M. J. De Rosa. 2013. "Detection of necrosis by release of lactate dehydrogenase activity." *Methods Mol Biol* 979:65-70. doi: 10.1007/978-1-62703-290-2_7.

Chen, Ko-Jie, Er-Yuan Chaung, Shiaw-Pyng Wey, Kun-Ju Lin, Felice Cheng, Chia-Chen Lin, Hao-Li Liu, Hsiang-Wen Tseng, Chih-Peng Liu, Ming-Cheng Wei, Chun-Min Liu, and Hsing-Wen Sung. 2014. "Hyperthermia-Mediated Local Drug Delivery by a Bubble-Generating Liposomal System for Tumor-Specific Chemotherapy." *ACS Nano* 8 (5):5105-5115. doi: 10.1021/nn501162x.

Chen, Rongjun, Sariah Khormaee, Mark E. Eccleston, and Nigel K. H. Slater. 2009. "The role of hydrophobic amino acid grafts in the enhancement of membrane-disruptive activity of

pH-responsive pseudo-peptides." *Biomaterials* 30 (10):1954-1961. doi: http://dx.doi.org/10.1016/j.biomaterials.2008.12.036.

Chen, Shao-Hua, and Getu Zhaori. 2011. "Potential clinical applications of siRNA technique: benefits and limitations." *European Journal of Clinical Investigation* 41 (2):221-232. doi: 10.1111/j.1365-2362.2010.02400.x.

Chu, Chih-Chien, Yih-Wen Wang, Chih-Fu Yeh, and Leeyih Wang. 2008. "Synthesis of Conductive Core−Shell Nanoparticles Based on Amphiphilic Starburst Poly(n-butyl acrylate)-b-poly(styrenesulfonate)." *Macromolecules* 41 (15):5632-5640. doi: 10.1021/ma7027243.

Coates, John. 2000. "Interpretation of infrared spectra, a practical approach." *Encyclopedia of analytical chemistry*.

Cross, Michael J., and Lena Claesson-Welsh. 2001. "FGF and VEGF function in angiogenesis: signalling pathways, biological responses and therapeutic inhibition." *Trends in Pharmacological Sciences* 22 (4):201-207. doi: http://dx.doi.org/10.1016/S0165-6147(00)01676-X.

Curcio, A., D. Torella, G. Cuda, C. Coppola, M. C. Faniello, F. Achille, V. G. Russo, M. Chiariello, and C. Indolfi. 2004. "Effect of stent coating alone on in vitro vascular smooth muscle cell proliferation and apoptosis." *Am J Physiol Heart Circ Physiol* 286 (3):H902-8. doi: 10.1152/ajpheart.00130.2003.

Dahan, A., and J. M. Miller. 2012. "The solubility-permeability interplay and its implications in formulation design and development for poorly soluble drugs." *Aaps j* 14 (2):244-51. doi: 10.1208/s12248-012-9337-6.

Davis, G. E., and D. R. Senger. 2005. "Endothelial extracellular matrix: biosynthesis, remodeling, and functions during vascular morphogenesis and neovessel stabilization." *Circ Res* 97 (11):1093-107. doi: 10.1161/01.RES.0000191547.64391.e3.

Denker, B. M., and S. K. Nigam. 1998. "Molecular structure and assembly of the tight junction." *Am J Physiol* 274 (1 Pt 2):F1-9.

des Rieux, A., V. Fievez, M. Garinot, Y. J. Schneider, and V. Preat. 2006. "Nanoparticles as potential oral delivery systems of proteins and vaccines: a mechanistic approach." *J Control Release* 116 (1):1-27. doi: 10.1016/j.jconrel.2006.08.013.

Dong, Liang, Abhishek K. Agarwal, David J. Beebe, and Hongrui Jiang. 2006. "Adaptive liquid microlenses activated by stimuli-responsive hydrogels." *Nature* 442 (7102):551-554. doi: http://www.nature.com/nature/journal/v442/n7102/suppinfo/nature05024_S1.html.

Du, Y., E. Lo, S. Ali, and A. Khademhosseini. 2008. "Directed assembly of cell-laden microgels for fabrication of 3D tissue constructs." *Proc Natl Acad Sci U S A* 105 (28):9522-7. doi: 10.1073/pnas.0801866105.

Duda, Dan G., and Rakesh K. Jain. 2010. "Premetastatic lung "niche": is vascular endothelial growth factor receptor 1 activation required?" *Cancer research* 70 (14):5670-5673. doi: 10.1158/0008-5472.can-10-0119.

Dudhani, Anitha R., and Shantha L. Kosaraju. 2010. "Bioadhesive chitosan nanoparticles: Preparation and characterization." *Carbohydrate Polymers* 81 (2):243-251. doi: http://dx.doi.org/10.1016/j.carbpol.2010.02.026.

DuFort, Christopher C., Matthew J. Paszek, and Valerie M. Weaver. 2011. "Balancing forces: architectural control of mechanotransduction." *Nat Rev Mol Cell Biol* 12 (5):308-319.

Ensign, Laura M., Richard Cone, and Justin Hanes. 2012. "Oral drug delivery with polymeric nanoparticles: The gastrointestinal mucus barriers." *Advanced Drug Delivery Reviews* 64 (6):557-570. doi: http://dx.doi.org/10.1016/j.addr.2011.12.009.

Famulok, M., and G. Mayer. "Aptamers as tools in molecular biology and immunology." (0070-217X (Print)).

Ferrara, N. 1999. "Role of vascular endothelial growth factor in the regulation of angiogenesis." *Kidney Int* 56 (3):794-814. doi: 10.1046/j.1523-1755.1999.00610.x.

Fischer, Christian, Massimiliano Mazzone, Bart Jonckx, and Peter Carmeliet. 2008. "FLT1 and its ligands VEGFB and PlGF: drug targets for anti-angiogenic therapy?" *Nat Rev Cancer* 8 (12):942-956.

Folkman, Judah. 1971. "Tumor Angiogenesis: Therapeutic Implications." *New England Journal of Medicine* 285 (21):1182-1186. doi: doi:10.1056/NEJM197111182852108.

Folkman, Judah. 1974. "Tumor Angiogenesis Factor." *Cancer Research* 34 (8):2109-2113.

Folkman, Judah. 2002. "Role of angiogenesis in tumor growth and metastasis." *Seminars in Oncology* 29 (6, Supplement 16):15-18. doi: http://dx.doi.org/10.1016/S0093-7754(02)70065-1.

Forbes, D. C., and N. A. Peppas. 2013. "Differences in molecular structure in cross-linked polycationic nanoparticles synthesized using ARGET ATRP or UV-initiated polymerization." *Polymer* 54 (17):4486-4492. doi: http://dx.doi.org/10.1016/j.polymer.2013.06.047.

Foss, Aaron C., and Nicholas A. Peppas. 2004. "Investigation of the cytotoxicity and insulin transport of acrylic-based copolymer protein delivery systems in contact with caco-2 cultures." *European Journal of Pharmaceutics and Biopharmaceutics* 57 (3):447-455. doi: http://dx.doi.org/10.1016/j.ejpb.2004.02.008.

Frohlich, E. 2012. "The role of surface charge in cellular uptake and cytotoxicity of medical nanoparticles." *Int J Nanomedicine* 7:5577-91. doi: 10.2147/IJN.S36111.

Fujisawa, S., T. Atsumi, and Y. Kadoma. 2000. "Cytotoxicity of methyl methacrylate (MMA) and related compounds and their interaction with dipalmitoylphosphatidylcholine (DPPC) liposomes as a model for biomembranes." *Oral Dis* 6 (4):215-21.

Garmy-Susini, B., H. Jin, Y. Zhu, R. J. Sung, R. Hwang, and J. Varner. 2005. "Integrin alpha4beta1-VCAM-1-mediated adhesion between endothelial and mural cells is required for blood vessel maturation." *J Clin Invest* 115 (6):1542-51. doi: 10.1172/jci23445.

Genis, L., P. Gonzalo, A. S. Tutor, B. G. Galvez, A. Martinez-Ruiz, C. Zaragoza, S. Lamas, K. Tryggvason, S. S. Apte, and A. G. Arroyo. 2007. "Functional interplay between endothelial nitric oxide synthase and membrane type 1 matrix metalloproteinase in migrating endothelial cells." *Blood* 110 (8):2916-23. doi: 10.1182/blood-2007-01-068080.

Gil, Eun Seok, and Samuel M. Hudson. 2004. "Stimuli-reponsive polymers and their bioconjugates." *Progress in Polymer Science* 29 (12):1173-1222. doi: http://dx.doi.org/10.1016/j.progpolymsci.2004.08.003.

Gref, R., A. Domb, P. Quellec, T. Blunk, R. H. Müller, J. M. Verbavatz, and R. Langer. 1995. "The controlled intravenous delivery of drugs using PEG-coated sterically stabilized nanospheres." *Advanced Drug Delivery Reviews* 16 (2–3):215-233. doi: http://dx.doi.org/10.1016/0169-409X(95)00026-4.

Gudeman, Linda F, and Nikolaos A Peppas. 1995. "pH-sensitive membranes from poly (vinyl alcohol)/poly (acrylic acid) interpenetrating networks." *Journal of membrane science* 107 (3):239-248.

Gumbiner, B. 1987. "Structure, biochemistry, and assembly of epithelial tight junctions." *Am J Physiol* 253 (6 Pt 1):C749-58.

Guo, Shutao, C. Michael Lin, Zhenghong Xu, Lei Miao, Yuhua Wang, and Leaf Huang. 2014. "Co-delivery of Cisplatin and Rapamycin for Enhanced Anticancer Therapy through Synergistic Effects and Microenvironment Modulation." *ACS Nano* 8 (5):4996-5009. doi: 10.1021/nn5010815.

Hagberg, Carolina E., Annelie Falkevall, Xun Wang, Erik Larsson, Jenni Huusko, Ingrid Nilsson, Laurens A. van Meeteren, Erik Samen, Li Lu, Maarten Vanwildemeersch, Joakim Klar, Guillem Genove, Kristian Pietras, Sharon Stone-Elander, Lena Claesson-Welsh, Seppo Yla-Herttuala, Per Lindahl, and Ulf Eriksson. 2010. "Vascular endothelial growth factor B controls endothelial fatty acid uptake." *Nature* 464 (7290):917-921. doi: http://www.nature.com/nature/journal/v464/n7290/suppinfo/nature08945_S1.html.

Hanahan, Douglas, and Judah Folkman. 1996. "Patterns and Emerging Mechanisms of the Angiogenic Switch during Tumorigenesis." *Cell* 86 (3):353-364. doi: http://dx.doi.org/10.1016/S0092-8674(00)80108-7.

Hancock, B. C., and M. Parks. 2000. "What is the true solubility advantage for amorphous pharmaceuticals?" *Pharm Res* 17 (4):397-404.

Hatakeyama, H., H. Akita, K. Kogure, M. Oishi, Y. Nagasaki, Y. Kihira, M. Ueno, H. Kobayashi, H. Kikuchi, and H. Harashima. 2006. "Development of a novel systemic gene delivery system for cancer therapy with a tumor-specific cleavable PEG-lipid." *Gene Ther* 14 (1):68-77. doi: http://www.nature.com/gt/journal/v14/n1/suppinfo/3302843s1.html.

Hicklin, D. J., L. Witte, Z. Zhu, F. Liao, Y. Wu, Y. Li, and P. Bohlen. 2001. "Monoclonal antibody strategies to block angiogenesis." *Drug Discov Today* 6 (10):517-528.

Hodivala-Dilke, K. M., A. R. Reynolds, and L. E. Reynolds. 2003. "Integrins in angiogenesis: multitalented molecules in a balancing act." *Cell Tissue Res* 314 (1):131-44. doi: 10.1007/s00441-003-0774-5.

Howes, P. D., R. Chandrawati, and M. M. Stevens. 2014. "Bionanotechnology. Colloidal nanoparticles as advanced biological sensors." *Science* 346 (6205):1247390. doi: 10.1126/science.1247390.

Hynes, R. O., J. C. Lively, J. H. McCarty, D. Taverna, S. E. Francis, K. Hodivala-Dilke, and Q. Xiao. 2002. "The diverse roles of integrins and their ligands in angiogenesis." *Cold Spring Harb Symp Quant Biol* 67:143-53.

Hynes, Richard O. 2009. "The Extracellular Matrix: Not Just Pretty Fibrils." *Science* 326 (5957):1216-1219.

Ichikawa, H., and N. A. Peppas. 2003. "Novel complexation hydrogels for oral peptide delivery: in vitro evaluation of their cytocompatibility and insulin-transport enhancing effects using Caco-2 cell monolayers." *J Biomed Mater Res A* 67 (2):609-17. doi: 10.1002/jbm.a.10128.

Jain, Rakesh K., Dan G. Duda, Christopher G. Willett, Dushyant V. Sahani, Andrew X. Zhu, Jay S. Loeffler, Tracy T. Batchelor, and A. Gregory Sorensen. 2009. "Biomarkers of response

and resistance to antiangiogenic therapy." *Nat Rev Clin Oncol* 6 (6):327-338. doi: http://www.nature.com/nrclinonc/journal/v6/n6/suppinfo/nrclinonc.2009.63_S1.html.

Jaruga, E., A. Sokal, S. Chrul, and G. Bartosz. 1998. "Apoptosis-independent alterations in membrane dynamics induced by curcumin." *Exp Cell Res* 245 (2):303-12. doi: 10.1006/excr.1998.4225.

Jellinek, Derek, Louis S. Green, Carol Bell, C. Kate Lynott, Nicole Gill, Chandra Vargeese, Gary Kirschenheuter, Daniel P. C. McGee, and Padmapriya Abesinghe. 1995. "Potent 2'-Amino-2'-deoxypyrimidine RNA Inhibitors of Basic Fibroblast Growth Factor." *Biochemistry* 34 (36):11363-11372. doi: 10.1021/bi00036a009.

Jones, M., and J. Leroux. 1999. "Polymeric micelles - a new generation of colloidal drug carriers." *Eur J Pharm Biopharm* 48 (2):101-11.

Kamiyama, E., D. Nakai, T. Mikkaichi, N. Okudaira, and O. Okazaki. 2010. "Interaction of angiotensin II type 1 receptor blockers with P-gp substrates in Caco-2 cells and hMDR1-expressing membranes." *Life Sci* 86 (1-2):52-8. doi: 10.1016/j.lfs.2009.11.006.

Kaplan, Rosandra N., Rebecca D. Riba, Stergios Zacharoulis, Anna H. Bramley, Loic Vincent, Carla Costa, Daniel D. MacDonald, David K. Jin, Koji Shido, Scott A. Kerns, Zhenping Zhu, Daniel Hicklin, Yan Wu, Jeffrey L. Port, Nasser Altorki, Elisa R. Port, Davide Ruggero, Sergey V. Shmelkov, Kristian K. Jensen, Shahin Rafii, and David Lyden. 2005. "VEGFR1-positive haematopoietic bone marrow progenitors initiate the pre-metastatic niche." *Nature* 438 (7069):820-827. doi: http://www.nature.com/nature/journal/v438/n7069/suppinfo/nature04186_S1.html.

Kerbel, R. S., A. Viloria-Petit, G. Klement, and J. Rak. 2000. "'Accidental' anti-angiogenic drugs. anti-oncogene directed signal transduction inhibitors and conventional chemotherapeutic agents as examples." *Eur J Cancer* 36 (10):1248-57.

Kim, S., K. Bell, S. A. Mousa, and J. A. Varner. 2000. "Regulation of angiogenesis in vivo by ligation of integrin alpha5beta1 with the central cell-binding domain of fibronectin." *Am J Pathol* 156 (4):1345-62.

Koetting, Michael C., and Nicholas A. Peppas. 2014. "pH-Responsive poly(itaconic acid-co-N-vinylpyrrolidone) hydrogels with reduced ionic strength loading solutions offer improved oral delivery potential for high isoelectric point-exhibiting therapeutic proteins." *International Journal of Pharmaceutics* 471 (1–2):83-91. doi: http://dx.doi.org/10.1016/j.ijpharm.2014.05.023.

Lai, Samuel K., Ying-Ying Wang, and Justin Hanes. 2009. "Mucus-penetrating nanoparticles for drug and gene delivery to mucosal tissues." *Advanced Drug Delivery Reviews* 61 (2):158-171. doi: http://dx.doi.org/10.1016/j.addr.2008.11.002.

Lanahan, Anthony A., Karlien Hermans, Filip Claes, Joanna S. Kerley-Hamilton, Zhen W. Zhuang, Frank J. Giordano, Peter Carmeliet, and Michael Simons. 2010. "VEGF Receptor 2 Endocytic Trafficking Regulates Arterial Morphogenesis." *Developmental Cell* 18 (5):713-724. doi: http://dx.doi.org/10.1016/j.devcel.2010.02.016.

Lee, S., T. T. Chen, C. L. Barber, M. C. Jordan, J. Murdock, S. Desai, N. Ferrara, A. Nagy, K. P. Roos, and M. L. Iruela-Arispe. 2007. "Autocrine VEGF signaling is required for vascular homeostasis." *Cell* 130 (4):691-703. doi: 10.1016/j.cell.2007.06.054.

Li, Junjie, Zhishen Ge, and Shiyong Liu. 2013. "PEG-sheddable polyplex micelles as smart gene carriers based on MMP-cleavable peptide-linked block copolymers." *Chemical Communications* 49 (62):6974-6976. doi: 10.1039/C3CC43576H.

Li, P. Y., P. S. Lai, W. C. Hung, and W. J. Syu. 2010. "Poly(L-lactide)-vitamin E TPGS nanoparticles enhanced the cytotoxicity of doxorubicin in drug-resistant MCF-7 breast cancer cells." *Biomacromolecules* 11 (10):2576-82. doi: 10.1021/bm1005195.

Liao, Fang, Jacqueline F. Doody, Jay Overholser, Bridget Finnerty, Rajiv Bassi, Yan Wu, Elisabetta Dejana, Paul Kussie, Peter Bohlen, and Daniel J. Hicklin. 2002. "Selective Targeting of Angiogenic Tumor Vasculature by Vascular Endothelial-cadherin Antibody Inhibits Tumor Growth without Affecting Vascular Permeability." *Cancer Research* 62 (9):2567-2575.

Lichtenberger, Beate M., Poi Kiang Tan, Heide Niederleithner, Napoleone Ferrara, Peter Petzelbauer, and Maria Sibilia. 2010. "Autocrine VEGF Signaling Synergizes with EGFR in Tumor Cells to Promote Epithelial Cancer Development." *Cell* 140 (2):268-279. doi: http://dx.doi.org/10.1016/j.cell.2009.12.046.

Liechty, William B., Mary Caldorera-Moore, Margaret A. Phillips, Cody Schoener, and Nicholas A. Peppas. 2011. "Advanced molecular design of biopolymers for transmucosal and intracellular delivery of chemotherapeutic agents and biological therapeutics." *Journal of Controlled Release* 155 (2):119-127. doi: http://dx.doi.org/10.1016/j.jconrel.2011.06.009.

Liechty, William B., Rebekah L. Scheuerle, and Nicholas A. Peppas. 2013. "Tunable, responsive nanogels containing t-butyl methacrylate and 2-(t-butylamino)ethyl methacrylate." *Polymer* 54 (15):3784-3795. doi: http://dx.doi.org/10.1016/j.polymer.2013.05.045.

Liu, D., Zhihong Liu F Fau - Liu, Lili Liu Z Fau - Wang, Na Wang L Fau - Zhang, and N. Zhang. "Tumor specific delivery and therapy by double-targeted nanostructured lipid carriers with anti-VEGFR-2 antibody." (1543-8392 (Electronic)).

Lobmann, K., H. Grohganz, R. Laitinen, C. Strachan, and T. Rades. 2013. "Amino acids as co-amorphous stabilizers for poorly water soluble drugs--Part 1: preparation, stability and dissolution enhancement." *Eur J Pharm Biopharm* 85 (3 Pt B):873-81. doi: 10.1016/j.ejpb.2013.03.014.

Lu, P., V. M. Weaver, and Z. Werb. 2012. "The extracellular matrix: a dynamic niche in cancer progression." *J Cell Biol* 196 (4):395-406. doi: 10.1083/jcb.201102147.

McNeil, C. 2006. "Two targets, one drug for new EGFR inhibitors." *J Natl Cancer Inst* 98 (16):1102-3. doi: 10.1093/jnci/djj350.

Miller, J. M., A. Beig, R. A. Carr, J. K. Spence, and A. Dahan. 2012. "A win-win solution in oral delivery of lipophilic drugs: supersaturation via amorphous solid dispersions increases apparent solubility without sacrifice of intestinal membrane permeability." *Mol Pharm* 9 (7):2009-16. doi: 10.1021/mp300104s.

Mistry, P., A. J. Stewart, W. Dangerfield, S. Okiji, C. Liddle, D. Bootle, J. A. Plumb, D. Templeton, and P. Charlton. 2001. "In vitro and in vivo reversal of P-glycoprotein-mediated multidrug resistance by a novel potent modulator, XR9576." *Cancer Res* 61 (2):749-58.

Mo, Ran, Tianyue Jiang, Rocco DiSanto, Wanyi Tai, and Zhen Gu. 2014. "ATP-triggered anticancer drug delivery." *Nat Commun* 5. doi: 10.1038/ncomms4364.

Mouw, Janna K., Guanqing Ou, and Valerie M. Weaver. 2014. "Extracellular matrix assembly: a multiscale deconstruction." *Nat Rev Mol Cell Biol* 15 (12):771-785. doi: 10.1038/nrm3902.

Na, K., E. S. Lee, and Y. H. Bae. 2007. "Self-organized nanogels responding to tumor extracellular pH: pH-dependent drug release and in vitro cytotoxicity against MCF-7 cells." *Bioconjug Chem* 18 (5):1568-74. doi: 10.1021/bc070052e.

Neufeld, Gera, and Ofra Kessler. 2008. "The semaphorins: versatile regulators of tumour progression and tumour angiogenesis." *Nat Rev Cancer* 8 (8):632-645.

Newman, A. C., M. N. Nakatsu, W. Chou, P. D. Gershon, and C. C. Hughes. 2011. "The requirement for fibroblasts in angiogenesis: fibroblast-derived matrix proteins are essential for endothelial cell lumen formation." *Mol Biol Cell* 22 (20):3791-800. doi: 10.1091/mbc.E11-05-0393.

Nomoto, Takahiro, Shigeto Fukushima, Michiaki Kumagai, Kaori Machitani, Arnida, Yu Matsumoto, Makoto Oba, Kanjiro Miyata, Kensuke Osada, Nobuhiro Nishiyama, and Kazunori Kataoka. 2014. "Three-layered polyplex micelle as a multifunctional nanocarrier platform for light-induced systemic gene transfer." *Nat Commun* 5. doi: 10.1038/ncomms4545.

O'Reilly, Michael S., Lars Holmgren, Yuen Shing, Catherine Chen, Rosalind A. Rosenthal, Marsha Moses, William S. Lane, Yihai Cao, E. Helene Sage, and Judah Folkman. 1994. "Angiostatin: A novel angiogenesis inhibitor that mediates the suppression of metastases by a lewis lung carcinoma." *Cell* 79 (2):315-328. doi: http://dx.doi.org/10.1016/0092-8674(94)90200-3.

Odian, George G, and George Odian. 2004. *Principles of polymerization*. Vol. 3: Wiley-Interscience New York.

Osborne, S. E., I. Matsumura, and A. D. Ellington. 1997. "Aptamers as therapeutic and diagnostic reagents: problems and prospects." *Curr Opin Chem Biol* 1 (1):5-9.

Otrock, Z. K., R. A. Mahfouz, J. A. Makarem, and A. I. Shamseddine. 2007. "Understanding the biology of angiogenesis: review of the most important molecular mechanisms." *Blood Cells Mol Dis* 39 (2):212-20. doi: 10.1016/j.bcmd.2007.04.001.

Panda, R. N., M. F. Hsieh, R. J. Chung, and T. S. Chin. 2003. "FTIR, XRD, SEM and solid state NMR investigations of carbonate-containing hydroxyapatite nano-particles synthesized by hydroxide-gel technique." *Journal of Physics and Chemistry of Solids* 64 (2):193-199. doi: http://dx.doi.org/10.1016/S0022-3697(02)00257-3.

Pasqualini, R., E. Koivunen, and E. Ruoslahti. 1997. "Alpha v integrins as receptors for tumor targeting by circulating ligands." *Nat Biotechnol* 15 (6):542-6. doi: 10.1038/nbt0697-542.

Peppas, Nicholas A, and Shelia L Wright. 1998. "Drug diffusion and binding in ionizable interpenetrating networks from poly (vinyl alcohol) and poly (acrylic acid)." *European journal of Pharmaceutics and Biopharmaceutics* 46 (1):15-29.

Peppas, Nikolaos A, and Shelia L Wright. 1996. "Solute diffusion in poly (vinyl alcohol)/poly (acrylic acid) interpenetrating networks." *Macromolecules* 29 (27):8798-8804.

Peppas, Nikolaos A. 1991. "Physiologically Responsive Hydrogels." *Journal of Bioactive and Compatible Polymers* 6 (3):241-246. doi: 10.1177/088391159100600303.

Peracchia, M. T., E. Fattal, D. Desmaële, M. Besnard, J. P. Noël, J. M. Gomis, M. Appel, J. d'Angelo, and P. Couvreur. 1999. "Stealth® PEGylated polycyanoacrylate nanoparticles for intravenous administration and splenic targeting." *Journal of Controlled Release* 60 (1):121-128. doi: http://dx.doi.org/10.1016/S0168-3659(99)00063-2.

Peracchia, M. T., C. Vauthier, D. Desmaele, A. Gulik, J. C. Dedieu, M. Demoy, J. d'Angelo, and P. Couvreur. 1998. "Pegylated nanoparticles from a novel methoxypolyethylene glycol cyanoacrylate-hexadecyl cyanoacrylate amphiphilic copolymer." *Pharm Res* 15 (4):550-6.

Persano, Luca, Marika Crescenzi, and Stefano Indraccolo. 2007. "Anti-angiogenic gene therapy of cancer: Current status and future prospects." *Molecular Aspects of Medicine* 28 (1):87-114. doi: http://dx.doi.org/10.1016/j.mam.2006.12.005.

Phelps, Edward A., and Andres J. Garcia. 2008. "Update on therapeutic vascularization strategies." *Regenerative Medicine* 4 (1):65-80. doi: 10.2217/17460751.4.1.65.

Phng, L. K., and H. Gerhardt. 2009. "Angiogenesis: a team effort coordinated by notch." *Dev Cell* 16 (2):196-208. doi: 10.1016/j.devcel.2009.01.015.

Plapied, Laurence, Nicolas Duhem, Anne des Rieux, and Véronique Préat. 2011. "Fate of polymeric nanocarriers for oral drug delivery." *Current Opinion in Colloid & Interface Science* 16 (3):228-237. doi: http://dx.doi.org/10.1016/j.cocis.2010.12.005.

Presta, M., L. Tiberio, M. Rusnati, P. Dell'Era, and G. Ragnotti. 1991. "Basic fibroblast growth factor requires a long-lasting activation of protein kinase C to induce cell proliferation in transformed fetal bovine aortic endothelial cells." *Cell regulation* 2 (9):719-726.

Primard, Charlotte, Nicolas Rochereau, Elsa Luciani, Christian Genin, Thierry Delair, Stéphane Paul, and Bernard Verrier. 2010. "Traffic of poly(lactic acid) nanoparticulate vaccine vehicle from intestinal mucus to sub-epithelial immune competent cells." *Biomaterials* 31 (23):6060-6068. doi: http://dx.doi.org/10.1016/j.biomaterials.2010.04.021.

Quinting, Gregory R., and Rubing Cai. 1994. "High-Resolution NMR Analysis of the Tacticity of Poly(n-butyl methacrylate)." *Macromolecules* 27 (22):6301-6306. doi: 10.1021/ma00100a012.

Randall, Cynthia S, William L Rocco, and Pierre Rico. 2010. "XRD: XRD in Pharmaceutical Analysis: A Versatile Tool for Problem-Solving." *American Pharmaceutical Review* 13 (6):52.

Rautio, J., J. E. Humphreys, L. O. Webster, A. Balakrishnan, J. P. Keogh, J. R. Kunta, C. J. Serabjit-Singh, and J. W. Polli. 2006. "In vitro p-glycoprotein inhibition assays for assessment of clinical drug interaction potential of new drug candidates: a recommendation for probe substrates." *Drug Metab Dispos* 34 (5):786-92. doi: 10.1124/dmd.105.008615.

Reilly, J. F., and P. A. Maher. 2001. "Importin beta-mediated nuclear import of fibroblast growth factor receptor: role in cell proliferation." *J Cell Biol* 152 (6):1307-12.

Richard, Robert E., Marlene Schwarz, Shrirang Ranade, A. Ken Chan, Krzysztof Matyjaszewski, and Brent Sumerlin. 2005. "Evaluation of Acrylate-Based Block Copolymers Prepared by Atom Transfer Radical Polymerization as Matrices for Paclitaxel Delivery from Coronary Stents." *Biomacromolecules* 6 (6):3410-3418. doi: 10.1021/bm050464v.

Rivera-Gil, Pilar, Stefaan De Koker, Bruno G. De Geest, and Wolfgang J. Parak. 2009. "Intracellular Processing of Proteins Mediated by Biodegradable Polyelectrolyte Capsules." *Nano Letters* 9 (12):4398-4402. doi: 10.1021/nl902697j.

Robson, C., K. A. Wright, P. R. Twentyman, P. A. Lambert, and R. J. Griffin. 1998. "Chemical synthesis and biological properties of novel fluorescent antifolates in Pgp- and MRP-overexpressing tumour cell lines." *Biochem Pharmacol* 56 (7):807-16.

Rolny, Charlotte, Massimiliano Mazzone, Sònia Tugues, Damya Laoui, Irja Johansson, Cathy Coulon, Mario Leonardo Squadrito, Inmaculada Segura, Xiujuan Li, Ellen Knevels, Sandra Costa, Stefan Vinckier, Tom Dresselaer, Peter Åkerud, Maria De Mol, Henriikka Salomäki, Mia Phillipson, Sabine Wyns, Erik Larsson, Ian Buysschaert, Johan Botling, Uwe Himmelreich, Jo A. Van Ginderachter, Michele De Palma, Mieke Dewerchin, Lena Claesson-Welsh, and Peter Carmeliet. 2011. "HRG Inhibits Tumor Growth and Metastasis by Inducing Macrophage Polarization and Vessel Normalization through Downregulation of PlGF." *Cancer Cell* 19 (1):31-44. doi: http://dx.doi.org/10.1016/j.ccr.2010.11.009.

Ruoslahti, E., and M. D. Pierschbacher. 1987. "New perspectives in cell adhesion: RGD and integrins." *Science* 238 (4826):491-7.

Ryan, G. M., L. M. Kaminskas, and C. J. Porter. 2014. "Nano-chemotherapeutics: Maximising lymphatic drug exposure to improve the treatment of lymph-metastatic cancers." *J Control Release*. doi: 10.1016/j.jconrel.2014.04.051.

Schlessinger, Joseph. 2000. "Cell Signaling by Receptor Tyrosine Kinases." *Cell* 103 (2):211-225. doi: http://dx.doi.org/10.1016/S0092-8674(00)00114-8.

Schmaljohann, Dirk. 2006. "Thermo- and pH-responsive polymers in drug delivery." *Advanced Drug Delivery Reviews* 58 (15):1655-1670. doi: http://dx.doi.org/10.1016/j.addr.2006.09.020.

Schwartz, Jonathan D., Eric K. Rowinsky, Hagop Youssoufian, Bronislaw Pytowski, and Yan Wu. 2010. "Vascular endothelial growth factor receptor-1 in human cancer." *Cancer* 116 (S4):1027-1032. doi: 10.1002/cncr.24789.

Scudiero, D. A., R. H. Shoemaker, K. D. Paull, A. Monks, S. Tierney, T. H. Nofziger, M. J. Currens, D. Seniff, and M. R. Boyd. 1988. "Evaluation of a soluble tetrazolium/formazan assay for cell growth and drug sensitivity in culture using human and other tumor cell lines." *Cancer Res* 48 (17):4827-33.

Semple, Sean C., Akin Akinc, Jianxin Chen, Ammen P. Sandhu, Barbara L. Mui, Connie K. Cho, Dinah W. Y. Sah, Derrick Stebbing, Erin J. Crosley, Ed Yaworski, Ismail M. Hafez, J. Robert Dorkin, June Qin, Kieu Lam, Kallanthottathil G. Rajeev, Kim F. Wong, Lloyd B. Jeffs, Lubomir Nechev, Merete L. Eisenhardt, Muthusamy Jayaraman, Mikameh Kazem, Martin A. Maier, Masuna Srinivasulu, Michael J. Weinstein, Qingmin Chen, Rene Alvarez, Scott A. Barros, Soma De, Sandra K. Klimuk, Todd Borland, Verbena Kosovrasti, William L. Cantley, Ying K. Tam, Muthiah Manoharan, Marco A. Ciufolini, Mark A. Tracy, Antonin de Fougerolles, Ian MacLachlan, Pieter R. Cullis, Thomas D. Madden, and Michael J. Hope. 2010. "Rational design of cationic lipids for siRNA delivery." *Nat Biotech* 28 (2):172-176. doi: 10.1038/nbt.1602

http://www.nature.com/nbt/journal/v28/n2/abs/nbt.1602.html#supplementary-information.

Sengupta, Shiladitya, David Eavarone, Ishan Capila, Ganlin Zhao, Nicki Watson, Tanyel Kiziltepe, and Ram Sasisekharan. 2005. "Temporal targeting of tumour cells and neovasculature with a nanoscale delivery system." *Nature* 436 (7050):568-572. doi: http://www.nature.com/nature/journal/v436/n7050/suppinfo/nature03794_S1.html.

Sharpe, Lindsey A., Adam M. Daily, Sarena D. Horava, and Nicholas A. Peppas. 2014. "Therapeutic applications of hydrogels in oral drug delivery." *Expert Opinion on Drug Delivery* 11 (6):901-915. doi: 10.1517/17425247.2014.902047.

Sheetal, R. D. Mello, K. Das Sudip, and G. Das Nandita. 2009. "Polymeric Nanoparticles for Small-Molecule Drugs: Biodegradation of Polymers and Fabrication of Nanoparticles." In *Drug Delivery Nanoparticles Formulation and Characterization*, 16-34. Informa Healthcare.

Sheikpranbabu, S., Deepak Kalishwaralal K Fau - Venkataraman, Soo Hyun Venkataraman D Fau - Eom, Jongsun Eom Sh Fau - Park, Sangiliyandi Park J Fau - Gurunathan, and S. Gurunathan. "Silver nanoparticles inhibit VEGF-and IL-1beta-induced vascular permeability via Src dependent pathway in porcine retinal endothelial cells." (1477-3155 (Electronic)). doi: D - NLM: PMC2776000 EDAT- 2009/11/03 06:00 MHDA- 2009/11/03 06:01 CRDT- 2009/11/03 06:00 PHST- 2009/06/26 [received] PHST- 2009/10/30 [accepted] PHST- 2009/10/30 [aheadofprint] AID - 1477-3155-7-8 [pii] AID - 10.1186/1477-3155-7-8 [doi] PST - epublish.

Shen, Q., Y. Lin, T. Handa, M. Doi, M. Sugie, K. Wakayama, N. Okada, T. Fujita, and A. Yamamoto. 2006a. "Modulation of intestinal P-glycoprotein function by polyethylene glycols and their derivatives by in vitro transport and in situ absorption studies." *Int J Pharm* 313 (1-2):49-56. doi: 10.1016/j.ijpharm.2006.01.020.

Shen, Qi, Yulian Lin, Takahiro Handa, Masamichi Doi, Masami Sugie, Kana Wakayama, Naoki Okada, Takuya Fujita, and Akira Yamamoto. 2006b. "Modulation of intestinal P-glycoprotein function by polyethylene glycols and their derivatives by in vitro transport and in situ absorption studies." *International Journal of Pharmaceutics* 313 (1–2):49-56. doi: http://dx.doi.org/10.1016/j.ijpharm.2006.01.020.

Shin, Junhwa, Pochi Shum, and David H. Thompson. 2003. "Acid-triggered release via dePEGylation of DOPE liposomes containing acid-labile vinyl ether PEG–lipids." *Journal of Controlled Release* 91 (1–2):187-200. doi: http://dx.doi.org/10.1016/S0168-3659(03)00232-3.

Solon, Jerome, Aynur Kaya-Çopur, Julien Colombelli, and Damian Brunner. 2009. "Pulsed Forces Timed by a Ratchet-like Mechanism Drive Directed Tissue Movement during Dorsal Closure." *Cell* 137 (7):1331-1342. doi: http://dx.doi.org/10.1016/j.cell.2009.03.050.

Spencer, David S., Amey S. Puranik, and Nicholas A. Peppas. 2015. "Intelligent nanoparticles for advanced drug delivery in cancer treatment." *Current Opinion in Chemical Engineering* 7 (0):84-92. doi: http://dx.doi.org/10.1016/j.coche.2014.12.003.

STACKER, STEVEN A., MEGAN E. BALDWIN, and MARC G. ACHEN. 2002. "The role of tumor lymphangiogenesis in metastatic spread." *The FASEB Journal* 16 (9):922-934. doi: 10.1096/fj.01-0945rev.

Stockmann, C., A. Doedens, A. Weidemann, N. Zhang, N. Takeda, J. I. Greenberg, D. A. Cheresh, and R. S. Johnson. 2008. "Deletion of vascular endothelial growth factor in myeloid cells accelerates tumorigenesis." *Nature* 456 (7223):814-8. doi: 10.1038/nature07445.

Sudhakar, A., H. Sugimoto, C. Yang, J. Lively, M. Zeisberg, and R. Kalluri. 2003. "Human tumstatin and human endostatin exhibit distinct antiangiogenic activities mediated by alpha v beta 3 and alpha 5 beta 1 integrins." *Proc Natl Acad Sci U S A* 100 (8):4766-71. doi: 10.1073/pnas.0730882100.

Synatschke, Christopher V., Takahiro Nomoto, Horacio Cabral, Melanie Förtsch, Kazuko Toh, Yu Matsumoto, Kozo Miyazaki, Andreas Hanisch, Felix H. Schacher, Akihiro Kishimura, Nobuhiro Nishiyama, Axel H. E. Müller, and Kazunori Kataoka. 2014. "Multicompartment Micelles with Adjustable Poly(ethylene glycol) Shell for Efficient in Vivo Photodynamic Therapy." *ACS Nano* 8 (2):1161-1172. doi: 10.1021/nn4028294.

Szakacs, G., J. K. Paterson, J. A. Ludwig, C. Booth-Genthe, and M. M. Gottesman. 2006. "Targeting multidrug resistance in cancer." *Nat Rev Drug Discov* 5 (3):219-34. doi: 10.1038/nrd1984.

Tammela, Tuomas, and Kari Alitalo. "Lymphangiogenesis: Molecular Mechanisms and Future Promise." *Cell* 140 (4):460-476. doi: 10.1016/j.cell.2010.01.045.

Ting, Jeffrey M., Tushar S. Navale, Frank S. Bates, and Theresa M. Reineke. 2013. "Precise Compositional Control and Systematic Preparation of Multimonomeric Statistical Copolymers." *ACS Macro Letters* 2 (9):770-774. doi: 10.1021/mz4003112.

Tokareva, Iryna, Sergiy Minko, Janos H. Fendler, and Eliza Hutter. 2004. "Nanosensors Based on Responsive Polymer Brushes and Gold Nanoparticle Enhanced Transmission Surface Plasmon Resonance Spectroscopy." *Journal of the American Chemical Society* 126 (49):15950-15951. doi: 10.1021/ja044575y.

Torchilin, V. P. 2007. "Micellar nanocarriers: pharmaceutical perspectives." *Pharm Res* 24 (1):1-16. doi: 10.1007/s11095-006-9132-0.

Tress, Martin, Emmanuel U. Mapesa, Wilhelm Kossack, Wycliffe K. Kipnusu, Manfred Reiche, and Friedrich Kremer. 2013. "Glassy Dynamics in Condensed Isolated Polymer Chains." *Science* 341 (6152):1371-1374.

Tvorogov, Denis, Andrey Anisimov, Wei Zheng, Veli-Matti Leppänen, Tuomas Tammela, Simonas Laurinavicius, Wolfgang Holnthoner, Hanna Heloterä, Tanja Holopainen, Michael Jeltsch, Nisse Kalkkinen, Hilkka Lankinen, Päivi M. Ojala, and Kari Alitalo. 2010. "Effective Suppression of Vascular Network Formation by Combination of Antibodies Blocking VEGFR Ligand Binding and Receptor Dimerization." *Cancer Cell* 18 (6):630-640. doi: http://dx.doi.org/10.1016/j.ccr.2010.11.001.

Wischke, C., A. T. Neffe, S. Steuer, E. Engelhardt, and A. Lendlein. 2010. "AB-polymer networks with cooligoester and poly(n-butyl acrylate) segments as a multifunctional matrix for controlled drug release." *Macromol Biosci* 10 (9):1063-72. doi: 10.1002/mabi.201000089.

Xu, Huan, Yihui Deng, Dawei Chen, Weiwei Hong, Yi Lu, and Xiaohui Dong. 2008. "Esterase-catalyzed dePEGylation of pH-sensitive vesicles modified with cleavable PEG-lipid derivatives." *Journal of Controlled Release* 130 (3):238-245. doi: http://dx.doi.org/10.1016/j.jconrel.2008.05.009.

Yun, Y., Kinam Cho Yw Fau - Park, and K. Park. "Nanoparticles for oral delivery: targeted nanoparticles with peptidic ligands for oral protein delivery." (1872-8294 (Electronic)). doi: D - NLM: NIHMS419181

D - NLM: PMC3574626 EDAT- 2012/11/06 06:00 MHDA- 2013/10/23 06:00 CRDT- 2012/11/06 06:00 PHST- 2012/06/28 [received] PHST- 2012/10/17 [revised] PHST- 2012/10/18 [accepted] PHST- 2012/11/02 [aheadofprint] AID - S0169-409X(12)00353-5 [pii] AID - 10.1016/j.addr.2012.10.007 [doi] PST - ppublish.

Zhang, Janny X., Samuel Zalipsky, Nasreen Mullah, Michal Pechar, and Theresa M. Allen. 2004. "Pharmaco attributes of dioleoylphosphatidylethanolamine/cholesterylhemisuccinate liposomes containing different types of cleavable lipopolymers." *Pharmacological Research* 49 (2):185-198. doi: http://dx.doi.org/10.1016/j.phrs.2003.09.003.

Zhang, Qian, Qiao Jiang, Na Li, Luru Dai, Qing Liu, Linlin Song, Jinye Wang, Yaqian Li, Jie Tian, Baoquan Ding, and Yang Du. 2014. "DNA Origami as an In Vivo Drug Delivery Vehicle for Cancer Therapy." *ACS Nano* 8 (7):6633-6643. doi: 10.1021/nn502058j.

Zhu, Lin, Tao Wang, Federico Perche, Anton Taigind, and Vladimir P. Torchilin. 2013. "Enhanced anticancer activity of nanopreparation containing an MMP2-sensitive PEG-drug conjugate and cell-penetrating moiety." *Proceedings of the National Academy of Sciences* 110 (42):17047-17052. doi: 10.1073/pnas.1304987110.